PENNSTATE

1855

FINAL REPORT

FINITE DIFFERENCE TIME DOMAIN ELECTROMAGNETIC SCATTERING FROM FREQUENCY-DEPENDENT LOSSY MATERIALS

Under Contract NAG 2-648
NASA Ames Research Center

Period Covered: 3/1/90-6/30/91

Submitted to

Captain Doug Havens
AFEWC/ESAS
San Antonio, TX 78243-5000

Submitted by

Raymond J. Luebbers (PI) and John H. Beggs
Electrical and Computer Engineering Department
The Pennsylvania State University
University Park, PA 16802

Tel. (814) 865-2362
FAX (814) 865-7065

July 1991

TABLE OF CONTENTS

INTRODUCTION

This final report summarizes the research accomplishments under Contract NAG 2-648 between NASA Ames Research Center and the Pennsylvania State University. More specific information on each topic covered in this report is contained in the manuals and preprints which have been submitted along with this report, as described in the Deliverables section of the Statement of Work for the subject contract. Also submitted with this report are 4 different FDTD computer codes and companion RCS conversion codes on magnetic media. In the remainder of this report the preprints, the computer codes and their user's manuals will be summarized.

COMPUTER CODES DELIVERED

Under this effort a single three dimensional dispersive FDTD code for both dispersive dielectric and magnetic materials was to be developed and delivered, along with a User's Manual. This code is included with this report on Magnetic Media, and is named "FDTDD", standing for the "D" version of a set of three-dimensional FDTD codes developed at Penn State. This code has the capability to calculate electromagnetic field interactions with objects which include both dispersive and non-dispersive dielectric and magnetic materials. Using a companion code, "RCS3D", the output from FDTDD can be converted to radar cross section vs frequency. A User's Manual describing the theory and use of the computer code FDTDD and showing validation results is included with this final report as attachment [1].

In addition to FDTDD, simpler (and somewhat faster) three-dimensional FDTD codes which have more limited or no dispersive material capability, "FDTDA" through "FDTDC", are also being delivered along with this final report. Version "A" is for frequency-independent materials, version "B" for frequency-dependent dielectric (non-magnetic) materials, and version "C" for frequency-independent dielectric and magnetic materials. While version "D" includes all of these cases, the simpler versions "A" through "C" are somewhat easier to use and will run faster than the more complicated "D" version. They are therefore preferred when the more extensive capabilities of the "D" version are not needed. All versions use the same "RCS3D" companion computer code to convert time domain output to RCS vs frequency. The User's Manuals for all four versions of the Penn State FDTD code are included with this report as attachments [1-4].

While three-dimensional FDTD codes are generally more useful, two-dimensional codes can be applied to geometries of interest, and have the advantage of requiring significantly less computer resources. A pair of two-dimensional FDTD codes, "TEA" and "TMA", for transverse electric and transverse magnetic excitation, respectively, are also included with this final report on magnetic media. Also included are companion

computer codes "SWTEA" and "SWTMA", which convert the time domain output of "TEA" and "TMA" to scattering width vs frequency. The user's manual for these codes is also included with this report as an attachment [5]. A theoretical description and validation results for the two-dimensional computer codes are contained in a preprint included with this report as attachment [6].

EXTENSIONS TO DISPERSIVE FDTD CAPABILITIES

During this effort two extensions to our dispersive material FDTD capability were made. One was the extension to include magnetic materials which have more complicated frequency dependence of their permittivity than considered previously. The time domain magnetic susceptibility has the form of a damped sinusoidal wave, resulting from the oscillations of the microscopic currents in the material. Dispersive FDTD was extended to include this class of materials, and these results are reported in a PhD dissertation by Forrest Hunsberger that is included with this final report as attachment [7]. Some of this material has already been presented at the recent IEEE AP-S conference [8], and Dr. Hunsberger is currently writing papers based on this dissertation for journal submission.

The other extension is to a time domain surface "impedance" formulation for lossy conductors. As explained in attachment [9], this removes a difficulty in applying FDTD to targets containing lossy materials. The difficulty is due to the necessity of reducing the size of the FDTD cells which are inside the conducting materials. With the FDTD surface "impedance" described in [9], FDTD cells need not be located inside the conducting material but only at the surface. The attachment [9] preprint has already been accepted for publication in IEEE Trans. on Antennas and Propagation. These results have in part been presented at the recent IEEE AP-S symposium [10].

The approach used in [9] also extends the basic frequency dependent FDTD to a wider class of materials. This is due to the method used in [9] to obtain the necessary time domain convolution coefficients. With this method ANY material whose frequency dependent behavior is known can have this information be transformed to the time domain, and then with application of Prony's method (see [9]) the necessary exponential coefficients for applying dispersive FDTD can be obtained.

PLATE SCATTERING

During the course of this research effort three different plate scattering geometries were given special consideration. The first of these was suggested by Dr. Randy Jost. It involved a conducting plate coated with a dielectric layer. This geometry cannot readily be modeled using other scattering calculation methods. Scattering results

for this geometry were calculated using one of our FDTD codes (the "FDTDA" code furnished under this effort). The results were documented and are attached to this report [11]. The results were previously furnished to Dr. Jost, and according to Dr. Jost they showed significant correlation with measurements. We hope to continue this investigation.

The second plate geometry considered was the "business card" plate geometry being used as a test case by Dr. Alex Woo of NASA Ames. This geometry is challenging since edge waves contribute to the scattering. Moment Method codes require approximately 10 times the usual density of modes to accurately compute the scattering from this geometry. Our results, shown in attachment [12] of this report, shown the difference in RCS computed using FDTD and a Moment Method code. Dr. Woo indicated that our results were quite accurate, considering that we used only 10 cells per wavelength running on a 486 PC. We hope to run this data again using more cells per wavelength, and compare our results directly with measurements.

The third topic considered was extending FDTD to include modeling of thin impedance sheets. While applicable to arbitrary shapes and in both two and three dimensions, the extension was validated by calculating RCS from thin flat impedance sheet plates. The results are reported in attachment [13].

NONLINEAR MATERIALS

Having extended the FDTD method to dispersive materials, another class of materials which it would be desirable to include are nonlinear materials. During this effort the current flowing in a wire antenna loaded with a nonlinear diode was successfully computed using FDTD. The results are shown in the attached preprint [14]. With this capability RCS from scatters including nonlinear loads or bulk materials may be computed using FDTD. Further extensions could include scattering of short pulses from nonlinear dispersive materials including ferrite absorbers.

WIRE ANTENNAS

The accuracy available from the FDTD method was demonstrated by computing the self impedance of a wire dipole antenna and the mutual impedance between two wire antennas. These results are reported in attachment [15].

CONCLUSIONS

During this effort the tasks specified in the Statement of Work have been successfully completed. The extension of FDTD to more complicated materials has been made. A three-dimensional FDTD code capable of modeling interactions with both dispersive dielectric and magnetic materials has been written, validated, and documented. This code is efficient and is capable of modeling interesting targets using a modest computer work station platform.

However, in addition to the tasks in the Statement of Work, a significant number of other FDTD extensions and calculations have been made. RCS results for two different plate geometries have been reported. The FDTD method has been extended to computing far zone time domain results in two dimensions. Finally, the capability to model nonlinear materials has been incorporated into FDTD and validated.

The FDTD computer codes developed have been supplied, along with documentation, and preprints describing the other FDTD advances have been included with this report as attachments.

ATTACHMENTS AND REFERENCES

1. John Beggs and Raymond Luebbers, "User's Manual for Three-Dimensional FDTD Version "D" Code for Scattering from Frequency-Dependent Dielectric and Magnetic Materials," July 1991.

2. John Beggs and Raymond Luebbers, "User's Manual for Three-Dimensional FDTD Version "A" Code for Scattering from Frequency-Independent Dielectric Materials," July 1991.

3. John Beggs and Raymond Luebbers, "User's Manual for Three-Dimensional FDTD Version "B" Code for Scattering from Frequency-Dependent Dielectric and Magnetic Materials," July 1991.

4. John Beggs and Raymond Luebbers, "User's Manual for Three-Dimensional FDTD Version "C" Code for Scattering from Frequency-Independent Dielectric Materials," July 1991.

5. John Beggs and Raymond Luebbers, "User's Manual for Two-Dimensional FDTD Version "A" Codes for TE and TM Scattering from Frequency-Independent Dielectric Materials," July 1991.

6. Raymond Luebbers, Deirdre Ryan, and John Beggs, "A Two-Dimensional Time Domain Near Zone to Far Zone Transformation," submitted to IEEE Transaction on Antennas and Propagation, May 1991.

7. Forrest Hunsberger, Jr., "Extension of the Finite Difference Time Domain Method to Gyrotropic Media," PhD Dissertation, The Pennsylvania State University, May 1991.

8. F. Hunsberger, R. Luebbers, K. Kunz, "Transient Analysis of Magnetoactive Plasma using Finite Difference Time Domain Method," IEEE Antennas and Propagation Society International Symposium, London, Ontario, Canada, June 24-28, 1991.

9. John Beggs, Raymond Luebbers, Kane Yee, and Karl Kunz, "Wideband Finite Difference Time Domain Implementation of Surface Impedance Boundary Conditions for Good Conductors," accepted for publication in IEEE Trans. on Antennas and Propagat.

10. J. Beggs, R. Luebbers, K. Kunz, K. Yee, "Wideband Finite Difference Time Domain Implementation of Surface Impedance Boundary Conditions for Good Conductors," IEEE Antennas and Propagation Society International Symposium, London, Ontario, Canada, June 24-28, 1991.

11. Raymond Lùebbers and John Beggs, "Time Domain Scattering and Radar Cross Section Calculations for a Thin, Perfectly Conducting Plate," February 1991.

12. Raymond Luebbers and John Beggs, "Conical Cut Radar Cross Section Calculations for a Thin, Perfectly Conducting Plate," March 1991.

13. Raymond Luebbers and Karl Kunz, "FDTD Modeling of Thin Impedance Sheets," submitted to IEEE Trans. Antennas and Propagation, June 1991.

14. Raymond Luebbers, John Beggs, and Karl Kunz, "Finite Difference Time Domain Calculation of Transients in Antennas with Nonlinear Loads," submitted to IEEE Trans. Antennas and Propagation, July 1991.

15. Raymond Luebbers and Karl Kunz, "Finite Difference Time Domain Calculations of Antenna Mutual Coupling," submitted to IEEE Trans. on Electromagnetic Compatibility, April 1991.

USER'S MANUAL FOR

THREE DIMENSIONAL FDTD VERSION A

CODE FOR SCATTERING FROM FREQUENCY-INDEPENDENT

DIELECTRIC MATERIALS

by

John H. Beggs, Raymond J. Luebbers and Karl S. Kunz
Electrical and Computer Engineering Department
The Pennsylvania State University
University Park, PA 16802

(814) 865-2362

January 1992

TABLE OF CONTENTS

TABLE OF CONTENTS (cont.)

I. INTRODUCTION

The Penn State Finite Difference Time Domain Electromagnetic Scattering Code Version A is a three dimensional numerical electromagnetic scattering code based upon the Finite Difference Time Domain Technique (FDTD). The supplied version of the code is one version of our current three dimensional FDTD code set. This manual provides a description of the code and corresponding results for the default scattering problem. The manual is organized into fourteen sections: introduction, description of the FDTD method, Operation, resource requirements, Version A code capabilities, a brief description of the default scattering geometry, a brief description of each subroutine, a description of the include file (COMMONA.FOR), a section briefly discussing Radar Cross Section (RCS) computations, a section discussing the scattering results, a sample problem setup section, a new problem checklist, references and figure titles.

II. FDTD METHOD

The Finite Difference Time Domain (FDTD) technique models transient electromagnetic scattering and interactions with objects of arbitrary shape and/or material composition. The technique was first proposed by Yee [1] for isotropic, non-dispersive materials in 1966; and has matured within the past twenty years into a robust and efficient computational method. The present FDTD technique is capabable of transient electromagnetic interactions with objects of arbitrary and complicated geometrical shape and material composition over a large band of frequencies. This technique has recently been extended to include dispersive dielectric materials, chiral materials and plasmas.

In the FDTD method, Maxwell's curl equations are discretized in time and space and all derivatives (temporal and spatial) are approximated by central differences. The electric and magnetic fields are interleaved in space and time and are updated in a second-order accurate leapfrog scheme. The computational space is divided into cells with the electric fields located on the edges and the magnetic fields on the faces (see Figure 1). FDTD objects are defined by specifying dielectric and/or magnetic material parameters at electric and/or magnetic field locations.

Two basic implementations of the FDTD method are widely used for electromagnetic analysis: total field formalism and scattered field formalism. In the total field formalism, the electric and magnetic field are updated based upon the material type present at each spatial location. In the scattered field formalism, the incident waveform is defined analytically and the scattered field is coupled to the incident field through the different material types. For the incident field, any waveform, angle of incidence and polarization is possible. The separation of the incident and

scattered fields conveniently allows an absorbing boundary to be employed at the extremities of the discretized problem space to absorb the scattered fields.

This code is a scattered field code, and the total E and H fields may be found by combining the incident and scattered fields. Any type of field quantity (incident, scattered, or total), Poynting vector or current are available anywhere within the computational space. These fields, incident, scattered and total, may be found within, on or about the interaction object placed in the problem space. By using a near to far field transformation, far fields can be determined from the near fields within the problem space thereby affording radiation patterns and RCS values. The accuracy of these calculations is typically within a dB of analytic solutions for dielectric and magnetic sphere scattering. Further improvements are expected as better absorbing boundary conditions are developed and incorporated.

III. OPERATION

Typically, a truncated Gaussian incident waveform is used to excite the system being modeled, however certain code versions also provide a smooth cosine waveform for convenience in modeling dispersive materials. The interaction object is defined in the discretized problem space with arrays at each cell location created by the discretization. All three dielectric material types for E field components within a cell can be individually specified by the arrays IDONE(I,J,K), IDTWO(I,J,K), IDTHRE(I,J,K). This models arbitrary dielectric materials with $\mu = \mu_0$. By an obvious extension to six arrays, magnetic materials with $\mu \neq \mu_0$ can be modeled.

Scattering occurs when the incident wave, marched forward in time in small steps set by the Courant stability condition, reaches the interaction object. Here a scattered wave must appear along with the incident wave so that the Maxwell equations are satisfied. If the material is a perfectly conductive metal then only the well known boundary condition

$$E_{tan}^{scat} = -E_{tan}^{inc} \tag{1}$$

must be satisfied. For a nondispersive dielectric the requirement is that the total field must satisfy the Maxwell equations in the material:

$$\nabla \times E^{tot} = \nabla \times (E^{inc} + E^{scat}) = -\frac{1}{\mu_o}\frac{\partial H^{tot}}{\partial t} = -\frac{1}{\mu_o}\frac{\partial (H^{inc} + H^{scat})}{\partial t} \tag{2}$$

$$\nabla \times H^{tot} = \nabla \times (H^{inc} + H^{scat}) = \varepsilon \frac{\partial E^{tot}}{\partial t} + \sigma E^{tot} \tag{3}$$

$$= \varepsilon \frac{\partial (E^{inc} + E^{scat})}{\partial t} + \sigma (E^{inc} + E^{scat}) \tag{4}$$

Additionally the incident wave, defined as moving unimpeded through a vacuum in the problem space, satisfies everywhere in the problem the Maxwell equations for free space

$$\nabla \times E^{inc} = -\frac{1}{\mu_o} \frac{\partial H^{inc}}{\partial t} \tag{5}$$

$$\nabla \times H^{inc} = \varepsilon_o \frac{\partial E^{inc}}{\partial t} \tag{6}$$

Subtracting the second set of equations from the first yields the Maxwell equations governing the scattered fields in the material:

$$\nabla \times E^{scat} = -\frac{1}{\mu_o} \frac{\partial H^{scat}}{\partial t} \tag{7}$$

$$\nabla \times H^{scat} = (\varepsilon - \varepsilon_o) \frac{\partial E^{inc}}{\partial t} + \sigma E^{inc} + \varepsilon \frac{\partial E^{scat}}{\partial t} + \sigma E^{scat} \tag{8}$$

Outside the material this simplifies to:

$$\nabla \times E^{scat} = -\frac{1}{\mu_o} \frac{\partial H^{scat}}{\partial t} \tag{9}$$

$$\nabla \times H^{scat} = \varepsilon_o \frac{\partial E^{scat}}{\partial t} \tag{10}$$

Magnetic materials, dispersive effects, non-linearities, etc., are further generalizations of the above approach. Based on the value of the material type, the subroutines for calculating scattered E and H field components branch to the appropriate expression for that scattered field component and

that component is advanced in time according to the selected algorithm. As many materials can be modeled as desired, the number equals the dimension selected for the flags. If materials with behavior different from those described above must be modeled, then after the appropriate algorithm is found, the code's branching structure allows easy incorporation of the new behavior.

IV. RESOURCE REQUIREMENTS

The number of cells the problem space is divided into times the six components per cell set the problem space storage requirements

$$\text{Storage} = NC \times 6 \text{ components/cell} \times 4 \text{ bytes/component} \tag{11}$$

and the computational cost

$$\text{Operations} = NC \times 6 \text{ comp/cell} \times 10 \text{ ops/component} \times N \tag{12}$$

where N is the number of time steps desired.

N typically is on the order of ten times the number of cells on one side of the problem space. More precisely for cubical cells it takes $\sqrt{3}$ time steps to traverse a single cell when the time step is set by the Courant stability condition

$$\Delta t = \frac{\Delta x}{\sqrt{3}c} \qquad \Delta x = \text{cell size dimension} \tag{13}$$

The condition on N is then that

$$N \sim 10 \times (\sqrt{3} NC^{\frac{1}{3}}) \qquad NC^{\frac{1}{3}} \sim \text{number cells on a side of the problem space} \tag{14}$$

The earliest aircraft modeling using FDTD with approximately 30 cells on a side required approximately 500 time steps. For more recent modeling with approximately 100 cells on a side, 2000 or more time steps are used.

For $(100 \text{ cell})^3$ problem spaces, 24 MBytes of memory are required to store the fields. Problems on the order of this size have been run on a Silicon Graphics 4D 220 with 32 MBytes of memory, IBM RISC 6000, an Intel 486 based machine, and VAX 11/785. Storage is only a problem as in the case of the 486 where only 16 MBytes of memory was available. This limited the problem space size to approximately $(80 \text{ cells})^3$.

For $(100 \text{ cell})^3$ problems with approximately 2000 time steps, there is a total of 120×10^9 operations to perform. The speeds of the previously mentioned machines are 24 MFLOPs (4 processor upgraded version), 10 MFLOPS, 1.5 MFLOPS, and 0.2 MFLOPs. The run times are then 5×10^3 seconds, 12×10^3 seconds, 80×10^3 seconds and 600×10^3 seconds, respectively. In hours the times are 1.4, 3.3, 22.2 and 167 hours. Problems of this size are possible on all but the last machine and can in fact be performed on a personal computer (486) if one day turnarounds are permissible.

V. VERSION A CODE CAPABILITIES

The Penn State University FDTD Electromagnetic Scattering Code Version A has the following capabilities:

1) Ability to model lossy dielectric and perfectly conducting scatterers.

2) First and second order outer radiation boundary condition (ORBC) operating on the electric fields for dielectric or perfectly conducting scatterers.

3) Near to far zone transformation capability to obtain far zone scattered fields.

4) Gaussian and smooth cosine incident waveforms with arbitrary incidence angles.

5) Near zone field, current or power sampling capability.

6) Companion code for computing Radar Cross Section (RCS).

VI. DEFAULT SCATTERING GEOMETRY

The code as delivered is set up to calculate the far zone backscatter fields for an infinitely thin, 29 cm square, perfectly conducting plate. The problem space size is 60 by 60 by 49 cells in the x, y and z directions, the cells are 1 cm cubes, and the incident waveform is a ϕ-polarized Gaussian pulse with incidence angles of θ=45 and ϕ=30 degrees. The output data files are included as a reference along with a code (RCS3D.FOR) for computing the frequency domain RCS using these output data files. The ORBC is the second order absorbing boundary condition set forth by Mur [2].

VII. SUBROUTINE DESCRIPTION

In the description for each subroutine, an asterisk (*) will be placed by the subroutine name if that particular subroutine is normally modified when defining a scattering problem.

MAIN ROUTINE

The main routine in the program contains the calls for all necessary subroutines to initialize the problem space and scattering object(s) and for the incident waveform, far zone transformation, field update subroutines, outer radiation boundary conditions and field sampling.

The main routine begins with the include statement and then appropriate data files are opened, and subroutines ZERO, BUILD and SETUP are called to initialize variables and/or arrays, build the object(s) and initialize the incident waveform and miscellaneous parameters, respectively. Subroutine SETFZ is called to intialize parameters for the near to far zone transformation if far zone fields are desired.

The main loop is entered next, where all of the primary field computations and data saving takes place. During each time step cycle, the EXSFLD, EYSFLD, and EZSFLD subroutines are called to update the x, y, and z components of the scattered electric field. The six electric field outer radiation boundary conditions (RADE??) are called next to absorb any outgoing scattered fields. Time is then advanced 1/2 time step according to the Yee algorithm and then the HXSFLD, HYSFLD, AND HZSFLD subroutines are called to update the x, y, and z components of scattered magnetic field. Time is then advanced another 1/2 step and then either near zone fields are sampled and written to disk in DATSAV, and/or the near zone to far zone vector potentials are updated in SAVFZ. The parameter NZFZ (described later) in the common file defines the type of output fields desired.

After execution of all time steps in the main field update loop, subroutine FAROUT is called if far zone fields are desired to compute the far zone fields and write them to disk. At this point, the execution is complete.

SUBROUTINE SETFZ

This subroutine initializes the necessary parameters required for far zone field computations. The code as furnished computes backscatter far zone fields and can compute bistatic far zone fields for one scattering angle (i.e. one θ and ϕ angle). Refer to reference [3] for a complete description of the near to far zone transformation. Other versions of this subroutine provide for multiple bistatic angles.

SUBROUTINE SAVFZ

This subroutine updates the near zone to far zone vector potentials.

SUBROUTINE FAROUT

This subroutine changes the near zone to far zone vector potentials to far zone electric field θ and ϕ components and writes them to disk.

SUBROUTINE BUILD *

This subroutine "builds" the scattering object(s) by initializing the IDONE, IDTWO, and IDTHRE arrays. The IDONE-IDTHRE arrays are for specifying perfectly conducting and lossy dielectric materials. Refer to Figure 1 for a diagram of the basic Yee cell. For example, setting an element of the IDONE array at some I,J,K location is actually locating dielectric material at a cell edge whose center location is I+0.5,J,K. Thus, materials with diagonal permittivity tensors can be modeled. The default material type for all ID??? arrays is 0, or free space. By initializing these arrays to values other than 0, the user is defining an object by determining what material types are present at each spatial location. Other material types available for IDONE-IDTHRE are 1 for perfectly conducting objects and 2-9 for lossy non-magnetic dielectrics. It is assumed throughout the code that <u>all</u> dielectric materials are non-magnetic (i.e. the materials have a permeability of μ_0). This subroutine also has a section that checks the ID??? arrays to determine if legal material types have been defined throughout the problem space. The actual material parameters (ϵ and σ) are defined in subroutine SETUP. The default geometry is a 29 cm square perfectly conducting plate.

The user must be careful that his/her object created in the BUILD subroutine is properly formed.

When it is important to place the object in the center of the problem space (to have lowest possible cross-pol scattering for symmetric objects), NX etc. should be odd. This is due to the field locations in the Yee cell and also the placement of the E field absorbing boundary condition surfaces.

If the object being modeled has curved surfaces, edges, etc. that are at an angle to one or more of the coordinate axes, then that shape must be approximately modeled by lines and faces in a "stair-stepped" (or stair-cased) fashion. This stair-cased approximation introduces errors into computations at higher frequencies. Intuitively, the error becomes smaller as more cells are used to stair-case a particular object.

SUBROUTINE DCUBE

This subroutine builds cubes of dielectric material by defining four each of IDONE, IDTWO and IDTHRE components corresponding to one spatial cube of dielectric material. It can

also be used to define thin (i.e. up to one cell thick) dielectric or perfectly conducting plates. Refer to comments within DCUBE for a description of the arguments and usage of the subroutine.

SUBROUTINE SETUP *

This subroutine initializes many of the constants required for incident field definition, field update equations, outer radiation boundary conditions and material parameters. The material parameters ϵ and σ are defined for each material type using the material arrays EPS and SIGMA respectively. The array EPS is used for the total permittivity and SIGMA is used for the electric conductivity. These arrays are initialized in SETUP to free space material parameters for all material types and then the user is required to modify these arrays for his/her scattering materials. Thus, for the lossy dielectric material type 2, the user must define EPS(2) and SIGMA(2). The remainder of the subroutine computes constants used in field update equations and boundary conditions and writes the diagnostics file.

SUBROUTINE EXSFLD

This subroutine updates all x components of scattered electric field at each time step except those on the outer boundaries of the problem space. IF statements based upon the IDONE array are used to determine the type of material present and the corresponding update equation to be used. These scattered field equations are based upon the development given in [4].

SUBROUTINE EYSFLD

This subroutine updates all y components of scattered electric field at each time step except those on the outer boundaries of the problem space. IF statements based upon the IDTWO array are used to determine the type of material present and the corresponding update equation to be used.

SUBROUTINE EZSFLD

This subroutine updates all z components of scattered electric field at each time step except those on the outer boundaries of the problem space. IF statements based upon the IDTHRE array are used to determine the type of material present and the corresponding update equation to be used.

SUBROUTINES RADEYX, RADEZX, RADEZY, RADEXY, RADEXZ and RADEYZ

These subroutines apply the outer radiation boundary conditions to the scattered electric field on the outer

boundaries of the problem space.

SUBROUTINE HXSFLD

This subroutine updates all x components of scattered magnetic field at each time step. The standard non-magnetic update equation is used.

SUBROUTINE HYSFLD

This subroutine updates all y components of scattered magnetic field at each time step. The standard non-magnetic update equation is used.

SUBROUTINE HZSFLD

This subroutine updates all z components of scattered magnetic field at each time step. The standard non-magnetic update equation is used.

SUBROUTINE DATSAV *

This subroutine samples near zone scattered field quantities and saves them to disk. This subroutine is where the quantities to be sampled and their spatial locations are to be specified and is only called if near zone fields only are desired or if both near and far zone fields are desired. Total field quantities can also be sampled. See comments within the subroutine for specifying sampled scattered and/or total field quantities. When sampling magnetic fields, remember the $\delta t/2$ time difference between E and H when writing the fields to disk. Sections of code within this subroutine determine if the sampled quantities and the spatial locations have been properly defined.

FUNCTIONS EXI, EYI and EZI

These functions are called to compute the x, y and z components of incident electric field. The functional form of the incident field is contained in a separate function SOURCE.

FUNCTION SOURCE *

This function contains the functional form of the incident field. The code as furnished uses the Gaussian form of the incident field. An incident smooth cosine pulse is also available by uncommenting the required lines and commenting out the Gaussian pulse. Thus, this function need only be modified if the user changes the incident pulse from Gaussian to smooth cosine. A slight improvement in computing speed and vectorization may be achieved by moving this function inside each of the incident field functions EXI, EYI and so on.

FUNCTIONS DEXI, DEYI and DEZI

These functions are called to compute the x, y and z components of the time derivative of incident electric field. The functional form of the incident field is contained in a separate function DSRCE.

FUNCTION DSRCE *

This function contains the functional form of the time derivative of the incident field. The code as furnished uses the time derivative of the Gaussian form of the incident field. A smooth cosine pulse time derivative is also available by uncommenting the required lines and commenting out the Gaussian pulse. Thus, the function need only be modified if the user changes from the Gaussian to smooth cosine pulse. Again, a slight improvement in computing speed and vectorization may be achieved by moving this function inside each of the time derivative incident field functions DEXI, DEYI and so on.

SUBROUTINE ZERO

This subroutine initializes various arrays and variables to zero.

VIII. INCLUDE FILE DESCRIPTION (COMMONA.FOR) *

The include file, COMMONA.FOR, contains all of the arrays and variables that are shared among the different subroutines. This file will require the most modifications when defining scattering problems. A description of the parameters that are normally modified follows.

The parameters NX, NY and NZ specify the size of the problem space in cells in the x, y and z directions respectively. For problems where it is crucial to center the object within the problem space, then NX, NY and NZ should be odd. The parameter NTEST defines the number of near zone quantities to be sampled and NZFZ defines the field output format. Set NZFZ=0 for near zone fields only, NZFZ=1 for far zone fields only and NZFZ=2 for both near and far zone fields. Parameter NSTOP defines the maximum number of time steps. DELX, DELY, and DELZ (in meters) define the cell size in the x, y and z directions respectively. The θ and ϕ incidence angles (in degrees) are defined by THINC and PHINC respectively and the polarization is defined by ETHINC and EPHINC. ETHINC=1.0, EPHINC=0.0 for θ-polarized incident field and ETHINC=0.0, EPHINC=1.0 for ϕ-polarized incident fields. Parameters AMP and BETA define the maximum amplitude and the e^{-2} temporal width of the incident pulse respectively. BETA automatically adjusts when the cell size is changed and normally should not be changed by the user. The far zone scattering angles are defined by THETFZ and PHIFZ. The code as furnished

performs backscatter computations, but these parameters could be modified for a bistatic computation.

IX. RCS COMPUTATIONS

A companion code, RCS3D.FOR, has been included to compute RCS versus frequency. It uses the file name of the FDTD far zone output data (FZOUT3D.DAT) and writes a data file of far zone electric fields versus time (FZTIME.DAT) and RCS versus frequency (3DRCS.DAT). The RCS computations are performed up to the 10 cell/λ_0 frequency limit. Refer to comments within this code for further details.

X. RESULTS

As previously mentioned, the code as furnished models an infinitely thin, 29 cm square, perfectly conducting plate and computes backscatter far zone scattered fields at angles of θ=45 and ϕ=30 degrees.

Figures 2-3 shows the co-polarized far zone electric field versus time and the co-polarized RCS for the 29 cm square perfectly conducting plate.

Figures 4-5 shows the cross-polarized far zone electric field versus time and the cross-polarized RCS for the 29 cm square perfectly conducting plate.

XI. SAMPLE PROBLEM SETUP

The code as furnished models an infinitely thin, 29 cm square, perfectly conducting plate and computes backscatter far zone scattered fields at angles of θ=45 and ϕ=30 degrees. The corresponding output data files are also provided, along with a code to compute RCS using these data files. In order to change the code to a new problem, many different parameters need to be modified. A sample problem setup will now be discussed.

Suppose that the problem to be studied is RCS backscatter versus frequency from a 28 cm by 31 cm perfectly conducting plate with a 3 cm dielectric coating with a dielectric constant of $4\epsilon_0$ using a θ-polarized field. The backscatter angles are θ=30.0 and ϕ=60.0 degrees and the frequency range is up to 3 Ghz.

Since the frequency range is up to 3 Ghz, the cell size must be chosen appropriately to resolve the field IN ANY MATERIAL at the highest frequency of interest. A general rule is that the cell size should be 1/10 of the wavelength at the highest frequency of interest. For difficult geometries, 1/20 of a wavelength may be necessary. The free space wavelength at 3 GHz is λ_0=10 cm and the wavelength in the dielectric coating at 3 GHz is 5 cm. The cell size is chosen as 1 cm, which provides a

resolution of 5 cells/λ in the dielectric coating and 10 cells/λ_0 in free space. Numerical studies have shown that choosing the cell size $\leq$ 1/4 of the shortest wavelength in any material is the practical lower limit. Thus the cell size of 1 cm is barely adequate. The cell size in the x, y and z directions is set in the common file through variables DELX, DELY and DELZ. Next the problem space size must be large enough to accomodate the scattering object, plus at least a five cell boundary (10 cells is more appropriate) on every side of the object to allow for the far zone field integration surface. It is advisable for plate scattering to have the plate centered in the x and y directions of the problem space in order to reduce the cross-polarized backscatter and to position the plate low in the z direction to allow strong specular reflections multiple encounters with the ORBC. A 10 cell border is chosen, and the problem space size is chosen as 49 by 52 by 49 cells in the x, y and z directions respectively. As an initial estimate, allow 2048 time steps so that energy trapped within the dielectric layer will radiate. Thus parameters NX, NY and NZ in COMMONA.FOR would be changed to reflect the new problem space size, and parameter NSTOP is changed to 2048. If all transients have not been dissipated after 2048 time steps, then NSTOP will have to be increased. Truncating the time record before all transients have dissipated will corrupt frequency domain results. Parameter NZFZ must be equal to 1 since we are interested in far zone fields only. To build the object, the following lines are inserted into the BUILD subroutine:

```
C
C     BUILD THE DIELECTRIC SLAB FIRST
C
      ISTART=11
      JSTART=11
      KSTART=11
      NXWIDE=28
      NYWIDE=31
      NZWIDE=3
      MTYPE=2
      CALL DCUBE(ISTART,JSTART,KSTART,NXWIDE,NYWIDE,NZWIDE,MTYPE)
C
C     BUILD PEC PLATE NEXT
C
      ISTART=11
      JSTART=11
      KSTART=11
      NXWIDE=28
      NYWIDE=31
      NZWIDE=0
      MTYPE=1
      CALL DCUBE(ISTART,JSTART,KSTART,NXWIDE,NYWIDE,NZWIDE,MTYPE)
```

The PEC plate is built last on the bottom of the dielectric slab to avoid any air gaps between the dielectric material and the PEC plate. In the common file, the incidence angles THINC and PHINC have to be changed to 30.0 and 60.0 respectively, the cell sizes (DELX, DELY, DELZ) are set to 0.01, and the polarization is set to ETHINC=1.0 and EPHINC=0.0 for θ-polarized fields. Since dielectric material 2 is being used for the dielectric coating, the constitutive parameters EPS(2) and SIGMA(2) are set to $4\epsilon_0$ and 0.0 respectively, in subroutine SETUP. This completes the code modifications for the sample problem.

XII. NEW PROBLEM CHECKLIST

This checklist provides a quick reference to determine if all parameters have been defined properly for a given scattering problem. A reminder when defining quantities within the code: use MKS units and specify all angles in degrees.

COMMONA.FOR:

1) Is the problem space sized correctly? (NX, NY, NZ)

2) For near zone fields, is the number of sample points correct? (NTEST)

3) Is parameter NZFZ defined correctly for desired field outputs?

4) Is the number of time steps correct? (NSTOP)

5) Are the cell dimensions (DELX, DELY, DELZ) defined correctly?

6) Are the incidence angles (THINC, PHINC) defined correctly?

7) Is the polarization of the incident wave defined correctly (ETHINC, EPHINC)?

8) For other than backscatter far zone field computations, are the scattering angles set correctly? (THETFZ, PHIFZ)

SUBROUTINE BUILD:

1) Is the object completely and correctly specified?

SUBROUTINE SETUP:

1) Are the constitutive parameters for each material specified correctly? (EPS and SIGMA)

FUNCTIONS SOURCE and DSRCE:

1) If the Gaussian pulse is not desired, is it commented out and the smooth cosine pulse uncommented?

SUBROUTINE DATSAV:

1) For near zone fields, are the sampled field types and spatial locations correct for each sampling point? (NTYPE, IOBS, JOBS, KOBS)

XIII. REFERENCES

[1] K. S. Yee, "Numerical solution of initial boundary value problems involving Maxwell's equations in isotropic media," IEEE Trans. Antennas Propagat., vol. AP-14, pp. 302-307, May 1966.

[2] G. Mur, "Absorbing boundary conditions for the Finite-Difference approximation of the Time-Domain Electromagnetic-Field Equations," IEEE Trans. Electromagn. Compat., vol. EMC-23, pp. 377-382, November 1981.

[3] R.J. Luebbers et. al., "A Finite Difference Time-Domain Near Zone to Far Zone Transformation," IEEE Trans. Antennas Propagat., vol. AP-39, no. 4, pp. 429-433, April 1991.

[4] R. Holland, L. Simpson and K. S. Kunz, "Finite-Difference Time-Domain Analysis of EMP Coupling to Lossy Dielectric Structures," IEEE Trans. Electromagn. Compat., vol. EMC-22, pp. 203-209, August 1980.

XIV. FIGURE TITLES

Fig. 1 Standard three dimensional Yee cell showing placement of electric and magnetic fields.

Fig. 2 Co-polarized far zone scattered field versus time for 29 cm square perfectly conducting plate.

Fig. 3 Co-polarized RCS versus frequency for 29 cm square perfectly conducting plate.

Fig. 4 Cross-polarized far zone scattered field versus time for 29 cm square perfectly conducting plate.

Fig. 5 Cross-polarized RCS versus frequency for 29 cm square perfectly conducting plate.

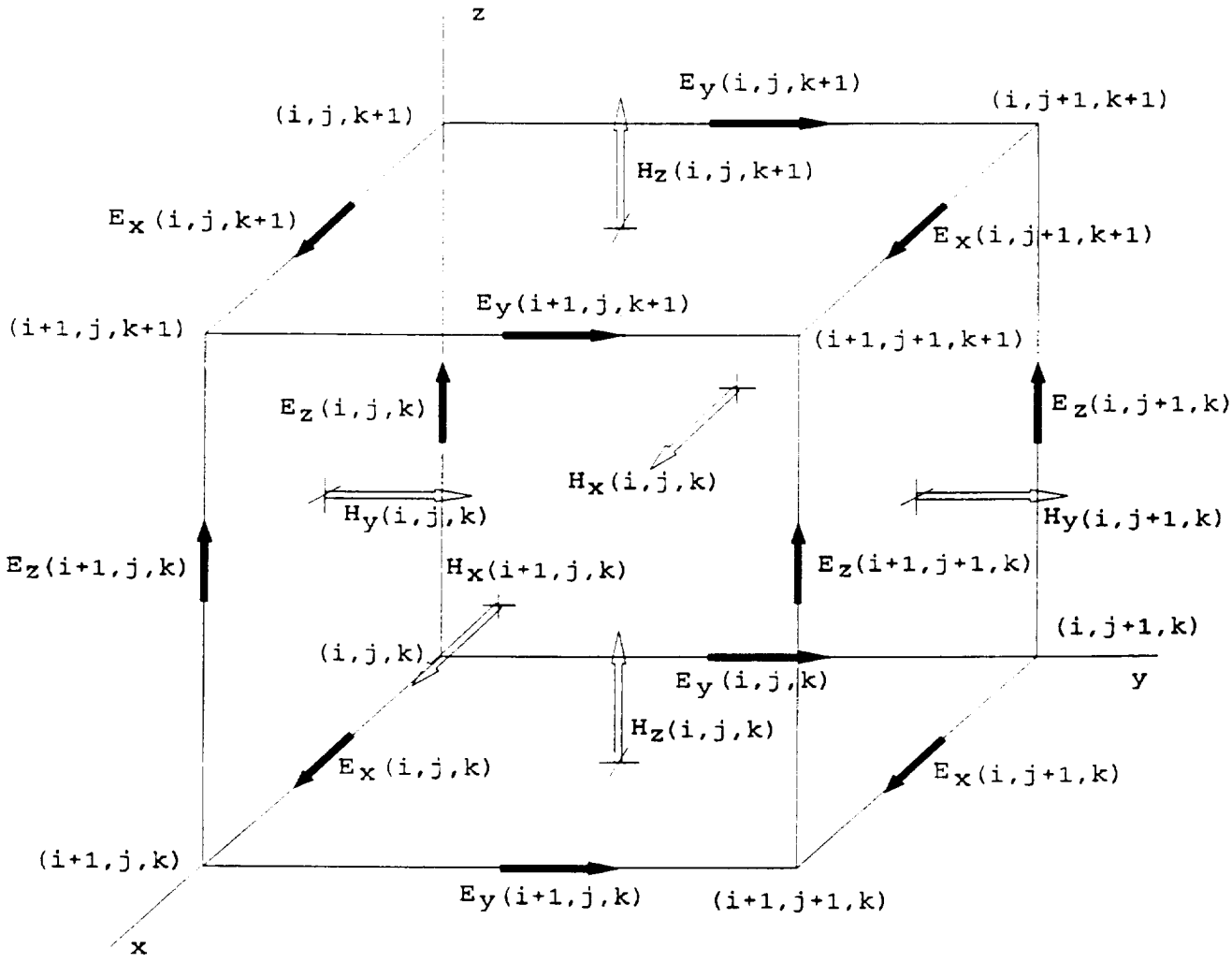
z
Ey(i,j,k+1)
(i,j,k+1)
(i,j+1,k+1)
Hz(i,j,k+1)
Ex(i,j,k+1)
Ex(i,j+1,k+1)
Ey(i+1,j,k+1)
(i+1,j,k+1)
(i+1,j+1,k+1)
Ez(i,j,k)
Ez(i,j+1,k)
Hx(i,j,k)
Hy(i,j,k)
Hy(i,j+1,k)
Ez(i+1,j,k)
Hx(i+1,j,k)
Ez(i+1,j+1,k)
(i,j+1,k)
(i,j,k)
Ey(i,j,k)
y
Hz(i,j,k)
Ex(i,j,k)
Ex(i,j+1,k)
(i+1,j,k)
Ey(i+1,j,k)
(i+1,j+1,k)
x

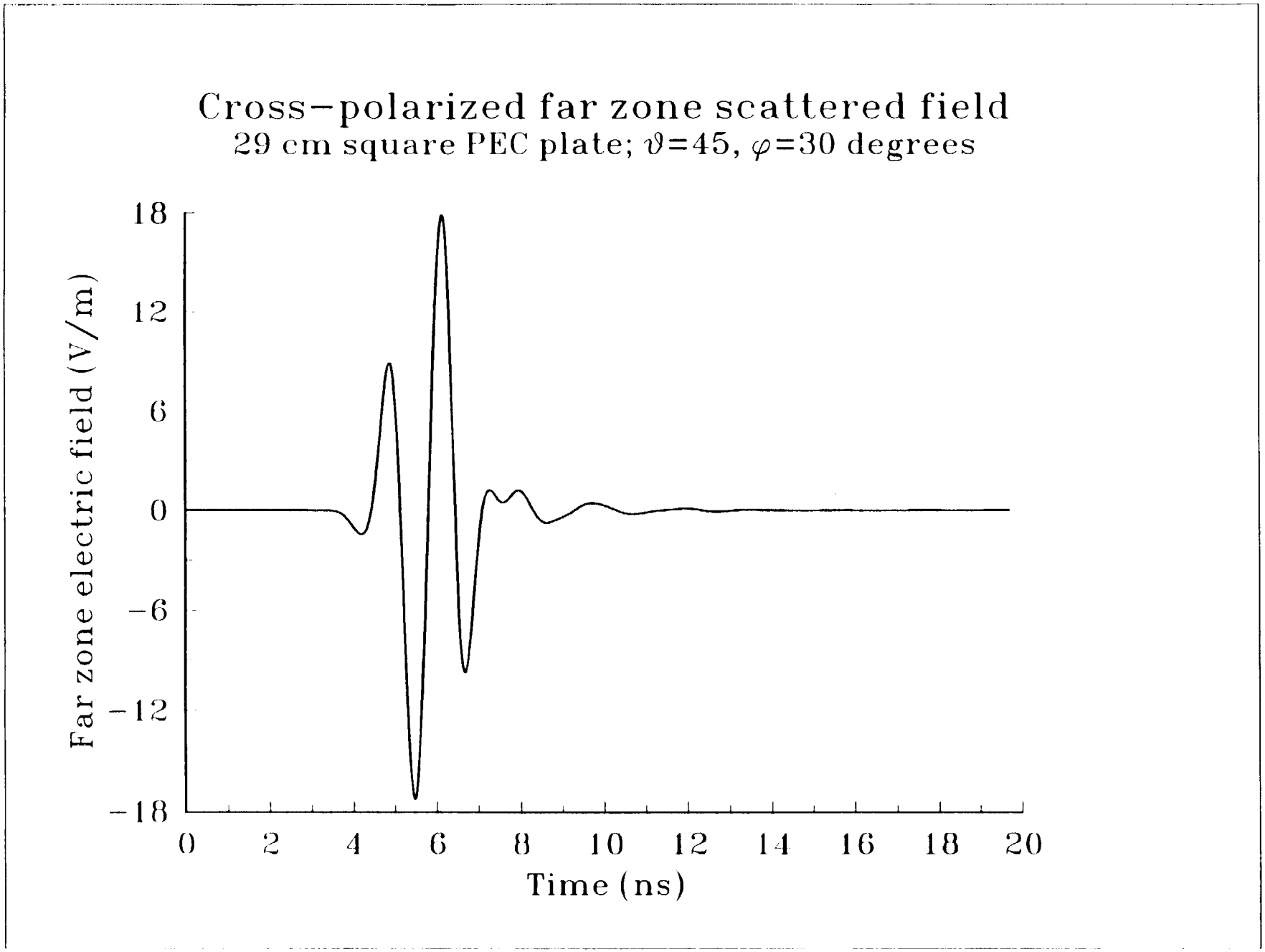
Cross-polarized far zone scattered field
29 cm square PEC plate; ϑ=45, φ=30 degrees
Far zone electric field (V/m)
18
12
6
0
-6
-12
-18
0
2
4
6
8
10
12
14
16
18
20
Time (ns)

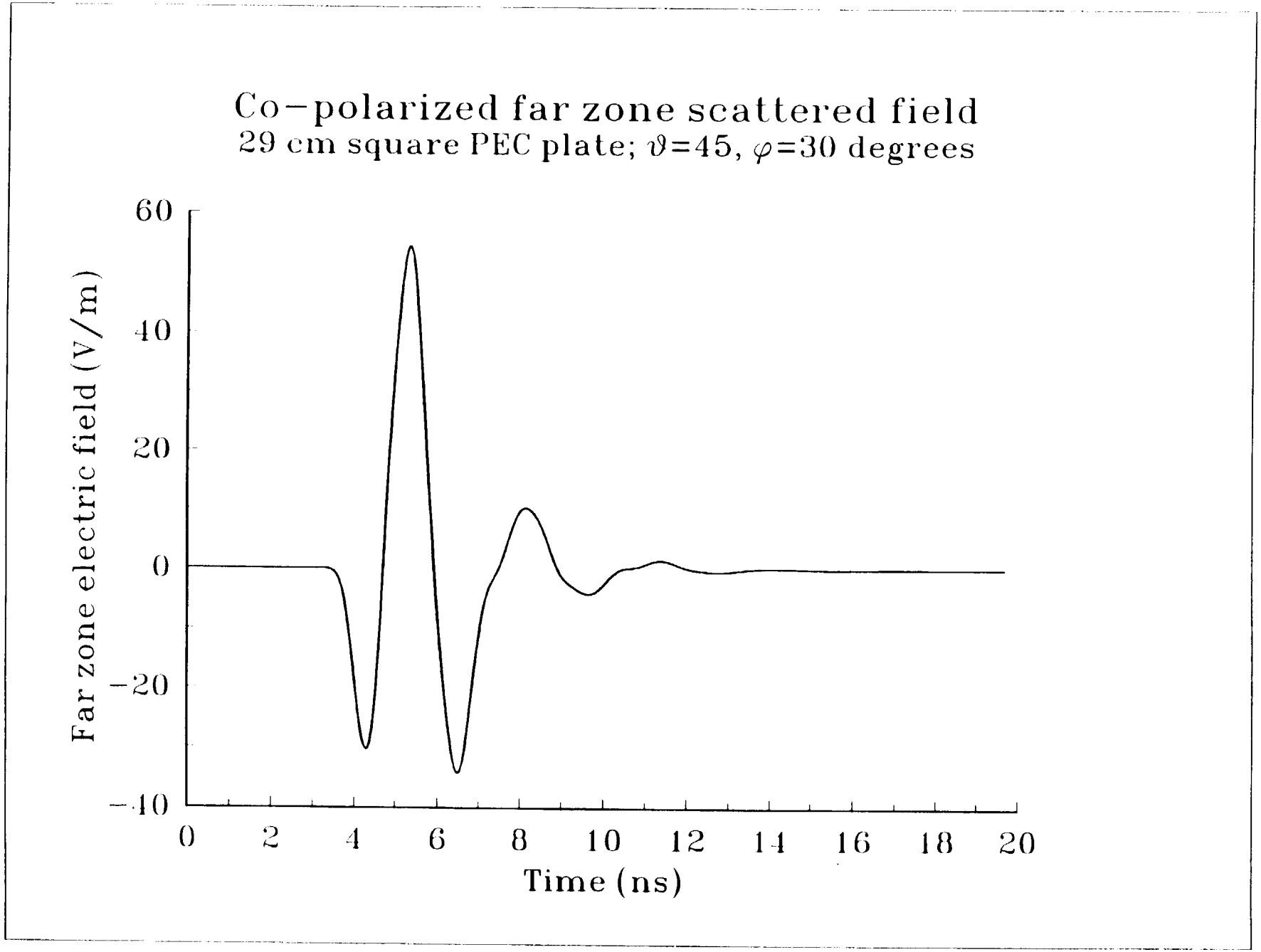
Co−polarized far zone scattered field
29 cm square PEC plate; ϑ=45, φ=30 degrees
Far zone electric field (V/m)
60
40
20
0
−20
−10
0
2
4
6
8
10
12
14
16
18
20
Time (ns)

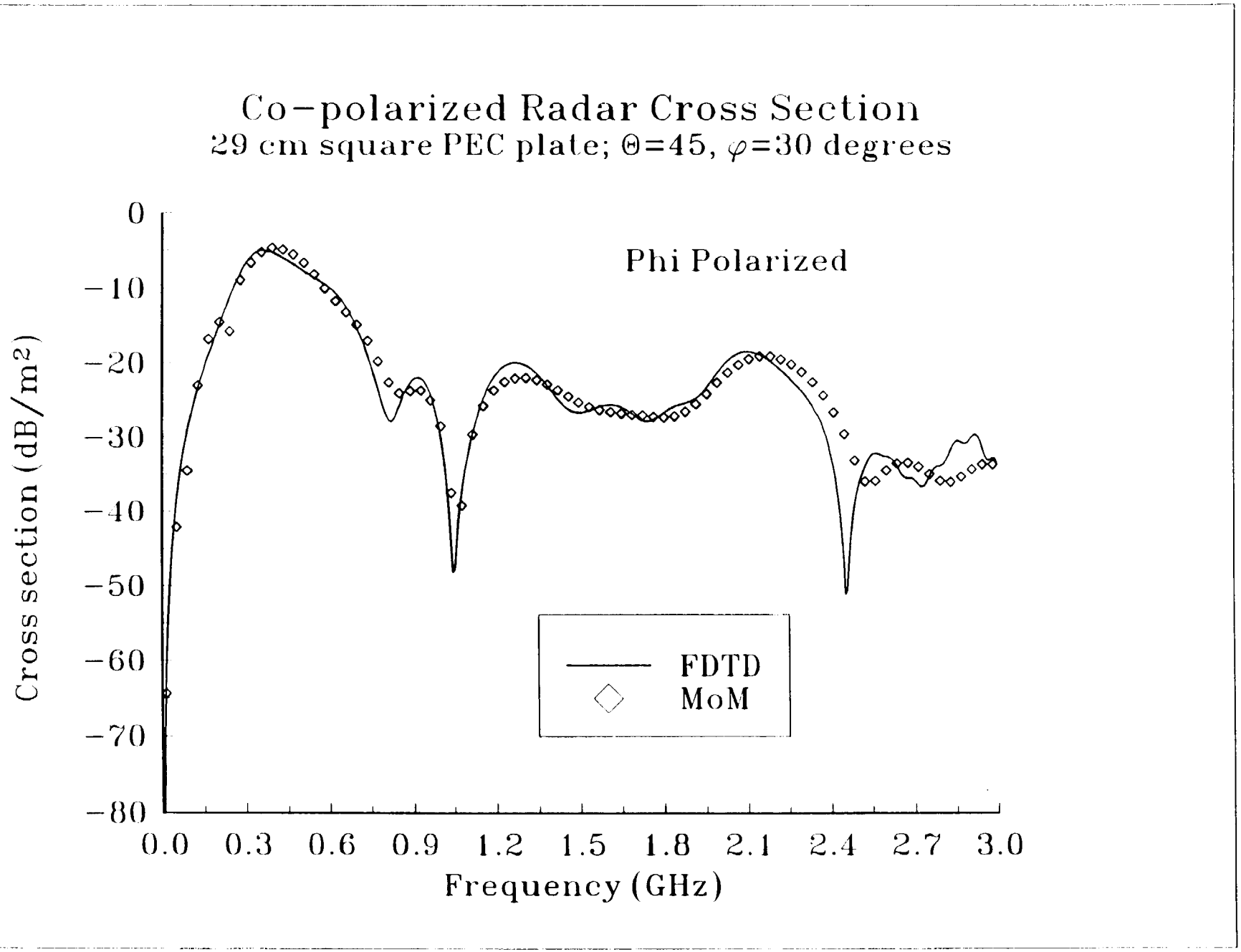
Co-polarized Radar Cross Section
29 cm square PEC plate; Θ=45, φ=30 degrees
Phi Polarized
Cross section (dB/m²)
0
-10
-20
-30
-40
-50
-60
-70
-80
0.0
0.3
0.6
0.9
1.2
1.5
1.8
2.1
2.4
2.7
3.0
Frequency (GHz)
FDTD
MoM

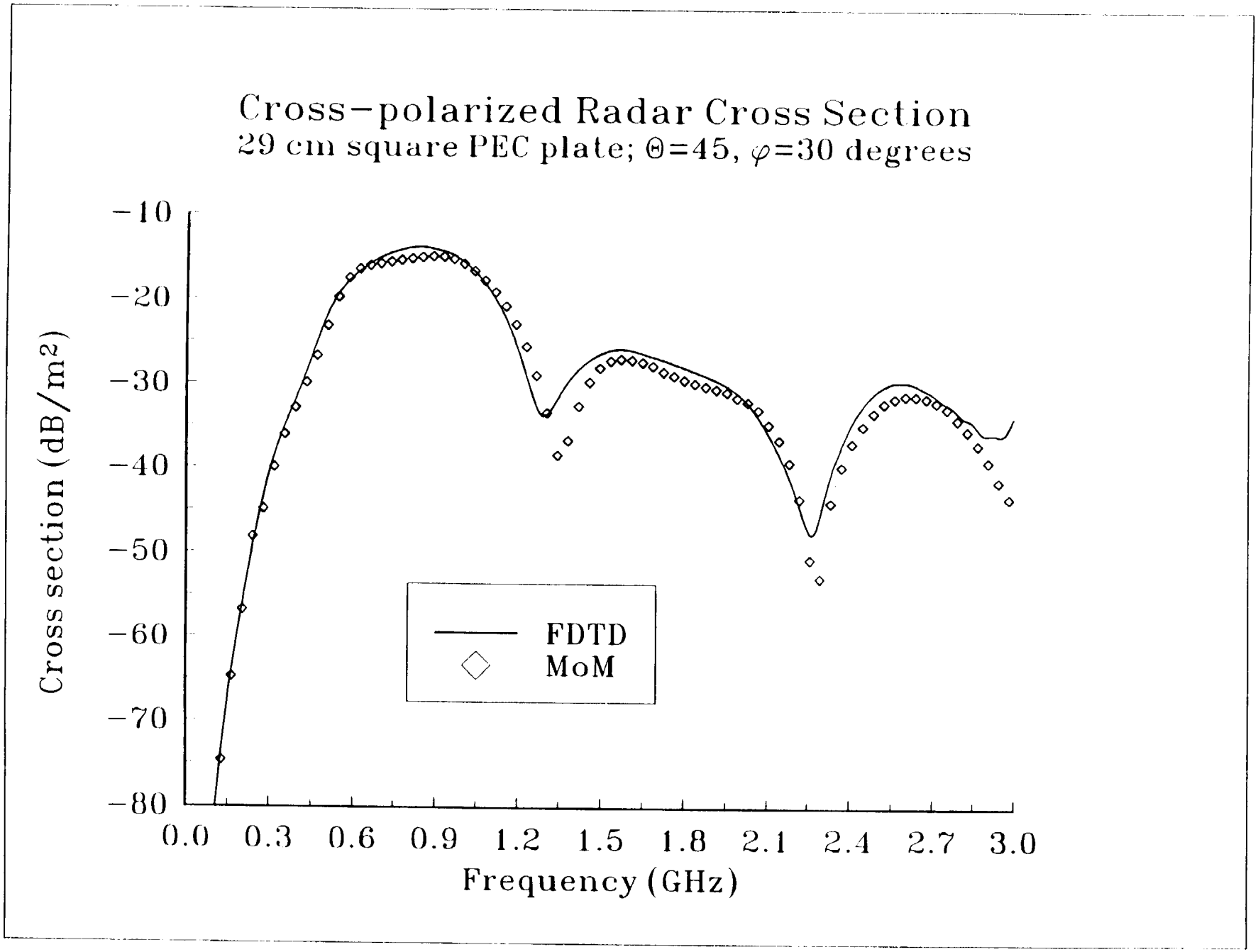
Cross-polarized Radar Cross Section
29 cm square PEC plate; Θ=45, φ=30 degrees
Cross section (dB/m²)
-10
-20
-30
-40
-50
-60
-70
-80
0.0
0.3
0.6
0.9
1.2
1.5
1.8
2.1
2.4
2.7
3.0
Frequency (GHz)
FDTD
MoM

USER'S MANUAL FOR

THREE DIMENSIONAL FDTD

VERSION B CODE FOR SCATTERING

FROM FREQUENCY-DEPENDENT DIELECTRIC MATERIALS

by

John H. Beggs, Raymond J. Luebbers and Karl S. Kunz
Electrical and Computer Engineering Department
The Pennsylvania State University
University Park, PA 16802

(814) 865-2362

January 1992

TABLE OF CONTENTS

TABLE OF CONTENTS (cont.)

I. INTRODUCTION

The Penn State Finite Difference Time Domain Electromagnetic Scattering Code Version B is a three dimensional numerical electromagnetic scattering code based upon the Finite Difference Time Domain Technique (FDTD). The supplied version of the code is one version of our current three dimensional FDTD code set. This manual provides a description of the code and corresponding results for several scattering problems. The manual is organized into fourteen sections: introduction, description of the FDTD method, operation, resource requirements, Version B code capabilities, a brief description of the default scattering geometry, a brief description of each subroutine, a description of the include file (COMMONB.FOR), a section briefly discussing Radar Cross Section (RCS) computations, a section discussing some scattering results, a sample problem setup section, a new problem checklist, references and figure titles.

II. FDTD METHOD

The Finite Difference Time Domain (FDTD) technique models transient electromagnetic scattering and interactions with objects of arbitrary shape and/or material composition. The technique was first proposed by Yee [1] for isotropic, non-dispersive materials in 1966; and has matured within the past twenty years into a robust and efficient computational method. The present FDTD technique is capabable of transient electromagnetic interactions with objects of arbitrary and complicated geometrical shape and material composition over a large band of frequencies. This technique has recently been extended to include dispersive dielectric materials, chiral materials and plasmas.

In the FDTD method, Maxwell's curl equations are discretized in time and space and all derivatives (temporal and spatial) are approximated by central differences. The electric and magnetic fields are interleaved in space and time and are updated in a second-order accurate leapfrog scheme. The computational space is divided into cells with the electric fields located on the edges and the magnetic fields on the faces (see Figure 1). FDTD objects are defined by specifying dielectric and/or magnetic material parameters at electric and/or magnetic field locations.

Two basic implementations of the FDTD method are widely used for electromagnetic analysis: total field formalism and scattered field formalism. In the total field formalism, the electric and magnetic field are updated based upon the material type present at each spatial location. In the scattered field formalism, the incident waveform is defined analytically and the scattered field is coupled to the incident field through the different material types. For the incident field, any waveform, angle of incidence and polarization is possible. The separation of the incident and

scattered fields conveniently allows an absorbing boundary to be employed at the extremities of the discretized problem space to absorb the scattered fields.

This code is a scattered field code, and the total E and H fields may be found by combining the incident and scattered fields. Any type of field quantity (incident, scattered, or total), Poynting vector or current are available anywhere within the computational space. These fields, incident, scattered and total, may be found within, on or about the interaction object placed in the problem space. By using a near to far field transformation, far fields can be determined from the near fields within the problem space thereby affording radiation patterns and RCS values. The accuracy of these calculations is typically within a dB of analytic solutions for dielectric and magnetic sphere scattering. Further improvements are expected as better absorbing boundary conditions are developed and incorporated.

III. OPERATION

Typically, a truncated Gaussian incident waveform is used to excite the system being modeled, however certain code versions also provide a smooth cosine waveform for convenience in modeling dispersive materials. The interaction object is defined in the discretized problem space with arrays at each cell location created by the discretization. All three dielectric material types for E field components within a cell can be individually specified by the arrays IDONE(I,J,K), IDTWO(I,J,K), IDTHRE(I,J,K). This models arbitrary dielectric materials with $\mu = \mu_0$. By an obvious extension to six arrays, magnetic materials with $\mu \neq \mu_0$ can be modeled.

Scattering occurs when the incident wave, marched forward in time in small steps set by the Courant stability condition, reaches the interaction object. Here a scattered wave must appear along with the incident wave so that the Maxwell equations are satisfied. If the material is a perfectly conductive metal then only the well known boundary condition

$$E_{tan}^{scat} = -E_{tan}^{inc} \tag{1}$$

must be satisfied. For a nondispersive dielectric the requirement is that the total field must satisfy the Maxwell equations in the material:

$$\nabla \times E^{tot} = \nabla \times (E^{inc} + E^{scat}) = -\frac{1}{\mu_o}\frac{\partial H^{tot}}{\partial t} = -\frac{1}{\mu_o}\frac{\partial (H^{inc} + H^{scat})}{\partial t} \tag{2}$$

$$\nabla \times H^{tot} = \nabla \times (H^{inc} + H^{scat}) = \varepsilon \frac{\partial E^{tot}}{\partial t} + \sigma E^{tot} \tag{3}$$

$$= \varepsilon \frac{\partial (E^{inc} + E^{scat})}{\partial t} + \sigma (E^{inc} + E^{scat}) \tag{4}$$

Additionally the incident wave, defined as moving unimpeded through a vacuum in the problem space, satisfies everywhere in the problem the Maxwell equations for free space

$$\nabla \times E^{inc} = -\frac{1}{\mu_o} \frac{\partial H^{inc}}{\partial t} \tag{5}$$

$$\nabla \times H^{inc} = \varepsilon_o \frac{\partial E^{inc}}{\partial t} \tag{6}$$

Subtracting the second set of equations from the first yields the Maxwell equations governing the scattered fields in the material:

$$\nabla \times E^{scat} = -\frac{1}{\mu_o} \frac{\partial H^{scat}}{\partial t} \tag{7}$$

$$\nabla \times H^{scat} = (\varepsilon - \varepsilon_o) \frac{\partial E^{inc}}{\partial t} + \sigma E^{inc} + \varepsilon \frac{\partial E^{scat}}{\partial t} + \sigma E^{scat} \tag{8}$$

Outside the material this simplifies to:

$$\nabla \times E^{scat} = -\frac{1}{\mu_o} \frac{\partial H^{scat}}{\partial t} \tag{9}$$

$$\nabla \times H^{scat} = \varepsilon_o \frac{\partial E^{scat}}{\partial t} \tag{10}$$

Magnetic materials, dispersive effects, non-linearities, etc., are further generalizations of the above approach. Based on the value of the material type, the subroutines for calculating scattered E and H field components branch to the appropriate expression for that scattered field component and

that component is advanced in time according to the selected algorithm. As many materials can be modeled as desired, the number equals the dimension selected for the flags. If materials with behavior different from those described above must be modeled, then after the appropriate algorithm is found, the code's branching structure allows easy incorporation of the new behavior.

IV. RESOURCE REQUIREMENTS

The number of cells the problem space is divided into times the six components per cell set the problem space storage requirements

$$\text{Storage} = NC \times 6 \text{ components/cell} \times 4 \text{ bytes/component} \tag{11}$$

and the computational cost

$$\text{Operations} = NC \times 6 \text{ comp/cell} \times 10 \text{ ops/component} \times N \tag{12}$$

where N is the number of time steps desired.

N typically is on the order of ten times the number of cells on one side of the problem space. More precisely for cubical cells it takes $\sqrt{3}$ time steps to traverse a single cell when the time step is set by the Courant stability condition

$$\Delta t = \frac{\Delta x}{\sqrt{3}c} \qquad \Delta x = \text{cell size dimension} \tag{13}$$

The condition on N is then that

$$N \approx 10 \times (\sqrt{3} NC^{\frac{1}{3}}) \qquad NC^{\frac{1}{3}} \sim \text{number cells on a side of the problem space} \tag{14}$$

The earliest aircraft modeling using FDTD with approximately 30 cells on a side required approximately 500 time steps. For more recent modeling with approximately 100 cells on a side, 2000 or more time steps are used.

For $(100 \text{ cell})^3$ problem spaces, 24 MBytes of memory are required to store the fields. Problems on the order of this size have been run on a Silicon Graphics 4D 220 with 32 MBytes of memory, IBM RISC 6000, an Intel 486 based machine, and VAX 11/785. Storage is only a problem as in the case of the 486 where only 16 MBytes of memory was available. This limited the problem space size to approximately $(80 \text{ cells})^3$.

For $(100 \text{ cell})^3$ problems with approximately 2000 time steps, there is a total of 120×10^9 operations to perform. The speeds of the previously mentioned machines are 24 MFLOPs (4 processor upgraded version), 10 MFLOPS, 1.5 MFLOPS, and 0.2 MFLOPs. The run times are then 5×10^3 seconds, 12×10^3 seconds, 80×10^3 seconds and 600×10^3 seconds, respectively. In hours the times are 1.4, 3.3, 22.2 and 167 hours. Problems of this size are possible on all but the last machine and can in fact be performed on a personal computer (486) if one day turnarounds are permissible.

V. VERSION B CODE CAPABILITIES

The Penn State University FDTD Electromagnetic Scattering Code Version B has the following capabilities:

1) Ability to model lossy dielectric and perfectly conducting scatterers.

2) Ability to model dispersive dielectric scatterers. This dispersive FDTD method is now designated $(FD)^2TD$ for Frequency-Dependent Finite Difference Time Domain.

3) First and second order outer radiation boundary condition (ORBC) operating on the electric fields.

4) Near to far zone transformation capability to obtain far zone scattered fields.

5) Gaussian and smooth cosine incident waveforms with arbitrary incidence angles.

6) Near zone field, current or power sampling capability.

7) Companion code for computing Radar Cross Section (RCS).

VI. DEFAULT SCATTERING GEOMETRY

The code as delivered is set up to calculate the far zone backscatter fields for a 20 cm radius, dispersive, 0.25 dB dielectric foam sphere. The 0.25 dB loaded foam is defined by a frequency dependent permittivity with an effective DC conductivity given by

$$\frac{\epsilon(\omega)}{\epsilon_0} = \epsilon_\infty + \frac{\epsilon_s - \epsilon_\infty}{1 + j\omega\tau_0} + \frac{\sigma}{j\omega\epsilon_0} \tag{15}$$

where ϵ_∞ is the infinite frequency permittivity, ϵ_s is the zero frequency permittivity, τ_0 is the relaxation time and ω is the

radian frequency. The 0.25 dB loaded foam parameters are ϵ_∞=1.06, ϵ_s=1.16, τ_0=0.6497 ns and σ=2.954e-4. The problem space size is 65 by 65 by 65 cells in the x, y and z directions, the cells are 1 cm cubes, and the incident waveform is a ϕ-polarized smooth cosine pulse with incidence angles of θ=22.5 and ϕ=22.5 degrees. The output data files are included as a reference along with a code (RCS3D.FOR) for computing the frequency domain RCS using these output data files. The ORBC is the second order absorbing boundary condition set forth by Mur [2].

VII. SUBROUTINE DESCRIPTION

In the description for each subroutine, an asterisk (*) will be placed by the subroutine name if that particular subroutine is normally modified when defining a scattering problem.

MAIN ROUTINE

The main routine in the program contains the calls for all necessary subroutines to initialize the problem space and scattering object(s) and for the incident waveform, far zone transformation, field update subroutines, outer radiation boundary conditions and field sampling.

The main routine begins with the include statement and then appropriate data files are opened, and subroutines ZERO, BUILD and SETUP are called to initialize variables and/or arrays, build the object(s) and initialize the incident waveform and miscellaneous parameters, respectively. Subroutine SETFZ is called to intialize parameters for the near to far zone transformation if far zone fields are desired.

The main loop is entered next, where all of the primary field computations and data saving takes place. During each time step cycle, the EXSFLD, EYSFLD, and EZSFLD subroutines are called to update the x, y, and z components of the scattered electric field. The six electric field outer radiation boundary conditions (RADE??) are called next to absorb any outgoing scattered fields. Time is then advanced 1/2 time step according to the Yee algorithm and then the HXSFLD, HYSFLD, AND HZSFLD subroutines are called to update the x, y, and z components of scattered magnetic field. Time is then advanced another 1/2 step and then either near zone fields are sampled and written to disk in DATSAV, and/or the near zone to far zone vector potentials are updated in SAVFZ. The parameter NZFZ (described later) in the common file defines the type of output fields desired.

After execution of all time steps in the main field update loop, subroutine FAROUT is called if far zone fields are desired to compute the far zone fields and write them to disk. At this point, the execution is complete.

SUBROUTINE SETFZ

This subroutine initializes the necessary parameters required for far zone field computations. The code as furnished computes backscatter far zone fields and can compute bistatic far zone fields for one scattering angle (i.e. one θ and ϕ angle). Refer to reference [3] for a complete description of the near to far zone transformation. Other versions of this subroutine provide for multiple bistatic angles.

SUBROUTINE SAVFZ

This subroutine updates the near zone to far zone vector potentials.

SUBROUTINE FAROUT

This subroutine changes the near zone to far zone vector potentials to far zone electric field θ and ϕ components and writes them to disk.

SUBROUTINE BUILD *

This subroutine "builds" the scattering object(s) by initializing the IDONE, IDTWO, and IDTHRE arrays to specify perfectly conducting, lossy dielectrics and dispersive dielectric materials. Refer to Figure 1 for a diagram of the basic Yee cell. Setting an element of the IDONE array at some I,J,K location is actually locating dielectric material at a cell edge whose center location is I+0.5,J,K. Thus, materials with diagonal permittivity tensors can be modeled. The default material type for all ID??? arrays is 0, or free space. By initializing these arrays to values other than 0, the user is defining an object by determining what material types are present at each spatial location. Other material types available for IDONE-IDTHRE are 1 for perfectly conducting objects, 2-9 for lossy non-magnetic dielectrics, 20-29 for dispersive dielectrics. This code assumes that <u>all</u> dielectric and dispersive dielectric materials have a permeability of μ_0. This subroutine also has a section that checks the ID??? arrays to determine if legal material types have been defined throughout the problem space. The actual non-dispersive material parameters (ϵ, μ, and σ) are defined in subroutine SETUP. The dispersive material parameters (ϵ_s, ϵ_∞, τ_0, σ) are also defined in a separate section in SETUP. The default geometry is a 20 cm radius, dispersive, 0.25 dB dielectric foam sphere.

The user must be careful that his/her object created in the BUILD subroutine is properly formed.

When it is important to place the object in the center of the problem space (to have lowest possible cross-pol scattering for symmetric objects), NX etc. should be odd. This is due to the field locations in the Yee cell and also the placement of the E field absorbing boundary condition surfaces.

If the object being modeled has curved surfaces, edges, etc. that are at an angle to one or more of the coordinate axes, then that shape must be approximately modeled by lines and faces in a "stair-stepped" (or stair-cased) fashion. This stair-cased approximation introduces errors into computations at higher frequencies. Intuitively, the error becomes smaller as more cells are used to stair-case a particular object. Thus, the default 0.25 dB dielectric foam sphere scattering geometry is a stair-cased sphere.

SUBROUTINE DCUBE

This subroutine builds cubes of dielectric material by defining four each of IDONE, IDTWO and IDTHRE components corresponding to one spatial cube of dielectric material. It can also be used to define thin (i.e. up to one cell thick) dielectric or perfectly conducting plates. Refer to comments within DCUBE for a description of the arguments and usage of the subroutine.

SUBROUTINE SETUP *

This subroutine initializes many of the constants required for incident field definition, field update equations, outer radiation boundary conditions and material parameters. The material parameters ϵ and σ are defined for each material type (non-dispersive) using the material arrays EPS and SIGMA respectively. The array EPS is used for the total permittivity, and SIGMA is used for the electric conductivity. These arrays are initialized in SETUP to free space material parameters for all material types and then the user is required to modify these arrays for his/her scattering materials. Thus, for the lossy dielectric material type 2, the user must define EPS(2) and SIGMA(2).

For dispersive dielectric materials, different material parameter arrays are used. The functional form of the frequency dependent permittivity that was implemented in the code is the Debye relaxation [4] with an effective DC conductivity given by

$$\epsilon(\omega) = \epsilon' - j\epsilon'' = \epsilon_\infty \epsilon_0 + \epsilon_0 \chi_e(\omega) + \frac{\sigma}{j\omega} \qquad (16)$$

where the frequency dependent electric susceptibility function is defined as

$$\chi_e(\omega) = \frac{\epsilon_s - \epsilon_\infty}{1 + j\omega\tau_0} \tag{17}$$

where ϵ_∞ is the infinite frequency permittivity, ϵ_s is the zero frequency permittivity, τ_0 is the relaxation time, σ is the effective electric conductivity, and ω is the radian frequency. The corresponding time domain susceptibility function is given by

$$\chi_e(t) = \left(\frac{\epsilon_s - \epsilon_\infty}{\tau_0}\right) e^{\left(-t/\tau_0\right)} u(t) \tag{18}$$

The FDTD implementation of frequency dependent permittivity involves a convolution with the electric field and interested readers are referred to references [5-6] for further details.

For dispersive dielectric materials, the corresponding material parameter arrays are EPSINF (ϵ_∞), EPSSTA (ϵ_s), RELAXT (τ_0), and RELSIG (σ). These dispersive material parameters are defined under the DISPERSIVE SETUP portion of the subroutine. The remainder of the subroutine computes constants used in field update equations and boundary conditions and writes the diagnostics file.

SUBROUTINE EXSFLD

This subroutine updates all x components of scattered electric field at each time step except those on the outer boundaries of the problem space. IF statements based upon the IDONE array are used to determine the type of material present and the corresponding update equation to be used. These scattered field equations are based upon the development given in [7].

SUBROUTINE EYSFLD

This subroutine updates all y components of scattered electric field at each time step except those on the outer boundaries of the problem space. IF statements based upon the IDTWO array are used to determine the type of material present and the corresponding update equation to be used.

SUBROUTINE EZSFLD

This subroutine updates all z components of scattered electric field at each time step except those on the outer boundaries of the problem space. IF statements based upon the IDTHRE array are used to determine the type of material present and the corresponding update equation to be used.

SUBROUTINES RADEYX, RADEZX, RADEZY, RADEXY, RADEXZ and RADEYZ

These subroutines apply the outer radiation boundary conditions to the scattered electric field on the outer boundaries of the problem space.

SUBROUTINE HXSFLD

This subroutine updates all x components of scattered magnetic field at each time step. The standard non-magnetic update equation is used.

SUBROUTINE HYSFLD

This subroutine updates all y components of scattered magnetic field at each time step. The standard non-magnetic update equation is used.

SUBROUTINE HZSFLD

This subroutine updates all z components of scattered magnetic field at each time step. The standard non-magnetic update equation is used.

SUBROUTINE DATSAV *

This subroutine samples near zone scattered field quantities and saves them to disk. This subroutine is where the quantities to be sampled and their spatial locations are to be specified and is only called if near zone fields only are desired or if both near and far zone fields are desired. Total field quantities can also be sampled. See comments within the subroutine for specifying sampled scattered and/or total field quantities. When sampling magnetic fields, remember the $\delta t/2$ time difference between E and H when writing the fields to disk. Sections of code within this subroutine determine if the sampled quantities and the spatial locations have been properly defined.

FUNCTIONS EXI, EYI and EZI

These functions are called to compute the x, y and z components of incident electric field. The functional form of the incident field is contained in a separate function SOURCE.

FUNCTION SOURCE *

This function contains the functional form of the incident field. The code as furnished uses the smooth cosine form of the incident field. An incident Gaussian pulse is also available by uncommenting the required lines and commenting out the smooth cosine pulse. Thus, this function need only be modified if the user changes the incident pulse from smooth cosine to Gaussian. Currently, only the smooth cosine pulse can be used for scattering from dispersive targets. A slight improvement in computing speed and vectorization may be achieved by moving this function inside each of the incident field functions EXI, EYI and so on.

FUNCTIONS DEXI, DEYI and DEZI

These functions are called to compute the x, y and z components of the time derivative of incident electric field. The functional form of the incident field is contained in a separate function DSRCE.

FUNCTIONS DEXIXE, DEYIXE and DEZIXE

These functions compute the x, y and z components of the convolution of the time derivative of the incident field with the electric Debye susceptibility function χ.

FUNCTION DSRCE *

This function contains the functional form of the time derivative of the incident field. The code as furnished uses the time derivative of the smooth cosine form of the incident field. A Gaussian pulse time derivative is also available by uncommenting the required lines and commenting out the smooth cosine pulse. Thus, the function need only be modified if the user changes from the smooth cosine to Gaussian pulse. Again, a slight improvement in computing speed and vectorization may be achieved by moving this function inside each of the time derivative incident field functions DEXI, DEYI and so on.

FUNCTION DCONV

This function evaluates the convolution of the time derivative of the incident field with the Debye susceptibility function χ.

SUBROUTINE ZERO

This subroutine initializes various arrays and variables to zero.

VIII. INCLUDE FILE DESCRIPTION (COMMONB.FOR) *

The include file, COMMONB.FOR, contains all of the arrays and variables that are shared among the different subroutines. This file will require the most modifications when defining scattering problems. A description of the parameters that are normally modified follows.

The parameters NX, NY and NZ specify the size of the problem space in cells in the x, y and z directions respectively. For problems where it is crucial to center the object within the problem space, then NX, NY and NZ should be odd. The parameter NTEST defines the number of near zone quantities to be sampled and NZFZ defines the field output format. Set NZFZ=0 for near zone fields only, NZFZ=1 for far zone fields only and NZFZ=2 for both near and far zone fields. Parameter NUMMAT defines the total number of material types that are available for use. NEDISP defines the number of dispersive dielectric materials that are being used. Parameter NSTOP defines the maximum number of time steps. DELX, DELY, and DELZ (in meters) define the cell size in the x, y and z directions respectively. The θ and ϕ incidence angles (in degrees) are defined by THINC and PHINC respectively and the polarization is defined by ETHINC and EPHINC. ETHINC=1.0, EPHINC=0.0 for θ-polarized incident field and ETHINC=0.0, EPHINC=1.0 for ϕ-polarized incident fields. Parameters AMP and BETA define the maximum amplitude and the e^{-2} temporal width of the incident pulse respectively. BETA automatically adjusts when the cell size is changed and normally should not be changed by the user. The far zone scattering angles are defined by THETFZ and PHIFZ. The code as furnished performs backscatter computations, but these parameters could be modified for a bistatic computation.

IX. RCS COMPUTATIONS

A companion code, RCS3D.FOR, has been included to compute RCS versus frequency. It uses the file name of the $(FD)^2TD$ far zone output data (FZOUT3D.DAT) and writes data files of far zone electric fields versus time (FZTIME.DAT) and RCS versus frequency (3DRCS.DAT). The RCS computations are performed up to the 10 cell/λ_0 frequency limit. Refer to comments within this code for further details.

X. RESULTS

As previously mentioned, the code as furnished models a 20 cm radius, dispersive, 0.25 dB dieletric foam sphere and computes backscatter far zone scattered fields at angles of θ=22.5 and ϕ=22.5 degrees. Results are included for the 0.25 dB dielectric foam sphere and for a 60 dB dielectric foam sphere. The material parameters for 0.25 dB and 60 dB loaded foam are:

0.25 DB FOAM		60 DB FOAM
1.16	ϵ_s	41.0
1.01	ϵ_∞	1.6
0.6497 ns	τ_0	0.3450 ns
2.954E-04 S/m	σ	3.902E-01 S/m

For the 0.25 dB foam there are 10 cells per wavelength at approximately 3.0 GHz. For the 60 dB foam there are 10 cells per wavelength at approximately 2.35 GHz, as the 60 dB foam has a higher dielectric constant.

Figures 2-7 show the real and imaginary parts of the 0.25 dB and 60 dB foam permeability and the dielectric susceptibilities versus time for both materials.

Figures 8-11 show the co-polarized far zone electric field versus time and the co-polarized RCS for the 0.25 dB and 60 dB dielectric foam spheres respectively.

XI. SAMPLE PROBLEM SETUP

The code as furnished models a 20 cm radius, dispersive, 0.25 dB dielectric foam sphere and computes backscatter far zone scattered fields at angles of θ=22.5 and ϕ=22.5 degrees. The corresponding output data files are also provided, along with a code to compute Radar Cross Section using these data files. In order to change the code to a new problem, many different parameters need to be modified. A sample problem setup will now be discussed.

Suppose that the problem to be studied is RCS backscatter versus frequency from a 28 cm by 31 cm perfectly conducting plate with a 3 cm dielectric coating with a dielectric constant of $4\epsilon_0$ using a θ-polarized field. The backscatter angles are θ=30.0 and ϕ=60.0 degrees and the frequency range is up to 3 Ghz.

Since the frequency range is up to 3 Ghz, the cell size must be chosen appropriately to resolve the field IN ANY MATERIAL at the highest frequency of interest. A general rule is that the cell size should be 1/10 of the wavelength at the highest frequency of interest. For difficult geometries, 1/20 of a wavelength may be necessary. The free space wavelength at 3 GHz is λ_0=10 cm and the wavelength in the dielectric coating at 3 GHz is 5 cm. The cell size is chosen as 1 cm, which provides a resolution of 5 cells/λ in the dielectric coating and 10 cells/λ_0 in free space. Numerical studies have shown that choosing the cell size $\leq$ 1/4 of the shortest wavelength in any material is the practical lower limit. Thus the cell size of 1 cm is barely adequate. The cell size in the x, y and z directions is set in

the common file through variables DELX, DELY and DELZ. Next the problem space size must be large enough to accomodate the scattering object, plus at least a five cell boundary (10 cells is more appropriate) on every side of the object to allow for the far zone field integration surface. It is advisable for plate scattering to have the plate centered in the x and y directions of the problem space in order to reduce the cross-polarized backscatter and to position the plate low in the z direction to allow strong specular reflections multiple encounters with the ORBC. A 10 cell border is chosen, and the problem space size is chosen as 49 by 52 by 49 cells in the x, y and z directions respectively. As an initial estimate, allow 2048 time steps so that energy trapped within the dielectric layer will radiate. Thus parameters NX, NY and NZ in COMMONB.FOR would be changed to reflect the new problem space size, and parameter NSTOP is changed to 2048. If all transients have not been dissipated after 2048 time steps, then NSTOP will have to be increased. Truncating the time record before all transients have dissipated will corrupt frequency domain results. Parameter NZFZ must be equal to 1 since we are interested in far zone fields only. To build the object, the following lines are inserted into the BUILD subroutine:

```
C
C     BUILD THE DIELECTRIC SLAB FIRST
C
      ISTART=11
      JSTART=11
      KSTART=11
      NXWIDE=28
      NYWIDE=31
      NZWIDE=3
      MTYPE=2
      CALL DCUBE(ISTART,JSTART,KSTART,NXWIDE,NYWIDE,NZWIDE,MTYPE)
C
C     BUILD PEC PLATE NEXT
C
      ISTART=11
      JSTART=11
      KSTART=11
      NXWIDE=28
      NYWIDE=31
      NZWIDE=0
      MTYPE=1
      CALL DCUBE(ISTART,JSTART,KSTART,NXWIDE,NYWIDE,NZWIDE,MTYPE)
```

The PEC plate is built last on the bottom of the dielectric slab to avoid any air gaps between the dielectric material and the PEC plate. In the common file, the incidence angles THINC and PHINC have to be changed to 30.0 and 60.0 respectively, the cell sizes (DELX, DELY, DELZ) are set to 0.01, and the polarization is set to ETHINC=1.0 and EPHINC=0.0 for θ-polarized

fields. Since dielectric material 2 is being used for the dielectric coating, the constitutive parameters EPS(2) and SIGMA(2) are set to $4\epsilon_0$ and 0.0 respectively, in subroutine SETUP. This completes the code modifications for the sample problem.

XII. NEW PROBLEM CHECKLIST

This checklist provides a quick reference to determine if all parameters have been defined properly for a given scattering problem. A reminder when defining quantities within the code: use MKS units and specify all angles in degrees.

COMMONB.FOR:

1) Is the problem space sized correctly? (NX, NY, NZ)

2) For near zone fields, is the number of sample points correct? (NTEST)

3) Is parameter NZFZ defined correctly for desired field outputs?

4) Is the number of dispersive dielectric (NEDISP) materials defined correctly?

5) Is the number of time steps correct? (NSTOP)

6) Are the cell dimensions (DELX, DELY, DELZ) defined correctly?

7) Are the incidence angles (THINC, PHINC) defined correctly?

8) Is the polarization of the incident wave defined correctly (ETHINC, EPHINC)?

9) For other than backscatter far zone field computations, are the scattering angles set correctly? (THETFZ, PHIFZ)

SUBROUTINE BUILD:

1) Is the object completely and correctly specified?

SUBROUTINE SETUP:

1) Are the constitutive parameters for each material specified correctly? (EPS and SIGMA)

2) Are the constitutive parameters for each dispersive material defined correctly? (EPSSTA, EPSINF, RELAXT, RELSIG)

FUNCTIONS SOURCE and DSRCE:

1) If the smooth cosine pulse is not desired, is it commented out and the Gaussian pulse uncommented?

SUBROUTINE DATSAV:

1) For near zone fields, are the sampled field types and spatial locations correct for each sampling point? (NTYPE, IOBS, JOBS, KOBS)

XIII. REFERENCES

[1] K. S. Yee, "Numerical solution of initial boundary value problems involving Maxwell's equations in isotropic media," IEEE Trans. Antennas Propagat., vol. AP-14, pp. 302-307, May 1966.

[2] G. Mur, "Absorbing boundary conditions for the Finite-Difference approximation of the Time-Domain Electromagnetic-Field Equations," IEEE Trans. Electromagn. Compat., vol. EMC-23, pp. 377-382, November 1981.

[3] R. J. Luebbers et. al., "A Finite Difference Time-Domain Near Zone to Far Zone Transformation," IEEE Trans. Antennas Propagat., vol. AP-39, no. 4, pp. 429-433, April 1991.

[4] C. Balanis, Advanced Engineering Electromagnetics, New York: Wiley, 1990, pp. 83-84.

[5] R. J. Luebbers et. al., "A frequency-dependent Finite-Difference Time-Domain formulation for dispersive materials," IEEE Trans. Electromagn. Compat., vol. EMC-32, pp. 222-227, August 1990.

[6] R. J. Luebbers et. al., "A frequency-dependent Finite-Difference Time-Domain formulation for transient propagation in plasma," IEEE Trans. Antennas Propagat., vol. AP-39, pp. 429-433, April 1991.

[7] R. Holland, L. Simpson and K. S. Kunz, "Finite-Difference Analysis of EMP Coupling to Lossy Dielectric Structures," IEEE Trans. Electromagn. Compat., vol. EMC-22, pp. 203-209, August 1980.

XIV. FIGURE TITLES

Fig. 1 Standard three dimensional Yee cell showing placement of electric and magnetic fields.

Fig. 2 Real part of relative permittivity versus frequency for 0.25 dB dielectric foam.

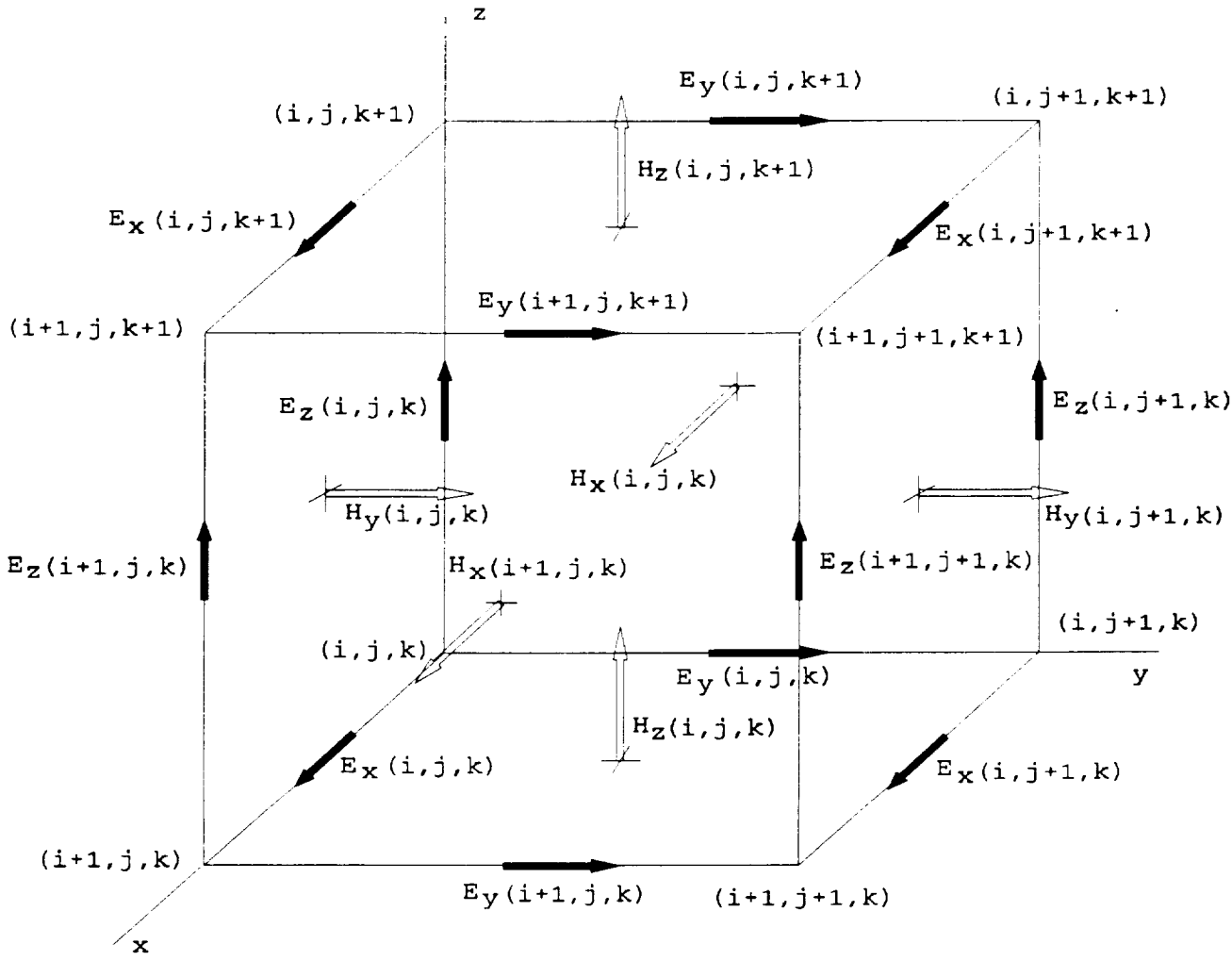
z
Ey(i,j,k+1)
(i,j,k+1)
(i,j+1,k+1)
Hz(i,j,k+1)
Ex(i,j,k+1)
Ex(i,j+1,k+1)
Ey(i+1,j,k+1)
(i+1,j,k+1)
(i+1,j+1,k+1)
Ez(i,j,k)
Ez(i,j+1,k)
Hx(i,j,k)
Hy(i,j,k)
Hy(i,j+1,k)
Ez(i+1,j,k)
Hx(i+1,j,k)
Ez(i+1,j+1,k)
(i,j+1,k)
(i,j,k)
Ey(i,j,k)
y
Hz(i,j,k)
Ex(i,j,k)
Ex(i,j+1,k)
(i+1,j,k)
Ey(i+1,j,k)
(i+1,j+1,k)
x

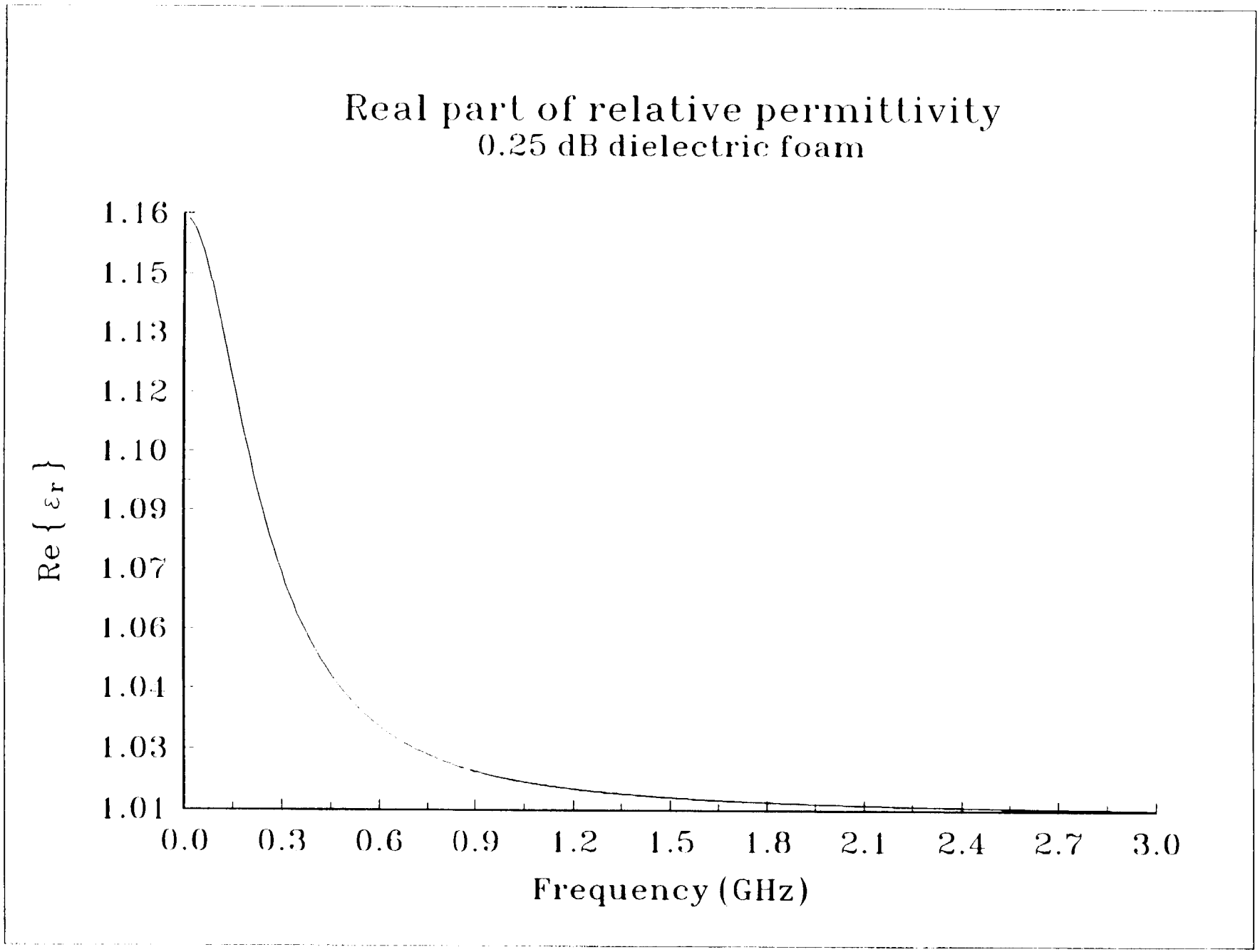
Real part of relative permittivity
0.25 dB dielectric foam
1.16
1.15
1.13
1.12
1.10
1.09
1.07
1.06
1.04
1.03
1.01
Re { εr }
0.0
0.3
0.6
0.9
1.2
1.5
1.8
2.1
2.4
2.7
3.0
Frequency (GHz)

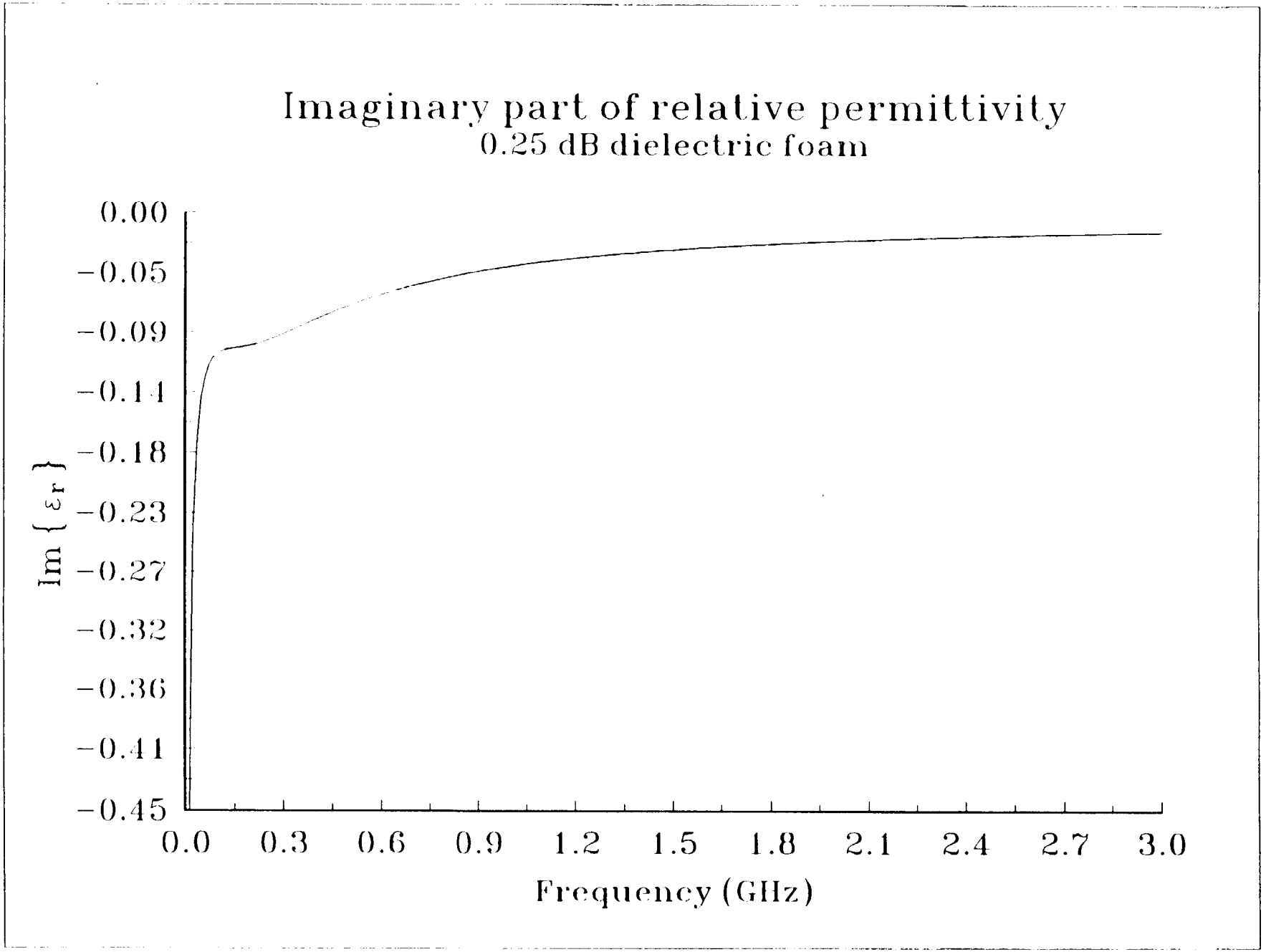
Imaginary part of relative permittivity
0.25 dB dielectric foam
0.00
−0.05
−0.09
−0.14
−0.18
−0.23
−0.27
−0.32
−0.36
−0.41
−0.45
Im { εr }
0.0
0.3
0.6
0.9
1.2
1.5
1.8
2.1
2.4
2.7
3.0
Frequency (GHz)

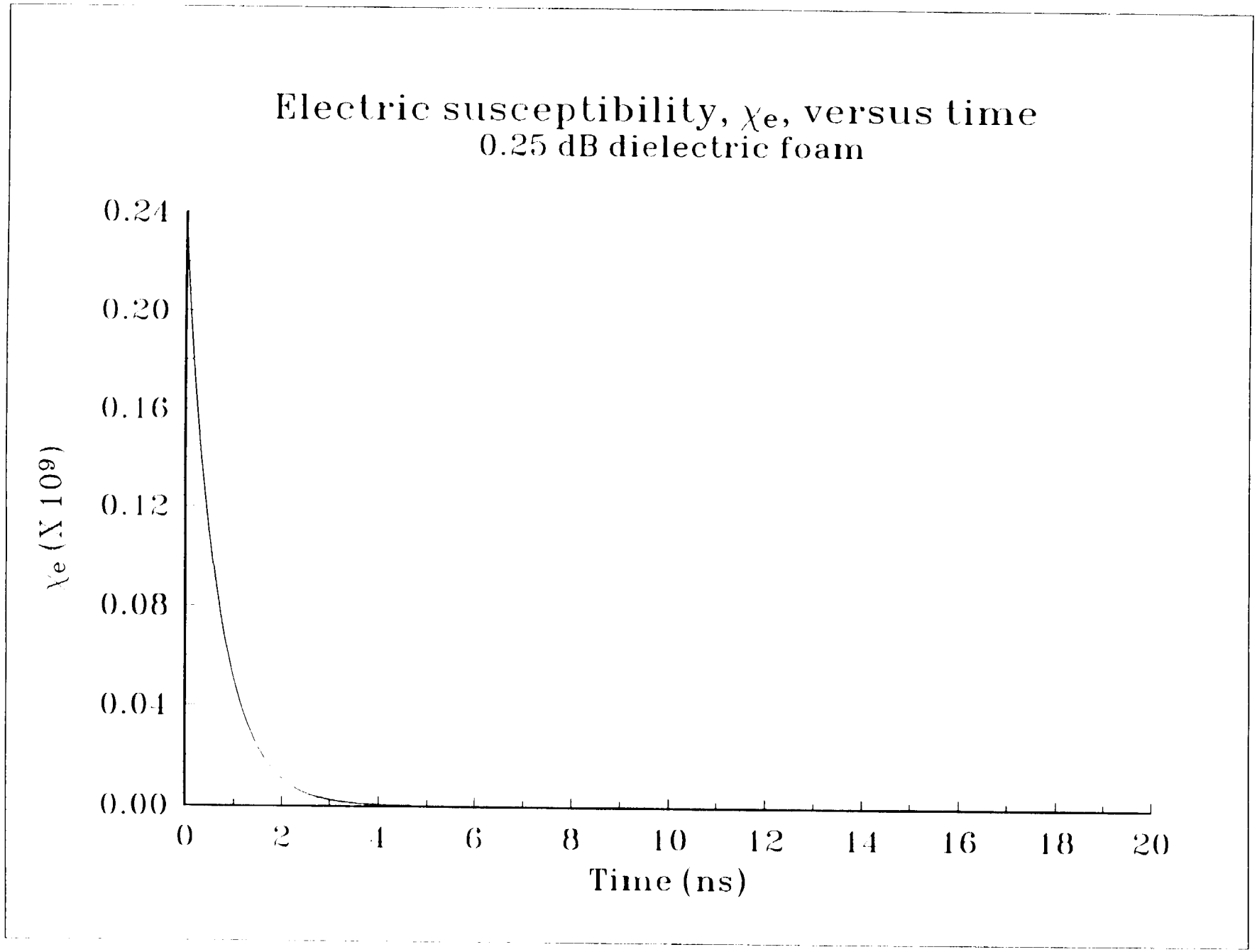
Electric susceptibility, χ_e, versus time
0.25 dB dielectric foam
0.24
0.20
0.16
0.12
0.08
0.04
0.00
χ_e (X 10^9)
0
2
4
6
8
10
12
14
16
18
20
Time (ns)

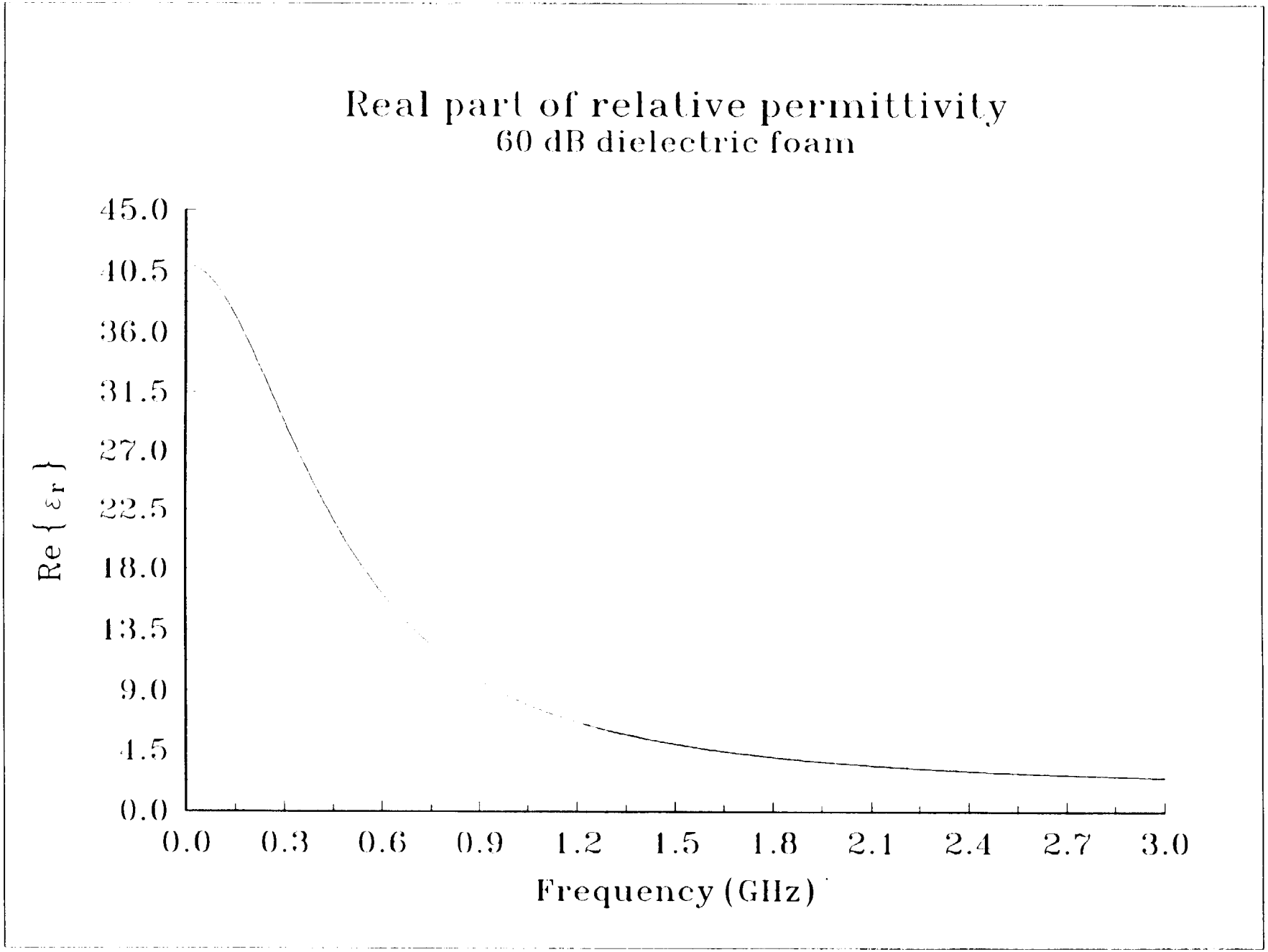
Real part of relative permittivity
60 dB dielectric foam
45.0
40.5
36.0
31.5
27.0
22.5
18.0
13.5
9.0
4.5
0.0
Re{ εr }
0.0
0.3
0.6
0.9
1.2
1.5
1.8
2.1
2.4
2.7
3.0
Frequency (GHz)

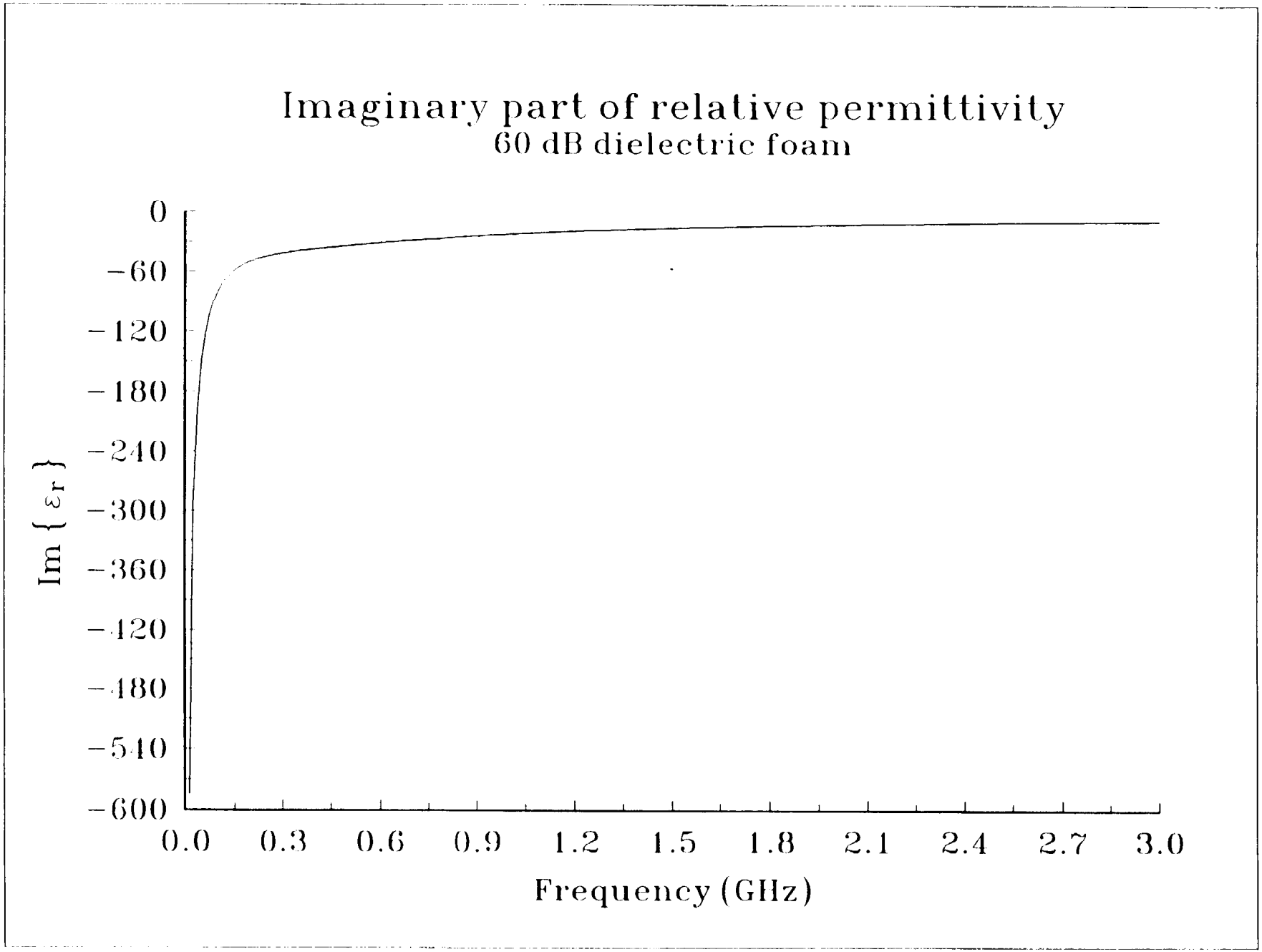
Imaginary part of relative permittivity
60 dB dielectric foam
0
−60
−120
−180
−240
−300
−360
−420
−480
−540
−600
Im { εr }
0.0
0.3
0.6
0.9
1.2
1.5
1.8
2.1
2.4
2.7
3.0
Frequency (GHz)

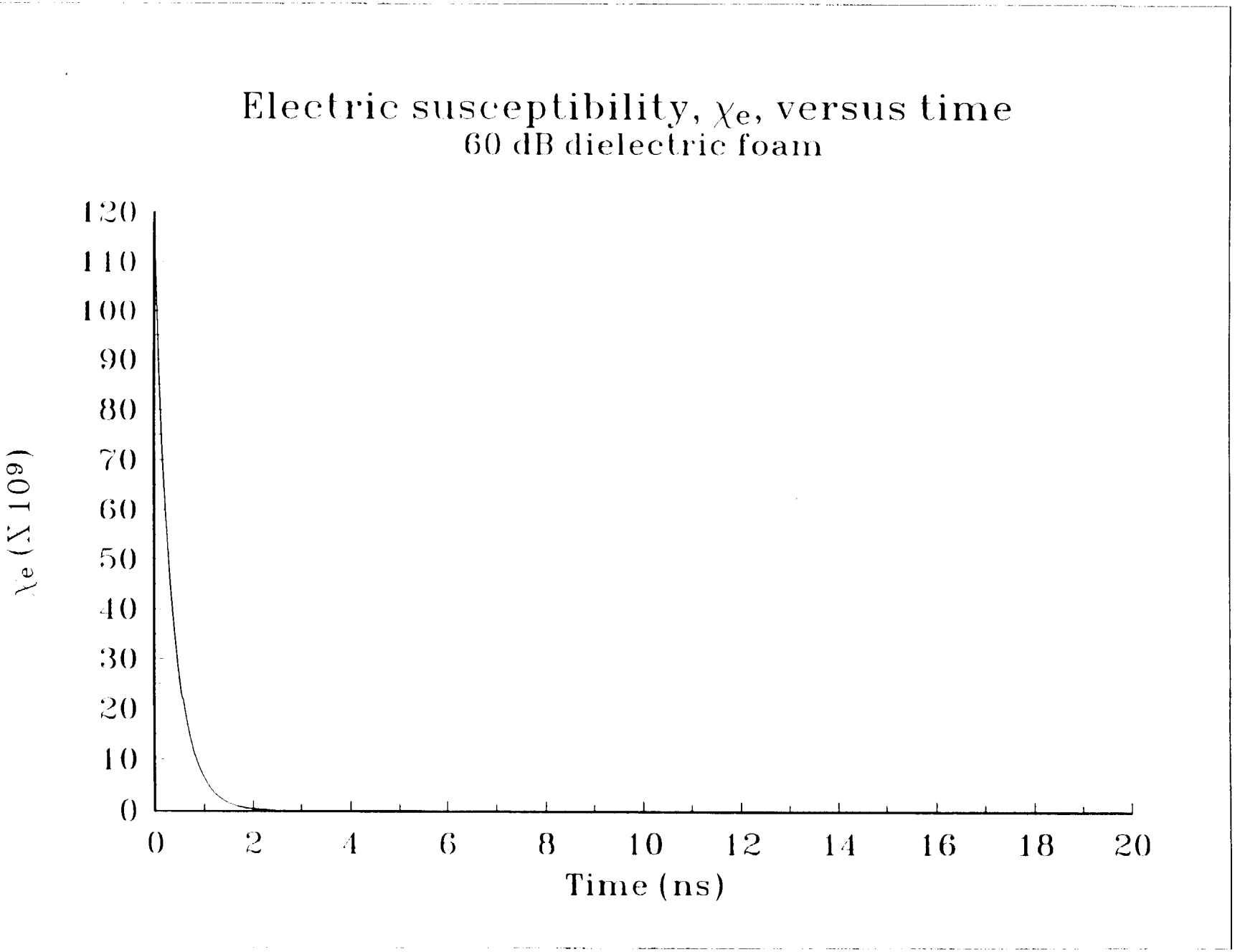
Electric susceptibility, χ_e, versus time
60 dB dielectric foam
χ_e (X 109)
120
110
100
90
80
70
60
50
40
30
20
10
0
0
2
4
6
8
10
12
14
16
18
20
Time (ns)

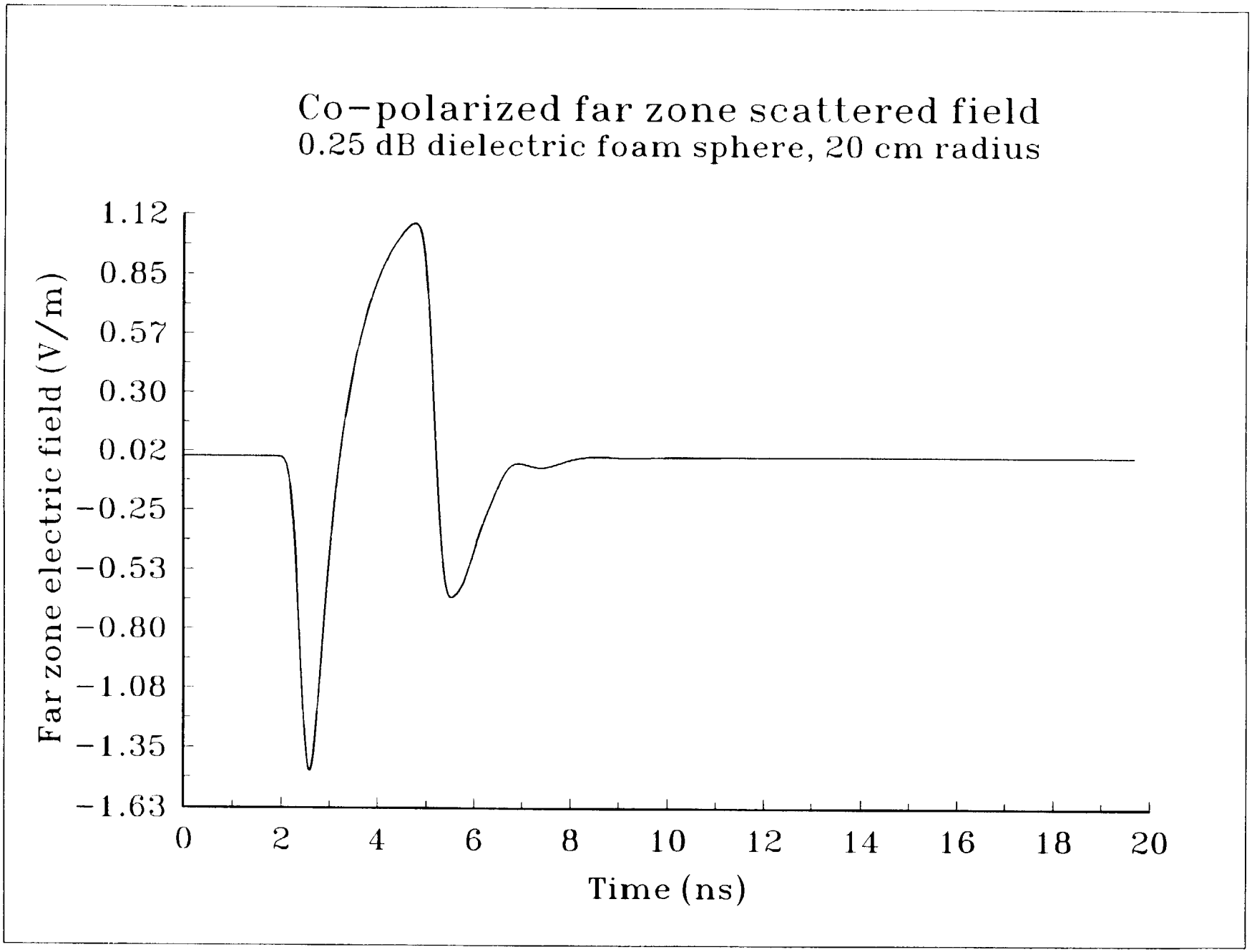
Co-polarized far zone scattered field
0.25 dB dielectric foam sphere, 20 cm radius
Far zone electric field (V/m)
1.12
0.85
0.57
0.30
0.02
-0.25
-0.53
-0.80
-1.08
-1.35
-1.63
0
2
4
6
8
10
12
14
16
18
20
Time (ns)

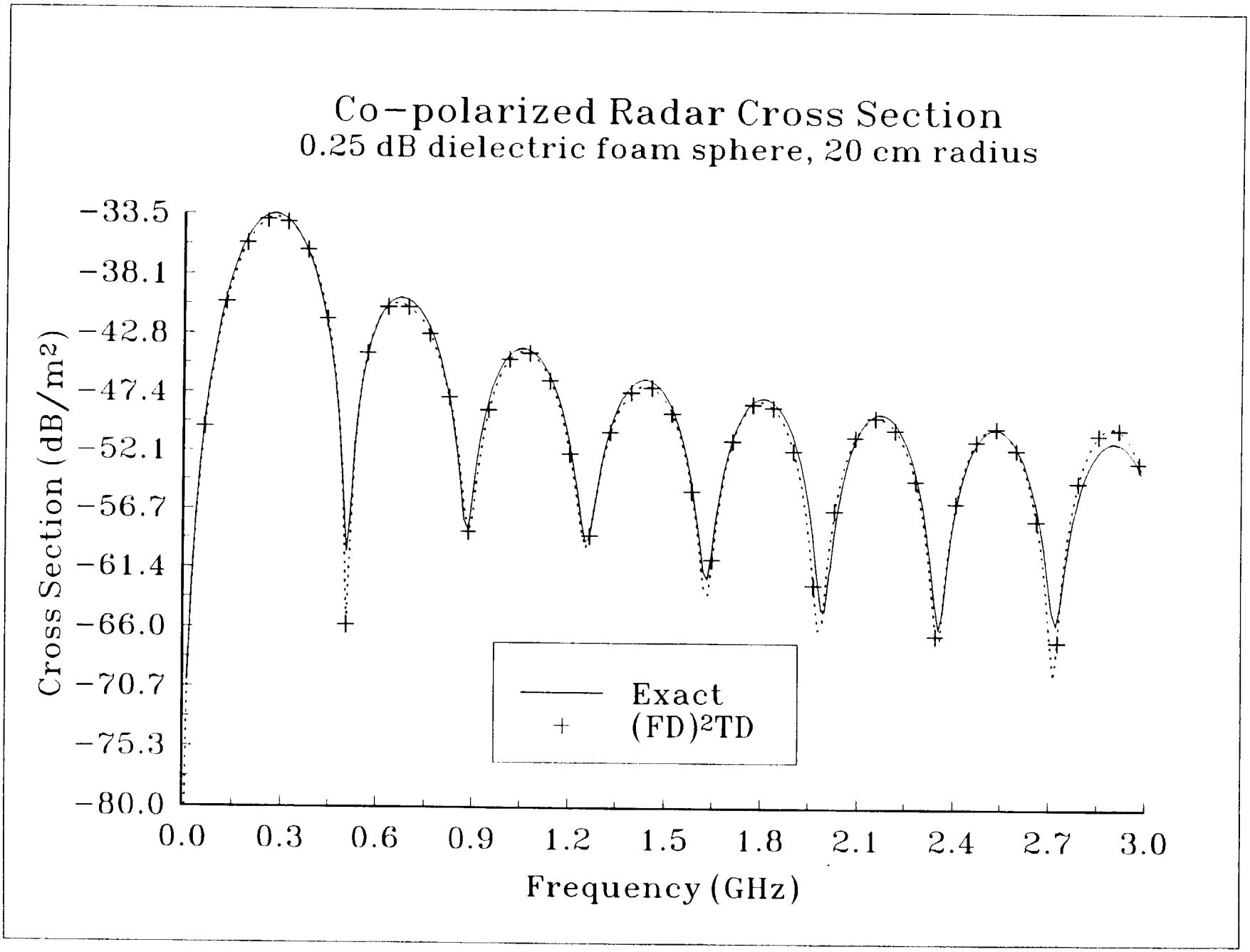
Co-polarized Radar Cross Section
0.25 dB dielectric foam sphere, 20 cm radius
Cross Section (dB/m²)
-33.5
-38.1
-42.8
-47.4
-52.1
-56.7
-61.4
-66.0
-70.7
-75.3
-80.0
0.0
0.3
0.6
0.9
1.2
1.5
1.8
2.1
2.4
2.7
3.0
Frequency (GHz)
Exact
(FD)²TD

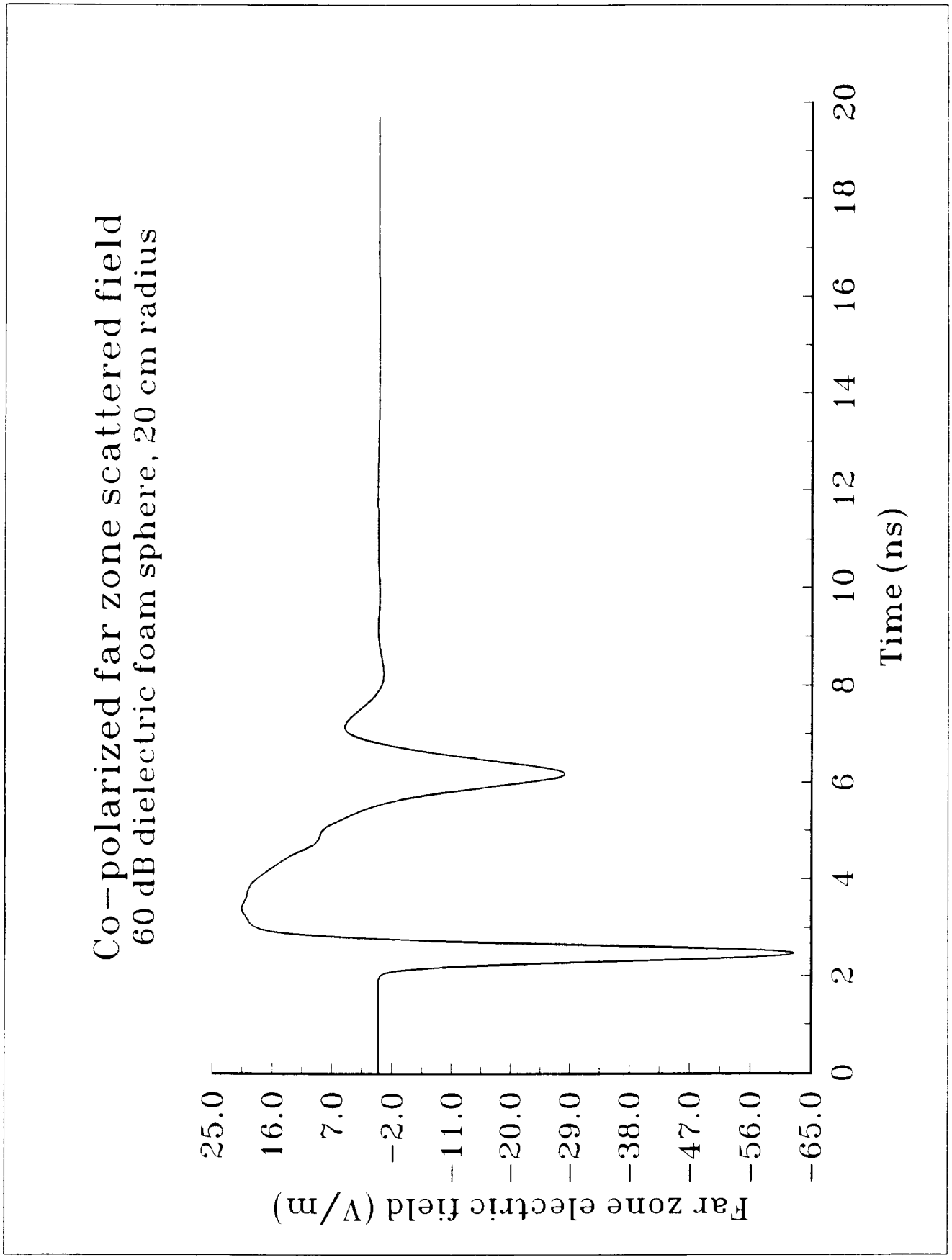

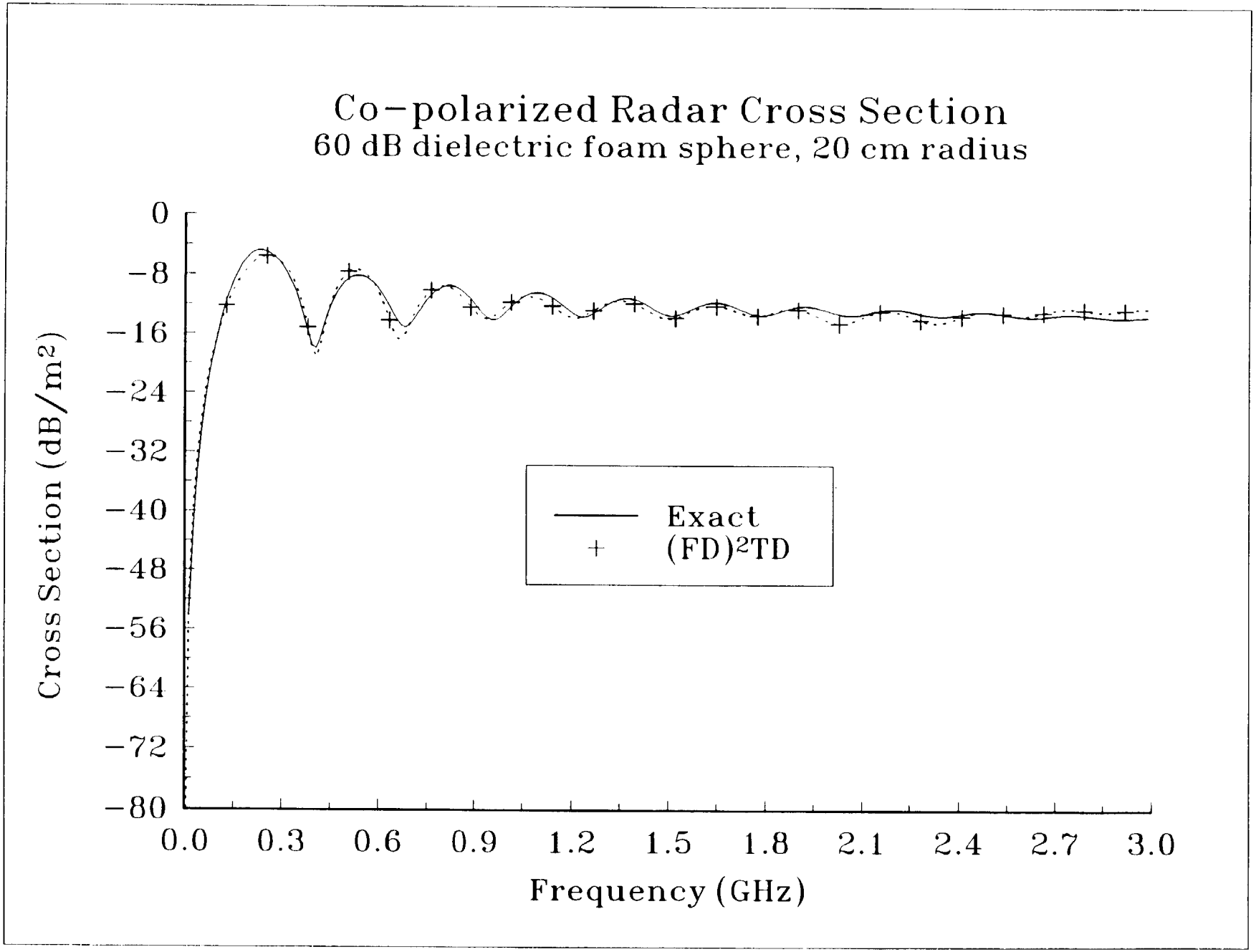
Co-polarized Radar Cross Section
60 dB dielectric foam sphere, 20 cm radius
Cross Section (dB/m²)
0
-8
-16
-24
-32
-40
-48
-56
-64
-72
-80
0.0
0.3
0.6
0.9
1.2
1.5
1.8
2.1
2.4
2.7
3.0
Frequency (GHz)
Exact
(FD)²TD

USER'S MANUAL FOR THREE DIMENSIONAL FDTD VERSION C CODE FOR SCATTERING FROM FREQUENCY-INDEPENDENT DIELECTRIC AND MAGNETIC MATERIALS

by

John H. Beggs, Raymond J. Luebbers and Karl S. Kunz
Electrical and Computer Engineering Department
The Pennsylvania State University
University Park, PA 16802

(814) 865-2362

January 1992

TABLE OF CONTENTS

TABLE OF CONTENTS (cont.)

I. INTRODUCTION

The Penn State Finite Difference Time Domain Electromagnetic Scattering Code Version C is a three dimensional numerical electromagnetic scattering code based upon the Finite Difference Time Domain Technique (FDTD). The supplied version of the code is one version of our current three dimensional FDTD code set. This manual provides a description of the code and corresponding results for several scattering problems. The manual is organized into fourteen sections: introduction, description of the FDTD method, operation, resource requirements, Version C code capabilities, a brief description of the default scattering geometry, a brief description of each subroutine, a description of the include file (COMMONC.FOR), a section briefly discussing Radar Cross Section (RCS) computations, a section discussing some scattering results, a sample problem setup section, a new problem checklist, references and figure titles.

II. FDTD METHOD

The Finite Difference Time Domain (FDTD) technique models transient electromagnetic scattering and interactions with objects of arbitrary shape and/or material composition. The technique was first proposed by Yee [1] for isotropic, non-dispersive materials in 1966; and has matured within the past twenty years into a robust and efficient computational method. The present FDTD technique is capabable of transient electromagnetic interactions with objects of arbitrary and complicated geometrical shape and material composition over a large band of frequencies. This technique has recently been extended to include dispersive dielectric materials, chiral materials and plasmas.

In the FDTD method, Maxwell's curl equations are discretized in time and space and all derivatives (temporal and spatial) are approximated by central differences. The electric and magnetic fields are interleaved in space and time and are updated in a second-order accurate leapfrog scheme. The computational space is divided into cells with the electric fields located on the edges and the magnetic fields on the faces (see Figure 1). FDTD objects are defined by specifying dielectric and/or magnetic material parameters at electric and/or magnetic field locations.

Two basic implementations of the FDTD method are widely used for electromagnetic analysis: total field formalism and scattered field formalism. In the total field formalism, the electric and magnetic field are updated based upon the material type present at each spatial location. In the scattered field formalism, the incident waveform is defined analytically and the scattered field is coupled to the incident field through the different material types. For the incident field, any waveform, angle of incidence and polarization is possible. The separation of the incident and

scattered fields conveniently allows an absorbing boundary to be employed at the extremities of the discretized problem space to absorb the scattered fields.

This code is a scattered field code, and the total E and H fields may be found by combining the incident and scattered fields. Any type of field quantity (incident, scattered, or total), Poynting vector or current are available anywhere within the computational space. These fields, incident, scattered and total, may be found within, on or about the interaction object placed in the problem space. By using a near to far field transformation, far fields can be determined from the near fields within the problem space thereby affording radiation patterns and RCS values. The accuracy of these calculations is typically within a dB of analytic solutions for dielectric and magnetic sphere scattering. Further improvements are expected as better absorbing boundary conditions are developed and incorporated.

III. OPERATION

Typically, a truncated Gaussian incident waveform is used to excite the system being modeled, however certain code versions also provide a smooth cosine waveform for convenience in modeling dispersive materials. The interaction object is defined in the discretized problem space with arrays at each cell location created by the discretization. All three dielectric material types for E field components within a cell can be individually specified by the arrays IDONE(I,J,K), IDTWO(I,J,K), IDTHRE(I,J,K). This models arbitrary dielectric materials with $\mu = \mu_0$. By an obvious extension to six arrays, magnetic materials with $\mu \neq \mu_0$ can be modeled.

Scattering occurs when the incident wave, marched forward in time in small steps set by the Courant stability condition, reaches the interaction object. Here a scattered wave must appear along with the incident wave so that the Maxwell equations are satisfied. If the material is a perfectly conductive metal then only the well known boundary condition

$$E_{tan}^{scat} = -E_{tan}^{inc} \tag{1}$$

must be satisfied. For a nondispersive dielectric the requirement is that the total field must satisfy the Maxwell equations in the material:

$$\nabla \times E^{tot} = \nabla \times (E^{inc} + E^{scat}) = -\frac{1}{\mu_o}\frac{\partial H^{tot}}{\partial t} = -\frac{1}{\mu_o}\frac{\partial (H^{inc} + H^{scat})}{\partial t} \tag{2}$$

$$\nabla \times H^{tot} = \nabla \times (H^{inc} + H^{scat}) = \varepsilon \frac{\partial E^{tot}}{\partial t} + \sigma E^{tot} \tag{3}$$

$$= \varepsilon \frac{\partial (E^{inc} + E^{scat})}{\partial t} + \sigma (E^{inc} + E^{scat}) \tag{4}$$

Additionally the incident wave, defined as moving unimpeded through a vacuum in the problem space, satisfies everywhere in the problem the Maxwell equations for free space

$$\nabla \times E^{inc} = -\frac{1}{\mu_o} \frac{\partial H^{inc}}{\partial t} \tag{5}$$

$$\nabla \times H^{inc} = \varepsilon_o \frac{\partial E^{inc}}{\partial t} \tag{6}$$

Subtracting the second set of equations from the first yields the Maxwell equations governing the scattered fields in the material:

$$\nabla \times E^{scat} = -\frac{1}{\mu_o} \frac{\partial H^{scat}}{\partial t} \tag{7}$$

$$\nabla \times H^{scat} = (\varepsilon - \varepsilon_o) \frac{\partial E^{inc}}{\partial t} + \sigma E^{inc} + \varepsilon \frac{\partial E^{scat}}{\partial t} + \sigma E^{scat} \tag{8}$$

Outside the material this simplifies to:

$$\nabla \times E^{scat} = -\frac{1}{\mu_o} \frac{\partial H^{scat}}{\partial t} \tag{9}$$

$$\nabla \times H^{scat} = \varepsilon_o \frac{\partial E^{scat}}{\partial t} \tag{10}$$

Magnetic materials, dispersive effects, non-linearities, etc., are further generalizations of the above approach. Based on the value of the material type, the subroutines for calculating scattered E and H field components branch to the appropriate expression for that scattered field component and

that component is advanced in time according to the selected algorithm. As many materials can be modeled as desired, the number equals the dimension selected for the flags. If materials with behavior different from those described above must be modeled, then after the appropriate algorithm is found, the code's branching structure allows easy incorporation of the new behavior.

IV. RESOURCE REQUIREMENTS

The number of cells the problem space is divided into times the six components per cell set the problem space storage requirements

$$\text{Storage} = NC \times 6 \text{ components/cell} \times 4 \text{ bytes/component} \quad (11)$$

and the computational cost

$$\text{Operations} = NC \times 6 \text{ comp/cell} \times 10 \text{ ops/component} \times N \quad (12)$$

where N is the number of time steps desired.

N typically is on the order of ten times the number of cells on one side of the problem space. More precisely for cubical cells it takes $\sqrt{3}$ time steps to traverse a single cell when the time step is set by the Courant stability condition

$$\Delta t = \frac{\Delta x}{\sqrt{3}c} \qquad \Delta x = \text{cell size dimension} \quad (13)$$

The condition on N is then that

$$N \sim 10 \times (\sqrt{3} NC^{\frac{1}{3}}) \qquad NC^{\frac{1}{3}} \sim \text{number cells on a side of the problem space} \quad (14)$$

The earliest aircraft modeling using FDTD with approximately 30 cells on a side required approximately 500 time steps. For more recent modeling with approximately 100 cells on a side, 2000 or more time steps are used.

For $(100 \text{ cell})^3$ problem spaces, 24 MBytes of memory are required to store the fields. Problems on the order of this size have been run on a Silicon Graphics 4D 220 with 32 MBytes of memory, IBM RISC 6000, an Intel 486 based machine, and VAX 11/785. Storage is only a problem as in the case of the 486 where only 16 MBytes of memory was available. This limited the problem space size to approximately $(80 \text{ cells})^3$.

For $(100 \text{ cell})^3$ problems with approximately 2000 time steps, there is a total of 120×10^9 operations to perform. The speeds of the previously mentioned machines are 24 MFLOPs (4 processor upgraded version), 10 MFLOPS, 1.5 MFLOPS, and 0.2 MFLOPs. The run times are then 5×10^3 seconds, 12×10^3 seconds, 80×10^3 seconds and 600×10^3 seconds, respectively. In hours the times are 1.4, 3.3, 22.2 and 167 hours. Problems of this size are possible on all but the last machine and can in fact be performed on a personal computer (486) if one day turnarounds are permissible.

V. VERSION C CODE CAPABILITIES

The Penn State University FDTD Electromagnetic Scattering Code Version C has the following capabilities:

1) Ability to model lossy dielectric and perfectly conducting scatterers.

2) Ability to model lossy magnetic scatterers.

3) First and second order outer radiation boundary condition (ORBC) operating on the electric fields for dielectric scatterers.

4) First and second order ORBC operating on the magnetic fields for magnetic scatterers.

5) Near to far zone transformation capability to obtain far zone scattered fields.

6) Gaussian and smooth cosine incident waveforms with arbitrary incidence angles.

7) Near zone field, current or power sampling capability.

8) Companion code for computing Radar Cross Section (RCS).

VI. DEFAULT SCATTERING GEOMETRY

The code as delivered is set up to calculate the far zone backscatter fields for a 20 cm radius, lossy magnetic sphere with parameters $\epsilon=\epsilon_0$, $\mu=4\mu_0$ and $\sigma^*=2.8413E+4$. The problem space size is 66 by 66 by 66 cells in the x, y and z directions, the cells are 0.01 cm cubes, and the incident waveform is a ϕ-polarized Gaussian pulse with incidence angles of $\theta=22.5$ and $\phi=22.5$ degrees. The output data files are included as a reference along with a code (RCS3D.FOR) for computing the frequency domain RCS using these output data files. The ORBC is the second order absorbing boundary condition set forth by Mur [2].

VII. SUBROUTINE DESCRIPTION

In the description for each subroutine, an asterisk (*) will be placed by the subroutine name if that particular subroutine is normally modified when defining a scattering problem.

MAIN ROUTINE

The main routine in the program contains the calls for all necessary subroutines to initialize the problem space and scattering object(s) and for the incident waveform, far zone transformation, field update subroutines, outer radiation boundary conditions and field sampling.

The main routine begins with the include statement and then appropriate data files are opened, and subroutines ZERO, BUILD and SETUP are called to initialize variables and/or arrays, build the object(s) and initialize the incident waveform and miscellaneous parameters, respectively. Subroutine SETFZ is called to intialize parameters for the near to far zone transformation if far zone fields are desired.

The main loop is entered next, where all of the primary field computations and data saving takes place. During each time step cycle, the EXSFLD, EYSFLD, and EZSFLD subroutines are called to update the x, y, and z components of the scattered electric field. The six electric field outer radiation boundary conditions (RADE??) are called next to absorb any outgoing scattered fields for perfectly conducting or lossy dielectric scatterers. Time is then advanced 1/2 time step according to the Yee algorithm and then the HXSFLD, HYSFLD, AND HZSFLD subroutines are called to update the x, y, and z components of scattered magnetic field. The six magnetic field outer radiation boundary conditions (RADH??) are called next to absorb any outgoing scattered fields for lossy magnetic scatterers. Time is then advanced another 1/2 step and then either near zone fields are sampled and written to disk in DATSAV, and/or the near zone to far zone vector potentials are updated in SAVFZ. The parameter NZFZ (described later) in the common file defines the type of output fields desired.

After execution of all time steps in the main field update loop, subroutine FAROUT is called if far zone fields are desired to compute the far zone fields and write them to disk. At this point, the execution is complete.

SUBROUTINE SETFZ

This subroutine initializes the necessary parameters required for far zone field computations. The code as furnished computes backscatter far zone fields and can compute bistatic far zone fields for one scattering angle (i.e. one θ and ϕ angle).

Refer to reference [3] for a complete description of the near to far zone transformation. Other versions of this subroutine provide for multiple bistatic angles.

SUBROUTINE SAVFZ

This subroutine updates the near zone to far zone vector potentials.

SUBROUTINE FAROUT

This subroutine changes the near zone to far zone vector potentials to far zone electric field θ and ϕ components and writes them to disk.

SUBROUTINE BUILD *

This subroutine "builds" the scattering object(s) by initializing the IDONE, IDTWO, IDTHRE, IDFOR, IDFIV and IDSIX arrays. The IDONE-IDTHRE arrays are for specifying perfectly conducting and lossy dielectric materials. The IDFOR-IDSIX arrays are for lossy magnetic materials. The reason for the separate arrays is so the user can independently control the exact placement of dielectric and magnetic material in the Yee cells. Refer to Figure 1 for a diagram of the basic Yee cell. For example, setting an element of the IDONE array at some I,J,K location is actually locating dielectric material at a cell edge whose center location is I+0.5,J,K. Setting an element of the IDFOR array at some I,J,K location is actually locating magnetic material perpendicular to a cell face whose center location is I,J+0.5,K+0.5, or equivalently, locating magnetic material at an edge on the dual H field mesh. The difference between the IDONE and IDFOR array locations is a direct result of the field offsets in the Yee cell (see Figure 1). Thus, materials with diagonal permittivity and/or diagonal permeability tensors can be modeled. The default material type for all ID??? arrays is 0, or free space. By initializing these arrays to values other than 0, the user is defining an object by determining what material types are present at each spatial location. Other material types available for IDONE-IDTHRE are 1 for perfectly conducting objects, and 2-9 for lossy dielectrics. IDONE-IDTHRE are normally set to 0 for magnetic scatterers. Other material types available for IDFOR-IDSIX are 10-19 for lossy magnetic materials. IDFOR-IDSIX are normally set to 0 for perfectly conducting or dielectric scatterers. If the user wants a material with both dielectric and magnetic properties (i.e. permittivity other than ϵ_0 for magnetic materials, and permeability other than μ_0 for dielectric materials), then he/she must define IDONE-IDSIX for that particular material. This subroutine also has a section that checks the ID??? arrays to determine if legal material types have been defined throughout the problem space. The actual material parameters (ϵ, μ, σ, and σ^*) are defined in subroutine SETUP.

The default geometry is a 20 cm radius, lossy magnetic sphere.

The user must be careful that his/her object created in the BUILD subroutine is properly formed. There is not a direct one-to-one correspondence between the dielectric and magnetic ID??? arrays. However, one can define a correspondence, so that code used to generate a dielectric object can be modified to generate a magnetic object.

To see this consider that we have set the permittivity at cell locations corresponding to

EX(I,J,K), EY(I,J,K), EZ(I,J,K)

using the IDONE, IDTWO, and IDTHRE arrays respectively. This determines one corner of a dielectric cube. If we wish to define the corner of a corresponding magnetic cube, offset 1/2 cell in the x, y, z directions, we would set the locations of the magnetic fields

HX(I+1,J,K), HY(I,J+1,K), HZ(I,J,K+1)

as magnetic material using the IDFOR, IDFIV, and IDSIX arrays.

This example indicates the following correspondence between BUILDing dielectric and magnetic objects:

Dielectric Object		Magnetic Object
IDONE(I,J,K)	=	IDFOR(I+1,J,K)
IDTWO(I,J,K)	=	IDFIV(I,J+1,K)
IDTHRE(I,J,K)	=	IDSIX(I,J,K+1)

To illustrate this for a somewhat more complicated case, consider an example of a 3x3 cell dielectric plate located in the XY plane at K=5. The plate can be generated with the following FORTRAN lines:

```
      DO 20 J=4,7
        DO 10 I=4,7
         IF(I.NE.7)IDONE(I,J,K)=2
         IF(J.NE.7)IDTWO(I,J,K)=2
 10     CONTINUE
 20   CONTINUE
```

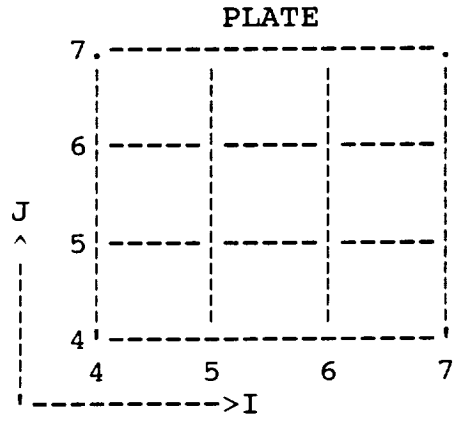

If the same FORTRAN lines were used to try to generate a magnetic plate, the object generated would actually be unconnected:

```
      DO 20 J=4,7
        DO 10 I=4,7
         IF(I.NE.7)IDFOR(I,J,K)=11
         IF(J.NE.7)IDFIV(I,J,K)=11
 10     CONTINUE
 20   CONTINUE
```

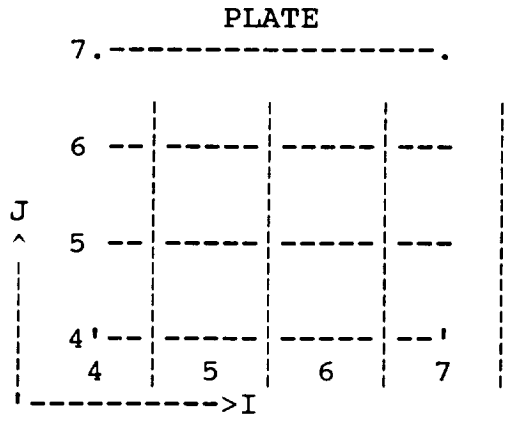

The correct way to build the magnetic plate is with the following FORTRAN code:

```
      DO 20 J=4,7
        DO 10 I=4,7
          IF(I.NE.4)IDFOR(I,J,K)=11
          IF(J.NE.4)IDFIV(I,J,K)=11
 10     CONTINUE
 20   CONTINUE
```

This is equivalent to the correspondence relationship given above. See comments in the BUILD subroutine for further explanation of the ID??? arrays.

When it is important to place the object in the center of the problem space (to have lowest possible cross-pol scattering for symmetric objects), NX etc. should be odd for dielectrics and even for magnetics. This is due to the field locations in the Yee cell and also the placement of the E and H field absorbing boundary condition surfaces.

If the object being modeled has curved surfaces, edges, etc. that are at an angle to one or more of the coordinate axes, then that shape must be approximately modeled by lines and faces in a "stair-stepped" (or stair-cased) fashion. This stair-cased approximation introduces errors into computations at higher frequencies. Intuitively, the error becomes smaller as more cells are used to stair-case a particular object. Thus, the default Nickel Ferrite sphere scattering geometry is a stair-cased sphere.

When the user's test object is dielectric it is apparently better to use the Mur E field boundary formulation. For a magnetic scattering object it seems better to use the Mur H field boundary formulation. The reason for this has to do with the

reactive part of the energy (near zone fields) reaching the absorbing boundary surface. These near zone fields differ for magnetic and dielectric objects, even for dual objects where the far fields are essentially identical.

One final comment on building dual dielectric vs magnetic objects can be explained by considering the duality between magnetic and dielectric materials. In testing the code, it was helpful to test dual dielectric/magnetic objects since they scatter identically in the far zone. In specifying the material of a magnetic scatterer to be the dual of a dielectric, the following transformation must be applied:

DIELECTRIC	<--DUAL-->	MAGNETIC
E field	<-------->	H field
H field	<-------->	-E field
ϵ	<-------->	μ
μ	<-------->	ϵ
ß (k)	<-------->	ß (k)
σ	<-------->	$\sigma \cdot (\mu_0/\epsilon_0) = \sigma^*$

The somewhat surprising entry in this table is the relationship between the dielectric and magnetic conductivities. The reason why the magnetic conductivity, σ^*, for magnetic materials has to be scaled as indicated is that for duality to be applied the free space impedance must be inverted. Although this is not generally possible for actual problems, identical far zone scattering for dielectric and magnetic scatterers can be achieved by this scaling of σ^* as above and realizing that E and H scattered field to incident field ratios will not invert. This scaling of σ^* is why conductivity for magnetic materials is usually not a dominating feature, and in fact is often neglected.

SUBROUTINE DCUBE

This subroutine builds cubes of dielectric material by defining four each of IDONE, IDTWO and IDTHRE components corresponding to one spatial cube of dielectric material. It can also be used to define thin (i.e. up to one cell thick) dielectric or perfectly conducting plates. Refer to comments within DCUBE for a description of the arguments and usage of the subroutine. This subroutine could be modified to build cubes and/or plates of magnetic materials by using a triple do-loop in BUILD (after calls to DCUBE) over coordinate indices I, J, K and applying the correspondence between the IDONE-IDTHRE and IDFOR-IDSIX arrays that was previously discussed.

SUBROUTINE SETUP *

This subroutine initializes many of the constants required for incident field definition, field update equations, outer

radiation boundary conditions and material parameters. The material parameters ϵ, μ, σ and σ^* are defined for each material type using the material arrays EPS, XMU, SIGMA and SIGMAC respectively. The array EPS is used for the total permittivity, XMU is used for the total permeability, SIGMA is used for the electric conductivity and SIGMAC is used for the magnetic conductivity (useful for running dual problems). These arrays are initialized in SETUP to free space material parameters for all material types and then the user is required to modify these arrays for his/her scattering materials. Thus, for the lossy dielectric material type 2, the user must define EPS(2) and SIGMA(2). The remainder of the subroutine computes constants used in field update equations and boundary conditions and writes the diagnostics file.

SUBROUTINE EXSFLD

This subroutine updates all x components of scattered electric field at each time step except those on the outer boundaries of the problem space. IF statements based upon the IDONE array are used to determine the type of material present and the corresponding update equation to be used. These scattered field equations are based on the development given in [4].

SUBROUTINE EYSFLD

This subroutine updates all y components of scattered electric field at each time step except those on the outer boundaries of the problem space. IF statements based upon the IDTWO array are used to determine the type of material present and the corresponding update equation to be used.

SUBROUTINE EZSFLD

This subroutine updates all z components of scattered electric field at each time step except those on the outer boundaries of the problem space. IF statements based upon the IDTHRE array are used to determine the type of material present and the corresponding update equation to be used.

SUBROUTINES RADEYX, RADEZX, RADEZY, RADEXY, RADEXZ and RADEYZ

These subroutines apply the outer radiation boundary conditions to the scattered electric field on the outer boundaries of the problem space for non-magnetic scatterers. The user controls selection of these routines through the parameter MAGNET (described later).

SUBROUTINE HXSFLD

This subroutine updates all x components of scattered magnetic field at each time step. IF statements based upon the

IDFOR array are used to determine the type of material present and the corresponding update equation to be used.

SUBROUTINE HYSFLD

This subroutine updates all y components of scattered magnetic field at each time step. IF statements based upon the IDFIV array are used to determine the type of material present and the corresponding update equation to be used.

SUBROUTINE HZSFLD

This subroutine updates all z components of scattered magnetic field at each time step. IF statements based upon the IDSIX array are used to determine the type of material present and the corresponding update equation to be used.

SUBROUTINES RADHXZ, RADHYX, RADHZY, RADHXY, RADHYZ and RADHZX

These subroutines apply the outer radiation boundary conditions to the scattered magnetic field on the outer boundaries of the problem space for magnetic scatterers. The user controls selection of these routines through the parameter MAGNET (described later).

SUBROUTINE DATSAV *

This subroutine samples near zone scattered field quantities and saves them to disk. This subroutine is where the quantities to be sampled and their spatial locations are to be specified and is only called if near zone fields only are desired or if both near and far zone fields are desired. Total field quantities can also be sampled. See comments within the subroutine for specifying sampled scattered and/or total field quantities. When sampling magnetic fields, remember the $\delta t/2$ time difference between E and H when writing the fields to disk. Sections of code within this subroutine determine if the sampled quantities and the spatial locations have been properly defined.

FUNCTIONS EXI, EYI, EZI, HXI, HYI and HZI

These functions are called to compute the x, y and z components of incident electric and magnetic field, respectively. The functional form of the incident field is contained in a separate function SOURCE.

FUNCTION SOURCE *

This function contains the functional form of the incident field. The code as furnished uses the Gaussian form of the incident field. An incident smooth cosine pulse is also available by uncommenting the required lines and commenting out the Gaussian pulse. Thus, this function need only be modified if the user changes the incident pulse from Gaussian to smooth cosine. A slight improvement in computing speed and vectorization may be achieved by moving this function inside each of the incident field functions EXI, EYI and so on.

FUNCTIONS DEXI, DEYI, DEZI, DHXI, DHYI and DHZI

These functions are called to compute the x, y and z components of the time derivative of incident electric and magnetic field, respectively. The functional form of the incident field is contained in a separate function DSRCE.

FUNCTION DSRCE *

This function contains the functional form of the time derivative of the incident field. The code as furnished uses the time derivative of the Gaussian form of the incident field. A smooth cosine pulse time derivative is also available by uncommenting the required lines and commenting out the Gaussian pulse. Thus, the function need only be modified if the user changes from the Gaussian to smooth cosine pulse. Again, a slight improvement in computing speed and vectorization may be achieved by moving this function inside each of the time derivative incident field functions DEXI, DEYI and so on.

SUBROUTINE ZERO

This subroutine initializes various arrays and variables to zero.

VIII. INCLUDE FILE DESCRIPTION (COMMONC.FOR) *

The include file, COMMONC.FOR, contains all of the arrays and variables that are shared among the different subroutines. This file will require the most modifications when defining scattering problems. A description of the parameters that are normally modified follows.

The parameters NX, NY and NZ specify the size of the problem space in cells in the x, y and z directions respectively. For problems where it is crucial to center the object within the problem space, then NX, NY and NZ should be odd for dielectric scatterers and even for magnetic scatterers. The parameter NTEST defines the number of near zone quantities to be sampled and NZFZ defines the field output format. Set NZFZ=0 for near zone fields

only, NZFZ=1 for far zone fields only and NZFZ=2 for both near and far zone fields. Parameter MAGNET is used to define magnetic scatterers and it controls the choice of RADE?? versus RADH?? absorbing boundary subroutines. It is set to 0 for dielectric scatterers and to 1 for magnetic scatterers. Parameter NSTOP defines the maximum number of time steps. DELX, DELY, and DELZ (in meters) define the cell size in the x, y and z directions respectively. The θ and ϕ incidence angles (in degrees) are defined by THINC and PHINC respectively and the polarization is defined by ETHINC and EPHINC. ETHINC=1.0, EPHINC=0.0 for θ-polarized incident field and ETHINC=0.0, EPHINC=1.0 for ϕ-polarized incident fields. Parameters AMP and BETA define the maximum amplitude and the e^{-2} temporal width of the incident pulse respectively. BETA automatically adjusts when the cell size is changed and normally should not be changed by the user. The far zone scattering angles are defined by THETFZ and PHIFZ. The code as furnished performs backscatter computations, but these parameters could be modified for a bistatic computation.

IX. RCS COMPUTATIONS

A companion code, RCS3D.FOR, has been included to compute RCS versus frequency. It uses the file name of the FDTD far zone output data (FZOUT3D.DAT) and writes data files of far zone electric fields versus time (FZTIME.DAT) and RCS versus frequency (3DRCS.DAT). The RCS computations are performed up to the 10 cell/λ_0 frequency limit. Refer to comments within this code for further details.

X. RESULTS

As previously mentioned, the code as furnished models a 20 cm radius, lossy magnetic sphere and computes backscatter far zone scattered fields at angles of θ=22.5 and ϕ=22.5 degrees. Results are included for the dual dielectric sphere and the default magnetic sphere. The material parameters for the dielectric dual of the magnetic material are $\epsilon=4\epsilon_0$, σ=0.2 and $\mu=\mu_0$. For these materials there are 5 cells per wavelength at approximately 3.0 GHz.

Figures 2-3 show the co-polarized far zone scattered field versus time and the co-polarized RCS versus frequency for the dielectric sphere.

Figures 4-5 show the co-polarized far zone electric field versus time and the co-polarized RCS for the magnetic sphere.

XI. SAMPLE PROBLEM SETUP

The code as furnished models a 20 cm radius, lossy magnetic sphere and computes backscatter far zone scattered fields at angles of θ=22.5 and ϕ=22.5 degrees. The corresponding output

data files are also provided, along with a code to compute Radar Cross Section using these data files. In order to change the code to a new problem, many different parameters need to be modified. A sample problem setup will now be discussed.

Suppose that the problem to be studied is RCS backscatter versus frequency from a 28 cm by 31 cm perfectly conducting plate with a 3 cm dielectric coating with a dielectric constant of $4\epsilon_0$ using a θ-polarized field. The backscatter angles are θ=30.0 and ϕ=60.0 degrees and the frequency range is up to 3 Ghz.

Since the frequency range is up to 3 Ghz, the cell size must be chosen appropriately to resolve the field IN ANY MATERIAL at the highest frequency of interest. A general rule is that the cell size should be 1/10 of the wavelength at the highest frequency of interest. For difficult geometries, 1/20 of a wavelength may be necessary. The free space wavelength at 3 GHz is λ_0=10 cm and the wavelength in the dielectric coating at 3 GHz is 5 cm. The cell size is chosen as 1 cm, which provides a resolution of 5 cells/λ in the dielectric coating and 10 cells/λ_0 in free space. Numerical studies have shown that choosing the cell size $\leq$ 1/4 of the shortest wavelength in any material is the practical lower limit. Thus the cell size of 1 cm is barely adequate. The cell size in the x, y and z directions is set in the common file through variables DELX, DELY and DELZ. Next the problem space size must be large enough to accomodate the scattering object, plus <u>at least</u> a five cell boundary (10 cells is more appropriate) on every side of the object to allow for the far zone field integration surface. It is advisable for plate scattering to have the plate centered in the x and y directions of the problem space in order to reduce the cross-polarized backscatter and to position the plate low in the z direction to allow strong specular reflections multiple encounters with the ORBC. A 10 cell border is chosen, and the problem space size is chosen as 49 by 52 by 49 cells in the x, y and z directions respectively. As an initial estimate, allow 2048 time steps so that energy trapped within the dielectric layer will radiate. Thus parameters NX, NY and NZ in COMMONC.FOR would be changed to reflect the new problem space size, and parameter NSTOP is changed to 2048. If all transients have not been dissipated after 2048 time steps, then NSTOP will have to be increased. Truncating the time record before all transients have dissipated will corrupt frequency domain results. Parameter NZFZ must be equal to 1 since we are interested in far zone fields only. Parameter MAGNET must be equal to 0 for the dielectric scatterer. To build the object, the following lines are inserted into the BUILD subroutine:

```
C
C     BUILD THE DIELECTRIC SLAB FIRST
C
      ISTART=11
```

```
      JSTART=11
      KSTART=11
      NXWIDE=28
      NYWIDE=31
      NZWIDE=3
      MTYPE=2
      CALL DCUBE(ISTART,JSTART,KSTART,NXWIDE,NYWIDE,NZWIDE,MTYPE)
C
C     BUILD PEC PLATE NEXT
C
      ISTART=11
      JSTART=11
      KSTART=11
      NXWIDE=28
      NYWIDE=31
      NZWIDE=0
      MTYPE=1
      CALL DCUBE(ISTART,JSTART,KSTART,NXWIDE,NYWIDE,NZWIDE,MTYPE)
```

The PEC plate is built last on the bottom of the dielectric slab to avoid any air gaps between the dielectric material and the PEC plate. In the common file, the incidence angles THINC and PHINC have to be changed to 30.0 and 60.0 respectively, the cell sizes (DELX, DELY, DELZ) are set to 0.01, and the polarization is set to ETHINC=1.0 and EPHINC=0.0 for θ-polarized fields. Since dielectric material 2 is being used for the dielectric coating, the constitutive parameters EPS(2) and SIGMA(2) are set to $4\epsilon_0$ and 0.0 respectively, in subroutine SETUP. This completes the code modifications for the sample problem.

XII. NEW PROBLEM CHECKLIST

This checklist provides a quick reference to determine if all parameters have been defined properly for a given scattering problem. A reminder when defining quantities within the code: use MKS units and specify all angles in degrees.

COMMONC.FOR:

1) Is the problem space sized correctly? (NX, NY, NZ)

2) For near zone fields, is the number of sample points correct? (NTEST)

3) Is parameter NZFZ defined correctly for desired field outputs?

4) Is parameter MAGNET defined correctly for the type of scatterer?

5) Is the number of time steps correct? (NSTOP)

6) Are the cell dimensions (DELX, DELY, DELZ) defined correctly?

7) Are the incidence angles (THINC, PHINC) defined correctly?

8) Is the polarization of the incident wave defined correctly (ETHINC, EPHINC)?

9) For other than backscatter far zone field computations, are the scattering angles set correctly? (THETFZ, PHIFZ)

SUBROUTINE BUILD:

1) Is the object completely and correctly specified?

SUBROUTINE SETUP:

1) Are the constitutive parameters for each material specified correctly? (EPS, XMU, SIGMA, SIGMAC)

FUNCTIONS SOURCE and DSRCE:

1) If the Gaussian pulse is not desired, is it commented out and the smooth cosine pulse uncommented?

SUBROUTINE DATSAV:

1) For near zone fields, are the sampled field types and spatial locations correct for each sampling point? (NTYPE, IOBS, JOBS, KOBS)

XIII. REFERENCES

[1] K. S. Yee, "Numerical solution of initial boundary value problems involving Maxwell's equations in isotropic media," IEEE Trans. Antennas Propagat., vol. AP-14, pp. 302-307, May 1966.

[2] G. Mur, "Absorbing boundary conditions for the Finite-Difference approximation of the Time-Domain Electromagnetic-Field Equations," IEEE Trans. Electromagn. Compat., vol. EMC-23, pp. 377-382, November 1981.

[3] R. J. Luebbers et. al., "A Finite Difference Time-Domain Near Zone to Far Zone Transformation," IEEE Trans. Antennas Propagat., vol. AP-39, no. 4, pp. 429-433, April 1991.

[4] R. Holland, L. Simpson and K. S. Kunz, "Finite-Difference Time-Domain Analysis of EMP Coupling to Lossy Dielectric Structures," IEEE Trans. Electromagn. Compat., vol. EMC-22, pp. 203-209, August 1980.

XIV. FIGURE TITLES

Fig. 1 Standard three dimensional Yee cell showing placement of electric and magnetic fields.

Fig. 2 Co-polarized far zone scattered field versus time for dielectric sphere with 20 cm radius.

Fig. 3 Co-polarized Radar Cross Section versus frequency for dielectric sphere with 20 cm radius.

Fig. 4 Co-polarized far zone scattered field versus time for magnetic sphere with 20 cm radius.

Fig. 5 Co-polarized Radar Cross Section versus frequency for magnetic sphere with 20 cm radius.

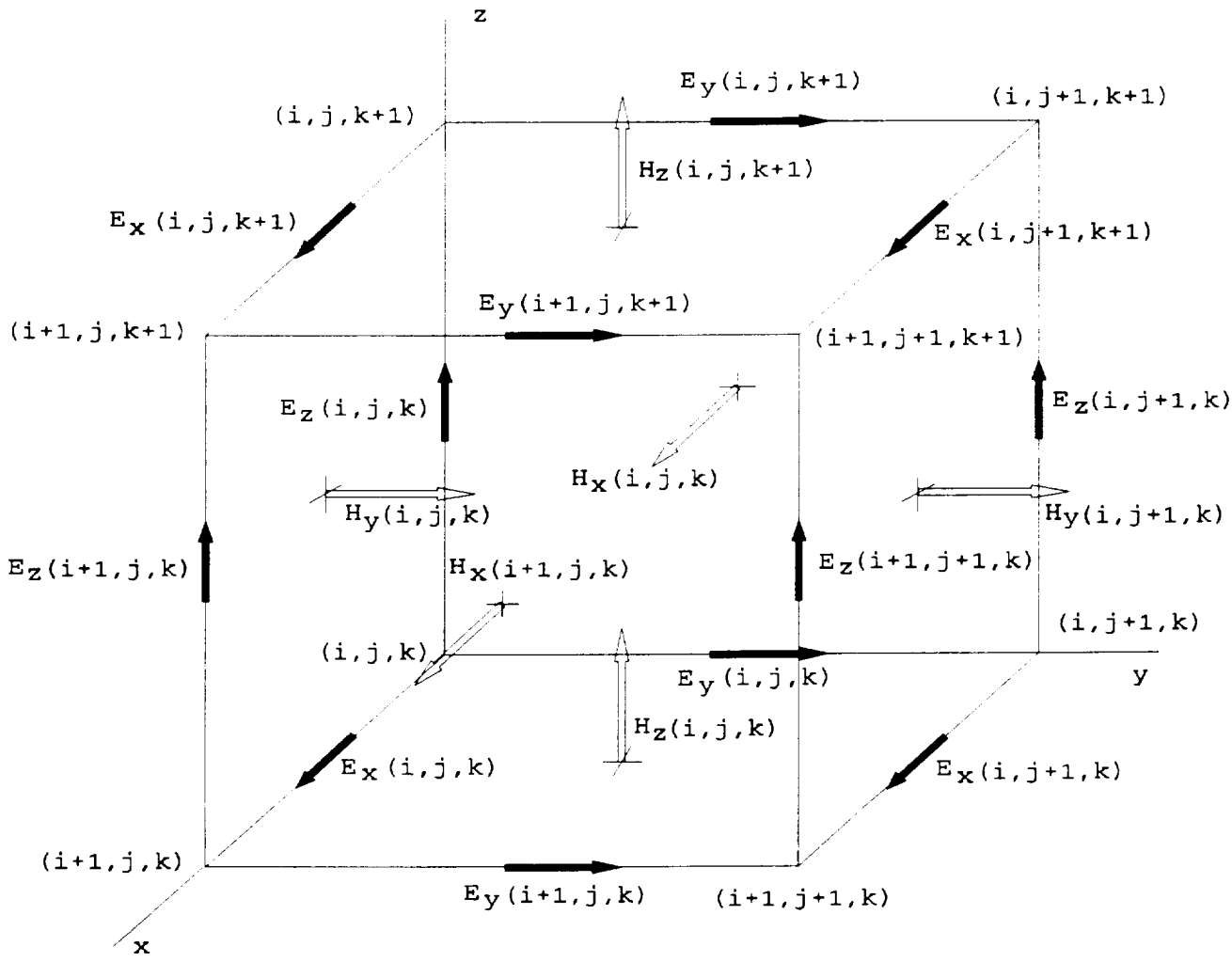
z
Ey(i,j,k+1)
(i,j,k+1)
(i,j+1,k+1)
Hz(i,j,k+1)
Ex(i,j,k+1)
Ex(i,j+1,k+1)
Ey(i+1,j,k+1)
(i+1,j,k+1)
(i+1,j+1,k+1)
Ez(i,j,k)
Ez(i,j+1,k)
Hx(i,j,k)
Hy(i,j,k)
Hy(i,j+1,k)
Ez(i+1,j,k)
Hx(i+1,j,k)
Ez(i+1,j+1,k)
(i,j+1,k)
(i,j,k)
Ey(i,j,k)
y
Hz(i,j,k)
Ex(i,j,k)
Ex(i,j+1,k)
(i+1,j,k)
Ey(i+1,j,k)
(i+1,j+1,k)
x

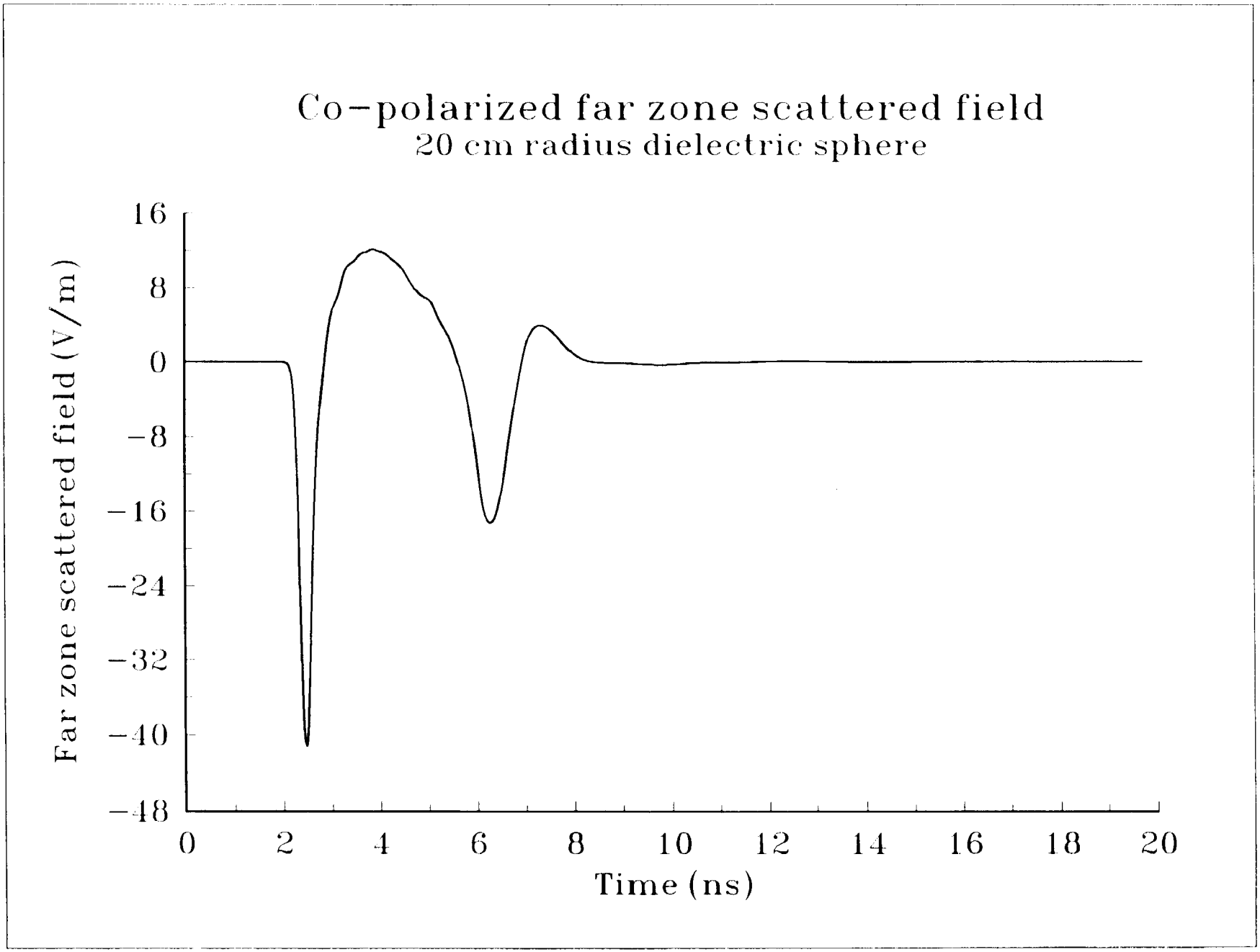
Co-polarized far zone scattered field
20 cm radius dielectric sphere
Far zone scattered field (V/m)
16
8
0
-8
-16
-24
-32
-40
-48
0
2
4
6
8
10
12
14
16
18
20
Time (ns)

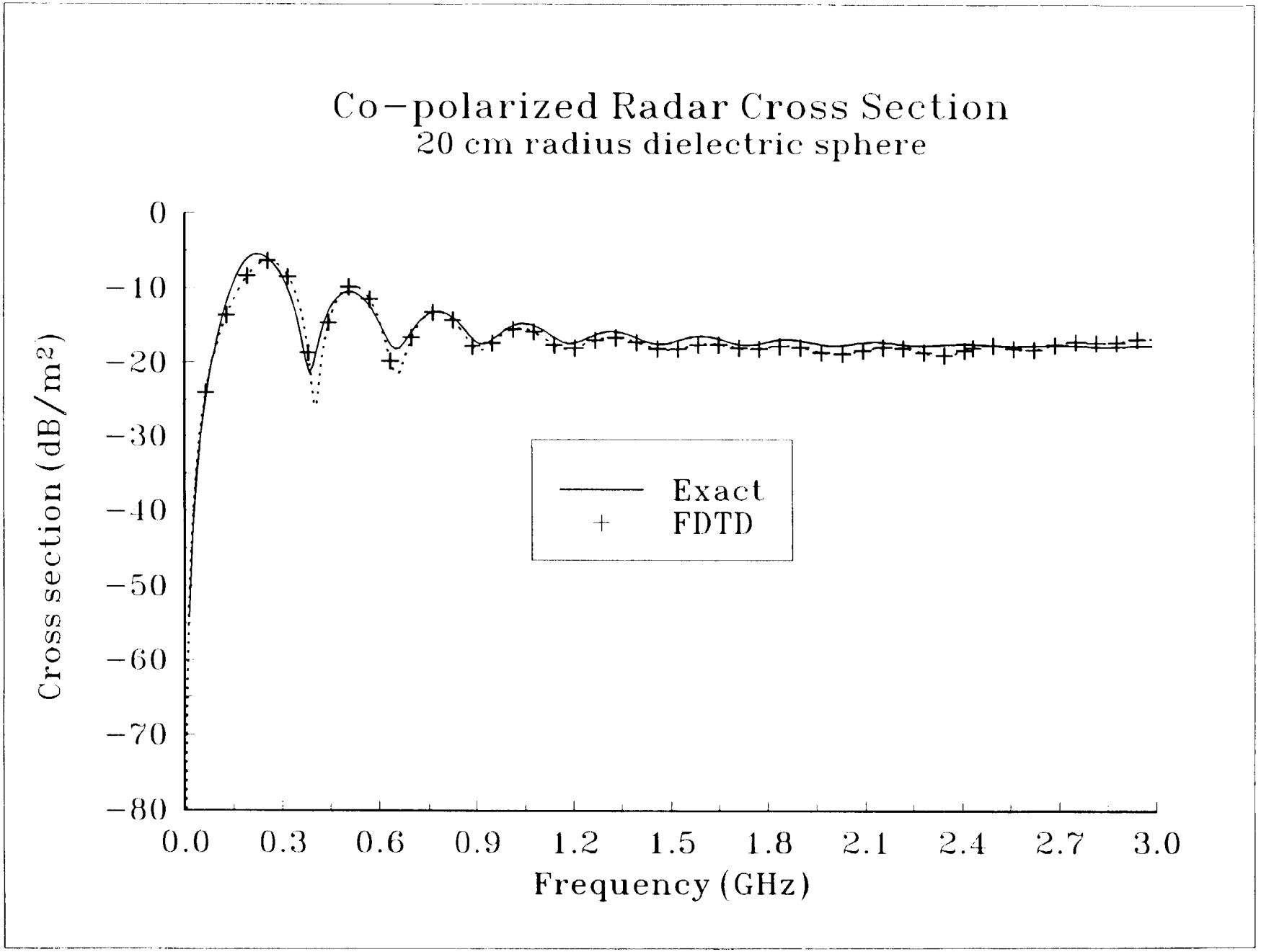
Co-polarized Radar Cross Section
20 cm radius dielectric sphere
Cross section (dB/m²)
0
−10
−20
−30
−40
−50
−60
−70
−80
0.0
0.3
0.6
0.9
1.2
1.5
1.8
2.1
2.4
2.7
3.0
Frequency (GHz)
Exact
FDTD

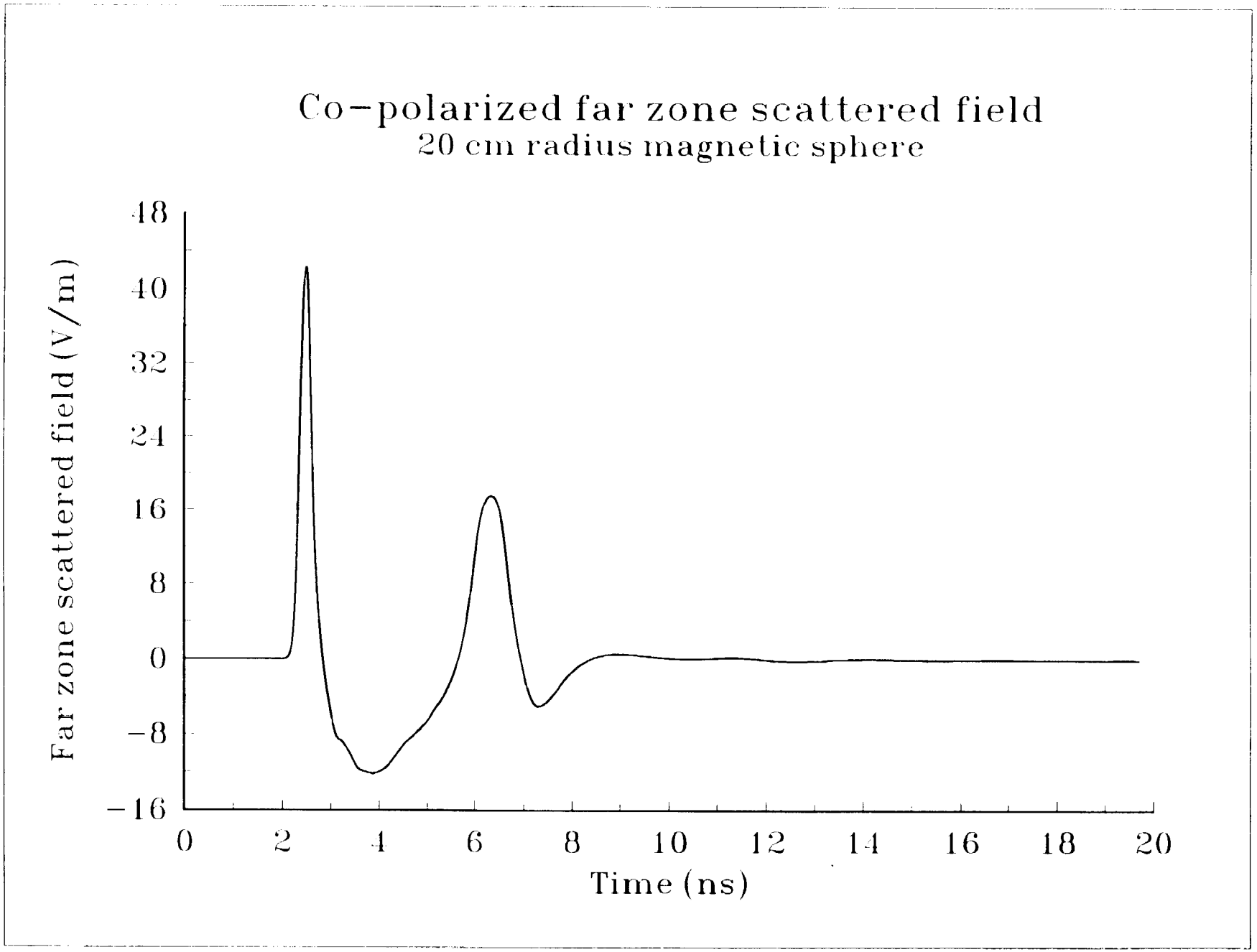
Co-polarized far zone scattered field
20 cm radius magnetic sphere
Far zone scattered field (V/m)
48
40
32
24
16
8
0
-8
-16
0
2
4
6
8
10
12
14
16
18
20
Time (ns)

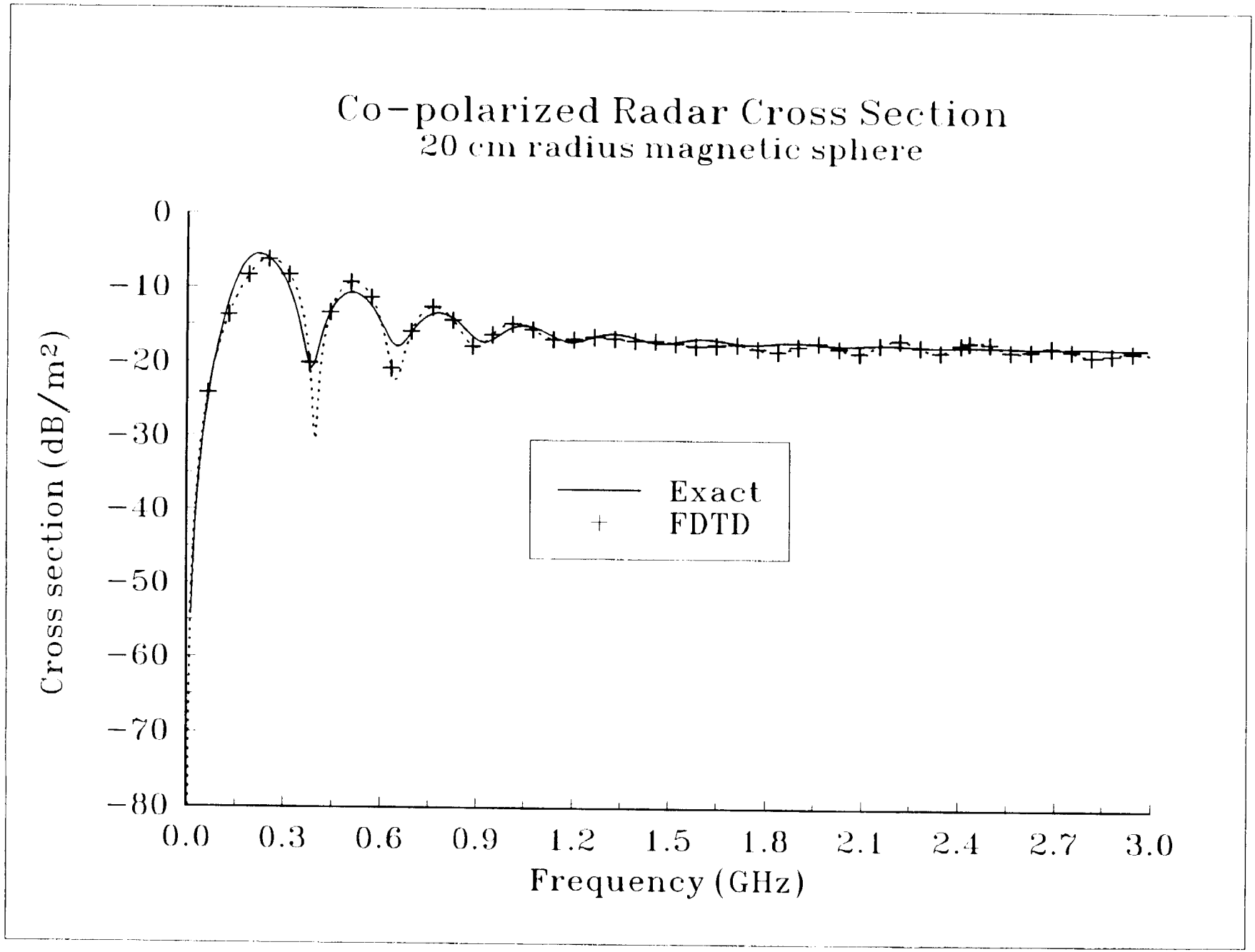
Co-polarized Radar Cross Section
20 cm radius magnetic sphere
Cross section (dB/m²)
0
−10
−20
−30
−40
−50
−60
−70
−80
0.0
0.3
0.6
0.9
1.2
1.5
1.8
2.1
2.4
2.7
3.0
Frequency (GHz)
Exact
FDTD

USER'S MANUAL FOR THREE DIMENSIONAL FDTD VERSION D CODE FOR SCATTERING FROM FREQUENCY-DEPENDENT DIELECTRIC AND MAGNETIC MATERIALS

by

John H. Beggs, Raymond J. Luebbers and Karl S. Kunz
Electrical and Computer Engineering Department
The Pennsylvania State University
University Park, PA 16802

(814) 865-2362

January 1992

TABLE OF CONTENTS

TABLE OF CONTENTS (cont.)

I. INTRODUCTION

The Penn State Finite Difference Time Domain Electromagnetic Scattering Code Version D is a three dimensional numerical electromagnetic scattering code based upon the Finite Difference Time Domain Technique (FDTD). The supplied version of the code is one version of our current three dimensional FDTD code set. This manual provides a description of the code and corresponding results for several scattering problems. The manual is organized into fourteen sections: introduction, description of the FDTD method, operation, resource requirements, Version D code capabilities, a brief description of the default scattering geometry, a brief description of each subroutine, a description of the include file (COMMOND.FOR), a section briefly discussing Radar Cross Section (RCS) computations, a section discussing some scattering results, a sample problem setup section, a new problem checklist, references and figure titles.

II. FDTD METHOD

The Finite Difference Time Domain (FDTD) technique models transient electromagnetic scattering and interactions with objects of arbitrary shape and/or material composition. The technique was first proposed by Yee [1] for isotropic, non-dispersive materials in 1966; and has matured within the past twenty years into a robust and efficient computational method. The present FDTD technique is capabable of transient electromagnetic interactions with objects of arbitrary and complicated geometrical shape and material composition over a large band of frequencies. This technique has recently been extended to include dispersive dielectric materials, chiral materials and plasmas.

In the FDTD method, Maxwell's curl equations are discretized in time and space and all derivatives (temporal and spatial) are approximated by central differences. The electric and magnetic fields are interleaved in space and time and are updated in a second-order accurate leapfrog scheme. The computational space is divided into cells with the electric fields located on the edges and the magnetic fields on the faces (see Figure 1). FDTD objects are defined by specifying dielectric and/or magnetic material parameters at electric and/or magnetic field locations.

Two basic implementations of the FDTD method are widely used for electromagnetic analysis: total field formalism and scattered field formalism. In the total field formalism, the electric and magnetic field are updated based upon the material type present at each spatial location. In the scattered field formalism, the incident waveform is defined analytically and the scattered field is coupled to the incident field through the different material types. For the incident field, any waveform, angle of incidence and polarization is possible. The separation of the incident and

scattered fields conveniently allows an absorbing boundary to be employed at the extremities of the discretized problem space to absorb the scattered fields.

This code is a scattered field code, and the total E and H fields may be found by combining the incident and scattered fields. Any type of field quantity (incident, scattered, or total), Poynting vector or current are available anywhere within the computational space. These fields, incident, scattered and total, may be found within, on or about the interaction object placed in the problem space. By using a near to far field transformation, far fields can be determined from the near fields within the problem space thereby affording radiation patterns and RCS values. The accuracy of these calculations is typically within a dB of analytic solutions for dielectric and magnetic sphere scattering. Further improvements are expected as better absorbing boundary conditions are developed and incorporated.

III. OPERATION

Typically, a truncated Gaussian incident waveform is used to excite the system being modeled, however certain code versions also provide a smooth cosine waveform for convenience in modeling dispersive materials. The interaction object is defined in the discretized problem space with arrays at each cell location created by the discretization. All three dielectric material types for E field components within a cell can be individually specified by the arrays IDONE(I,J,K), IDTWO(I,J,K), IDTHRE(I,J,K). This models arbitrary dielectric materials with $\mu = \mu_0$. By an obvious extension to six arrays, magnetic materials with $\mu \neq \mu_0$ can be modeled.

Scattering occurs when the incident wave, marched forward in time in small steps set by the Courant stability condition, reaches the interaction object. Here a scattered wave must appear along with the incident wave so that the Maxwell equations are satisfied. If the material is a perfectly conductive metal then only the well known boundary condition

$$E_{tan}^{scat} = -E_{tan}^{inc} \tag{1}$$

must be satisfied. For a nondispersive dielectric the requirement is that the total field must satisfy the Maxwell equations in the material:

$$\nabla \times E^{tot} = \nabla \times (E^{inc} + E^{scat}) = -\frac{1}{\mu_o}\frac{\partial H^{tot}}{\partial t} = -\frac{1}{\mu_o}\frac{\partial (H^{inc} + H^{scat})}{\partial t} \tag{2}$$

$$\nabla \times H^{tot} = \nabla \times (H^{inc} + H^{scat}) = \varepsilon \frac{\partial E^{tot}}{\partial t} + \sigma E^{tot} \tag{3}$$

$$= \varepsilon \frac{\partial (E^{inc} + E^{scat})}{\partial t} + \sigma (E^{inc} + E^{scat}) \tag{4}$$

Additionally the incident wave, defined as moving unimpeded through a vacuum in the problem space, satisfies everywhere in the problem the Maxwell equations for free space

$$\nabla \times E^{inc} = -\frac{1}{\mu_o} \frac{\partial H^{inc}}{\partial t} \tag{5}$$

$$\nabla \times H^{inc} = \varepsilon_o \frac{\partial E^{inc}}{\partial t} \tag{6}$$

Subtracting the second set of equations from the first yields the Maxwell equations governing the scattered fields in the material:

$$\nabla \times E^{scat} = -\frac{1}{\mu_o} \frac{\partial H^{scat}}{\partial t} \tag{7}$$

$$\nabla \times H^{scat} = (\varepsilon - \varepsilon_o) \frac{\partial E^{inc}}{\partial t} + \sigma E^{inc} + \varepsilon \frac{\partial E^{scat}}{\partial t} + \sigma E^{scat} \tag{8}$$

Outside the material this simplifies to:

$$\nabla \times E^{scat} = -\frac{1}{\mu_o} \frac{\partial H^{scat}}{\partial t} \tag{9}$$

$$\nabla \times H^{scat} = \varepsilon_o \frac{\partial E^{scat}}{\partial t} \tag{10}$$

Magnetic materials, dispersive effects, non-linearities, etc., are further generalizations of the above approach. Based on the value of the material type, the subroutines for calculating scattered E and H field components branch to the appropriate expression for that scattered field component and

that component is advanced in time according to the selected algorithm. As many materials can be modeled as desired, the number equals the dimension selected for the flags. If materials with behavior different from those described above must be modeled, then after the appropriate algorithm is found, the code's branching structure allows easy incorporation of the new behavior.

IV. RESOURCE REQUIREMENTS

The number of cells the problem space is divided into times the six components per cell set the problem space storage requirements

$$\text{Storage} = NC \times 6 \text{ components/cell} \times 4 \text{ bytes/component} \quad (11)$$

and the computational cost

$$\text{Operations} = NC \times 6 \text{ comp/cell} \times 10 \text{ ops/component} \times N \quad (12)$$

where N is the number of time steps desired.

N typically is on the order of ten times the number of cells on one side of the problem space. More precisely for cubical cells it takes $\sqrt{3}$ time steps to traverse a single cell when the time step is set by the Courant stability condition

$$\Delta t = \frac{\Delta x}{\sqrt{3}c} \qquad \Delta x = \text{cell size dimension} \quad (13)$$

The condition on N is then that

$$N \sim 10 \times (\sqrt{3} NC^{\frac{1}{3}}) \qquad NC^{\frac{1}{3}} \sim \text{number cells on a side of the problem space} \quad (14)$$

The earliest aircraft modeling using FDTD with approximately 30 cells on a side required approximately 500 time steps. For more recent modeling with approximately 100 cells on a side, 2000 or more time steps are used.

For $(100 \text{ cell})^3$ problem spaces, 24 MBytes of memory are required to store the fields. Problems on the order of this size have been run on a Silicon Graphics 4D 220 with 32 MBytes of memory, IBM RISC 6000, an Intel 486 based machine, and VAX 11/785. Storage is only a problem as in the case of the 486 where only 16 MBytes of memory was available. This limited the problem space size to approximately $(80 \text{ cells})^3$.

For $(100 \text{ cell})^3$ problems with approximately 2000 time steps, there is a total of 120×10^9 operations to perform. The speeds of the previously mentioned machines are 24 MFLOPs (4 processor upgraded version), 10 MFLOPS, 1.5 MFLOPS, and 0.2 MFLOPs. The run times are then 5×10^3 seconds, 12×10^3 seconds, 80×10^3 seconds and 600×10^3 seconds, respectively. In hours the times are 1.4, 3.3, 22.2 and 167 hours. Problems of this size are possible on all but the last machine and can in fact be performed on a personal computer (486) if one day turnarounds are permissible.

V. VERSION D CODE CAPABILITIES

The Penn State University FDTD Electromagnetic Scattering Code Version D has the following capabilities:

1) Ability to model lossy dielectric and perfectly conducting scatterers.

2) Ability to model lossy magnetic scatterers.

3) Ability to model dispersive dielectric and dispersive magnetic scatterers. This dispersive FDTD method is now designated $(FD)^2TD$ for Frequency-Dependent Finite Difference Time Domain.

4) First and second order outer radiation boundary condition (ORBC) operating on the electric fields for dielectric and dispersive dielectric scatterers.

5) First and second order ORBC operating on the magnetic fields for magnetic and dispersive magnetic scatterers.

6) Near to far zone transformation capability to obtain far zone scattered fields.

7) Gaussian and smooth cosine incident waveforms with arbitrary incidence angles.

8) Near zone field, current or power sampling capability.

9) Companion code for computing Radar Cross Section (RCS).

VI. DEFAULT SCATTERING GEOMETRY

The code as delivered is set up to calculate the far zone backscatter fields for a 6.67 meter radius, dispersive, Nickel Ferrite sphere. Nickel Ferrite is defined by a frequency dependent permeability given by

where μ_∞ is the infinite frequency permeability, μ_s is the zero

$$\frac{\mu(\omega)}{\mu_0} = \mu_\infty + \frac{\mu_s - \mu_\infty}{1 + j\omega\tau_0} \qquad (15)$$

frequency permeability, τ_0 is the relaxation time and ω is the radian frequency. The Nickel Ferrite parameters are μ_∞=1, μ_s=100 and τ_0=20 ns. The problem space size is 66 by 66 by 66 cells in the x, y and z directions, the cells are 1/3 m cubes, and the incident waveform is a ϕ-polarized smooth cosine pulse with incidence angles of θ=22.5 and ϕ=22.5 degrees. The output data files are included as a reference along with a code (RCS3D.FOR) for computing the frequency domain RCS using these output data files. The ORBC is the second order absorbing boundary condition set forth by Mur [2].

VII. SUBROUTINE DESCRIPTION

In the description for each subroutine, an asterisk (*) will be placed by the subroutine name if that particular subroutine is normally modified when defining a scattering problem.

MAIN ROUTINE

The main routine in the program contains the calls for all necessary subroutines to initialize the problem space and scattering object(s) and for the incident waveform, far zone transformation, field update subroutines, outer radiation boundary conditions and field sampling.

The main routine begins with the include statement and then appropriate data files are opened, and subroutines ZERO, BUILD and SETUP are called to initialize variables and/or arrays, build the object(s) and initialize the incident waveform and miscellaneous parameters, respectively. Subroutine SETFZ is called to intialize parameters for the near to far zone transformation if far zone fields are desired.

The main loop is entered next, where all of the primary field computations and data saving takes place. During each time step cycle, the EXSFLD, EYSFLD, and EZSFLD subroutines are called to update the x, y, and z components of the scattered electric field. The six electric field outer radiation boundary conditions (RADE??) are called next to absorb any outgoing scattered fields for perfectly conducting, dielectric, or dispersive dielectric scatterers. Time is then advanced 1/2 time step according to the Yee algorithm and then the HXSFLD, HYSFLD, AND HZSFLD subroutines are called to update the x, y, and z components of scattered magnetic field. The six magnetic field

outer radiation boundary conditions (RADH??) are called next to absorb any outgoing scattered fields for magnetic or dispersive magnetic scatterers. Time is then advanced another 1/2 step and then either near zone fields are sampled and written to disk in DATSAV, and/or the near zone to far zone vector potentials are updated in SAVFZ. The parameter NZFZ (described later) in the common file defines the type of output fields desired.

After execution of all time steps in the main field update loop, subroutine FAROUT is called if far zone fields are desired to compute the far zone fields and write them to disk. At this point, the execution is complete.

SUBROUTINE SETFZ

This subroutine initializes the necessary parameters required for far zone field computations. The code as furnished computes backscatter far zone fields and can compute bistatic far zone fields for one scattering angle (i.e. one θ and ϕ angle). Refer to reference [3] for a complete description of the near to far zone transformation. Other versions of this subroutine provide for multiple bistatic angles.

SUBROUTINE SAVFZ

This subroutine updates the near zone to far zone vector potentials.

SUBROUTINE FAROUT

This subroutine changes the near zone to far zone vector potentials to far zone electric field θ and ϕ components and writes them to disk.

SUBROUTINE BUILD *

This subroutine "builds" the scattering object(s) by initializing the IDONE, IDTWO, IDTHRE, IDFOR, IDFIV and IDSIX arrays. The IDONE-IDTHRE arrays are for specifying perfectly conducting, lossy dielectrics and dispersive dielectric materials. The IDFOR-IDSIX arrays are for lossy magnetic and dispersive magnetic materials. The reason for the separate arrays is so the user can independently control the exact placement of dielectric and magnetic material in the Yee cells. Refer to Figure 1 for a diagram of the basic Yee cell. For example, setting an element of the IDONE array at some I,J,K location is actually locating dielectric material at a cell edge whose center location is I+0.5,J,K. Setting an element of the IDFOR array at some I,J,K location is actually locating magnetic material perpendicular to a cell face whose center location is I,J+0.5,K+0.5, or equivalently, locating magnetic material at an edge on the dual H field mesh. The difference between the IDONE

and IDFOR array locations is a direct result of the field offsets in the Yee cell (see Figure 1). Thus, materials with diagonal permittivity and/or diagonal permeability tensors can be modeled. The default material type for all ID??? arrays is 0, or free space. By initializing these arrays to values other than 0, the user is defining an object by determining what material types are present at each spatial location. Other material types available for IDONE-IDTHRE are 1 for perfectly conducting objects, 2-9 for lossy non-magnetic dielectrics, 20-29 for dispersive dielectrics. IDONE-IDTHRE are normally set to 0 for magnetic scatterers. Other material types available for IDFOR-IDSIX are 10-19 for lossy magnetic materials and 30-39 for dispersive magnetic materials. IDFOR-IDSIX are normally set to 0 for perfectly conducting or dielectric scatterers. If the user wants a material with both dielectric and magnetic properties (i.e. permittivity other than ϵ_0 for magnetic materials, and permeability other than μ_0 for dielectric materials), then he/she must define IDONE-IDSIX for that particular material. This subroutine also has a section that checks the ID??? arrays to determine if legal material types have been defined throughout the problem space. The actual non-dispersive material parameters (ϵ, μ, σ, and σ^*) are defined in subroutine SETUP. The dispersive material parameters (ϵ_s, ϵ_∞, τ_0, σ, μ_s, μ_∞, τ_0, and σ^*) are also defined in a separate section in SETUP. The default geometry is a 6.67 m radius, dispersive, Nickel Ferrite sphere.

The user must be careful that his/her object created in the BUILD subroutine is properly formed. There is not a direct one-to-one correspondence between the dielectric and magnetic ID??? arrays. However, one can define a correspondence, so that code used to generate a dielectric object can be modified to generate a magnetic object.

To see this consider that we have set the permittivity at cell locations corresponding to

EX(I,J,K), EY(I,J,K), EZ(I,J,K)

using the IDONE, IDTWO, and IDTHRE arrays respectively. This determines one corner of a dielectric cube. If we wish to define the corner of a corresponding magnetic cube, offset 1/2 cell in the x, y, z directions, we would set the locations of the magnetic fields

HX(I+1,J,K), HY(I,J+1,K), HZ(I,J,K+1)

as magnetic material using the IDFOR, IDFIV, and IDSIX arrays.

This example indicates the following correspondence between BUILDing dielectric and magnetic objects:

Dielectric Object		Magnetic Object
IDONE(I,J,K)	=	IDFOR(I+1,J,K)
IDTWO(I,J,K)	=	IDFIV(I,J+1,K)
IDTHRE(I,J,K)	=	IDSIX(I,J,K+1)

To illustrate this for a somewhat more complicated case, consider an example of a 3x3 cell dielectric plate located in the XY plane at K=5. The plate can be generated with the following FORTRAN lines:

```
     DO 20 J=4,7
       DO 10 I=4,7
        IF(I.NE.7)IDONE(I,J,K)=2
        IF(J.NE.7)IDTWO(I,J,K)=2
10     CONTINUE
20   CONTINUE
```

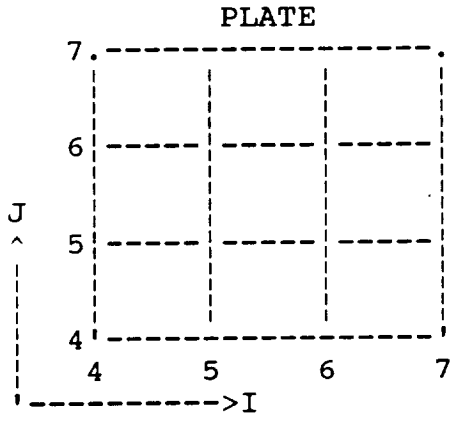

If the same FORTRAN lines were used to try to generate a magnetic plate, the object generated would actually be unconnected:

```
     DO 20 J=4,7
       DO 10 I=4,7
        IF(I.NE.7)IDFOR(I,J,K)=11
        IF(J.NE.7)IDFIV(I,J,K)=11
10     CONTINUE
20   CONTINUE
```

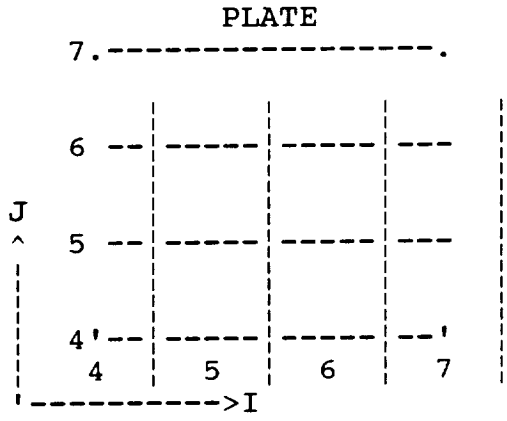

The correct way to build the magnetic plate is with the following FORTRAN code:

```
     DO 20 J=4,7
       DO 10 I=4,7
         IF(I.NE.4)IDFOR(I,J,K)=11

         IF(J.NE.4)IDFIV(I,J,K)=11
10     CONTINUE
20   CONTINUE
```

This is equivalent to the correspondence relationship given above. See comments in the BUILD subroutine for further explanation of the ID??? arrays.

When it is important to place the object in the center of the problem space (to have lowest possible cross-pol scattering for symmetric objects), NX etc. should be odd for dielectrics and even for magnetics. This is due to the field locations in the Yee cell and also the placement of the E and H field absorbing boundary condition surfaces.

If the object being modeled has curved surfaces, edges, etc. that are at an angle to one or more of the coordinate axes, then that shape must be approximately modeled by lines and faces in a "stair-stepped" (or stair-cased) fashion. This stair-cased approximation introduces errors into computations at higher frequencies. Intuitively, the error becomes smaller as more cells are used to stair-case a particular object. Thus, the default Nickel Ferrite sphere scattering geometry is a stair-cased sphere.

When the user's test object is dielectric it is apparently better to use the Mur E field boundary formulation. For a magnetic scattering object it seems better to use the Mur H field boundary formulation. The reason for this has to do with the reactive part of the energy (near zone fields) reaching the absorbing boundary surface. These near zone fields differ for magnetic and dielectric objects, even for dual objects where the far fields are essentially identical.

One final comment on building dual dielectric vs magnetic objects can be explained by considering the duality between magnetic and dielectric materials. In testing the code, it was helpful to test dual dielectric/magnetic objects since they scatter identically in the far zone. In specifying the material of a magnetic scatterer to be the dual of a dielectric, the following transformation must be applied:

DIELECTRIC	<--DUAL-->	MAGNETIC
E field	<--------->	H field
H field	<--------->	-E field
ϵ	<--------->	μ
μ	<--------->	ϵ
ß (k)	<--------->	ß (k)
σ	<--------->	$\sigma \cdot (\mu_0/\epsilon_0) = \sigma^*$

The somewhat surprising entry in this table is the relationship between the dielectric and magnetic conductivities. The reason why the magnetic conductivity, σ^*, for magnetic materials has to be scaled as indicated is that for duality to be applied the free

space impedance must be inverted. Although this is not generally possible for actual problems, identical far zone scattering for dielectric and magnetic scatterers can be achieved by this scaling of σ^* as above and realizing that E and H scattered field to incident field ratios will not invert. This scaling of σ^* is why conductivity for magnetic materials is usually not a dominating feature, and in fact is often neglected.

SUBROUTINE DCUBE

This subroutine builds cubes of dielectric material by defining four each of IDONE, IDTWO and IDTHRE components corresponding to one spatial cube of dielectric material. It can also be used to define thin (i.e. up to one cell thick) dielectric or perfectly conducting plates. Refer to comments within DCUBE for a description of the arguments and usage of the subroutine. This subroutine could be modified to build cubes and/or plates of magnetic materials by using a triple do-loop in BUILD (after calls to DCUBE) over coordinate indices I, J, K and applying the correspondence between the IDONE-IDTHRE and IDFOR-IDSIX arrays that was previously discussed.

SUBROUTINE SETUP *

This subroutine initializes many of the constants required for incident field definition, field update equations, outer radiation boundary conditions and material parameters. The material parameters ϵ, μ, σ and σ^* are defined for each material type (non-dispersive) using the material arrays EPS, XMU, SIGMA and SIGMAC respectively. The array EPS is used for the total permittivity, XMU is used for the total permeability, SIGMA is used for the electric conductivity and SIGMAC is used for the magnetic conductivity (useful for running dual problems). These arrays are initialized in SETUP to free space material parameters for all material types and then the user is required to modify these arrays for his/her scattering materials. Thus, for the lossy dielectric material type 2, the user must define EPS(2) and SIGMA(2).

For dispersive dielectric and magnetic materials, different material parameter arrays are used. The functional form of the frequency dependent permittivity/permeability that was implemented in the code is the Debye relaxation [4] with an effective DC conductivity given by

$$\epsilon(\omega) = \epsilon' - j\epsilon'' = \epsilon_\infty \epsilon_0 + \epsilon_0 \chi_e(\omega) + \frac{\sigma}{j\omega} \qquad (16)$$

where the frequency dependent electric susceptibility function is defined as

$$\chi_e(\omega) = \frac{\epsilon_s - \epsilon_\infty}{1 + j\omega\tau_0} \tag{17}$$

where ϵ_∞ is the infinite frequency permittivity, ϵ_s is the zero frequency permittivity, τ_0 is the relaxation time, σ is the effective electric conductivity, and ω is the radian frequency. The same expressions were used for the frequency dependent permeability and can be written from equations (16) and (17) by replacing ϵ by μ and σ by σ^*. The corresponding time domain susceptibility function is given by

$$\chi_e(t) = \left(\frac{\epsilon_s - \epsilon_\infty}{\tau_0}\right) e^{\left(-t/\tau_0\right)} u(t) \tag{18}$$

The FDTD implementation of frequency dependent permittivity and/or permeability involves a convolution with the electric and/or magnetic field and interested readers are referred to references [5-6] for further details.

For dispersive dielectric materials, the corresponding material parameter arrays are EPSINF (ϵ_∞), EPSSTA (ϵ_s), RELAXT (τ_0), and RELSIG (σ). For dispersive magnetic materials, the arrays are XMUINF (μ_∞), XMUSTA (μ_s), RELAXT (τ_0) and RELSIG (σ^*). These dispersive material parameters are defined under the DISPERSIVE SETUP portion of the subroutine. The remainder of the subroutine computes constants used in field update equations and boundary conditions and writes the diagnostics file.

SUBROUTINE EXSFLD

This subroutine updates all x components of scattered electric field at each time step except those on the outer boundaries of the problem space. IF statements based upon the IDONE array are used to determine the type of material present and the corresponding update equation to be used. These scattered field equations are based on the development given in [7].

SUBROUTINE EYSFLD

This subroutine updates all y components of scattered electric field at each time step except those on the outer boundaries of the problem space. IF statements based upon the IDTWO array are used to determine the type of material present

and the corresponding update equation to be used.

SUBROUTINE EZSFLD

This subroutine updates all z components of scattered electric field at each time step except those on the outer boundaries of the problem space. IF statements based upon the IDTHRE array are used to determine the type of material present and the corresponding update equation to be used.

SUBROUTINES RADEYX, RADEZX, RADEZY, RADEXY, RADEXZ and RADEYZ

These subroutines apply the outer radiation boundary conditions to the scattered electric field on the outer boundaries of the problem space for non-magnetic scatterers. The user controls selection of these routines through the parameter MAGNET (described later).

SUBROUTINE HXSFLD

This subroutine updates all x components of scattered magnetic field at each time step. IF statements based upon the IDFOR array are used to determine the type of material present and the corresponding update equation to be used.

SUBROUTINE HYSFLD

This subroutine updates all y components of scattered magnetic field at each time step. IF statements based upon the IDFIV array are used to determine the type of material present and the corresponding update equation to be used.

SUBROUTINE HZSFLD

This subroutine updates all z components of scattered magnetic field at each time step. IF statements based upon the IDSIX array are used to determine the type of material present and the corresponding update equation to be used.

SUBROUTINES RADHXZ, RADHYX, RADHZY, RADHXY, RADHYZ and RADHZX

These subroutines apply the outer radiation boundary conditions to the scattered magnetic field on the outer boundaries of the problem space for magnetic scatterers. The user controls selection of these routines through the parameter MAGNET (described later).

SUBROUTINE DATSAV *

This subroutine samples near zone scattered field quantities and saves them to disk. This subroutine is where the quantities to be sampled and their spatial locations are to be specified and is only called if near zone fields only are desired or if both near and far zone fields are desired. Total field quantities can also be sampled. See comments within the subroutine for specifying sampled scattered and/or total field quantities. When sampling magnetic fields, remember the $\delta t/2$ time difference between E and H when writing the fields to disk. Sections of code within this subroutine determine if the sampled quantities and the spatial locations have been properly defined.

FUNCTIONS EXI, EYI, EZI, HXI, HYI and HZI

These functions are called to compute the x, y and z components of incident electric and magnetic field, respectively. The functional form of the incident field is contained in a separate function SOURCE.

FUNCTION SOURCE *

This function contains the functional form of the incident field. The code as furnished uses the smooth cosine form of the incident field. An incident Gaussian pulse is also available by uncommenting the required lines and commenting out the smooth cosine pulse. Thus, this function need only be modified if the user changes the incident pulse from smooth cosine to Gaussian. Currently, only the smooth cosine pulse can be used for scattering from dispersive targets. A slight improvement in computing speed and vectorization may be achieved by moving this function inside each of the incident field functions EXI, EYI and so on.

FUNCTIONS DEXI, DEYI, DEZI, DHXI, DHYI and DHZI

These functions are called to compute the x, y and z components of the time derivative of incident electric and magnetic field, respectively. The functional form of the incident field is contained in a separate function DSRCE.

FUNCTIONS DEXIXE, DEYIXE, DEZIXE, DHXIXE, DHYIXE and DHZIXE

These functions compute the x, y and z components of the convolution of the time derivative of the incident field with the electric or magnetic Debye susceptibility function χ.

FUNCTION DSRCE *

This function contains the functional form of the time derivative of the incident field. The code as furnished uses the time derivative of the smooth cosine form of the incident field. A Gaussian pulse time derivative is also available by uncommenting the required lines and commenting out the smooth cosine pulse. Thus, the function need only be modified if the user changes from the smooth cosine to Gaussian pulse. Again, a slight improvement in computing speed and vectorization may be achieved by moving this function inside each of the time derivative incident field functions DEXI, DEYI and so on.

FUNCTION DCONV

This function evaluates the convolution of the time derivative of the incident field with the Debye susceptibility function χ.

SUBROUTINE ZERO

This subroutine initializes various arrays and variables to zero.

VIII. INCLUDE FILE DESCRIPTION (COMMOND.FOR) *

The include file, COMMOND.FOR, contains all of the arrays and variables that are shared among the different subroutines. This file will require the most modifications when defining scattering problems. A description of the parameters that are normally modified follows.

The parameters NX, NY and NZ specify the size of the problem space in cells in the x, y and z directions respectively. For problems where it is crucial to center the object within the problem space, then NX, NY and NZ should be odd for dielectric scatterers and even for magnetic scatterers. The parameter NTEST defines the number of near zone quantities to be sampled and NZFZ defines the field output format. Set NZFZ=0 for near zone fields only, NZFZ=1 for far zone fields only and NZFZ=2 for both near and far zone fields. Parameter MAGNET is used to define magnetic scatterers and it controls the choice of RADE?? versus RADH?? absorbing boundary subroutines. It is set to 0 for dielectric scatterers and to 1 for magnetic scatterers. Parameter NUMMAT defines the total number of material types that are available for use. NEDISP and NHDISP define the number of dispersive dielectric and magnetic materials that are being used. Parameter NSTOP defines the maximum number of time steps. DELX, DELY, and DELZ (in meters) define the cell size in the x, y and z directions respectively. The θ and ϕ incidence angles (in degrees) are defined by THINC and PHINC respectively and the polarization is defined by ETHINC and EPHINC. ETHINC=1.0, EPHINC=0.0 for θ-polarized incident field and ETHINC=0.0,

EPHINC=1.0 for ϕ-polarized incident fields. Parameters AMP and BETA define the maximum amplitude and the e^{-2} temporal width of the incident pulse respectively. BETA automatically adjusts when the cell size is changed and normally should not be changed by the user. The far zone scattering angles are defined by THETFZ and PHIFZ. The code as furnished performs backscatter computations, but these parameters could be modified for a bistatic computation.

IX. RCS COMPUTATIONS

A companion code, RCS3D.FOR, has been included to compute RCS versus frequency. It uses the file name of the $(FD)^2TD$ far zone output data (FZOUT3D.DAT) and writes data files of far zone electric fields versus time (FZTIME.DAT) and RCS versus frequency (3DRCS.DAT). The RCS computations are performed up to the 10 cell/λ_0 frequency limit. Refer to comments within this code for further details.

X. RESULTS

As previously mentioned, the code as furnished models a 6.67 m radius, dispersive, Nickel Ferrite sphere and computes backscatter far zone scattered fields at angles of θ=22.5 and ϕ=22.5 degrees. Results are included for 0.25 dB loaded dielectric and magnetic foam spheres, 60 dB dielectric and magnetic foam spheres and the Nickel Ferrite magnetic sphere. The material parameters for 0.25 dB and 60 dB loaded foam are:

0.25 DB FOAM		60 DB FOAM
1.16	ϵ_s	41.0
1.01	ϵ_∞	1.6
0.6497 ns	τ_0	0.3450 ns
2.954E-04 S/m	σ	3.902E-01 S/m

The magnetic materials are duals of the above as described earlier with the relative conductivity scaled by the ratio μ_0/ϵ_0. The Nickel Ferrite parameters are μ_∞=1, μ_s=100, τ_0=20 ns and σ^*=0.0. For the 0.25 dB foams there are 10 cells per wavelength at approximately 3.0 GHz. For the 60 dB foam there are 10 cells per wavelength at approximately 2.35 GHz, as the 60 dB foam has a higher dielectric constant.

Figures 2-10 show the real and imaginary parts of the 0.25 dB and 60 dB foam permeability, the real and imaginary parts of the Nickel Ferrite permeability, and the magnetic susceptibilities versus time for all three materials.

Figures 11-14 show the co-polarized far zone electric field versus time and the co-polarized RCS for the 0.25 dB and 60 dB dielectric foam spheres respectively.

Figures 15-18 show the co-polarized far zone electric field versus time and the co-polarized RCS for the 0.25 dB and 60 dB mangetic foam spheres respectively.

Figures 19-20 show the co-polarized far zone electric field versus time and the co-polarized RCS for the default Nickel Ferrite sphere using the dispersive FDTD method and the non-dispersive FDTD method. For the non-dispersive method, an equivalent permeability and magnetic conductivity were defined at 30 MHz from (16) with μ replacing ϵ as

$$\mu_r = \mu' \big|_{(\omega=2\pi 30E6)}, \quad \sigma^* = \omega\mu'' \mu_0 \big|_{(\omega=2\pi 30E6)}$$

XI. SAMPLE PROBLEM SETUP

The code as furnished models a 6.67 m radius Nickel Ferrite dispersive magnetic sphere and computes backscatter far zone scattered fields at angles of θ=22.5 and ϕ=22.5 degrees. The corresponding output data files are also provided, along with a code to compute Radar Cross Section using these data files. In order to change the code to a new problem, many different parameters need to be modified. A sample problem setup will now be discussed.

Suppose that the problem to be studied is RCS backscatter versus frequency from a 28 cm by 31 cm perfectly conducting plate with a 3 cm dielectric coating with a dielectric constant of $4\epsilon_0$ using a θ-polarized field. The backscatter angles are θ=30.0 and ϕ=60.0 degrees and the frequency range is up to 3 Ghz.

Since the frequency range is up to 3 Ghz, the cell size must be chosen appropriately to resolve the field IN ANY MATERIAL at the highest frequency of interest. A general rule is that the cell size should be 1/10 of the wavelength at the highest frequency of interest. For difficult geometries, 1/20 of a wavelength may be necessary. The free space wavelength at 3 GHz is λ_0=10 cm and the wavelength in the dielectric coating at 3 GHz is 5 cm. The cell size is chosen as 1 cm, which provides a resolution of 5 cells/λ in the dielectric coating and 10 cells/λ_0 in free space. Numerical studies have shown that choosing the cell size $\leq$ 1/4 of the shortest wavelength in any material is the practical lower limit. Thus the cell size of 1 cm is barely adequate. The cell size in the x, y and z directions is set in the common file through variables DELX, DELY and DELZ. Next the problem space size must be large enough to accomodate the

scattering object, plus at least a five cell boundary (10 cells is more appropriate) on every side of the object to allow for the far zone field integration surface. It is advisable for plate scattering to have the plate centered in the x and y directions of the problem space in order to reduce the cross-polarized backscatter and to position the plate low in the z direction to allow strong specular reflections multiple encounters with the ORBC. A 10 cell border is chosen, and the problem space size is chosen as 49 by 52 by 49 cells in the x, y and z directions respectively. As an initial estimate, allow 2048 time steps so that energy trapped within the dielectric layer will radiate. Thus parameters NX, NY and NZ in COMMOND.FOR would be changed to reflect the new problem space size, and parameter NSTOP is changed to 2048. If all transients have not been dissipated after 2048 time steps, then NSTOP will have to be increased. Truncating the time record before all transients have dissipated will corrupt frequency domain results. Parameter NZFZ must be equal to 1 since we are interested in far zone fields only. Parameter MAGNET must be equal to 0 for the dielectric scatterer. To build the object, the following lines are inserted into the BUILD subroutine:

```
C
C     BUILD THE DIELECTRIC SLAB FIRST
C
      ISTART=11
      JSTART=11
      KSTART=11
      NXWIDE=28
      NYWIDE=31
      NZWIDE=3
      MTYPE=2
      CALL DCUBE(ISTART,JSTART,KSTART,NXWIDE,NYWIDE,NZWIDE,MTYPE)
C
C     BUILD PEC PLATE NEXT
C
      ISTART=11
      JSTART=11
      KSTART=11
      NXWIDE=28
      NYWIDE=31
      NZWIDE=0
      MTYPE=1
      CALL DCUBE(ISTART,JSTART,KSTART,NXWIDE,NYWIDE,NZWIDE,MTYPE)
```

The PEC plate is built last on the bottom of the dielectric slab to avoid any air gaps between the dielectric material and the PEC plate. In the common file, the incidence angles THINC and PHINC have to be changed to 30.0 and 60.0 respectively, the cell sizes (DELX, DELY, DELZ) are set to 0.01, and the polarization is set to ETHINC=1.0 and EPHINC=0.0 for θ-polarized fields. Since dielectric material 2 is being used for the dielectric coating, the constitutive parameters EPS(2) and

SIGMA(2) are set to $4\epsilon_0$ and 0.0 respectively, in subroutine SETUP. This completes the code modifications for the sample problem.

XII. NEW PROBLEM CHECKLIST

This checklist provides a quick reference to determine if all parameters have been defined properly for a given scattering problem. A reminder when defining quantities within the code: use MKS units and specify all angles in degrees.

COMMOND.FOR:

1) Is the problem space sized correctly? (NX, NY, NZ)

2) For near zone fields, is the number of sample points correct? (NTEST)

3) Is parameter NZFZ defined correctly for desired field outputs?

4) Is parameter MAGNET defined correctly for the type of scatterer?

5) Is the number of dispersive dielectric (NEDISP) and dispersive magnetic (NHDISP) materials defined correctly?

6) Is the number of time steps correct? (NSTOP)

7) Are the cell dimensions (DELX, DELY, DELZ) defined correctly?

8) Are the incidence angles (THINC, PHINC) defined correctly?

9) Is the polarization of the incident wave defined correctly (ETHINC, EPHINC)?

10) For other than backscatter far zone field computations, are the scattering angles set correctly? (THETFZ, PHIFZ)

SUBROUTINE BUILD:

1) Is the object completely and correctly specified?

SUBROUTINE SETUP:

1) Are the constitutive parameters for each material specified correctly? (EPS, XMU, SIGMA, SIGMAC)

2) Are the constitutive parameters for each dispersive material defined correctly? (EPSSTA, EPSINF, RELAXT, RELSIG, XMUINF, XMUSTA, RELAXT, RELSIG)

FUNCTIONS SOURCE and DSRCE:

1) If the smooth cosine pulse is not desired, is it commented out and the Gaussian pulse uncommented?

SUBROUTINE DATSAV:

1) For near zone fields, are the sampled field types and spatial locations correct for each sampling point? (NTYPE, IOBS, JOBS, KOBS)

XIII. REFERENCES

[1] K. S. Yee, "Numerical solution of initial boundary value problems involving Maxwell's equations in isotropic media," IEEE Trans. Antennas Propagat., vol. AP-14, pp. 302-307, May 1966.

[2] G. Mur, "Absorbing boundary conditions for the Finite-Difference approximation of the Time-Domain Electromagnetic-Field Equations," IEEE Trans. Electromagn. Compat., vol. EMC-23, pp. 377-382, November 1981.

[3] R. J. Luebbers et. al., "A Finite Difference Time-Domain Near Zone to Far Zone Transformation," IEEE Trans. Antennas Propagat., vol. AP-39, no. 4, pp. 429-433, April 1991.

[4] C. Balanis, Advanced Engineering Electromagnetics, New York: Wiley, 1990, pp. 83-84.

[5] R. J. Luebbers et. al., "A frequency-dependent Finite-Difference Time-Domain formulation for dispersive materials," IEEE Trans. Electromagn. Compat., vol. EMC-32, pp. 222-227, August 1990.

[6] R. J. Luebbers et. al., "A frequency-dependent Finite-Difference Time-Domain formulation for transient propagation in plasma," IEEE Trans. Antennas Propagat., vol. AP-39, pp. 429-433, April 1991.

[7] R. Holland, L. Simpson, K. S. Kunz, "Finite-Difference Analysis of EMP Coupling to Lossy Dielectric Structures," IEEE Trans. Electromagn. Compat., vol. EMC-22, pp. 203-209, August 1980.

XI. FIGURE TITLES

Fig. 1 Standard three dimensional Yee cell showing placement of electric and magnetic fields.

Fig. 2 Real part of relative permeability versus frequency for 0.25 dB magnetic foam.

Fig. 3 Imaginary part of relative permeability versus frequency for 0.25 dB magnetic foam.

Fig. 4 Relative magnetic susceptibility versus time for 0.25 dB magnetic foam.

Fig. 5 Real part of relative permeability versus frequency for 60 dB magnetic foam.

Fig. 6 Imaginary part of relative permeability versus frequency for 60 dB magnetic foam.

Fig. 7 Relative magnetic susceptibility versus time for 60 dB magnetic foam.

Fig. 8 Real part of relative permeability versus frequency for Nickel Ferrite with $\mu_s = 100$, $\mu_\infty = 1$, $\tau_0 = 20$ ns.

Fig. 9 Imaginary part of relative permeability versus frequency for Nickel Ferrite with $\mu_s = 100$, $\mu_\infty = 1$, $\tau_0 = 20$ ns.

Fig. 10 Relative magnetic susceptibility versus time for Nickel Ferrite.

Fig. 11 Co-polarized far zone scattered field versus time for 0.25 dB dielectric foam sphere with 20 cm radius.

Fig. 12 Co-polarized Radar Cross Section versus frequency for 0.25 dB dielectric foam sphere with 20 cm radius.

Fig. 13 Co-polarized far zone scattered field versus time for 0.25 dB magnetic foam sphere with 20 cm radius.

Fig. 14 Co-polarized Radar Cross Section versus frequency for 0.25 dB magnetic foam sphere with 20 cm radius.

Fig. 15 Co-polarized far zone scattered field versus time for 60 dB dielectric foam sphere with 20 cm radius.

Fig. 16 Co-polarized Radar Cross Section versus frequency for 60 dB dielectric foam sphere with 20 cm radius.

Fig. 17 Co-polarized far zone scattered field versus time for 60 dB magnetic foam sphere with 20 cm radius.

Fig. 18 Co-polarized Radar Cross Section versus frequency for 60 dB magnetic foam sphere with 20 cm radius.

Fig. 19 Co-polarized far zone scattered field versus time for Nickel Ferrite sphere with 6.67 m radius using both dispersive FDTD and non-dispersive FDTD.

Fig. 20 Co-polarized Radar Cross Section versus frequency for Nickel Ferrite sphere with 6.67 m radius using both dispersive FDTD and non-dispersive FDTD.

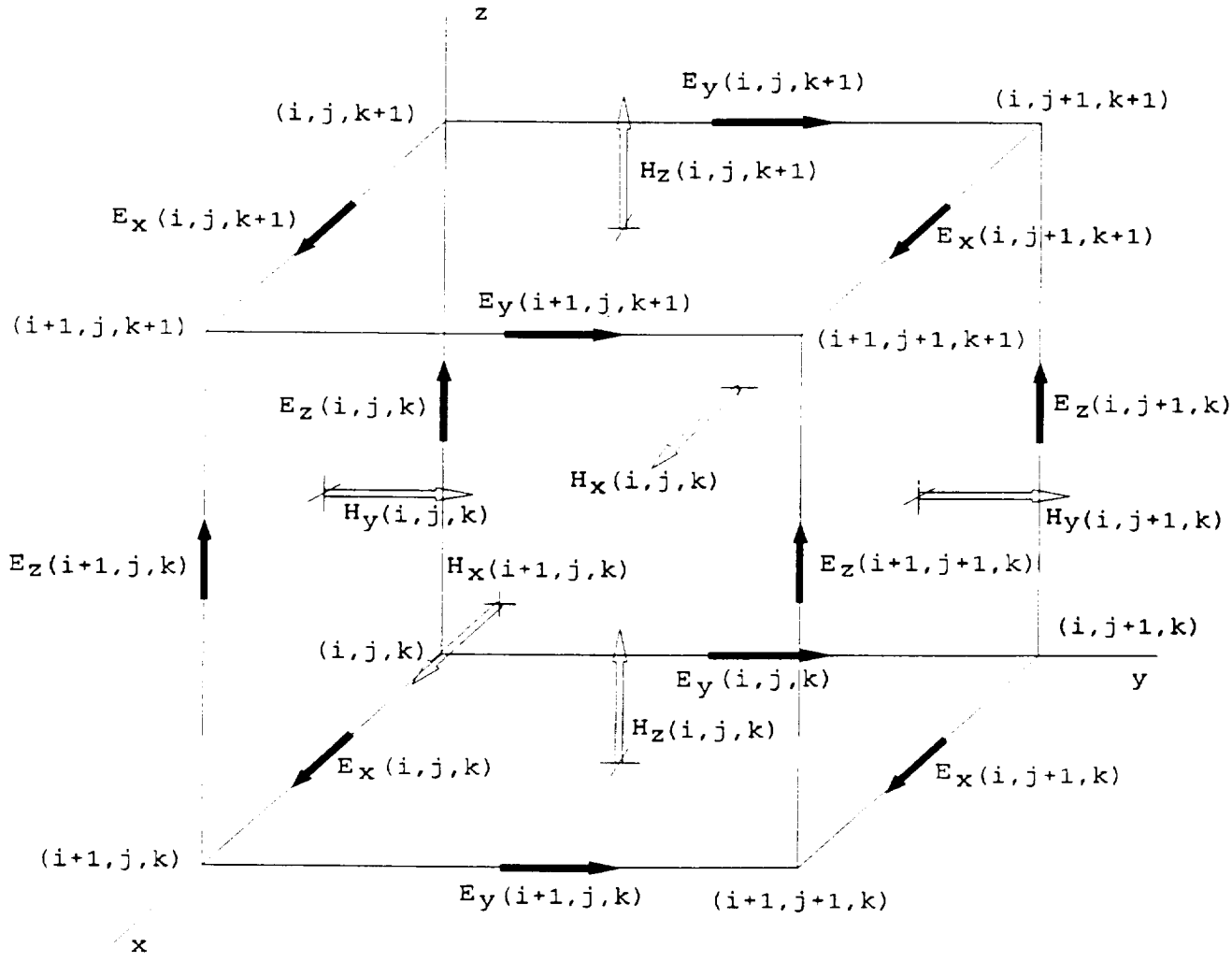
z
Ey(i,j,k+1)
(i,j,k+1)
(i,j+1,k+1)
Hz(i,j,k+1)
Ex(i,j,k+1)
Ex(i,j+1,k+1)
Ey(i+1,j,k+1)
(i+1,j,k+1)
(i+1,j+1,k+1)
Ez(i,j,k)
Ez(i,j+1,k)
Hx(i,j,k)
Hy(i,j,k)
Hy(i,j+1,k)
Ez(i+1,j,k)
Hx(i+1,j,k)
Ez(i+1,j+1,k)
(i,j+1,k)
(i,j,k)
Ey(i,j,k)
y
Hz(i,j,k)
Ex(i,j,k)
Ex(i,j+1,k)
(i+1,j,k)
Ey(i+1,j,k)
(i+1,j+1,k)
x

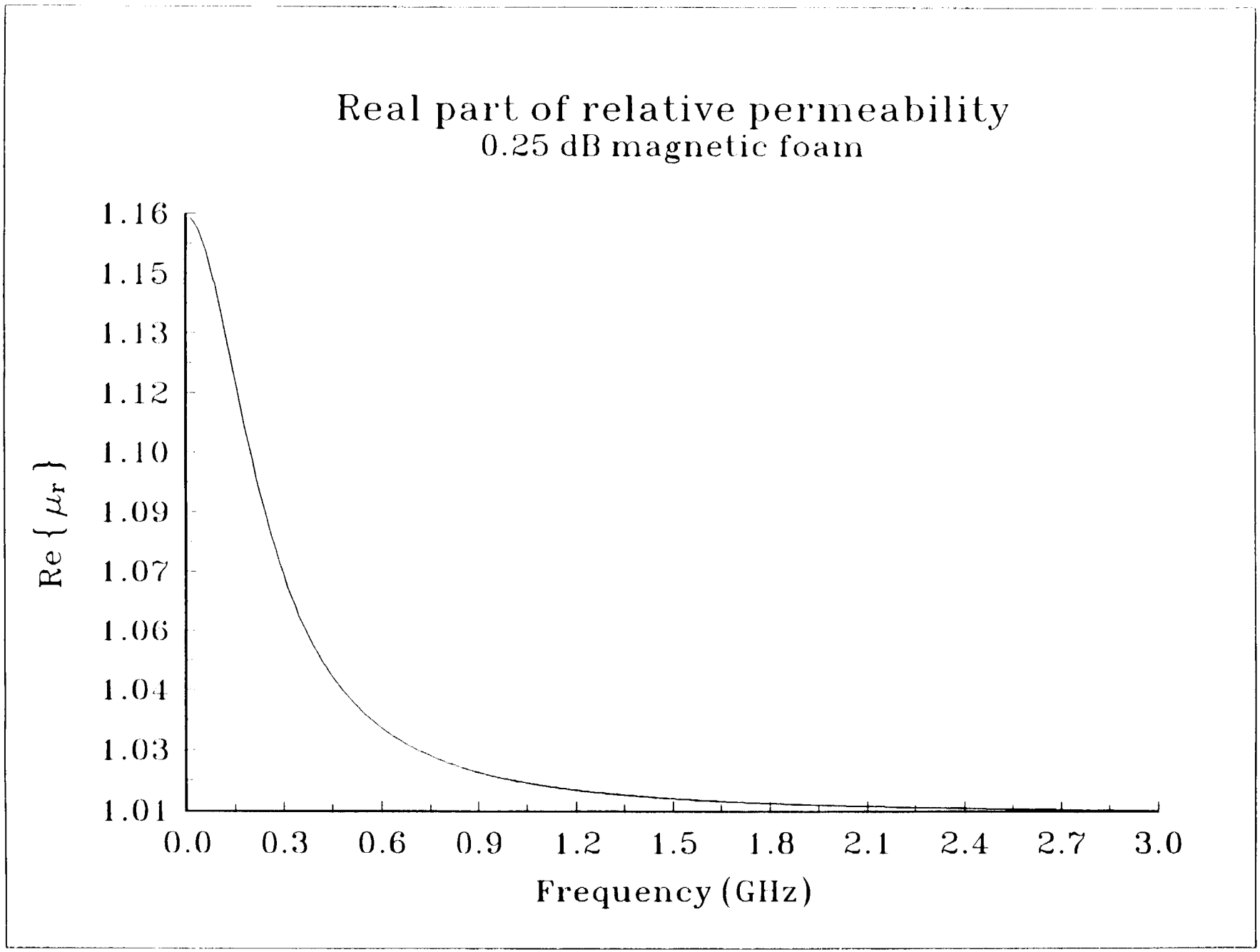
Real part of relative permeability
0.25 dB magnetic foam
1.16
1.15
1.13
1.12
1.10
1.09
1.07
1.06
1.04
1.03
1.01
Re { μ_r }
0.0
0.3
0.6
0.9
1.2
1.5
1.8
2.1
2.4
2.7
3.0
Frequency (GHz)

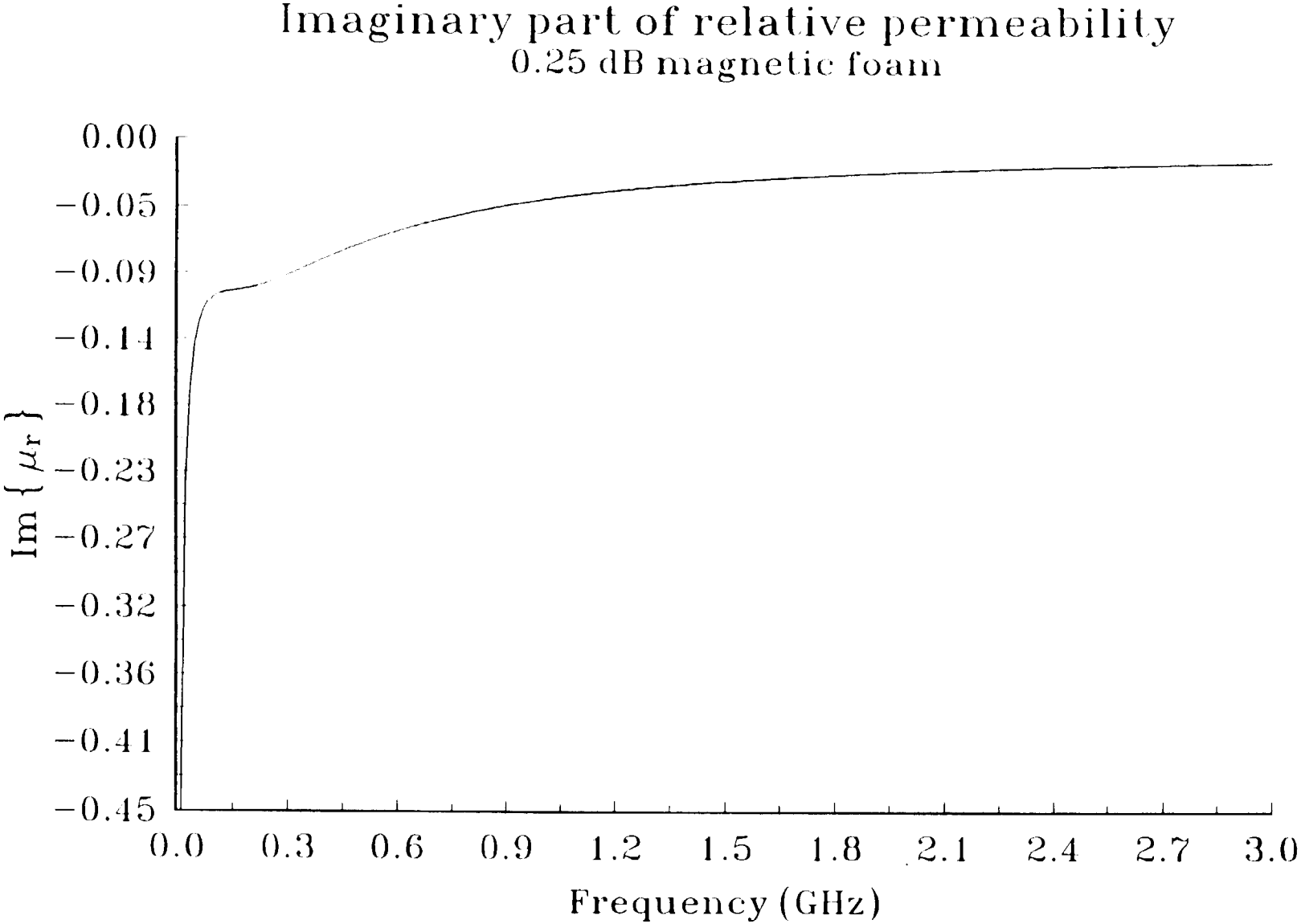
Imaginary part of relative permeability
0.25 dB magnetic foam
0.00
−0.05
−0.09
−0.14
−0.18
−0.23
−0.27
−0.32
−0.36
−0.41
−0.45
Im {μr}
0.0
0.3
0.6
0.9
1.2
1.5
1.8
2.1
2.4
2.7
3.0
Frequency (GHz)

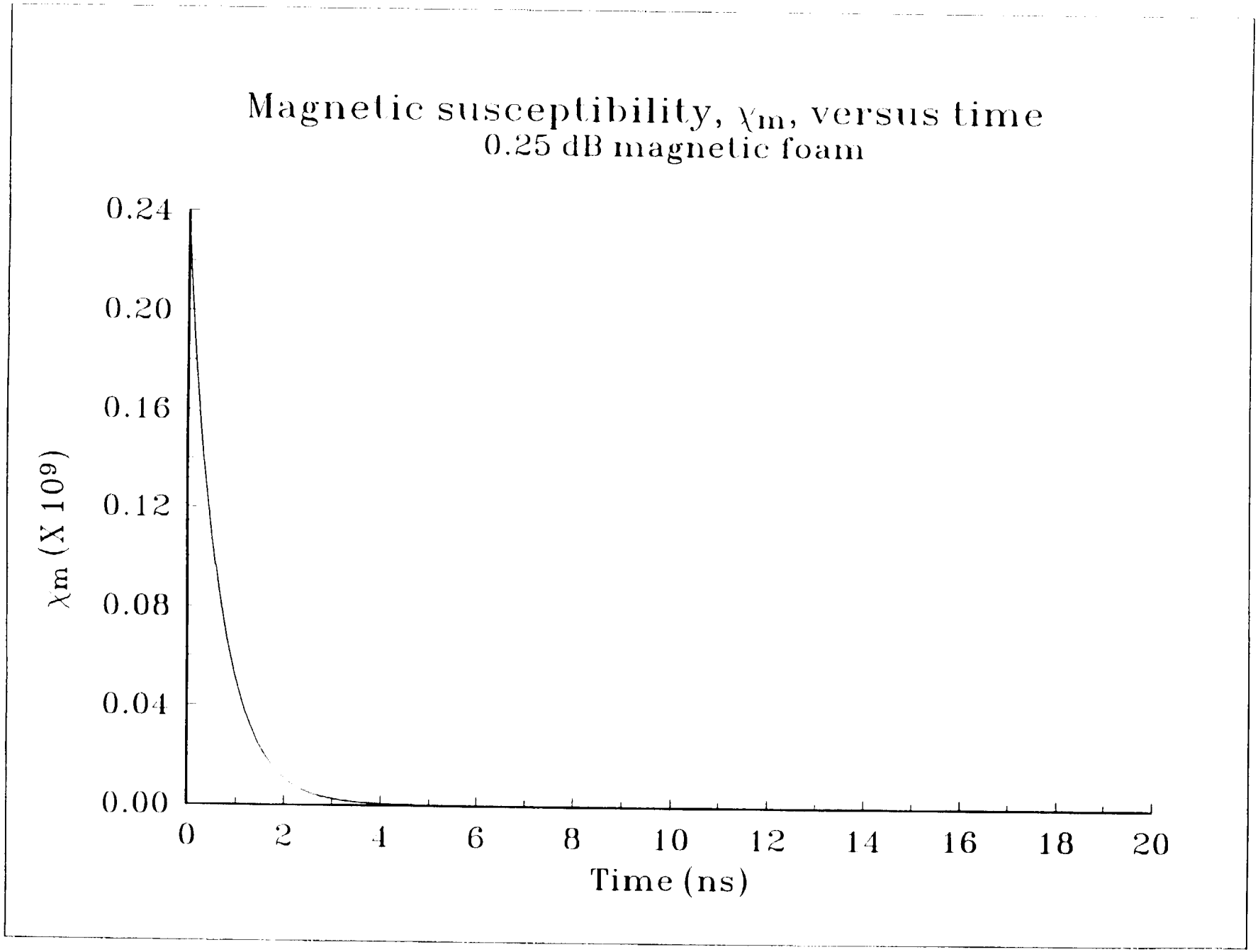
Magnetic susceptibility, χ_m, versus time
0.25 dB magnetic foam
0.24
0.20
0.16
0.12
0.08
0.04
0.00
χ_m (X 109)
0
2
4
6
8
10
12
14
16
18
20
Time (ns)

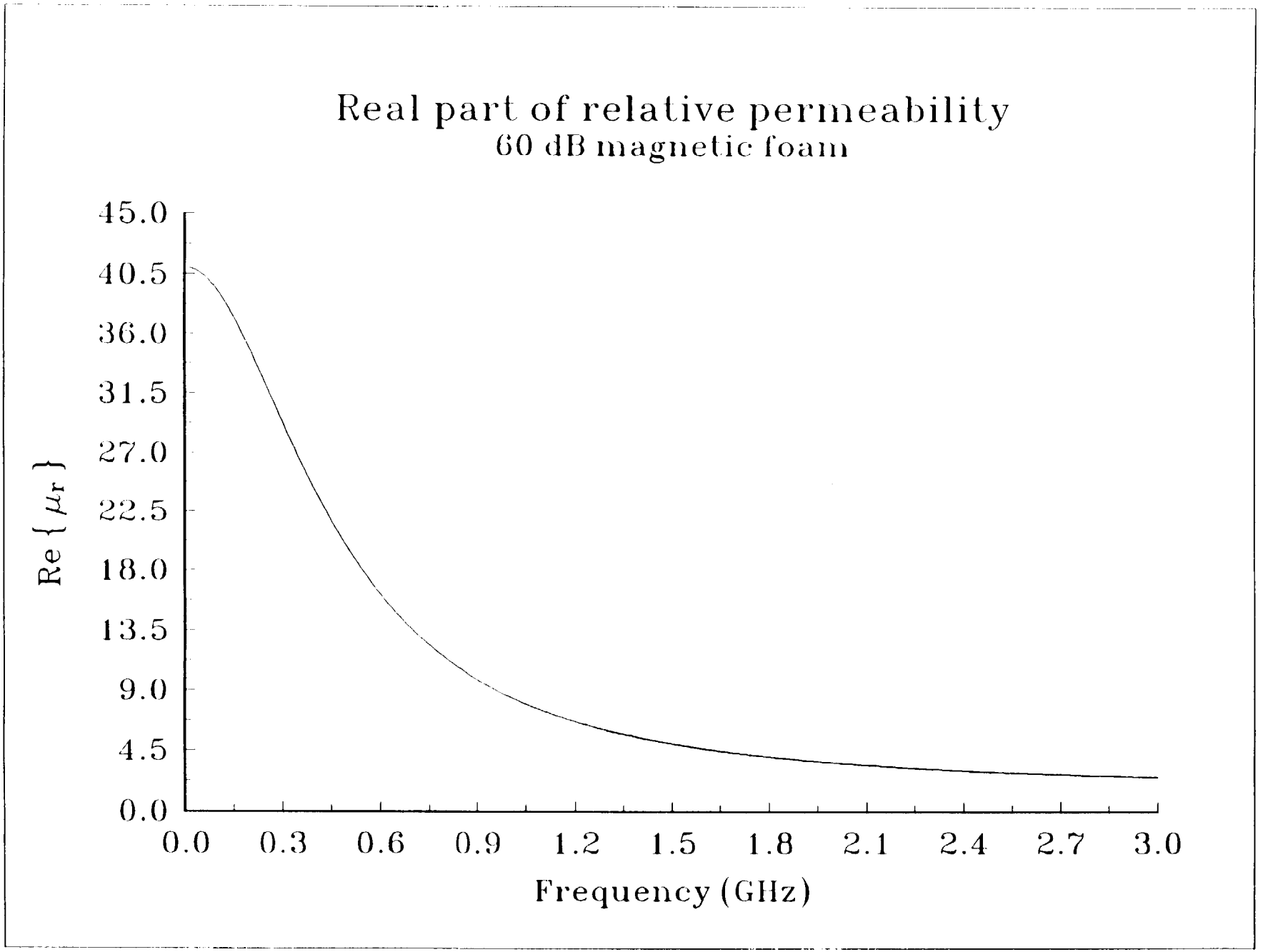
Real part of relative permeability
60 dB magnetic foam
45.0
40.5
36.0
31.5
27.0
22.5
18.0
13.5
9.0
4.5
0.0
Re { μr }
0.0
0.3
0.6
0.9
1.2
1.5
1.8
2.1
2.4
2.7
3.0
Frequency (GHz)

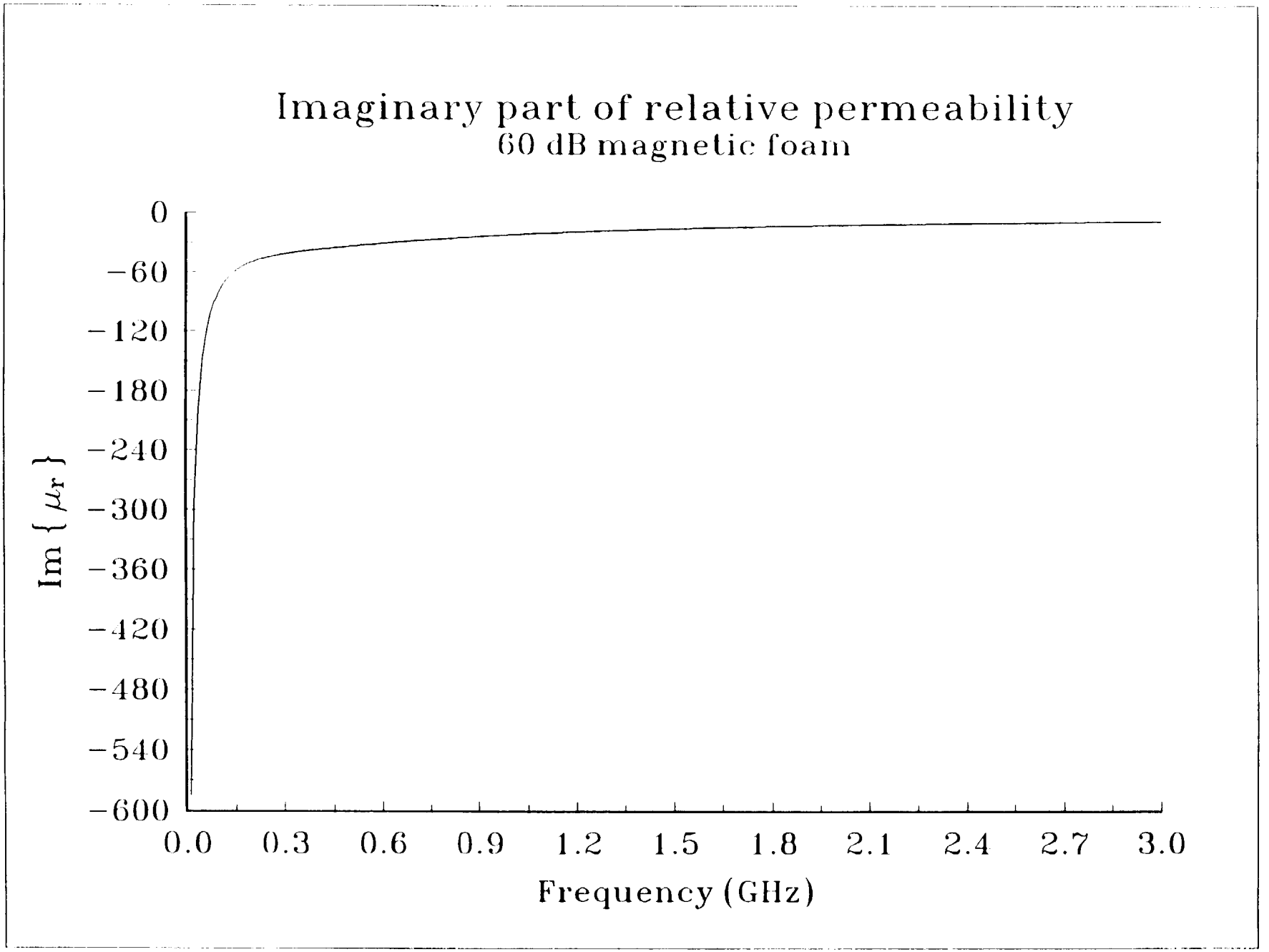
Imaginary part of relative permeability
60 dB magnetic foam
0
−60
−120
−180
−240
−300
−360
−420
−480
−540
−600
Im { μr }
0.0
0.3
0.6
0.9
1.2
1.5
1.8
2.1
2.4
2.7
3.0
Frequency (GHz)

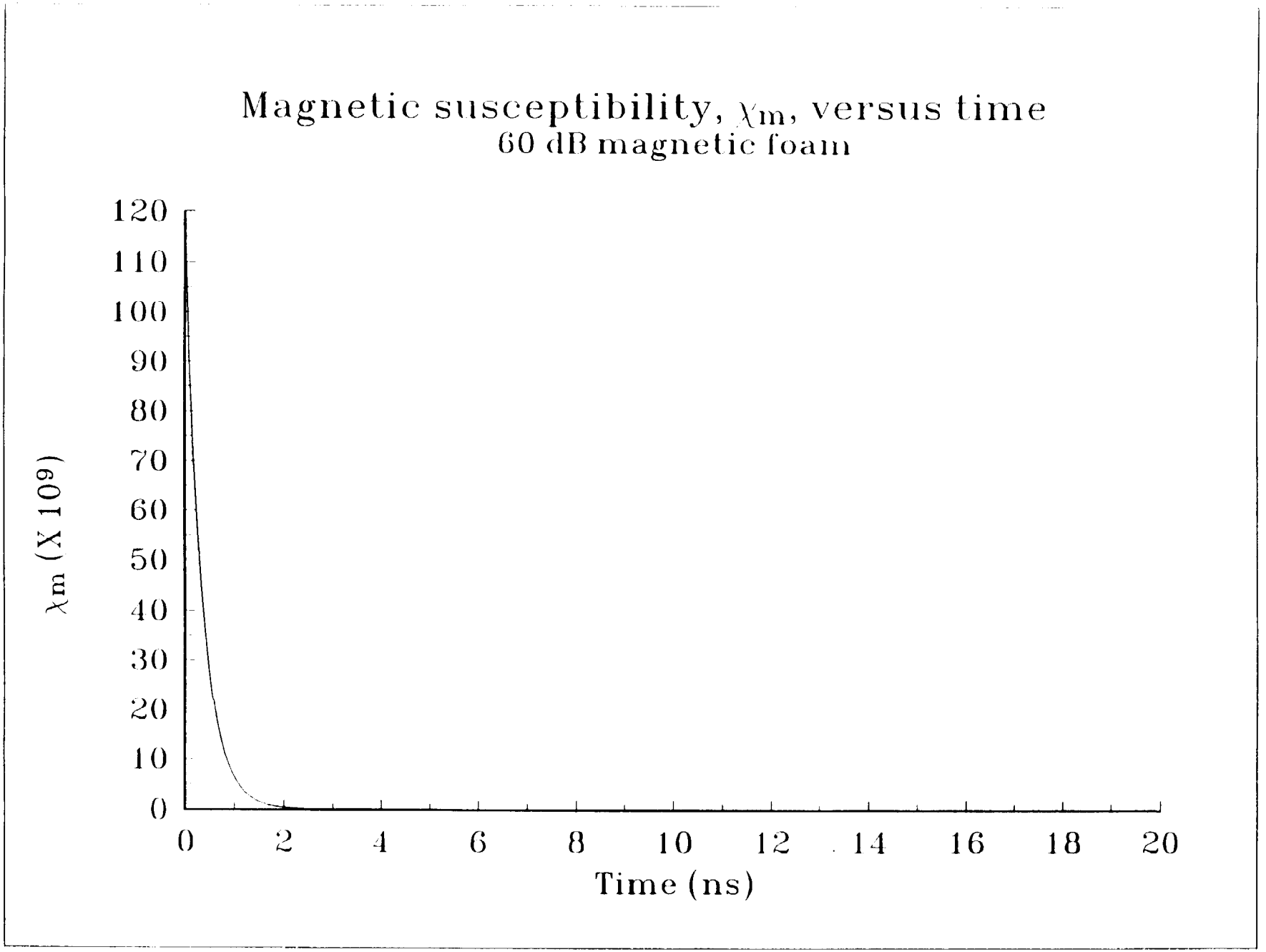
Magnetic susceptibility, χ_m, versus time
60 dB magnetic foam
χ_m (X 10^9)
120
110
100
90
80
70
60
50
40
30
20
10
0
0
2
4
6
8
10
12
14
16
18
20
Time (ns)

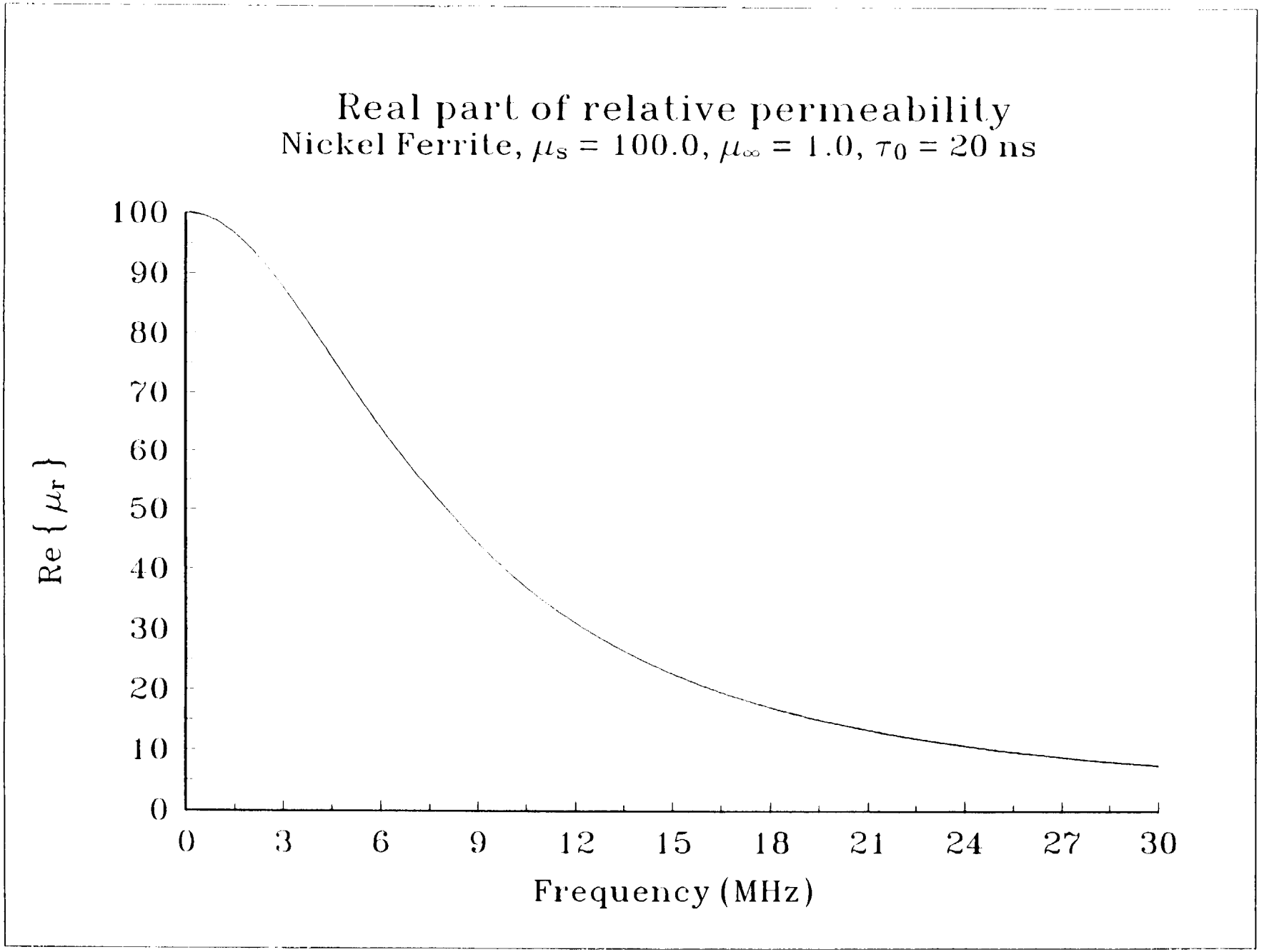
Real part of relative permeability
Nickel Ferrite, $\mu_s = 100.0$, $\mu_\infty = 1.0$, $\tau_0 = 20$ ns
Re $\{\mu_r\}$
100
90
80
70
60
50
40
30
20
10
0
0
3
6
9
12
15
18
21
24
27
30
Frequency (MHz)

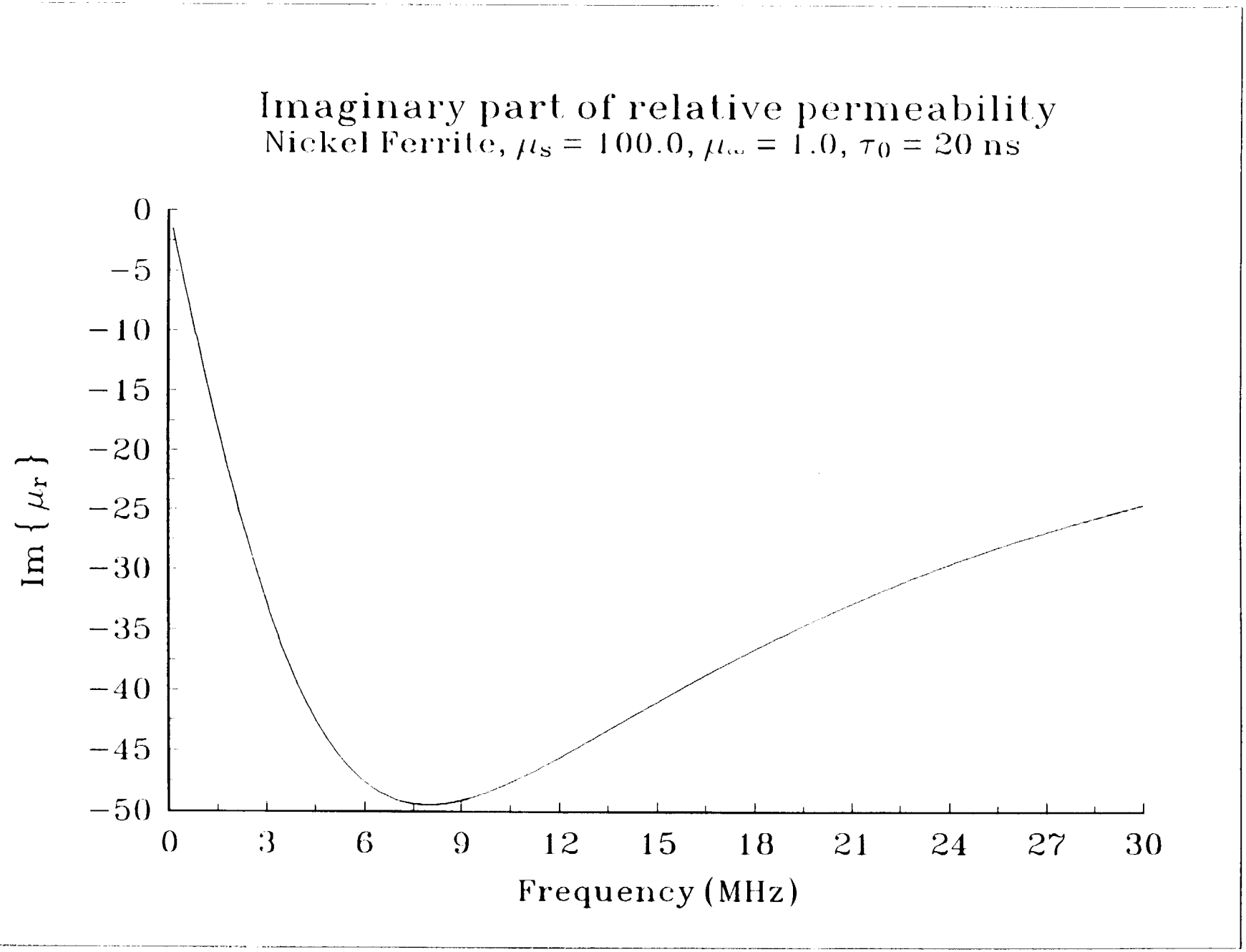
Imaginary part of relative permeability
Nickel Ferrite, $\mu_s = 100.0$, $\mu_\infty = 1.0$, $\tau_0 = 20$ ns
Im { μ_r }
0
−5
−10
−15
−20
−25
−30
−35
−40
−45
−50
0
3
6
9
12
15
18
21
24
27
30
Frequency (MHz)

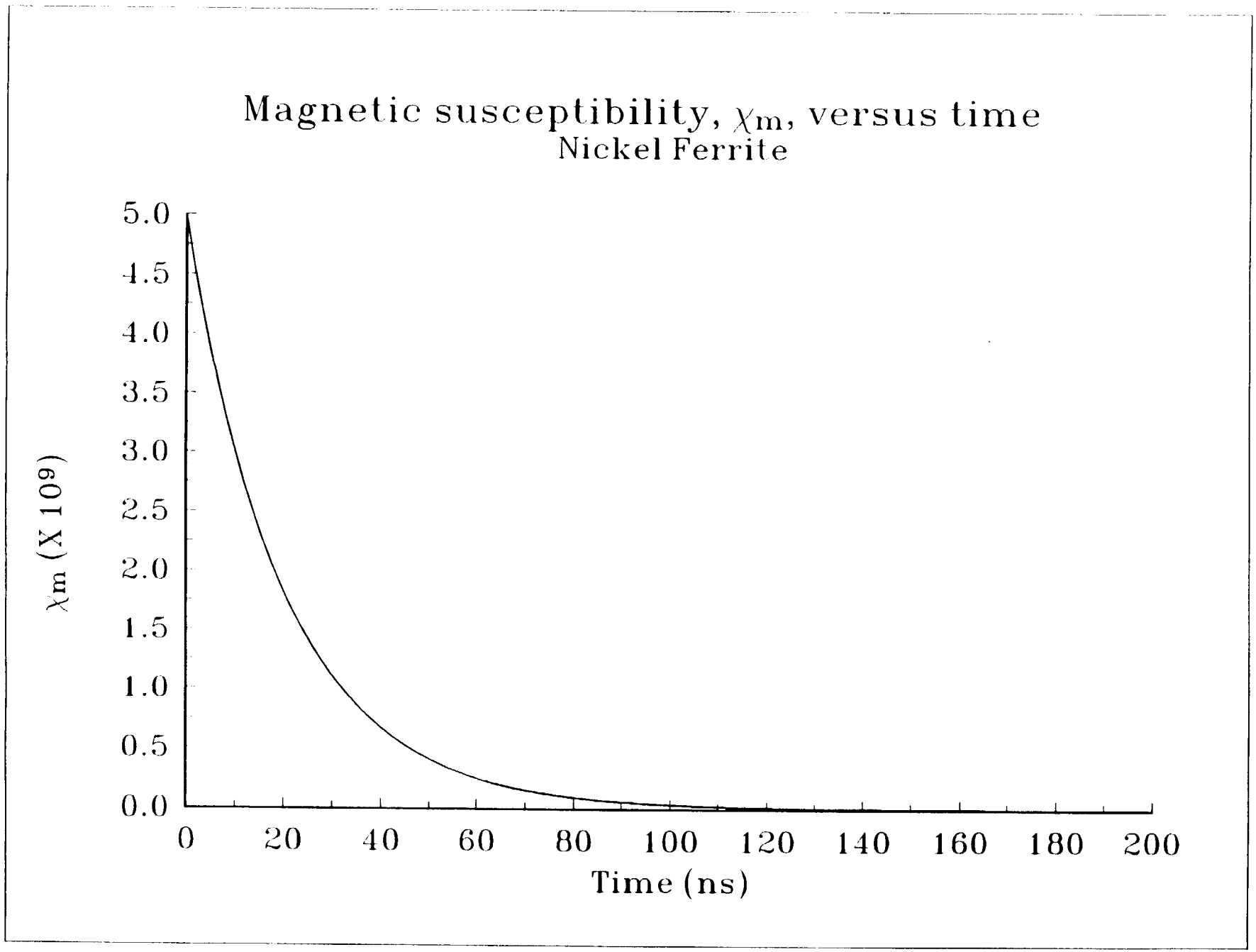
Magnetic susceptibility, χ_m, versus time
Nickel Ferrite
χ_m (X 10^9)
5.0
4.5
4.0
3.5
3.0
2.5
2.0
1.5
1.0
0.5
0.0
0
20
40
60
80
100
120
140
160
180
200
Time (ns)

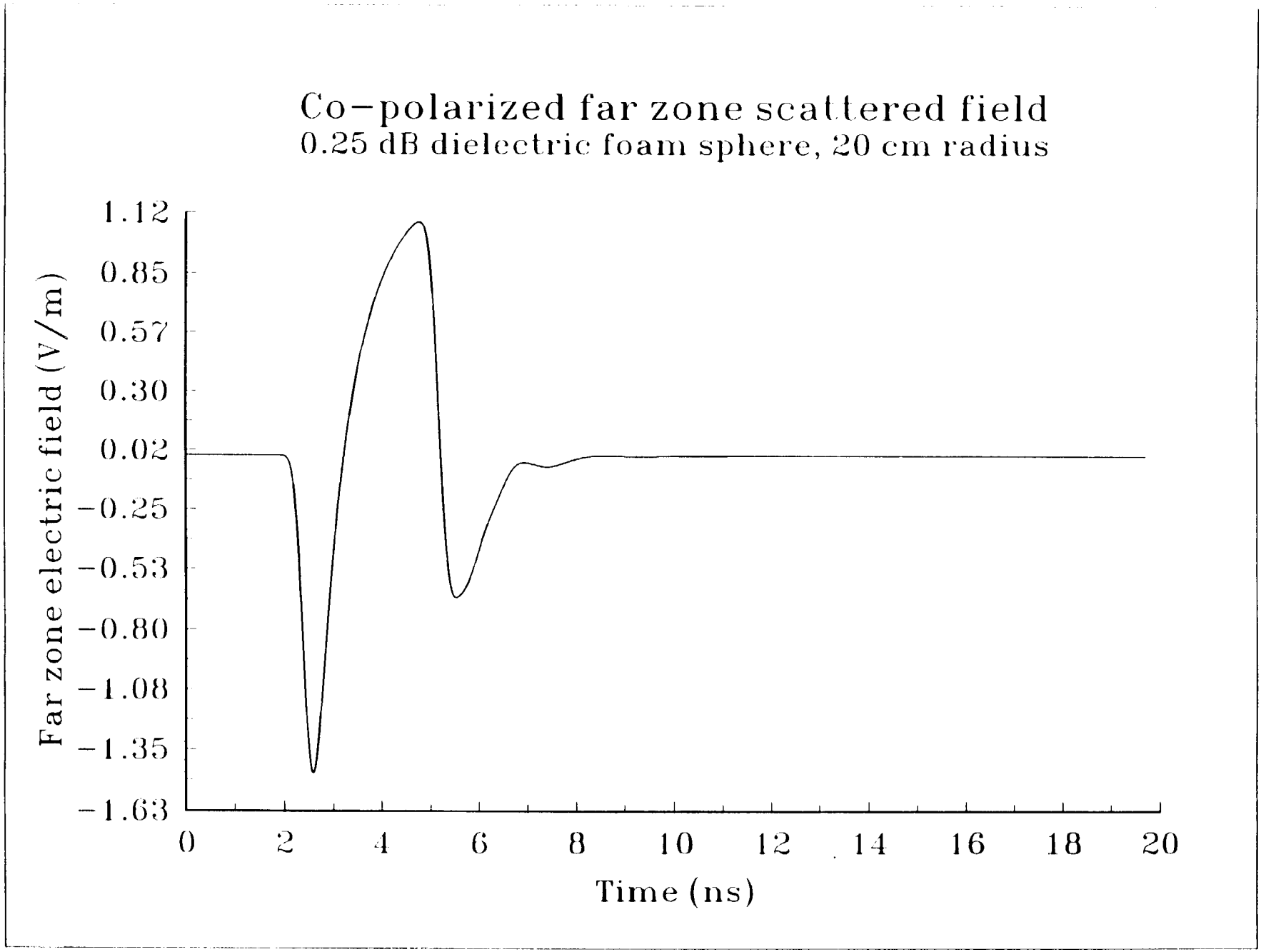
Co-polarized far zone scattered field
0.25 dB dielectric foam sphere, 20 cm radius
Far zone electric field (V/m)
1.12
0.85
0.57
0.30
0.02
-0.25
-0.53
-0.80
-1.08
-1.35
-1.63
0
2
4
6
8
10
12
14
16
18
20
Time (ns)

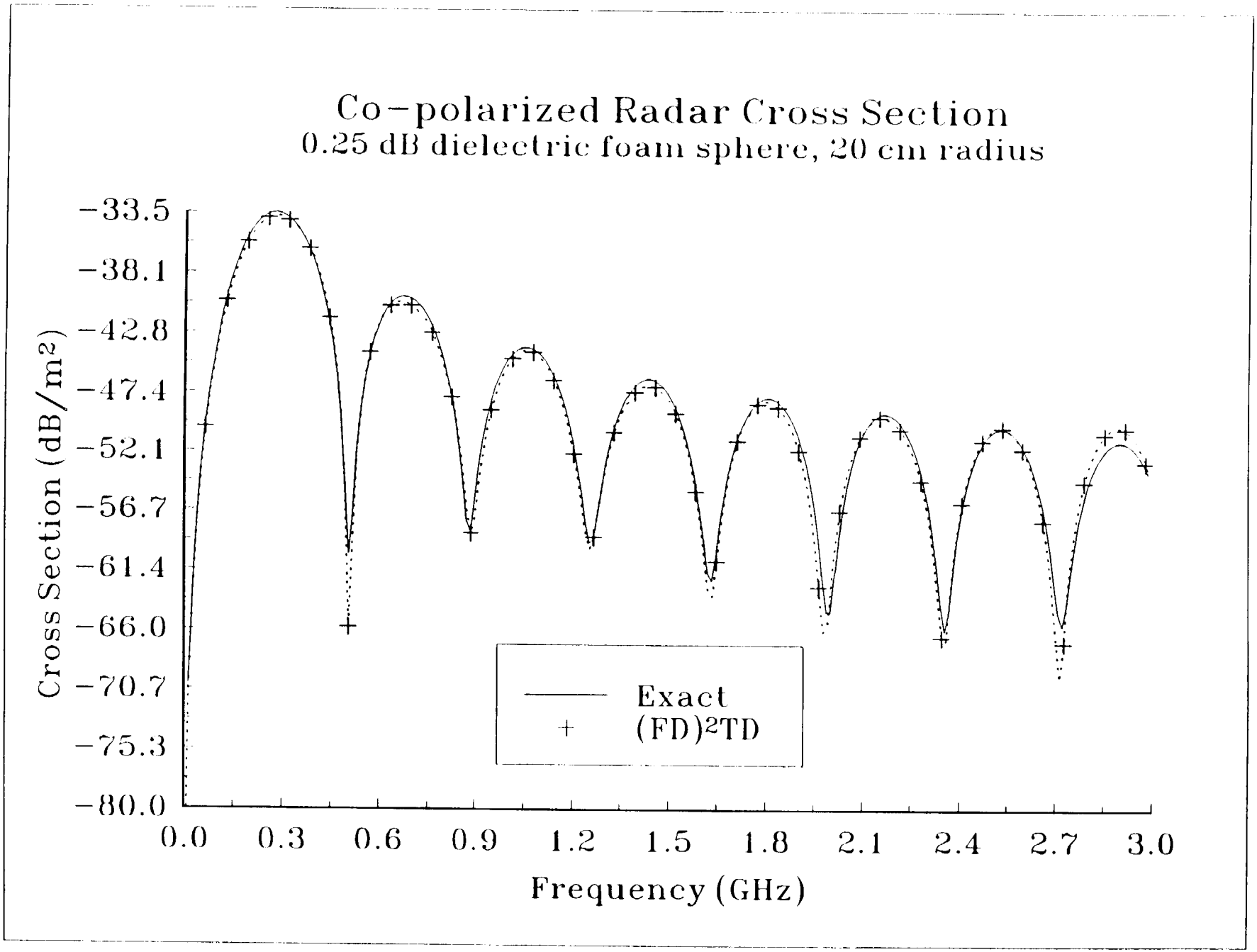
Co-polarized Radar Cross Section
0.25 dB dielectric foam sphere, 20 cm radius
Cross Section (dB/m²)
-33.5
-38.1
-42.8
-47.4
-52.1
-56.7
-61.4
-66.0
-70.7
-75.3
-80.0
0.0
0.3
0.6
0.9
1.2
1.5
1.8
2.1
2.4
2.7
3.0
Frequency (GHz)
Exact
(FD)²TD

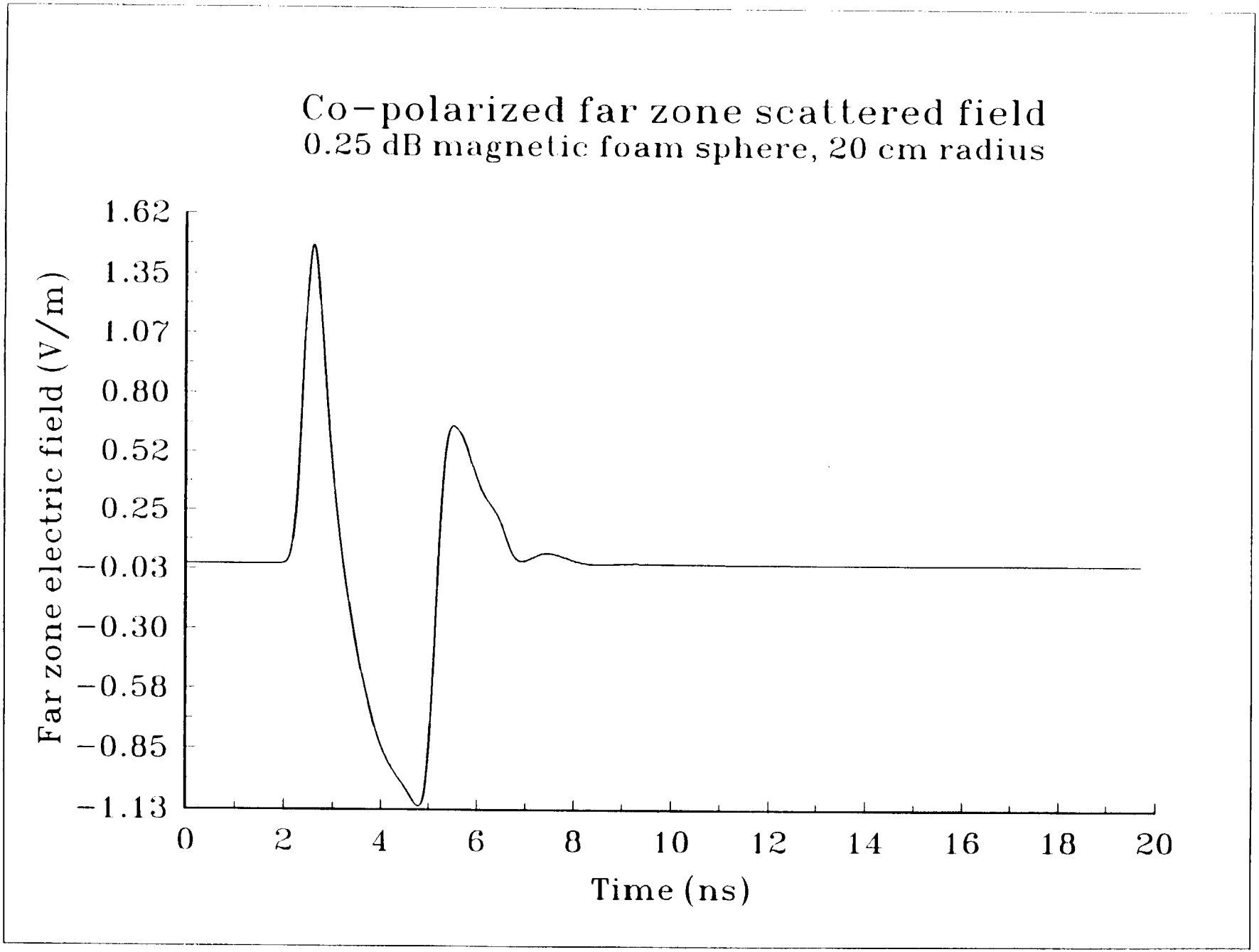
Co-polarized far zone scattered field
0.25 dB magnetic foam sphere, 20 cm radius
Far zone electric field (V/m)
1.62
1.35
1.07
0.80
0.52
0.25
-0.03
-0.30
-0.58
-0.85
-1.13
0
2
4
6
8
10
12
14
16
18
20
Time (ns)

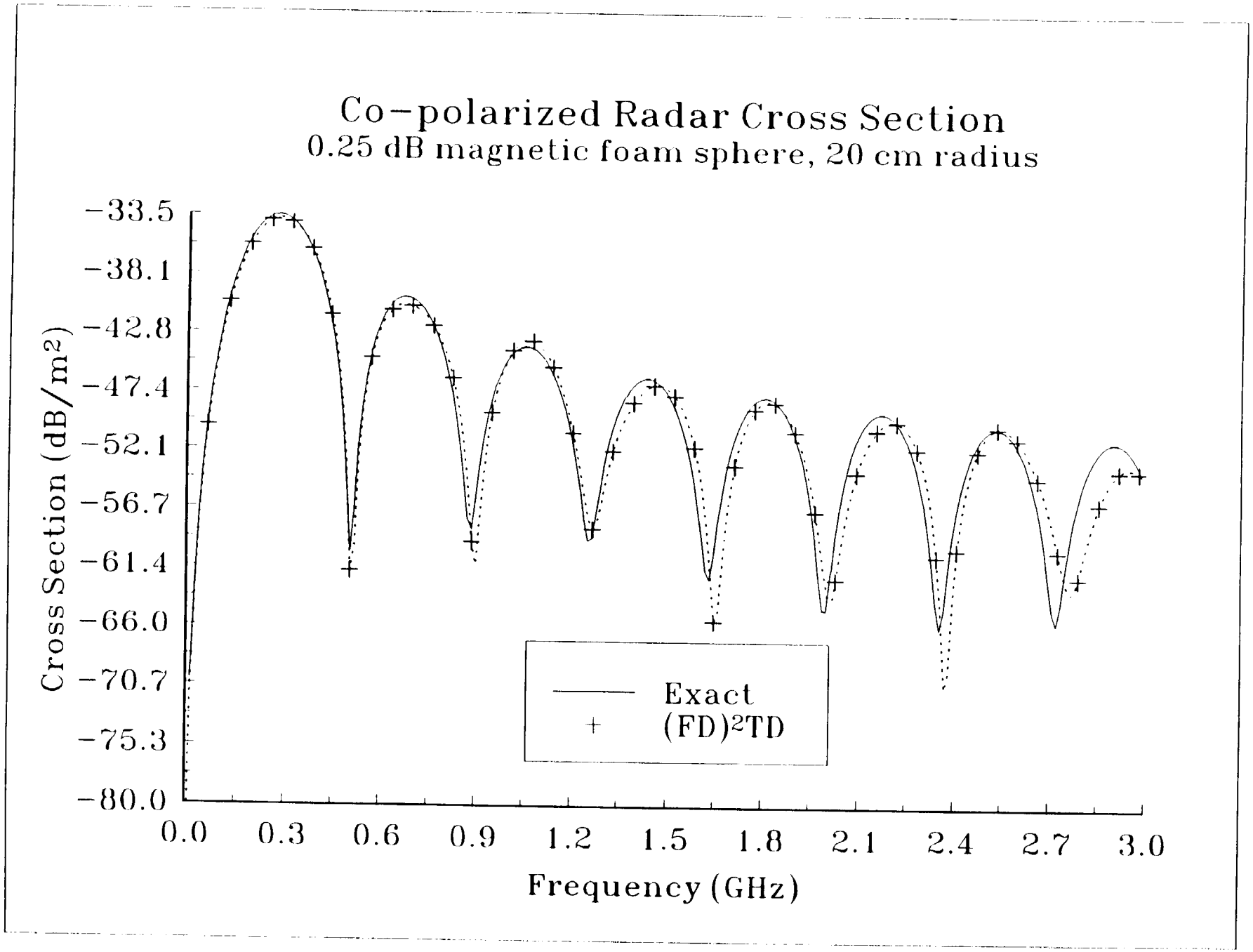
Co-polarized Radar Cross Section
0.25 dB magnetic foam sphere, 20 cm radius
Cross Section (dB/m²)
-33.5
-38.1
-42.8
-47.4
-52.1
-56.7
-61.4
-66.0
-70.7
-75.3
-80.0
0.0
0.3
0.6
0.9
1.2
1.5
1.8
2.1
2.4
2.7
3.0
Frequency (GHz)
Exact
(FD)²TD

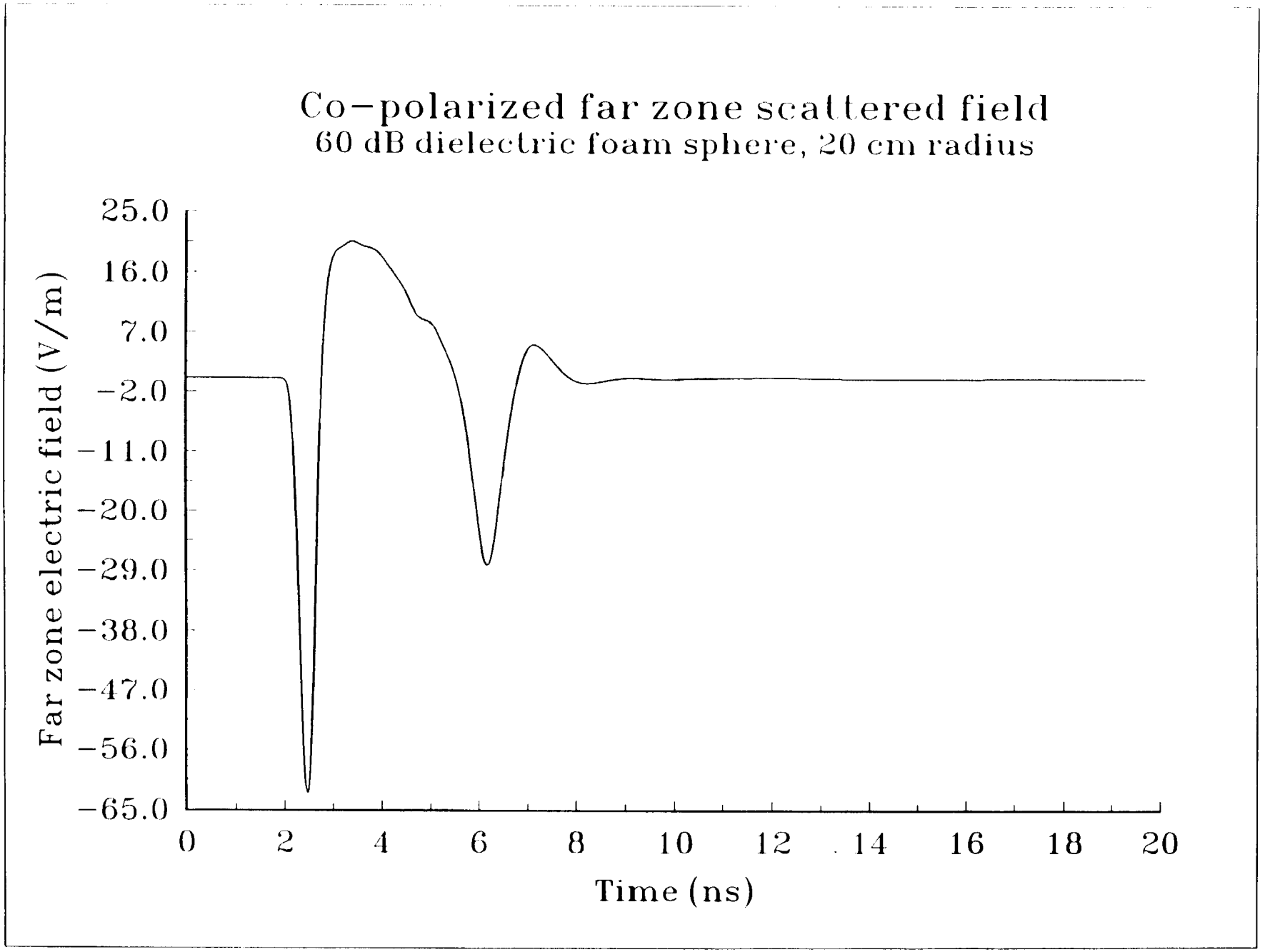
Co-polarized far zone scattered field
60 dB dielectric foam sphere, 20 cm radius
Far zone electric field (V/m)
25.0
16.0
7.0
-2.0
-11.0
-20.0
-29.0
-38.0
-47.0
-56.0
-65.0
0
2
4
6
8
10
12
14
16
18
20
Time (ns)

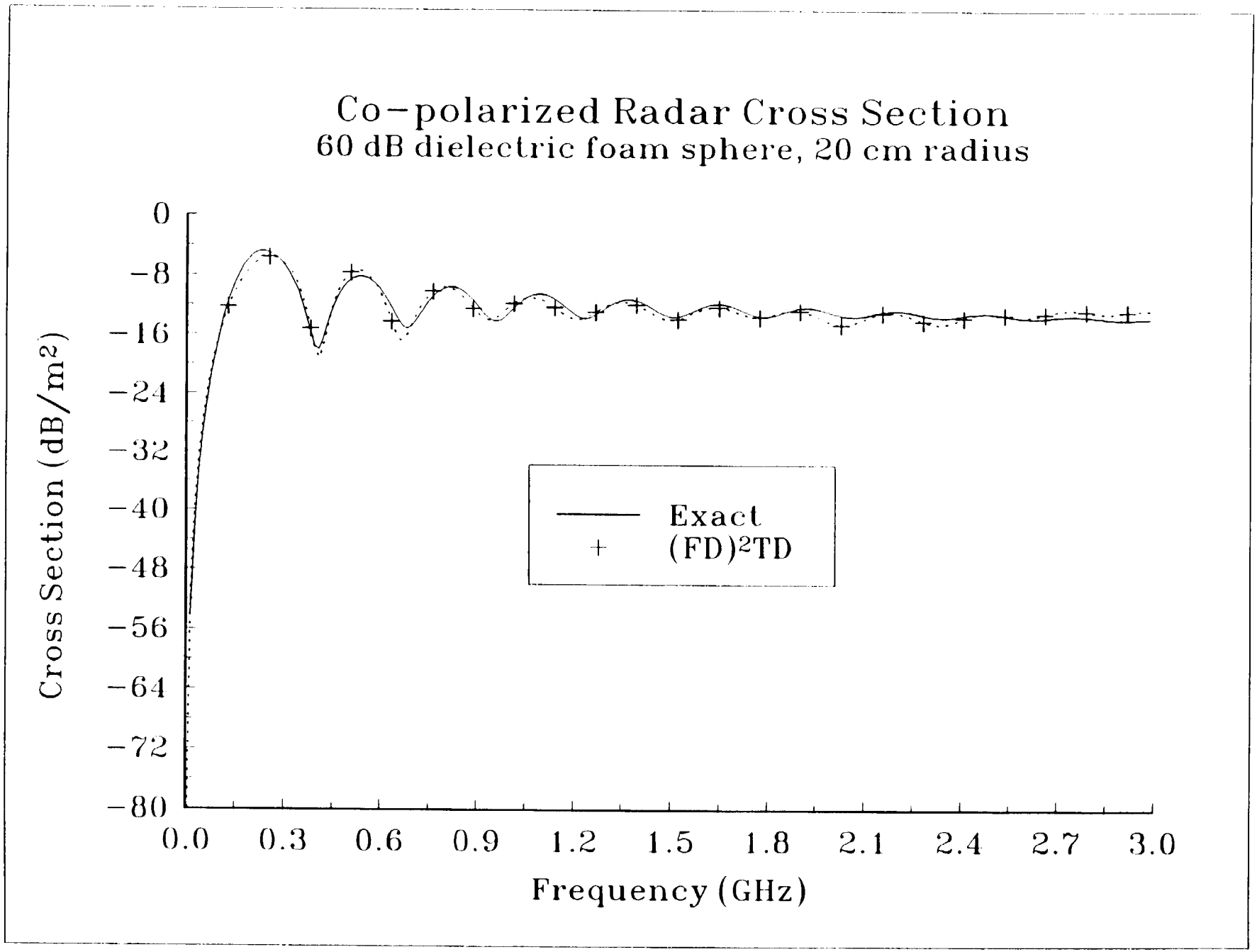
Co-polarized Radar Cross Section
60 dB dielectric foam sphere, 20 cm radius
Cross Section (dB/m²)
0
-8
-16
-24
-32
-40
-48
-56
-64
-72
-80
0.0
0.3
0.6
0.9
1.2
1.5
1.8
2.1
2.4
2.7
3.0
Frequency (GHz)
Exact
(FD)²TD

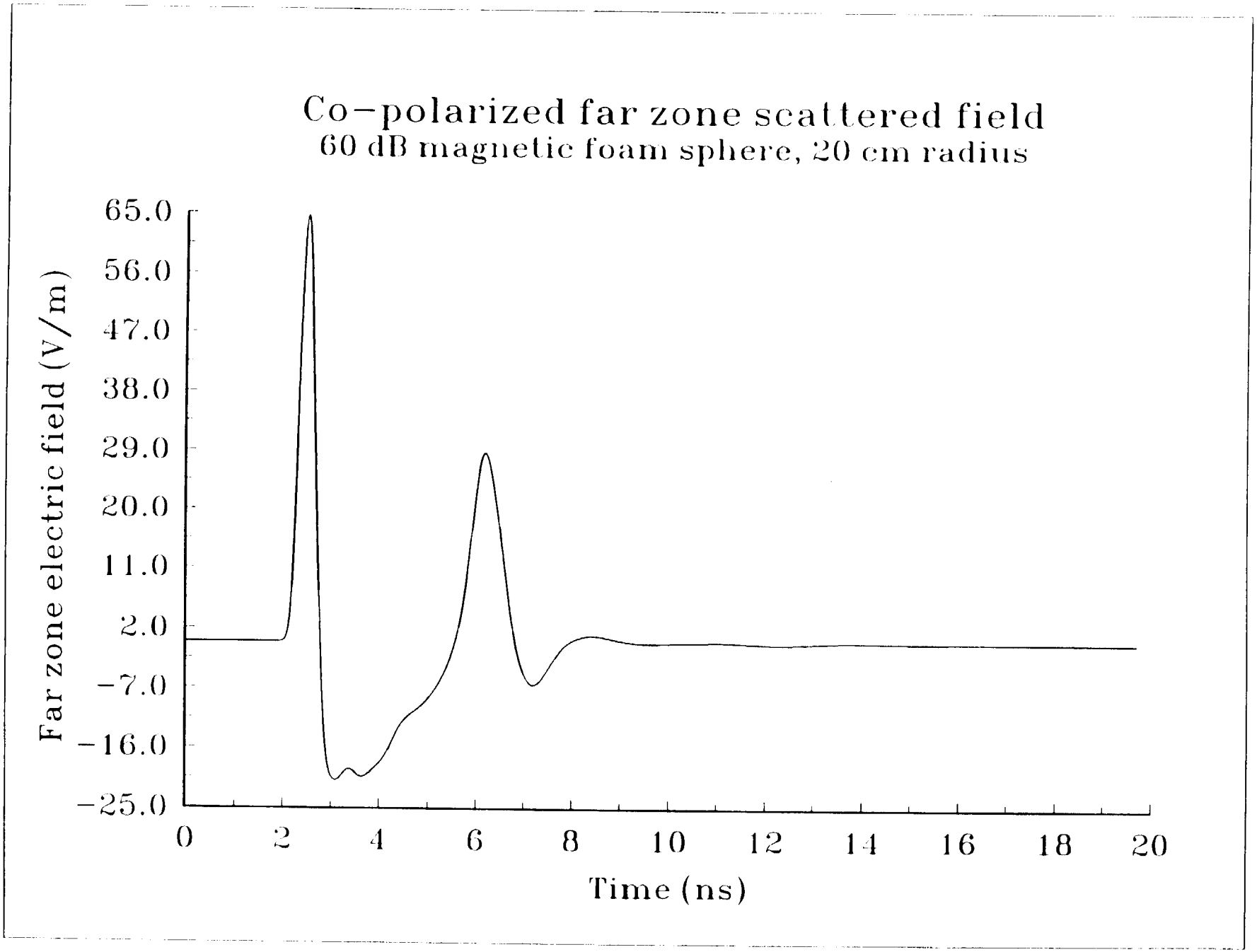
Co-polarized far zone scattered field
60 dB magnetic foam sphere, 20 cm radius
Far zone electric field (V/m)
65.0
56.0
47.0
38.0
29.0
20.0
11.0
2.0
-7.0
-16.0
-25.0
0
2
4
6
8
10
12
14
16
18
20
Time (ns)

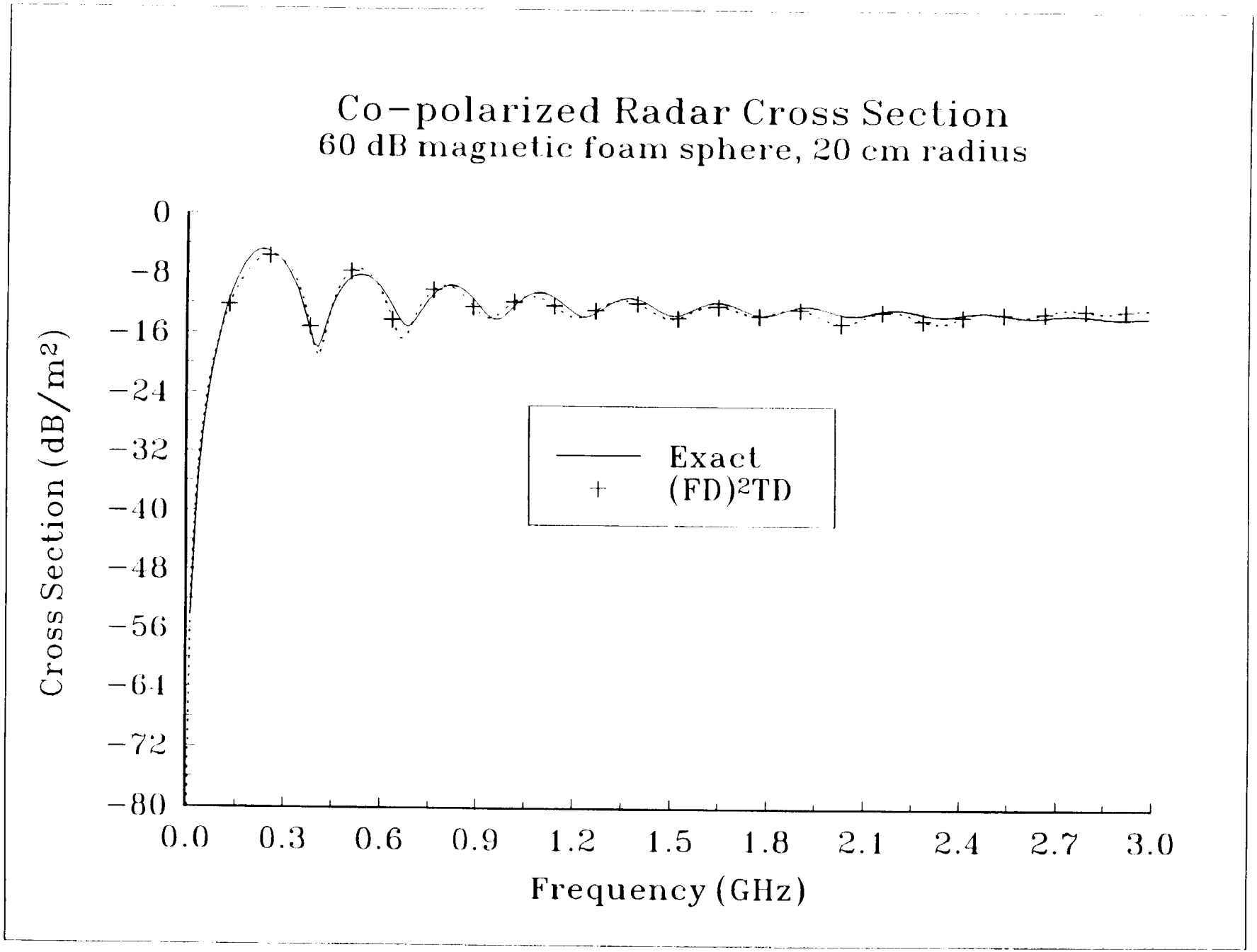
Co-polarized Radar Cross Section
60 dB magnetic foam sphere, 20 cm radius
Cross Section (dB/m²)
0
-8
-16
-24
-32
-40
-48
-56
-64
-72
-80
0.0
0.3
0.6
0.9
1.2
1.5
1.8
2.1
2.4
2.7
3.0
Frequency (GHz)
Exact
(FD)²TD

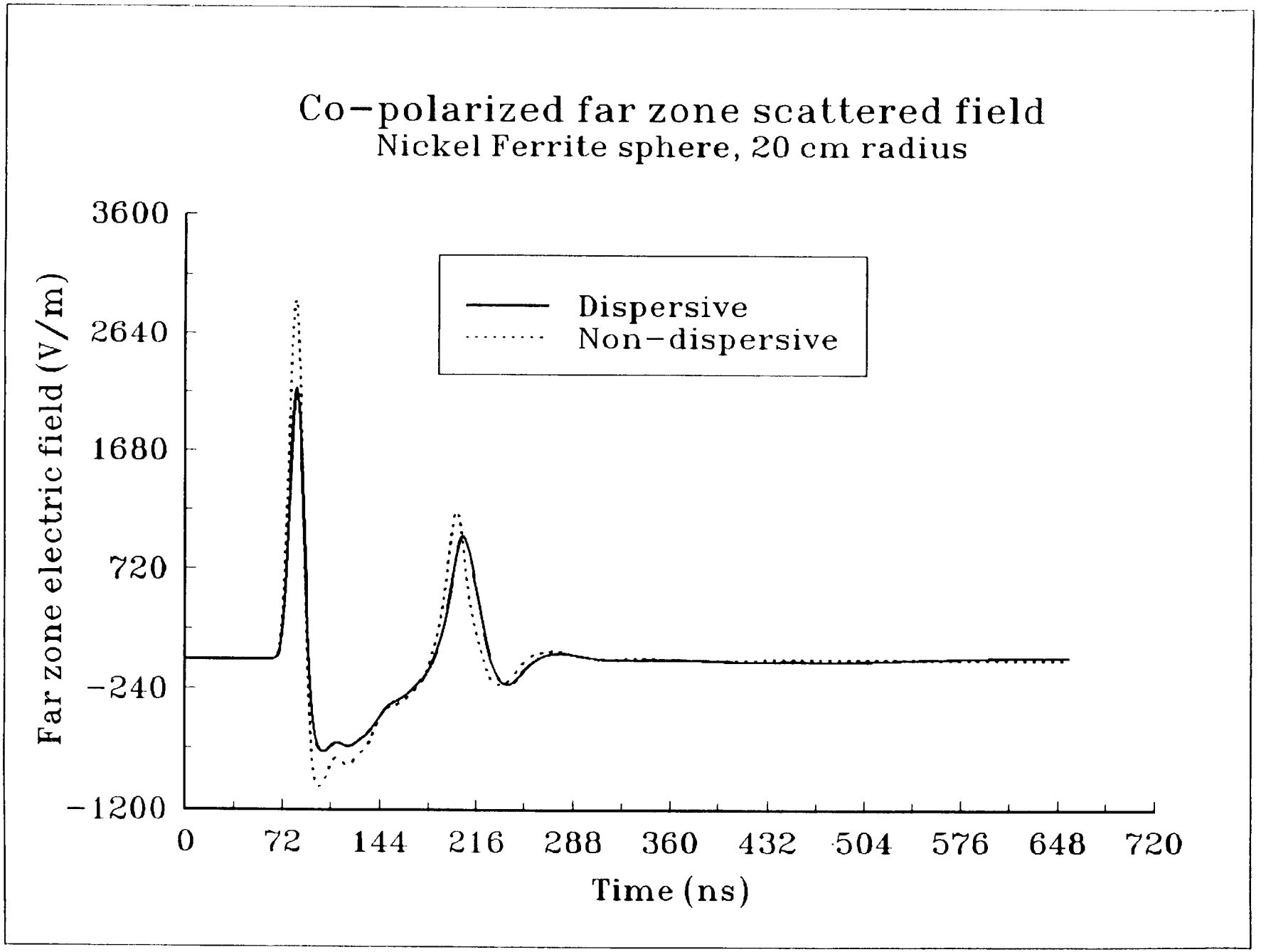
Co-polarized far zone scattered field
Nickel Ferrite sphere, 20 cm radius
Dispersive
Non-dispersive
Far zone electric field (V/m)
3600
2640
1680
720
-240
-1200
0
72
144
216
288
360
432
504
576
648
720
Time (ns)

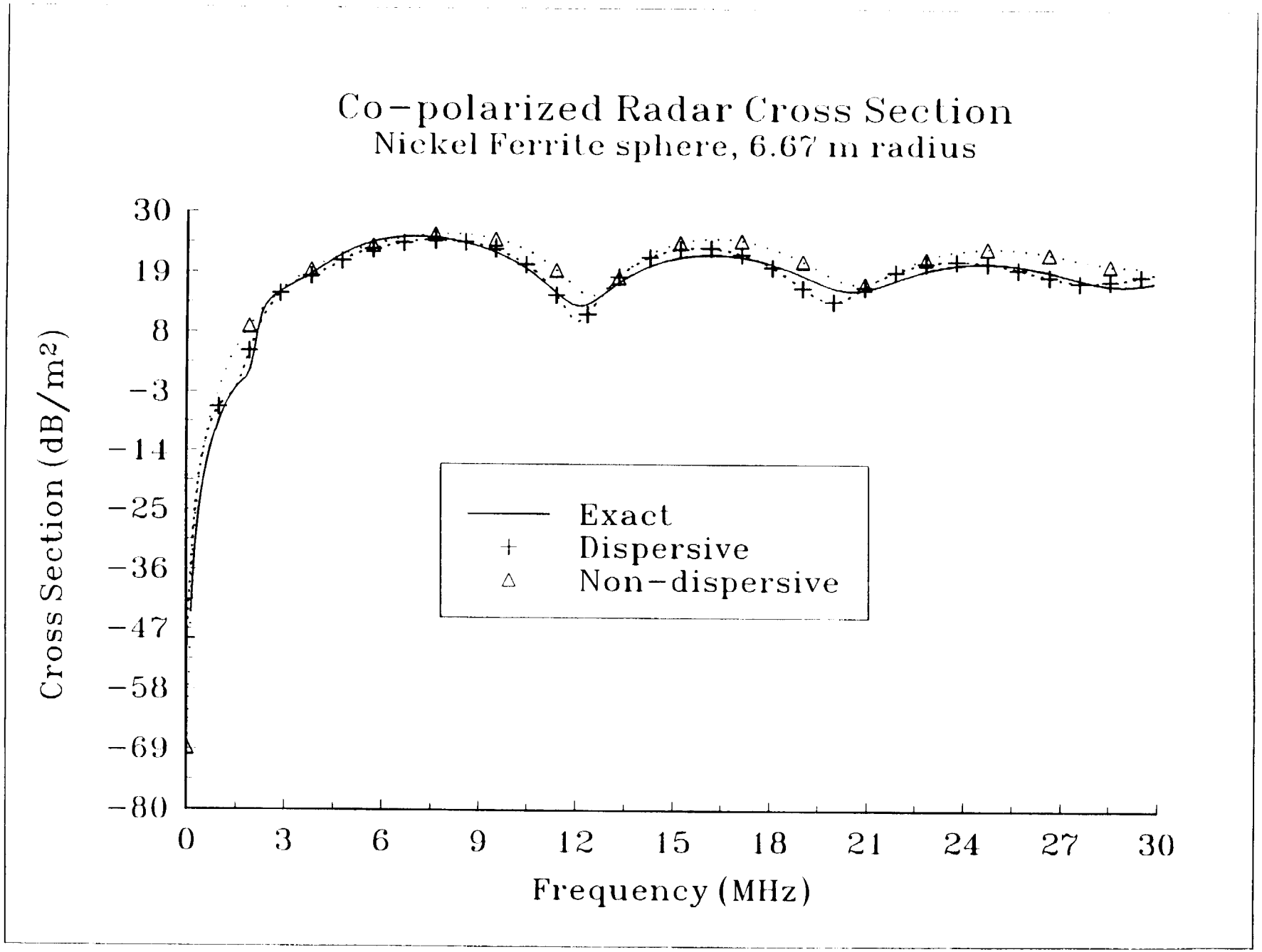
Co-polarized Radar Cross Section
Nickel Ferrite sphere, 6.67 m radius
Cross Section (dB/m²)
30
19
8
-3
-14
-25
-36
-47
-58
-69
-80
0
3
6
9
12
15
18
21
24
27
30
Frequency (MHz)
Exact
Dispersive
Non-dispersive

USER'S MANUAL FOR TWO DIMENSIONAL FDTD VERSION TEA AND TMA CODES FOR SCATTERING FROM FREQUENCY-INDEPENDENT DIELECTRIC MATERIALS

by

John H. Beggs, Raymond J. Luebbers and Karl S. Kunz
Electrical and Computer Engineering Department
The Pennsylvania State University
University Park, PA 16802

(814) 865-2362

November 1991

TABLE OF CONTENTS

I. INTRODUCTION

The Penn State Finite Difference Time Domain Electromagnetic Scattering Code Versions TEA and TMA are two dimensional numerical electromagnetic scattering codes based upon the Finite Difference Time Domain Technique (FDTD) first proposed by Yee [1] in 1966. The supplied version of the codes are two versions of our current two dimensional FDTD code set. This manual provides a description of the codes and corresponding results for the default scattering problem. The manual is organized into eleven sections: introduction, Version TEA and TMA code capabilities, a brief description of the default scattering geometry, a brief description of each subroutine, a description of the include files (TEACOM.FOR TMACOM.FOR), a section briefly discussing scattering width computations, a section discussing the scattering results, a sample problem setup section, a new problem checklist, references and figure titles.

II. VERSION TEA AND TMA CODE CAPABILITIES

The Penn State University FDTD Electromagnetic Scattering Code Versions TEA and TMA have identical capabilities except the TEA code has electric field perpendicular to the z axis and the TMA code has electric field parallel to the z axis. Each code has the following capabilities:

1) Ability to model lossy dielectric and perfectly conducting scatterers.

2) First and second order outer radiation boundary condition (ORBC) operating on the electric fields for dielectric or perfectly conducting scatterers.

3) Near to far zone transformation capability to obtain far zone scattered fields.

4) Gaussian and smooth cosine incident waveforms with arbitrary incidence angles.

5) Near zone field, current or power sampling capability.

6) Companion codes for computing scattering width.

III. DEFAULT SCATTERING GEOMETRY

The codes as delivered are set up to calculate the far zone backscatter fields for an infinite, 0.25 m radius, perfectly conducting cylinder. The problem space size is 201 by 201 cells in the x and y directions, the cells are 1 cm squares, and the incident waveform is a Gaussian pulse with incidence angle of ϕ=180 degrees. The output data files are included as a reference along with codes (SWTEA.FOR, SWTMA.FOR) for computing the

frequency domain scattering width using these output data files. The ORBC is the second order absorbing boundary condition set forth by Mur [2].

IV. SUBROUTINE DESCRIPTION

In the description for each subroutine, an asterisk (*) will be placed by the subroutine name if that particular subroutine is normally modified when defining a scattering problem. Also, each subroutine will be denoted if it is applicable to the TE code only, the TM code only, or to both codes.

MAIN ROUTINE (TE, TM)

The main routine in the program contains the calls for all necessary subroutines to initialize the problem space and scattering object(s) and for the incident waveform, far zone transformation, field update subroutines, outer radiation boundary conditions and field sampling.

The main routine begins with the include statement and then appropriate data files are opened, and subroutines ZERO, BUILD and SETUP are called to initialize variables and/or arrays, build the object(s) and initialize the incident waveform and miscellaneous parameters, respectively. Subroutine SETFZ is called to intialize parameters for the near to far zone transformation if far zone fields are desired.

The main loop is entered next, where all of the primary field computations and data saving takes place. During each time step cycle, the EXSFLD (TE), EYSFLD (TE), and EZSFLD (TM) subroutines are called to update the x, y, and z components of the scattered electric field. These scattered field equations are based upon the development given in [3]. RADEXY, RADEYX (TE) and RADEZX, RADEZY (TM) outer radiation boundary conditions are called next to absorb any outgoing scattered fields. Time is then advanced 1/2 time step according to the Yee algorithm and then the HXSFLD (TM), HYSFLD (TM), AND HZSFLD (TE) subroutines are called to update the x, y, and z components of scattered magnetic field. Time is then advanced another 1/2 step and then either near zone fields are sampled and written to disk in DATSAV, and/or the near zone to far zone vector potentials are updated in SAVFZ. The parameter NZFZ (described later) in the common file defines the type of output fields desired.

After execution of all time steps in the main field update loop, subroutine FAROUT is called if far zone fields are desired to compute the far zone fields and write them to disk. At this point, the execution is complete.

SUBROUTINE SETFZ (TE, TM)

This subroutine initializes the necessary parameters required for far zone field computations. The codes as furnished compute backscatter far zone field and can compute bistatic far zone fields for one scattering angle (i.e. one ϕ angle). Refer to reference [4] for a complete description of the two dimensional near to far zone transformation. Other versions of this subroutine provide for multiple bistatic angles.

SUBROUTINE SAVFZ (TE, TM)

This subroutine updates the near zone to far zone vector potentials.

SUBROUTINE FAROUT (TE, TM)

This subroutine changes the near zone to far zone vector potentials to far zone electric field θ (TM) and ϕ (TE) components and writes them to disk.

SUBROUTINE BUILD (TE, TM) *

This subroutine "builds" the scattering object(s) by initializing the IDONE (TE), IDTWO (TE), and IDTHRE (TM) arrays. The IDONE-IDTHRE arrays are for specifying perfectly conducting and lossy dielectric materials. Refer to Figure 1 for a diagram of the basic two dimensional Yee cell for the TE and TM case. For example, setting an element of the IDONE array at some I,J location is actually locating dielectric material at a cell edge whose center location is I+0.5,J. Thus, materials with diagonal permittivity tensors can be modeled. The default material type for all ID??? arrays is 0, or free space. By initializing these arrays to values other than 0, the user is defining an object by determining what material types are present at each spatial location. Other material types available for IDONE-IDTHRE are 1 for perfectly conducting objects and 2-9 for lossy non-magnetic dielectrics. It is assumed throughout the code that <u>all</u> dielectric materials are non-magnetic (i.e. the materials have a permeability of μ_0). This subroutine also has a section that checks the ID??? arrays to determine if legal material types have been defined throughout the problem space. The actual material parameters (ϵ and σ) are defined in subroutine SETUP. The default geometry is a 0.25 m radius, perfectly conducting cylinder.

The user must be careful that his/her object created in the BUILD subroutine is properly formed.

When it is important to place the object in the center of the problem space, NX and NY should be odd. This is due to the

field locations in the Yee cell and also the placement of the E field absorbing boundary condition surfaces.

If the object being modeled has curved surfaces, edges, etc. that are at an angle to one or more of the coordinate axes, then that shape must be approximately modeled by lines and faces in a "stair-stepped" (or stair-cased) fashion. This stair-cased approximation introduces errors into computations at higher frequencies. Intuitively, the error becomes smaller as more cells are used to stair-case a particular object.

SUBROUTINE DPLATE (TE)

This subroutine builds squares of dielectric material by defining two each of IDONE and IDTWO components corresponding to one spatial square of dielectric material. It can also be used to define thin (i.e. up to one cell thick) dielectric or perfectly conducting wires. Refer to comments within DPLATE for a description of the arguments and usage of the subroutine.

SUBROUTINE SETUP (TE, TM) *

This subroutine initializes many of the constants required for incident field definition, field update equations, outer radiation boundary conditions and material parameters. The material parameters ϵ and σ are defined for each material type using the material arrays EPS and SIGMA respectively. The array EPS is used for the total permittivity and SIGMA is used for the electric conductivity. These arrays are initialized in SETUP to free space material parameters for all material types and then the user is required to modify these arrays for his/her scattering materials. Thus, for the lossy dielectric material type 2, the user must define EPS(2) and SIGMA(2). The remainder of the subroutine computes constants used in field update equations and boundary conditions and writes the diagnostics file.

SUBROUTINE EXSFLD (TE)

This subroutine updates all x components of scattered electric field at each time step except those on the outer boundaries of the problem space. IF statements based upon the IDONE array are used to determine the type of material present and the corresponding update equation to be used.

SUBROUTINE EYSFLD (TE)

This subroutine updates all y components of scattered electric field at each time step except those on the outer boundaries of the problem space. IF statements based upon the IDTWO array are used to determine the type of material present and the corresponding update equation to be used.

SUBROUTINE EZSFLD (TM)

This subroutine updates all z components of scattered electric field at each time step except those on the outer boundaries of the problem space. IF statements based upon the IDTHRE array are used to determine the type of material present and the corresponding update equation to be used.

SUBROUTINES RADEYX, RADEXY (TE) and RADEZX, RADEZY (TM)

These subroutines apply the outer radiation boundary conditions to the scattered electric field on the outer boundaries of the problem space.

SUBROUTINE HXSFLD (TM)

This subroutine updates all x components of scattered magnetic field at each time step. The standard non-magnetic update equation is used.

SUBROUTINE HYSFLD (TM)

This subroutine updates all y components of scattered magnetic field at each time step. The standard non-magnetic update equation is used.

SUBROUTINE HZSFLD (TE)

This subroutine updates all z components of scattered magnetic field at each time step. The standard non-magnetic update equation is used.

SUBROUTINE DATSAV (TE, TM) *

This subroutine samples near zone scattered field quantities and saves them to disk. This subroutine is where the quantities to be sampled and their spatial locations are to be specified and is only called if near zone fields only are desired or if both near and far zone fields are desired. Total field quantities can also be sampled. See comments within the subroutine for specifying sampled scattered and/or total field quantities. When sampling magnetic fields, remember the $\delta t/2$ time difference between E and H when writing the fields to disk. Sections of code within this subroutine determine if the sampled quantities and the spatial locations have been properly defined.

FUNCTIONS EXI, EYI (TE) and EZI (TM)

These functions are called to compute the x, y and z components of incident electric field. The functional form of the incident field is contained in a separate function SOURCE.

FUNCTION SOURCE (TE, TM) *

This function contains the functional form of the incident field. The code as furnished uses the Gaussian form of the incident field. An incident smooth cosine pulse is also available by uncommenting the required lines and commenting out the Gaussian pulse. Thus, this function need only be modified if the user changes the incident pulse from Gaussian to smooth cosine. A slight improvement in computing speed and vectorization may be achieved by moving this function inside each of the incident field functions EXI, EYI and so on.

FUNCTIONS DEXI, DEYI (TE) and DEZI (TM)

These functions are called to compute the x, y and z components of the time derivative of incident electric field. The functional form of the incident field is contained in a separate function DSRCE.

FUNCTION DSRCE (TE, TM) *

This function contains the functional form of the time derivative of the incident field. The code as furnished uses the time derivative of the Gaussian form of the incident field. A smooth cosine pulse time derivative is also available by uncommenting the required lines and commenting out the Gaussian pulse. Thus, the function need only be modified if the user changes from the Gaussian to smooth cosine pulse. Again, a slight improvement in computing speed and vectorization may be achieved by moving this function inside each of the time derivative incident field functions DEXI, DEYI and so on.

SUBROUTINE ZERO (TE, TM)

This subroutine initializes various arrays and variables to zero.

V. INCLUDE FILE DESCRIPTION (TEACOM.FOR, TMACOM.FOR) *

The include files, TEACOM.FOR, TMACOM.FOR, contain all of the arrays and variables that are shared among the different subroutines. These files will require the most modifications when defining scattering problems. A description of the parameters that are normally modified follows.

The parameters NX and NY specify the size of the problem space in cells in the x and y directions respectively. For problems where it is crucial to center the object within the problem space, then NX and NY should be odd. The parameter NTEST defines the number of near zone quantities to be sampled and NZFZ defines the field output format. Set NZFZ=0 for near zone fields only, NZFZ=1 for far zone fields only and NZFZ=2 for both near

and far zone fields. Parameter NSTOP defines the maximum number of time steps. DELX and DELY (in meters) define the cell size in the x and y directions respectively. The ϕ incidence angle (in degrees) is defined by PHINC and the polarization is defined by the code that is being used. Parameters AMP and BETA define the maximum amplitude and the e^{-2} temporal width of the incident pulse respectively. BETA automatically adjusts when the cell size is changed and normally should not be changed by the user. The far zone scattering angle is defined by PHIFZ. The codes as furnished perform backscatter computations, but this parameter could be modified for a bistatic computation.

VI. SCATTERING WIDTH COMPUTATIONS

Companion codes, SWTEA.FOR, SWTMA.FOR, have been included to compute scattering width versus frequency. Each code uses the file name of the FDTD far zone output data (FZOUTTE.DAT, FZOUTTM.DAT) and writes data files of far zone electric field versus time (FZTE.DAT, FZTM.DAT) and scattering width versus frequency (SWTE.DAT, SWTM.DAT). The scattering width computations are performed up to the 10 cell/λ_0 frequency limit. Refer to comments within these codes for further details.

VII. RESULTS

As previously mentioned, the codes as furnished model an infinite, 0.25 m radius, perfectly conducting cylinder and compute backscatter far zone scattered field at an angles of ϕ=180 degrees.

Figures 2-4 show the TM far zone electric field versus time and the scattering width magnitude and phase for the 0.25 m radius perfectly conducting cylinder. Keep in mind that the far zone time domain electric field shown here is <u>not</u> the actual time domain scattered field. The actual far zone time domain scattered field can be obtained by an FFT of the FDTD time domain results, then multiplying the FFT by the appropriate frequency domain factor (described in [4]) and performing an inverse FFT.

Figures 5-7 show the TE far zone electric field versus time and the scattering width magnitude and phase for the 0.25 m radius perfectly conducting cylinder.

VIII. SAMPLE PROBLEM SETUP

The codes as furnished model an infinite, 0.25 m radius, perfectly conducting cylinder and compute backscatter far zone scattered field at an angle of ϕ=180 degrees. The corresponding output data files are also provided, along with codes to compute scattering width using these data files. In order to change the code to a new problem, many different parameters need to be modified. A sample problem setup will now be discussed.

Suppose that the problem to be studied is scattering width backscatter versus frequency from a 0.30 m radius dielectric cylinder with a dielectric constant of $4\epsilon_0$ using a θ-polarized field. The backscatter angle is ϕ=60.0 degrees and the frequency range is up to 3 Ghz.

The incident field is θ-polarized which indicates the TM code must be used. Since the frequency range is up to 3 Ghz, the cell size must be chosen appropriately to resolve the field IN ANY MATERIAL at the highest frequency of interest. A general rule is that the cell size should be 1/10 of the wavelength at the highest frequency of interest. For difficult geometries, 1/20 of a wavelength may be necessary. The free space wavelength at 3 GHz is λ_0=10 cm and the wavelength in the dielectric coating at 3 GHz is 5 cm. The cell size is chosen as 1 cm, which provides a resolution of 5 cells/λ in the dielectric coating and 10 cells/λ_0 in free space. Numerical studies have shown that choosing the cell size $\leq$ 1/4 of the shortest wavelength in any material is the practical lower limit. Thus the cell size of 1 cm is barely adequate. The cell size in the x and y directions is set in the common file through variables DELX and DELY. Next the problem space size must be large enough to accomodate the scattering object, plus <u>at least</u> a five cell boundary (10 cells is more appropriate) on every side of the object to allow for the far zone field integration surface. The default problem space size of 201 by 201 is adequate and provides a 75 cell border around the cylinder. As an initial estimate, allow 2048 time steps so that energy trapped within the dielectric layer will radiate. Thus parameter NSTOP is changed to 2048. If all transients have not been dissipated after 2048 time steps, then NSTOP will have to be increased. Truncating the time record before all transients have dissipated will corrupt frequency domain results. Parameter NZFZ must be equal to 1 since we are interested in far zone fields only. To build the object, simply change the RADIUS variable in the BUILD subroutine to 0.30. In the common file, the incidence angle PHINC has to be changed to 60.0 respectively, and the cell sizes (DELX and DELY) are set to 0.01. Since dielectric material 2 is being used for the dielectric coating, the constitutive parameters EPS(2) and SIGMA(2) are set to $4\epsilon_0$ and 0.0 respectively, in subroutine SETUP. This completes the code modifications for the sample problem.

IX. NEW PROBLEM CHECKLIST

This checklist provides a quick reference to determine if all parameters have been defined properly for a given scattering problem. A reminder when defining quantities within the code: use MKS units and specify all angles in degrees.

TEACOM.FOR, TMACOM.FOR:

1) Is the problem space sized correctly? (NX, NY)

2) For near zone fields, is the number of sample points correct? (NTEST)

3) Is parameter NZFZ defined correctly for desired field outputs?

4) Is the number of time steps correct? (NSTOP)

5) Are the cell dimensions (DELX, DELY) defined correctly?

6) Is the incidence angle (PHINC) defined correctly?

7) For other than backscatter far zone field computations, is the scattering angle set correctly? (PHIFZ)

SUBROUTINE BUILD:

1) Is the object completely and correctly specified?

SUBROUTINE SETUP:

1) Are the constitutive parameters for each material specified correctly? (EPS and SIGMA)

FUNCTIONS SOURCE and DSRCE:

1) If the Gaussian pulse is not desired, is it commented out and the smooth cosine pulse uncommented?

SUBROUTINE DATSAV:

1) For near zone fields, are the sampled field types and spatial locations correct for each sampling point? (NTYPE, IOBS, JOBS)

X. REFERENCES

[1] K. S. Yee, "Numerical solution of initial boundary value problems involving Maxwell's equations in isotropic media," IEEE Trans. Antennas Propagat., vol. AP-14, pp. 302-307, May 1966.

[2] G. Mur, "Absorbing boundary conditions for the Finite-Difference approximation of the Time-Domain Electromagnetic-Field Equations," IEEE Trans. Electromagn. Compat., vol. EMC-23, pp. 377-382, November 1981.

[3] R. Holland, L. Simpson and K. S. Kunz, "Finite-Difference Analysis of EMP Coupling to Lossy Dielectric Structures," IEEE Trans. Electromagn. Compat., vol. EMC-22, pp. 203-209, August 1980.

[4] R.J. Luebbers et. al., "A Two-Dimensional Time-Domain Near Zone to Far Zone Transformation," submitted to IEEE Trans. Antennas Propagat. for publication, May 1991.

XI. FIGURE TITLES

Fig. 1 Standard two dimensional Yee cell showing placement of electric and magnetic fields for the TE and TM case.

Fig. 2 Far zone scattered field versus time for 0.25 m radius perfectly conducting cylinder using TM polarization.

Fig. 3 Scattering width magnitude versus frequency for 0.25 m radius perfectly conducting cylinder using TM polarization.

Fig. 4 Scattering width phase versus frequency for 0.25 m radius perfectly conducting cylinder using TM polarization.

Fig. 5 Far zone scattered field versus time for 0.25 m radius perfectly conducting cylinder using TE polarization.

Fig. 6 Scattering width magnitude versus frequency for 0.25 m radius perfectly conducting cylinder using TE polarization.

Fig. 7 Scattering width phase versus frequency for 0.25 m radius perfectly conducting cylinder using TE polarization.

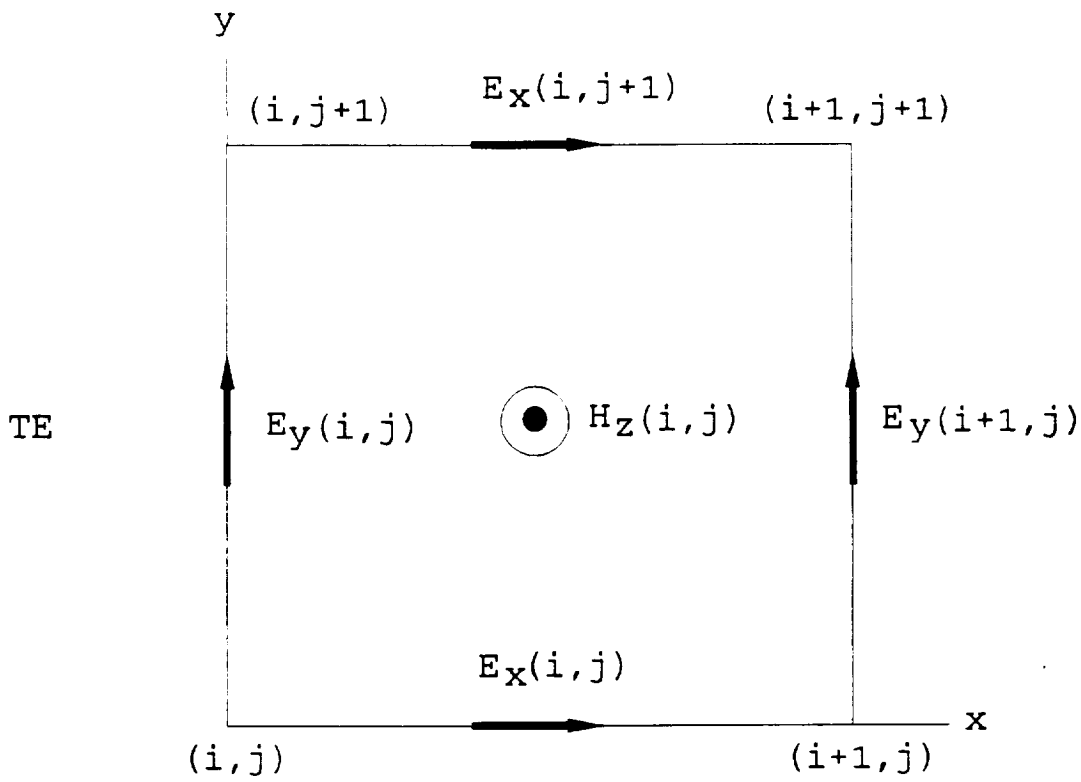
y
(i,j+1)
Ex(i,j+1)
(i+1,j+1)
TE
Ey(i,j)
Hz(i,j)
Ey(i+1,j)
Ex(i,j)
x
(i,j)
(i+1,j)

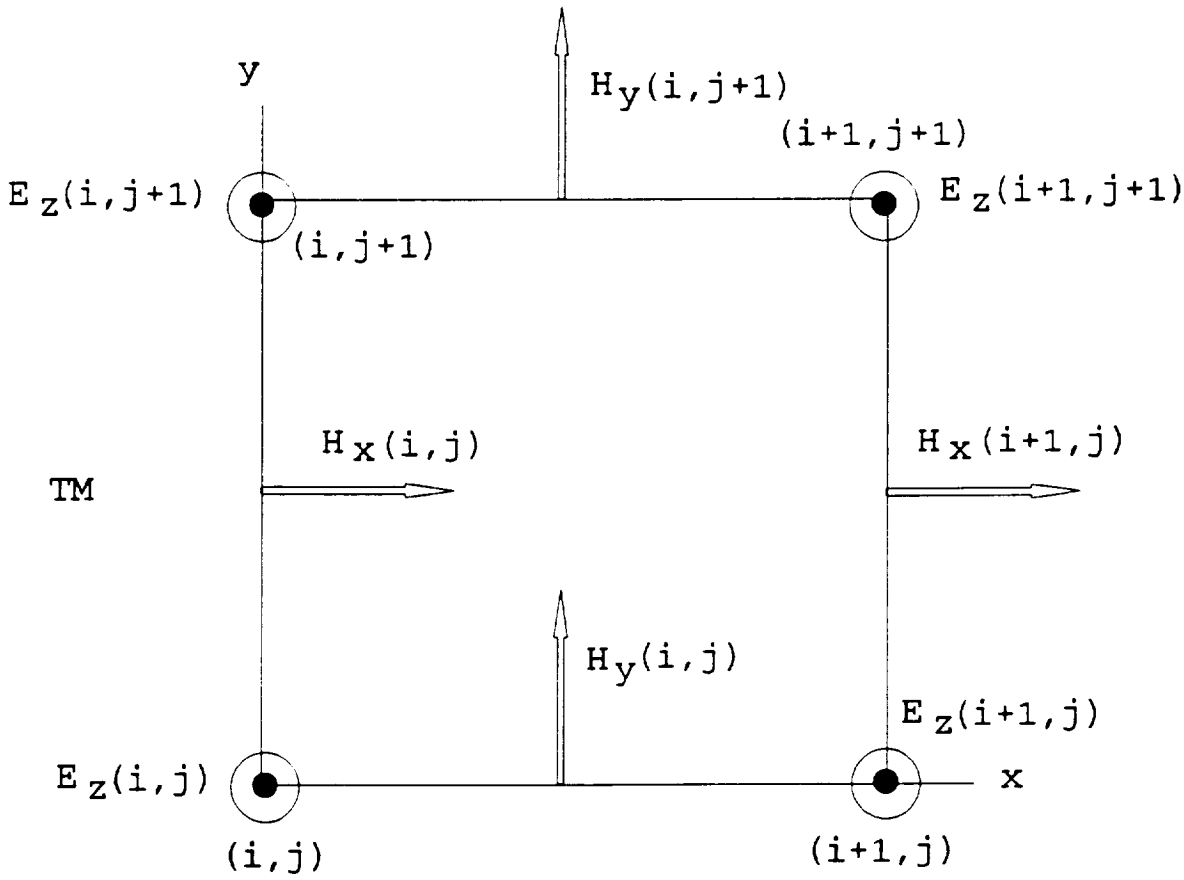
y
Hy(i,j+1)
(i+1,j+1)
Ez(i,j+1)
Ez(i+1,j+1)
(i,j+1)
Hx(i,j)
Hx(i+1,j)
TM
Hy(i,j)
Ez(i+1,j)
Ez(i,j)
x
(i,j)
(i+1,j)

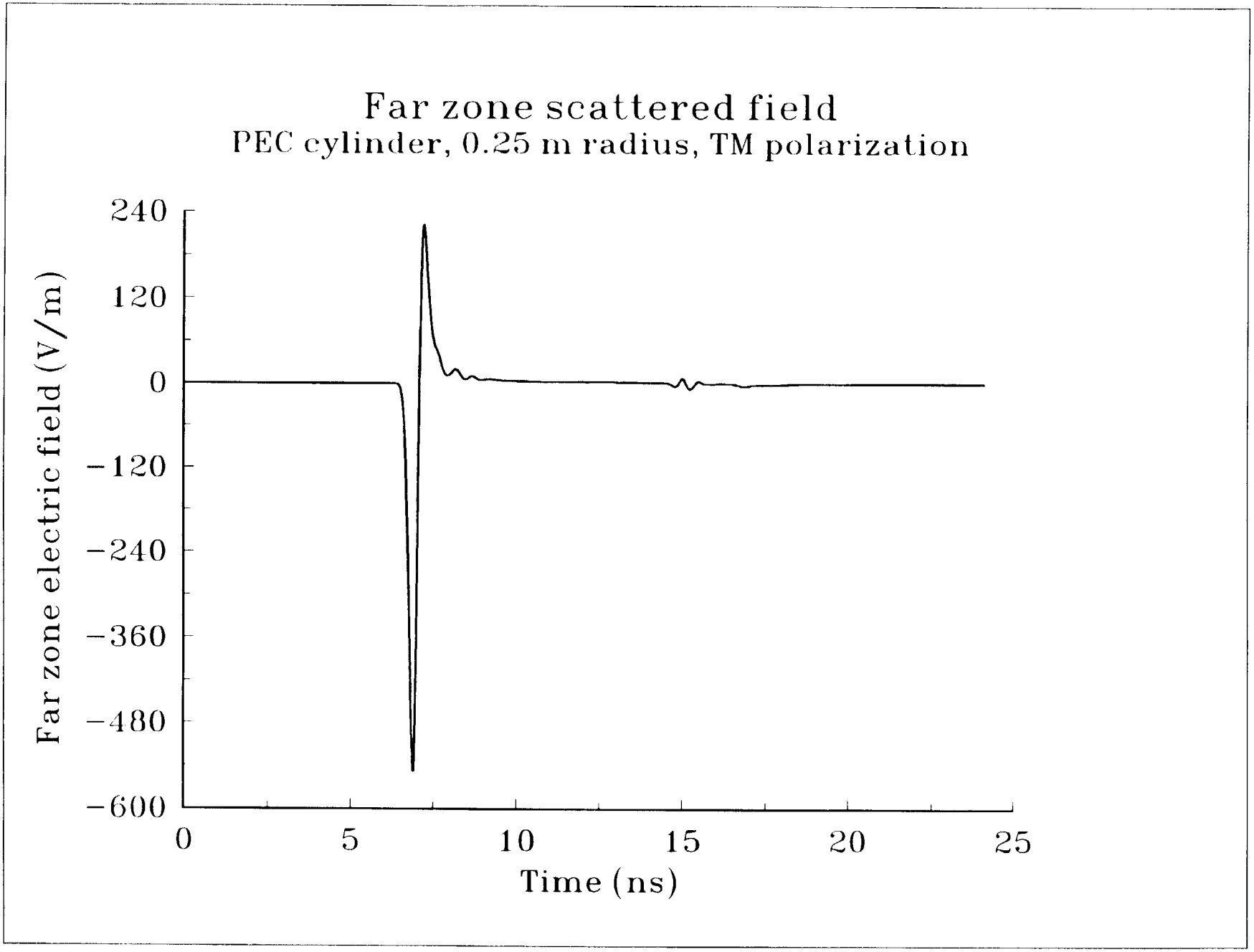
Far zone scattered field
PEC cylinder, 0.25 m radius, TM polarization
Far zone electric field (V/m)
240
120
0
−120
−240
−360
−480
−600
0
5
10
15
20
25
Time (ns)

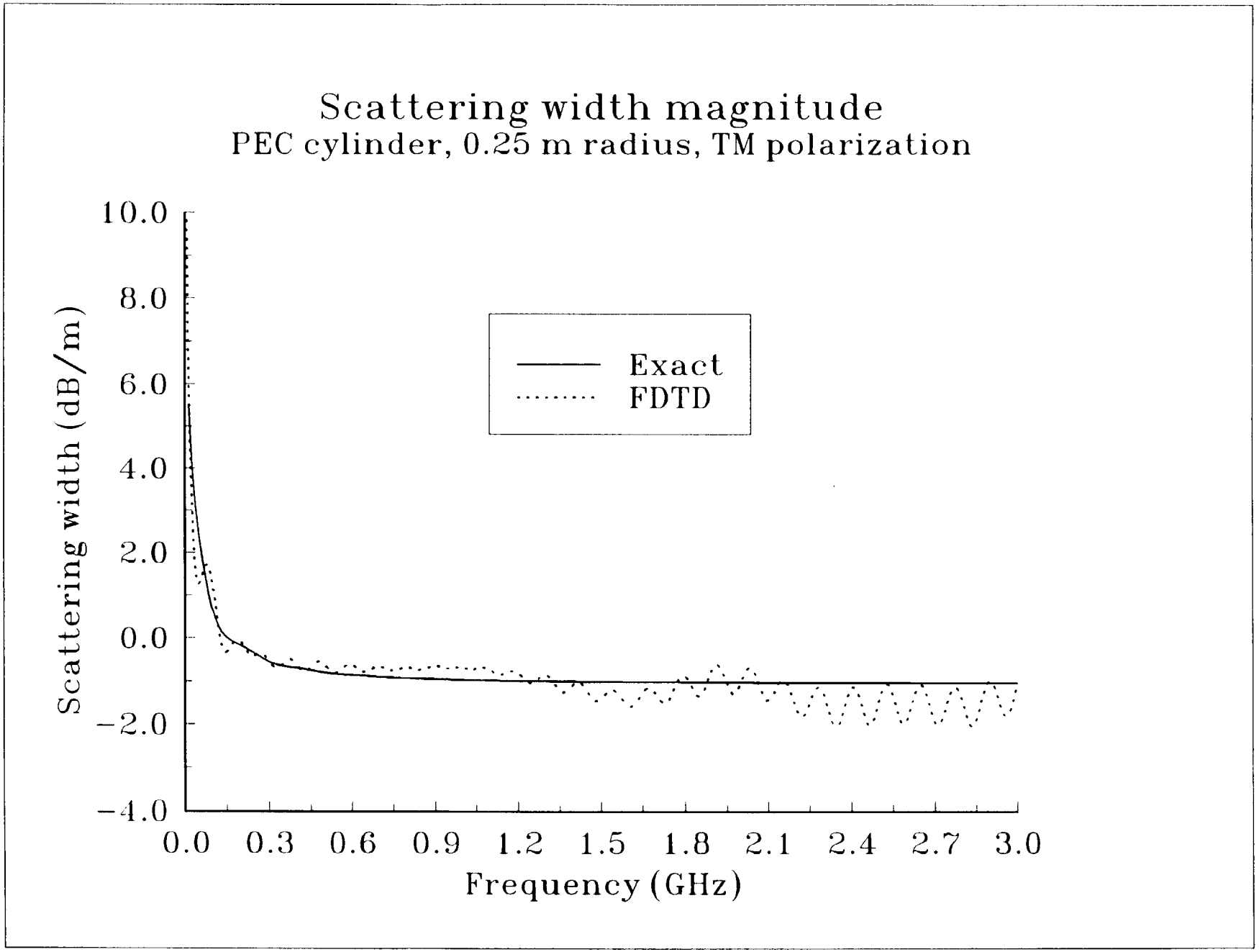
Scattering width magnitude
PEC cylinder, 0.25 m radius, TM polarization
Scattering width (dB/m)
10.0
8.0
6.0
4.0
2.0
0.0
−2.0
−4.0
Exact
FDTD
0.0
0.3
0.6
0.9
1.2
1.5
1.8
2.1
2.4
2.7
3.0
Frequency (GHz)

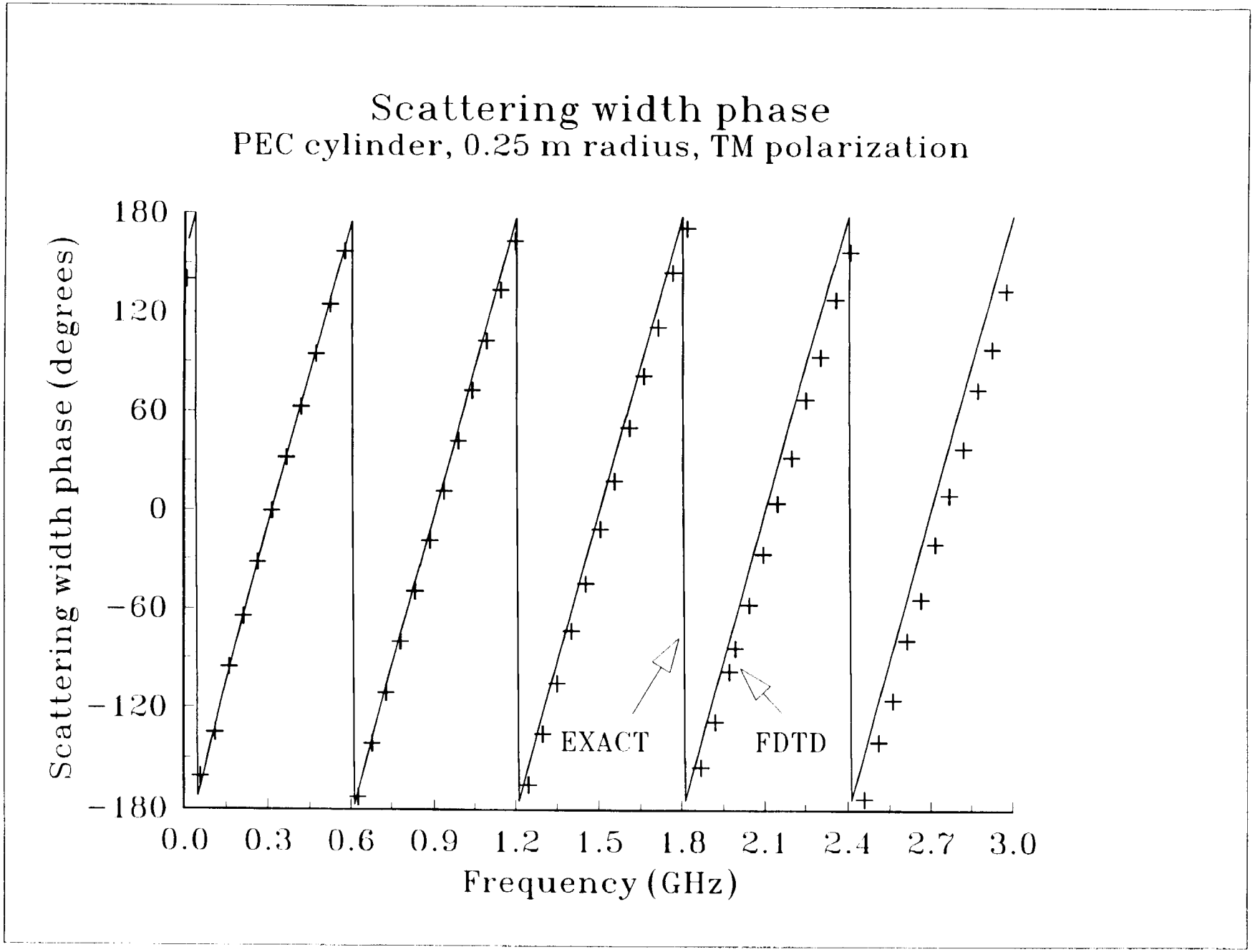
Scattering width phase
PEC cylinder, 0.25 m radius, TM polarization
Scattering width phase (degrees)
180
120
60
0
−60
−120
−180
0.0
0.3
0.6
0.9
1.2
1.5
1.8
2.1
2.4
2.7
3.0
Frequency (GHz)
EXACT
FDTD

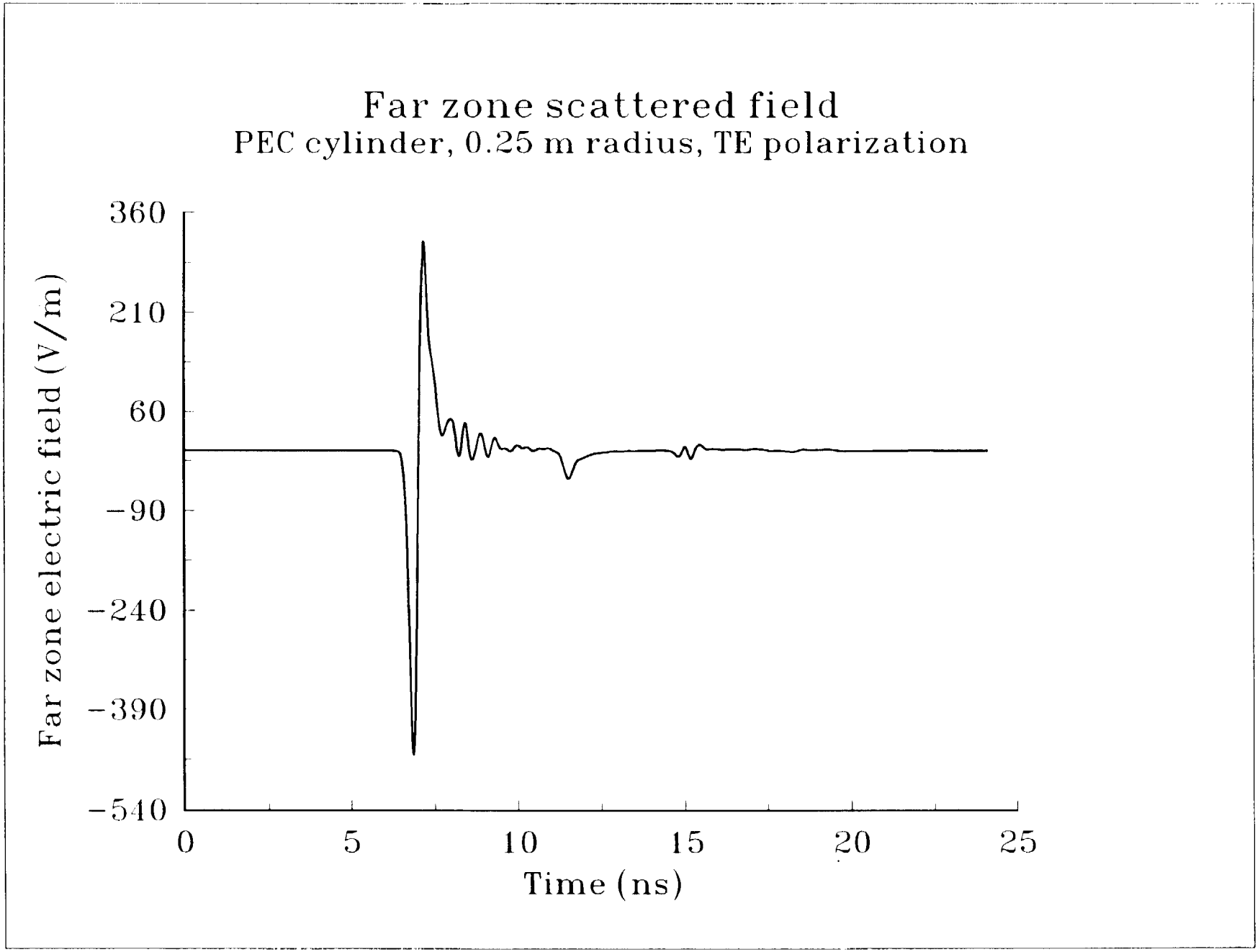
Far zone scattered field
PEC cylinder, 0.25 m radius, TE polarization
Far zone electric field (V/m)
360
210
60
−90
−240
−390
−540
0
5
10
15
20
25
Time (ns)

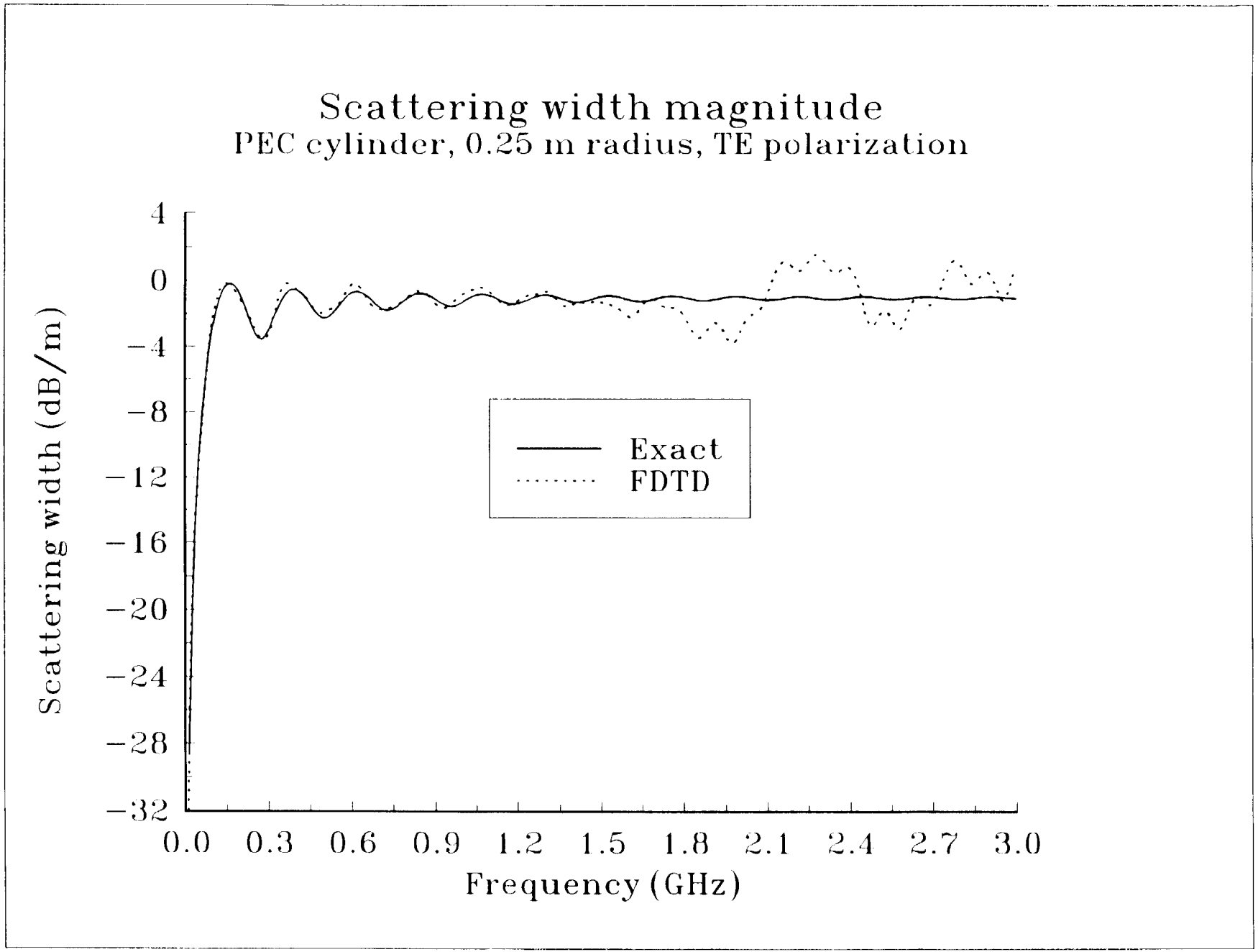
Scattering width magnitude
PEC cylinder, 0.25 m radius, TE polarization
Scattering width (dB/m)
4
0
−4
−8
−12
−16
−20
−24
−28
−32
0.0
0.3
0.6
0.9
1.2
1.5
1.8
2.1
2.4
2.7
3.0
Frequency (GHz)
Exact
FDTD

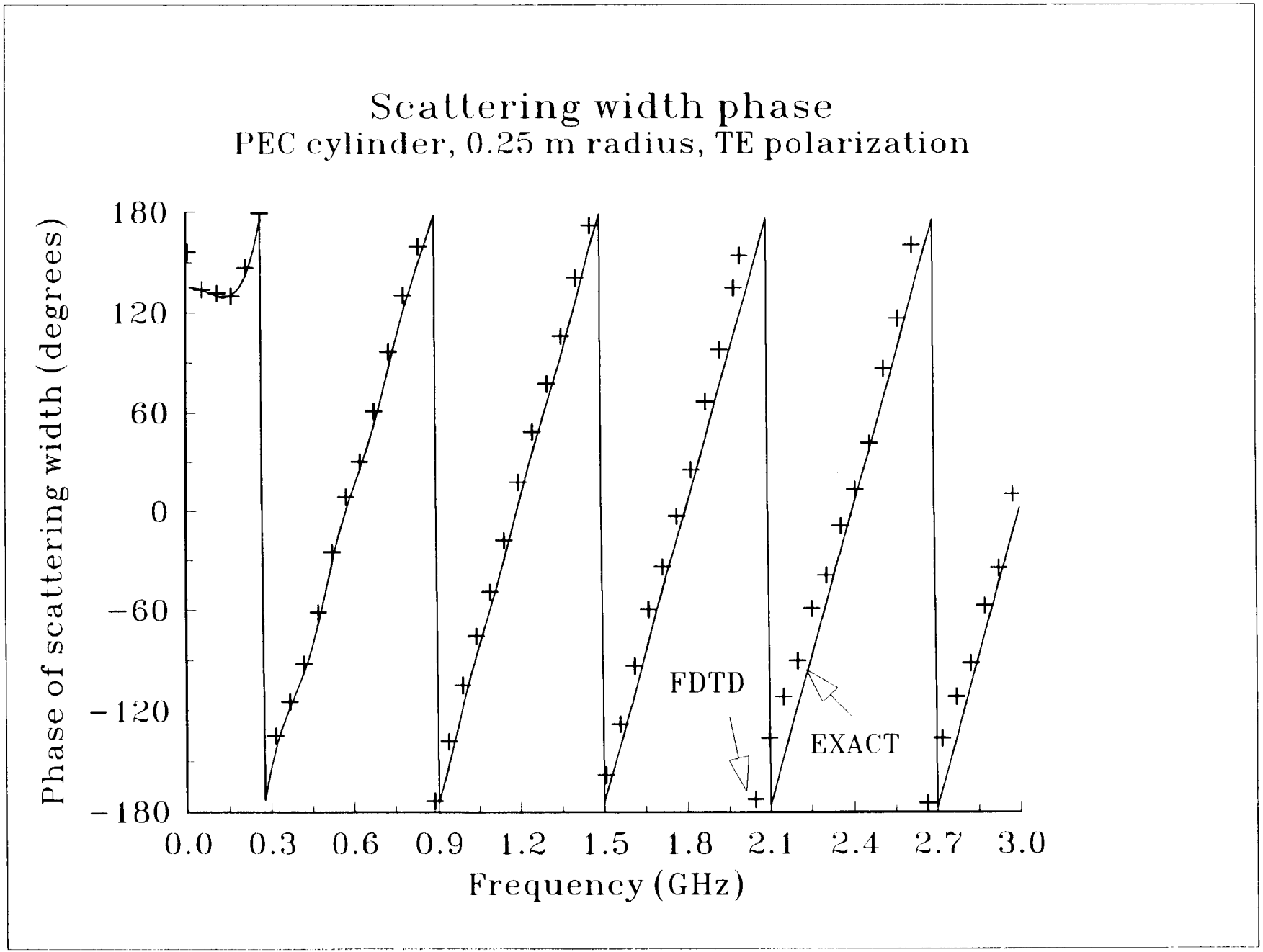
Scattering width phase
PEC cylinder, 0.25 m radius, TE polarization
Phase of scattering width (degrees)
180
120
60
0
−60
−120
−180
0.0
0.3
0.6
0.9
1.2
1.5
1.8
2.1
2.4
2.7
3.0
Frequency (GHz)
FDTD
EXACT

A TWO-DIMENSIONAL TIME DOMAIN NEAR ZONE TO FAR ZONE TRANSFORMATION

by

Raymond Luebbers, Deirdre Ryan, John Beggs
and Karl Kunz

Electrical and Computer Engineering Department
The Pennsylvania State University
University Park, PA 16802

May 1991

Abstract

In a previous paper [1] a time domain transformation useful for extrapolating three dimensional near zone finite difference time domain (FDTD) results to the far zone was presented. In this paper the corresponding two dimensional transform is outlined. While the three dimensional transformation produced a physically observable far zone time domain field, this is not convenient to do directly in two dimensions, since a convolution would be required. However, a representative two dimensional far zone time domain result can be obtained directly. This result can then be transformed to the frequency domain using a Fast Fourier Transform, corrected with a simple multiplicative factor, and used, for example, to calculate the complex wideband scattering width of a target. If an actual time domain far zone result is required it can be obtained by inverse Fourier transform of the final frequency domain result.

Introduction

A previous paper [1] described a method for transforming near zone Finite Difference Time Domain (FDTD) results directly to the far zone without first transforming to the frequency domain. This far zone field could then be used to compute the scattering cross section of an illuminated target or an antenna radiation pattern over the entire frequency band of the FDTD calculations. A similar result was published in [2]. In this paper the corresponding two dimensional transform is presented, and validated by comparison with calculated results for a perfectly conducting circular cylinder.

Approach

In [1] the frequency domain far zone transformation equations were Fourier transformed to the time domain and used in that form to derive an approach to transform near zone FDTD fields to the far zone directly in the time domain. Our approach here will be to present the fundamental frequency domain equations for both two and three dimensions, and by comparing them obtain the factor needed to convert the three dimensional far zone transform to function in two dimensions.

We again surround the scatterer with a closed surface S', and consider that equivalent tangential electric and magnetic time harmonic surface currents may exist on this surface. Referring to [3], we obtain the vector potentials for the three dimensional case as

$$\bar{A} = \frac{e^{-jkr}}{4\pi r} \int_{S'} \bar{J}_s \, e^{jk\bar{r}'\cdot\hat{r}} \, ds' \qquad (1)$$

$$\bar{F} = \frac{e^{-jkr}}{4\pi r} \int_{S'} \bar{M}_s \, e^{jk\bar{r}'\cdot\hat{r}} \, ds' \qquad (2)$$

with $j=\sqrt{-1}$, $k = \omega\sqrt{\mu\epsilon}$ (the wave number), $\hat{r}$ the unit vector to the far zone field point, $\bar{r}'$ the vector to the source point of integration, r the distance to the far zone field point, and S' the closed surface surrounding the scatterer.

The far zone frequency domain electric fields of the scatterer are then obtained from

$$E_\theta = -j\omega\mu A_\theta - j\omega\sqrt{\mu\epsilon}\, F_\phi \qquad (3)$$

$$E_\phi = -j\omega\mu A_\phi + j\omega\sqrt{\mu\epsilon}\, F_\theta \qquad (4)$$

One can then easily convert to radar cross section (RCS), if desired, by applying

$$\sigma_{3D} = \lim_{r\to\infty} \left(4\pi r^2 \frac{|E^s_{3D}|^2}{|E^i|^2}\right) \qquad (5)$$

where E^s_{3D} is either E_θ or E_ϕ of (2) or (3), and E^i is the incident plane wave electric field.

In [1] the equations corresponding to (1,2) were easily transformed to the time domain since the exponential phase term inside the integrals corresponds to a time shift relative to an arbitrary time reference point. Equations corresponding to (2,3) were also readily transformed to the time domain since the $j\omega$ factor in these equations corresponds to a time derivative. Thus the resulting time domain fields can be obtained conveniently directly in the time domain, as shown in [1].

Now consider the corresponding equations in two dimensions. The vector potentials are given by

$$\bar{A} = \frac{e^{-jk\rho}}{\sqrt{8jk\pi\rho}} \int_{s'} \bar{J}_s \, e^{jk\rho'\cos(\phi-\phi')} \, ds' \tag{6}$$

$$\bar{F} = \frac{e^{-jk\rho}}{\sqrt{8jk\pi\rho}} \int_{s'} \bar{M}_s \, e^{jk\rho'\cos(\phi-\phi')} \, ds' \tag{7}$$

where ρ' and ϕ' are the coordinates of the source point of integration, and ρ and ϕ the coordinates of the far zone field point. The corresponding far zone radiated fields are obtained from

$$E_z = -j\omega\mu A_z + j\omega\sqrt{\mu\epsilon}\, F_\phi \tag{8}$$

$$E_\phi = -j\omega\mu A_\phi - j\omega\sqrt{\mu\epsilon}\, F_z \tag{9}$$

Also, the two dimensional scattering width is defined as

$$\sigma_{2D} = \lim_{\rho\to\infty} \left(2\pi\rho \frac{|E^s_{2D}|^2}{|E^i|^2}\right) \tag{10}$$

where E^s_{2D} is either E_z or E_ϕ of (8,9).

The approach applied in [1] cannot be conveniently applied in the two dimensional case due to the factor of $1/\sqrt{jk}$ (actually $1/\sqrt{j\omega\sqrt{\mu\epsilon}}$) in (6,7). In order to evaluate the Fourier transform of (6,7) directly in the time domain a convolution operation would be required. To avoid this complication our approach will be to modify the results in [1] to provide representative two dimensional time domain far zone fields which can then be converted to the actual frequency domain fields by a multiplication in the frequency domain rather than the time domain convolution. Should the actual time domain far zone fields be required, they can then be obtained by an additional Fourier transform of these results back to the time domain.

In order to convert our previous three dimensional results to two dimensions, we compare the two sets of equations. First, comparing (3,4) with (8,9), since the spherical unit θ vector is equal to the negative of the cylindrical unit z vector, (3,4) and (8,9) correspond exactly, and no adjustment between two and three dimensional transforms is needed.

Next, comparing (1,2) with (6,7) the r^2 and ρ factors are compensated by the definitions in (5) and (10) respectively, as expected, and no compensation is needed here either.

Finally, consider equations (1,2) vs (6,7). The additional dimension of integration in (1,2) is compensated for by defining a scattering width per unit length (in z) in (10). This

corresponds in (1,2) to having no z variation and integrating the z' variable over a unit distance. The exponents provide equivalent phase (time) delays and need not be compensated for. Considering the remaining factors, it is easily determined that in the frequency domain, the relationship between far zone electric fields obtained from a three dimensional far zone transformation with no z variation and the two dimensional far zone fields is

$$E^s_{2D} = \sqrt{\frac{2\pi c}{j\omega}}\; E^s_{3D} \tag{11}$$

where $c = 1/\sqrt{\mu\epsilon}$.

With these results the time domain far zone transform given in [1] can be easily adapted to two dimensions as follows:

1) Consider only the field components and corresponding surface currents excited in the two dimensional problem. For example, for a TE_z computation only H_z, E_x, E_y, and the corresponding surface currents are included.

2) Calculate the far zone time domain fields using the method described in [1], but for a two dimensional integration surface which encloses the scatterer. Let δz, the z coordinate unit cell dimension used in [1], equal 1 (meter). (This field is not a physically observable field. It represents the radiation from a unit length of the scatterer in the time domain.)

3) Fourier transform the result of step 2) and multiply the result by the factor in (11). This result is the frequency domain two dimensional far zone field, which can then be used in

(10) to calculate the scattering width as a function of frequency.

4) If the actual time domain two dimensional far zone field is desired, it can be obtained by an additional Fourier transformation of the result obtained in 3) back to the time domain.

Demonstration

In order to demonstrate the capabilities of the above approach a pair (TE_z and TM_z) of FDTD codes were developed from the three dimensional FDTD code described in [1]. These codes utilize second order Mur absorbing boundary conditions acting on the electric fields. The test geometry was a circular perfectly conducting cylinder of radius 0.25 meters.

Both TE and TM polarization was considered, and two sets of calculations were made for each polarization. For the first set the FDTD cells were 1 cm squares, with a problem space 200x200 cells. For the second set the cells were 0.5 cm squares in a 500x500 cell problem space. On a 25 MHz 486 PC (approximately 1 MFLOP) each of the first set required about 20 minutes to compute, with each of the second set requiring a few minutes less than 2 hours.

For all cases the incident plane wave traveled in the x direction, backscatter was calculated, and 2048 time steps were evaluated. In order to clearly show the response, not all time steps are included in the Figures.

Figure 1 shows the relative far zone fields computed directly in the time domain as outlined above for the TM polarization. The small ripple at approximately 15 ns on Figure 1 is due to reflections from the Mur outer boundary. Figures 2 and 3 show comparison with the exact solution for the scattering

width amplitude and phase. The upper frequency limit of 3.0 GHz corresponds to 10 cells per wavelength. The agreement is quite good.

A similar set of data for TE polarization is shown in Figures 4-6. The time domain far zone results in Figure 4 has ripples in the 6-8 ns range due to the staircasing of the round cylinder with square FDTD cells. The small negative pulse at 10 ns is the creeping wave which has traveled around the cylinder. Again, there is a small ripple at 14 ns due to the Mur boundary reflection. This is the difficult polarization for approximating a smooth surface with a "staircased" FDTD code, yet the agreement in Figures 5 and 6 is reasonably good, reproducing the first 6 1/2 ripples in the scattering width.

The above calculations are repeated in Figures 7-13 with a greater expenditure of computer resources. For these results the cell size of 0.5 cm changes the 3.0 GHz upper frequency limit of the plots to correspond to 20 cells per wavelength. The improvement in the agreement with the exact solution is clear, indicating the accuracy that can be obtained from this approach. Note especially Figure 12, which shows on a expanded dB scale agreement with the exact solution within a fraction of a dB for the first 9 lobes of the response.

Conclusions

A simple approach to calculating a wide bandwidth time domain transformation of near zone FDTD fields to the far zone has been presented. It is based on simple modifications to the previous three dimensional method presented in [1]. Results obtained using this transformation show good agreement with the exact solution for a circular cylinder for both polarizations.

References

1. R. J. Luebbers, K. S. Kunz, M. Schneider, and F. Hunsberger, "A Finite Difference Time-Domain Near Zone to Far Zone Transformation," IEEE Trans. Ant. Prop., Vol. 39, No. 4, April 1991, pp 429-433.

2. K. S. Yee, D. Ingham, and K. Shlager, "Time-Domain Extrapolation to the Far Field Based on FDTD Calculations," IEEE Trans. Ant. Prop., Vol. 39, No. 3, March 1991, pp 410-412.

3. R. F. Harrington, Time-Harmonic Electromagnetic Fields, McGraw-Hill, 1961.

Figure Titles

Fig 1. Far Zone relative electric field vs time for TM_z polarized incident Gaussian pulsed plane wave illuminating a perfectly conducting circular cylinder. FDTD cells are 1 cm squares.

Fig 2. Scattering width amplitude obtained from far zone time domain results and compared with exact solution. FDTD cells are 1 cm squares.

Fig 3. Scattering width phase obtained from far zone time domain results and compared with exact solution. FDTD cells are 1 cm squares.

Fig 4. Far Zone relative electric field vs time for TE_z polarized incident Gaussian pulsed plane wave illuminating a perfectly conducting circular cylinder. FDTD cells are 1 cm squares.

Fig 5. Scattering width amplitude obtained from far zone time domain results and compared with exact solution. FDTD cells are 1 cm squares.

Fig 6. Scattering width phase obtained from far zone time domain results and compared with exact solution. FDTD cells are 1 cm squares.

Fig 7. Far Zone relative electric field vs time for TM_z polarized incident Gaussian pulsed plane wave illuminating a perfectly conducting circular cylinder. FDTD cells are 0.5 cm squares.

Fig 8. Scattering width amplitude obtained from far zone time domain results and compared with exact solution. FDTD cells are 0.5 cm squares.

Fig 9. Scattering width phase obtained from far zone time domain results and compared with exact solution. FDTD cells are 0.5 cm squares.

Fig 10. Far Zone relative electric field vs time for TE_z polarized incident Gaussian pulsed plane wave illuminating a perfectly conducting circular cylinder. FDTD cells are 0.5 cm squares.

Fig 11. Scattering width amplitude obtained from far zone time domain results and compared with exact solution. FDTD cells are 0.5 cm squares.

Fig 12. Scattering width amplitude obtained from far zone time domain results and compared with exact solution on an expanded dB scale. FDTD cells are 0.5 cm squares.

Fig 13. Scattering width phase obtained from far zone time domain results and compared with exact solution. FDTD cells are 0.5 cm squares.

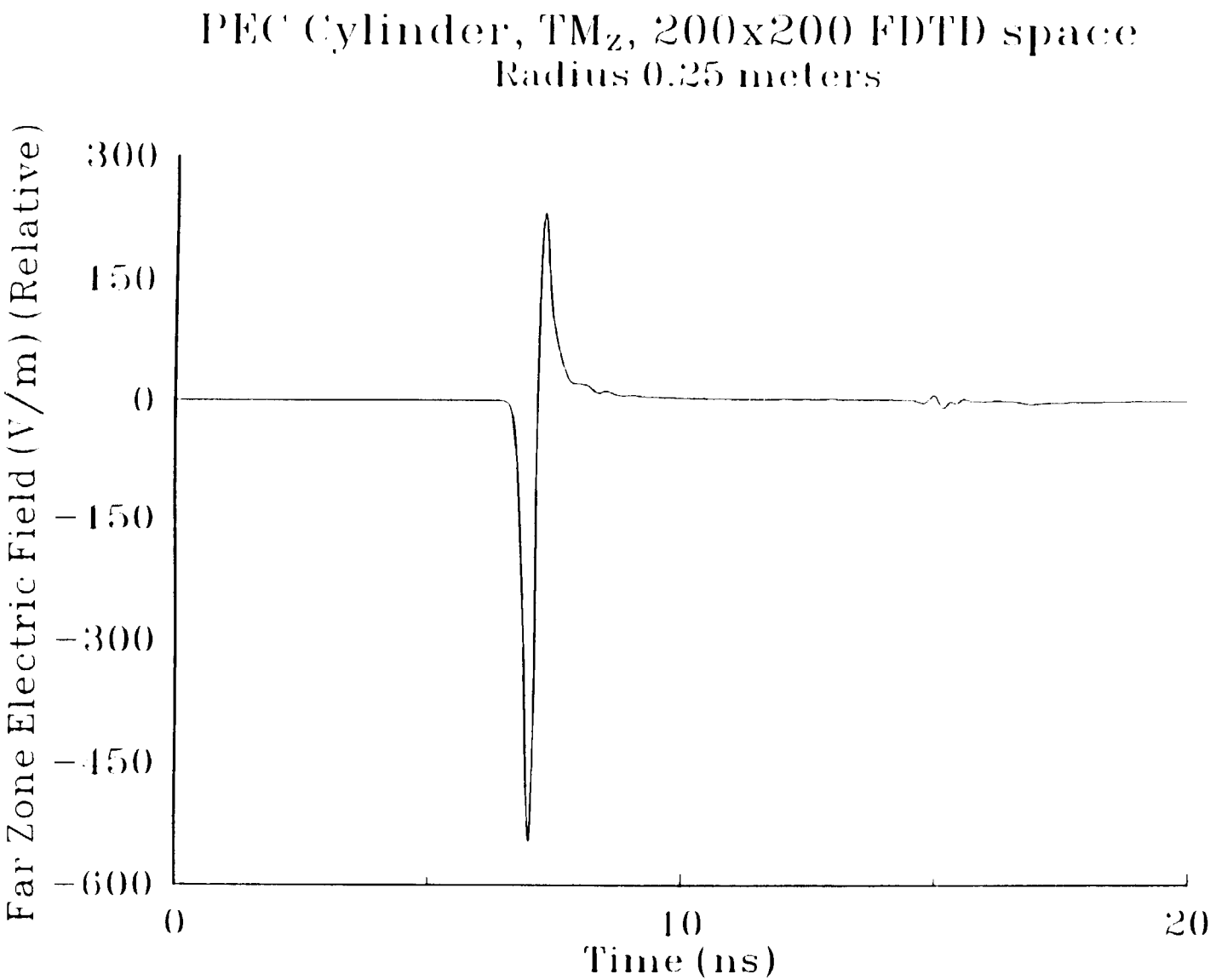
PEC Cylinder, TMz, 200x200 FDTD space
Radius 0.25 meters
Far Zone Electric Field (V/m) (Relative)
300
150
0
−150
−300
−450
−600
0
10
20
Time (ns)

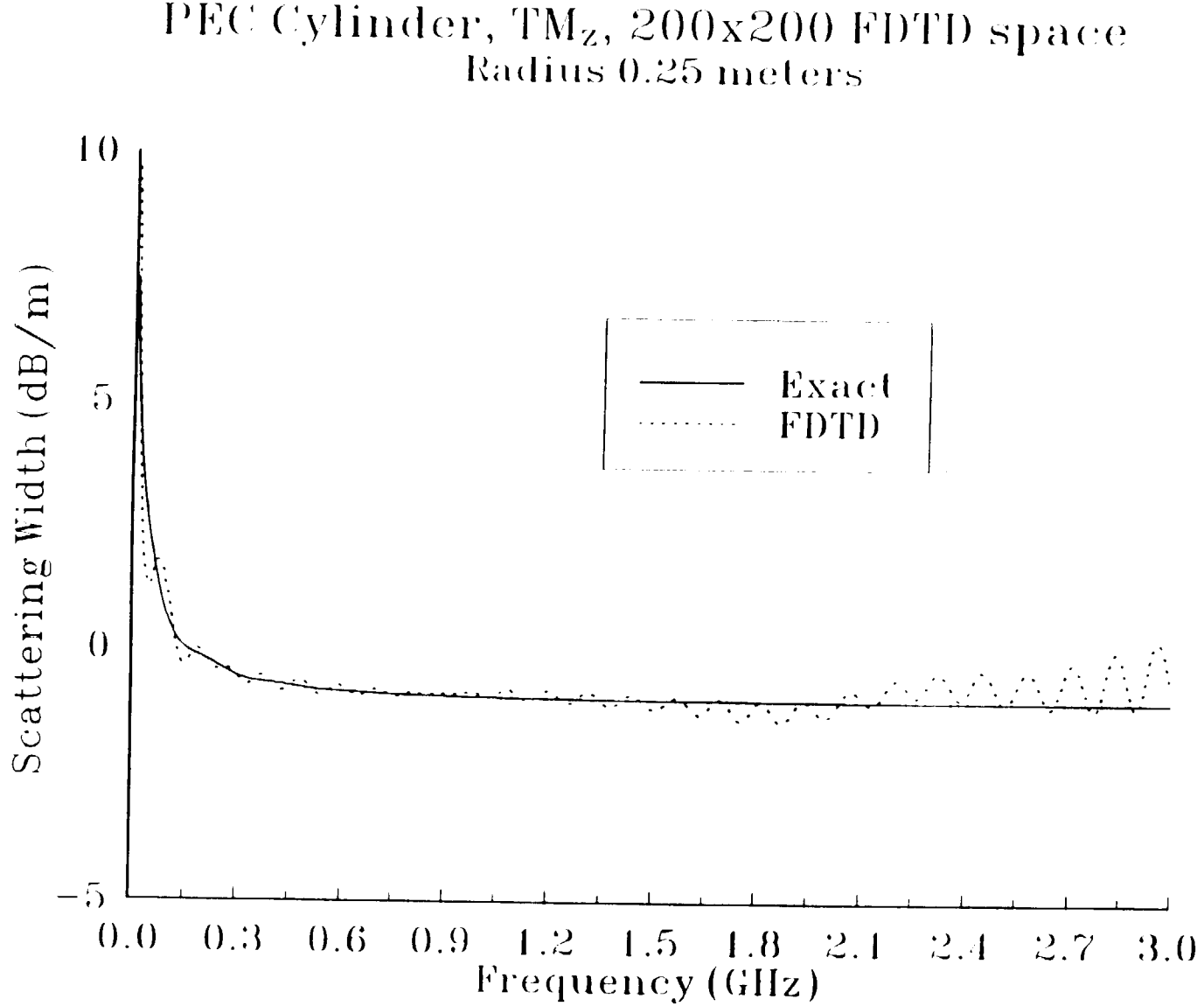
PEC Cylinder, TMz, 200x200 FDTD space
Radius 0.25 meters
Scattering Width (dB/m)
10
5
0
−5
0.0
0.3
0.6
0.9
1.2
1.5
1.8
2.1
2.4
2.7
3.0
Frequency (GHz)
Exact
FDTD

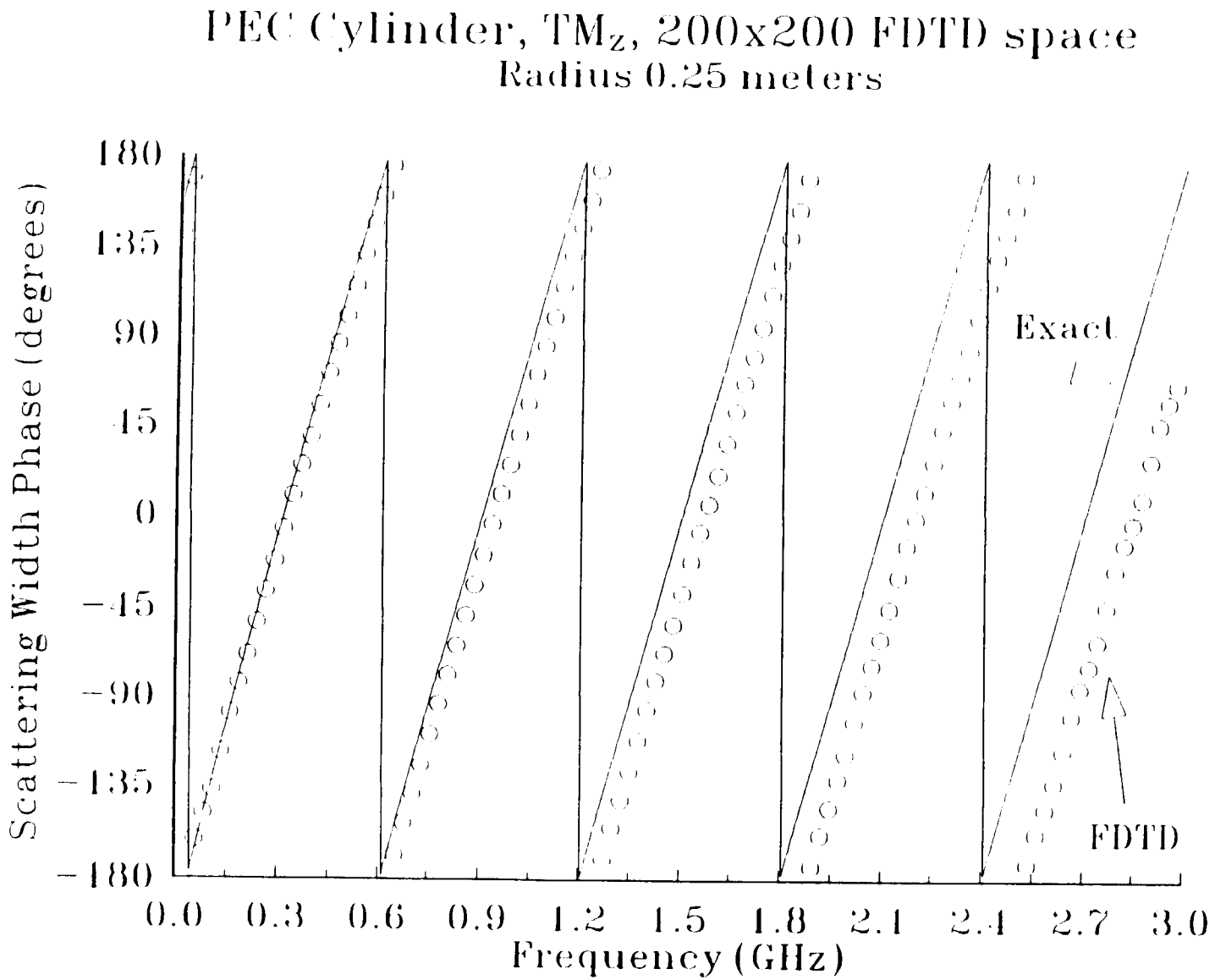
PEC Cylinder, TMz, 200x200 FDTD space
Radius 0.25 meters
Scattering Width Phase (degrees)
180
135
90
45
0
-45
-90
-135
-180
0.0
0.3
0.6
0.9
1.2
1.5
1.8
2.1
2.4
2.7
3.0
Frequency (GHz)
Exact
FDTD

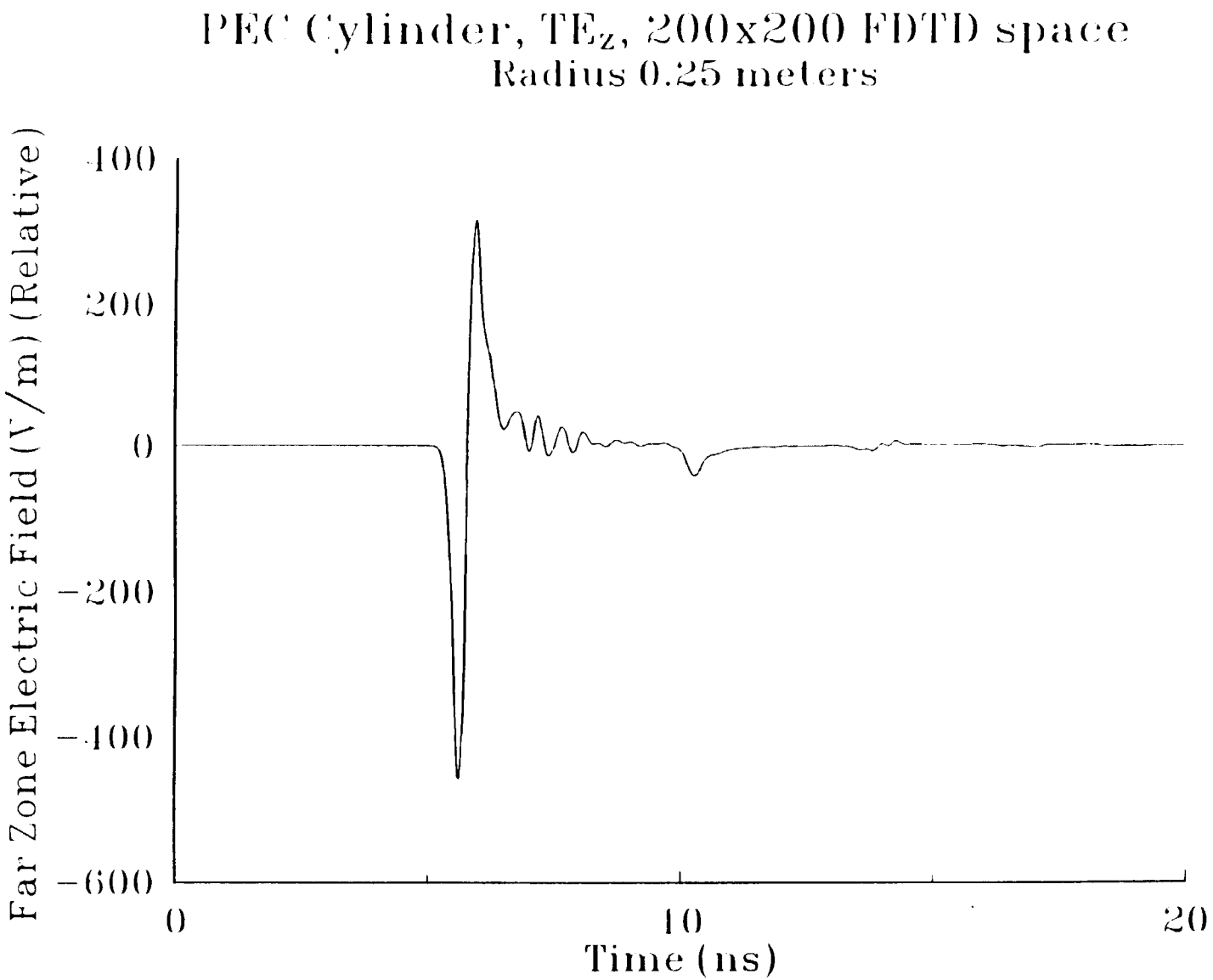
PEC Cylinder, TEz, 200x200 FDTD space
Radius 0.25 meters
Far Zone Electric Field (V/m) (Relative)
400
200
0
−200
−400
−600
0
10
20
Time (ns)

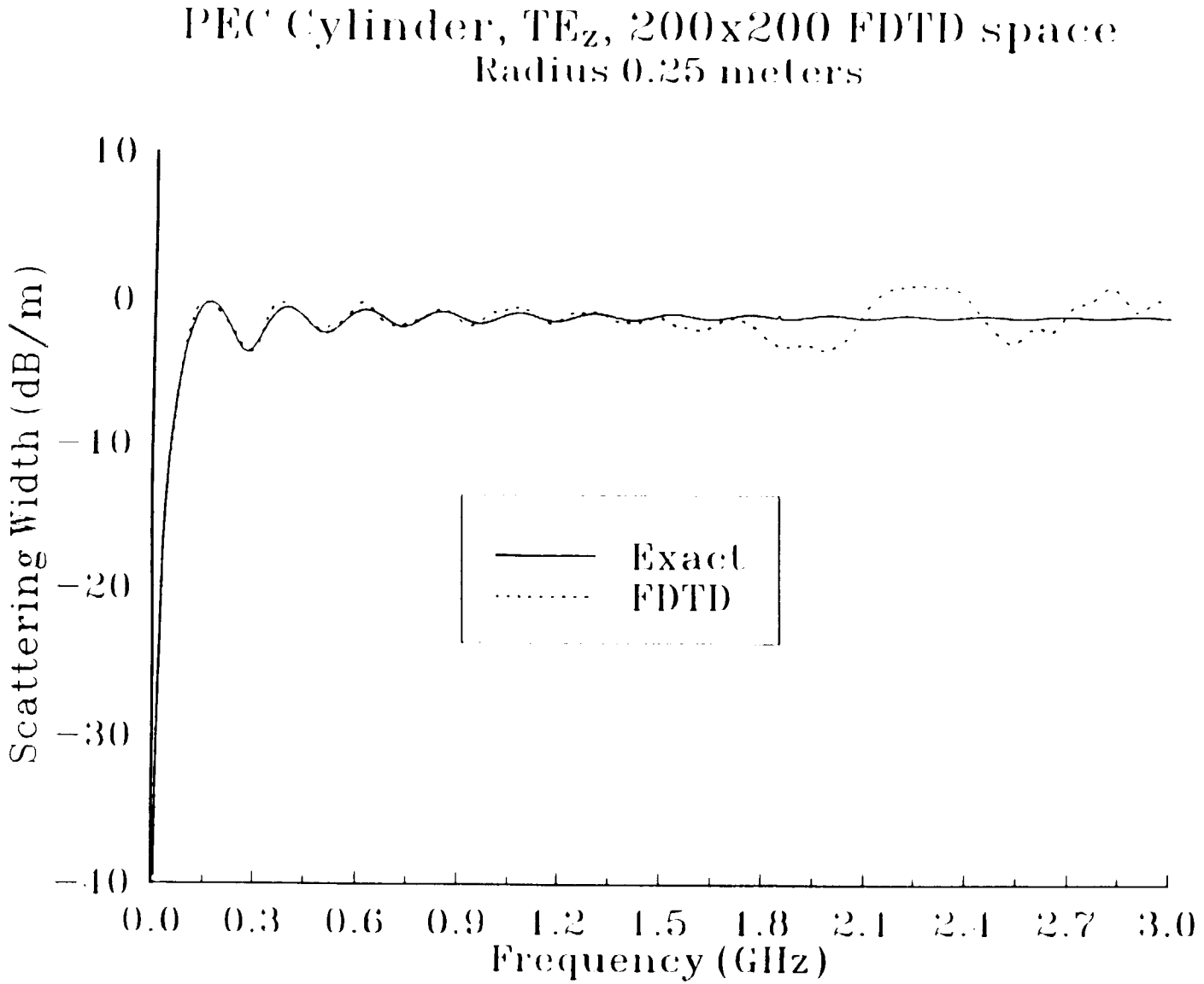
PEC Cylinder, TEz, 200x200 FDTD space
Radius 0.25 meters
Scattering Width (dB/m)
10
0
-10
-20
-30
-40
0.0
0.3
0.6
0.9
1.2
1.5
1.8
2.1
2.4
2.7
3.0
Frequency (GHz)
Exact
FDTD

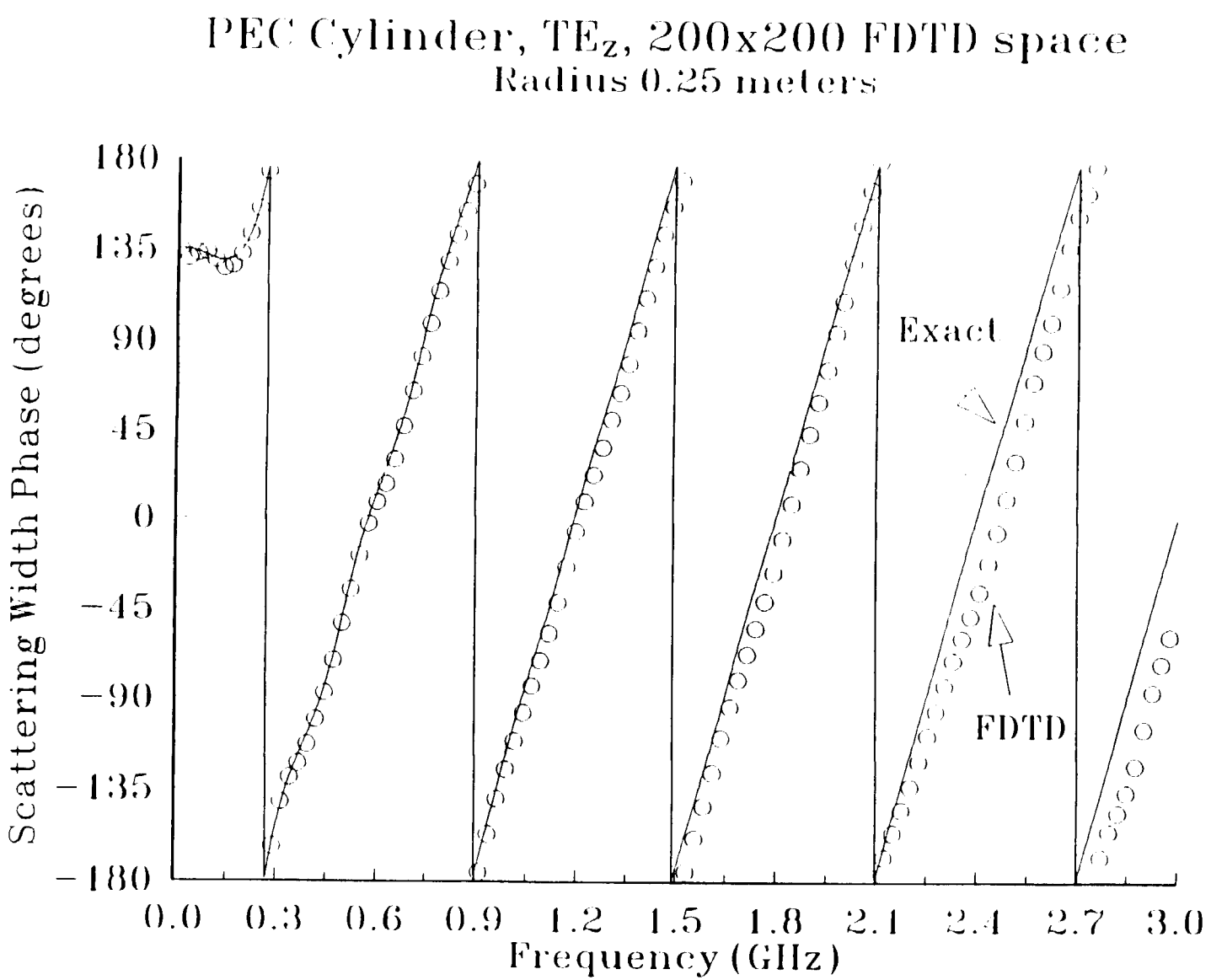
PEC Cylinder, TEz, 200x200 FDTD space
Radius 0.25 meters
Scattering Width Phase (degrees)
180
135
90
45
0
-45
-90
-135
-180
0.0
0.3
0.6
0.9
1.2
1.5
1.8
2.1
2.4
2.7
3.0
Frequency (GHz)
Exact
FDTD

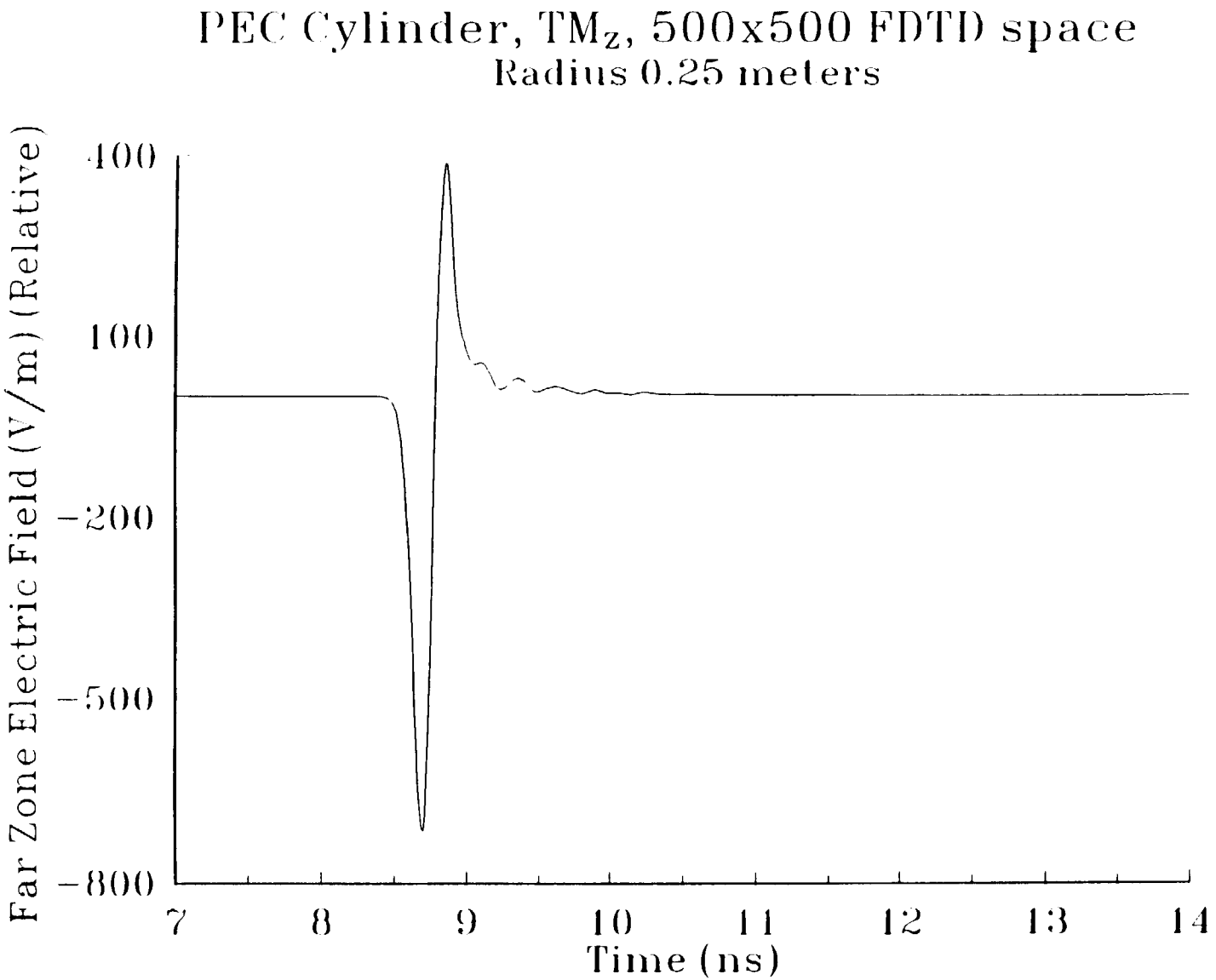
PEC Cylinder, TMz, 500x500 FDTD space
Radius 0.25 meters
Far Zone Electric Field (V/m) (Relative)
400
100
-200
-500
-800
7
8
9
10
11
12
13
14
Time (ns)

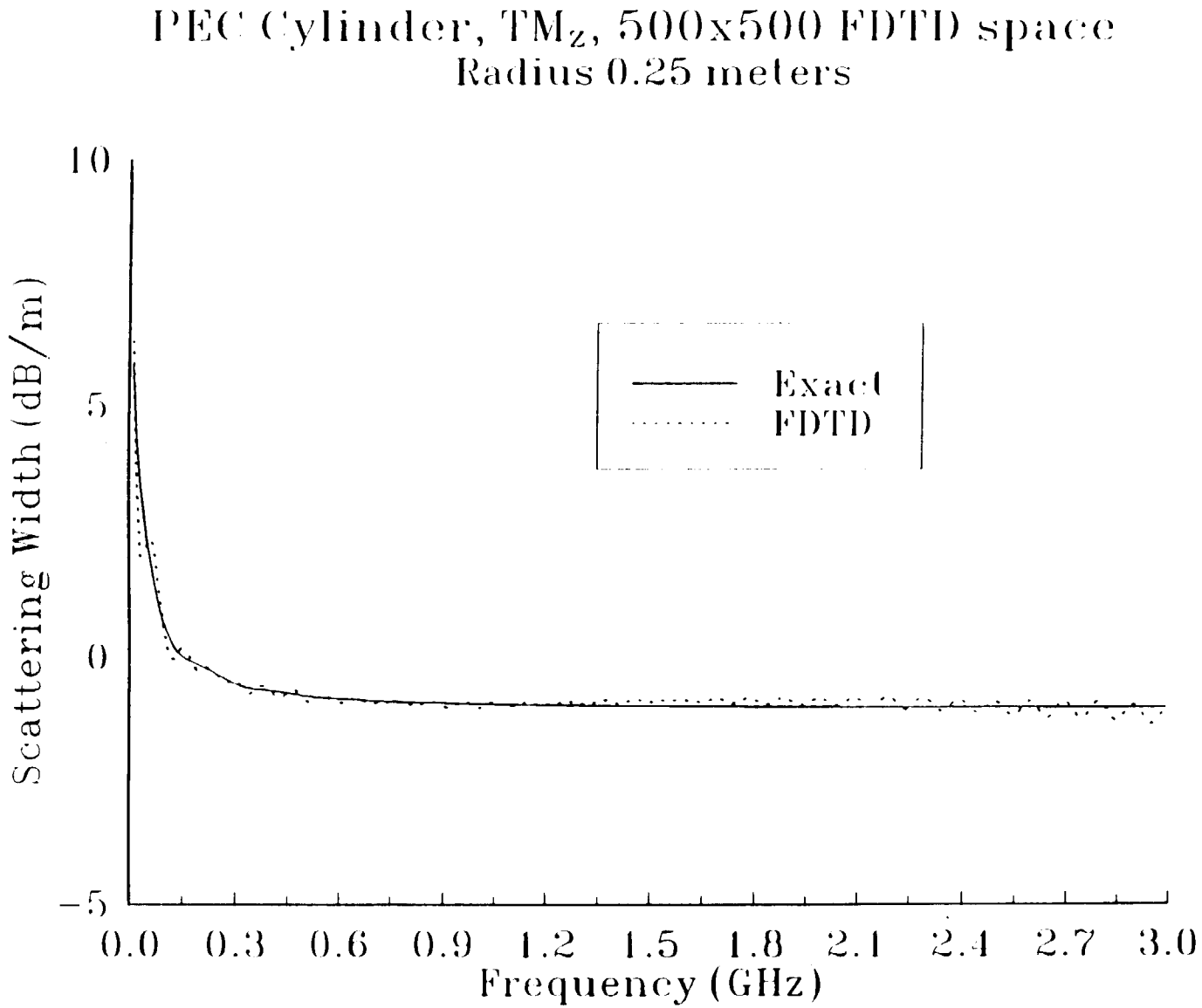
PEC Cylinder, TMz, 500x500 FDTD space
Radius 0.25 meters
Scattering Width (dB/m)
10
5
0
−5
0.0
0.3
0.6
0.9
1.2
1.5
1.8
2.1
2.4
2.7
3.0
Frequency (GHz)
Exact
FDTD

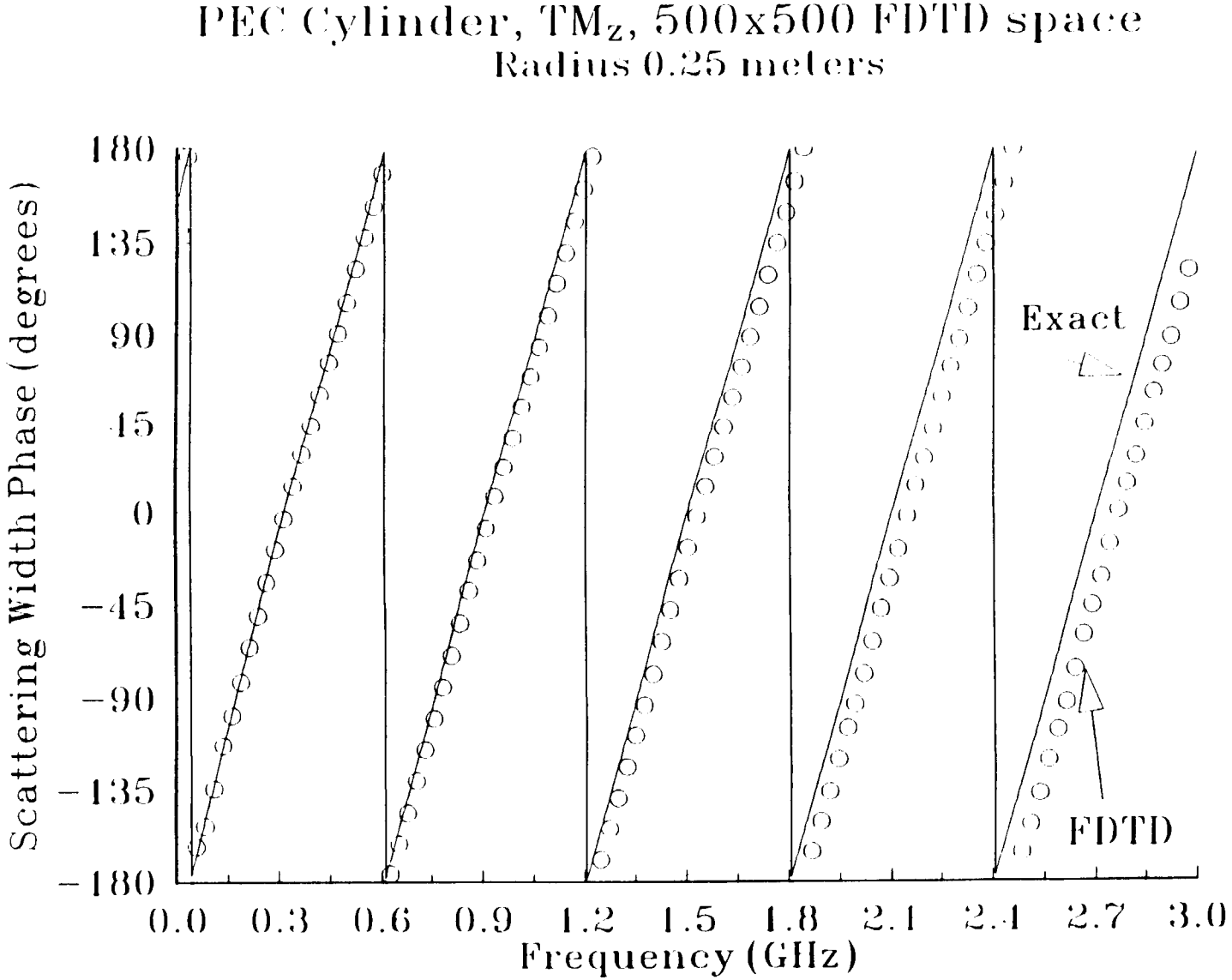
PEC Cylinder, TMz, 500x500 FDTD space
Radius 0.25 meters
Scattering Width Phase (degrees)
180
135
90
45
0
-45
-90
-135
-180
0.0
0.3
0.6
0.9
1.2
1.5
1.8
2.1
2.4
2.7
3.0
Frequency (GHz)
Exact
FDTD

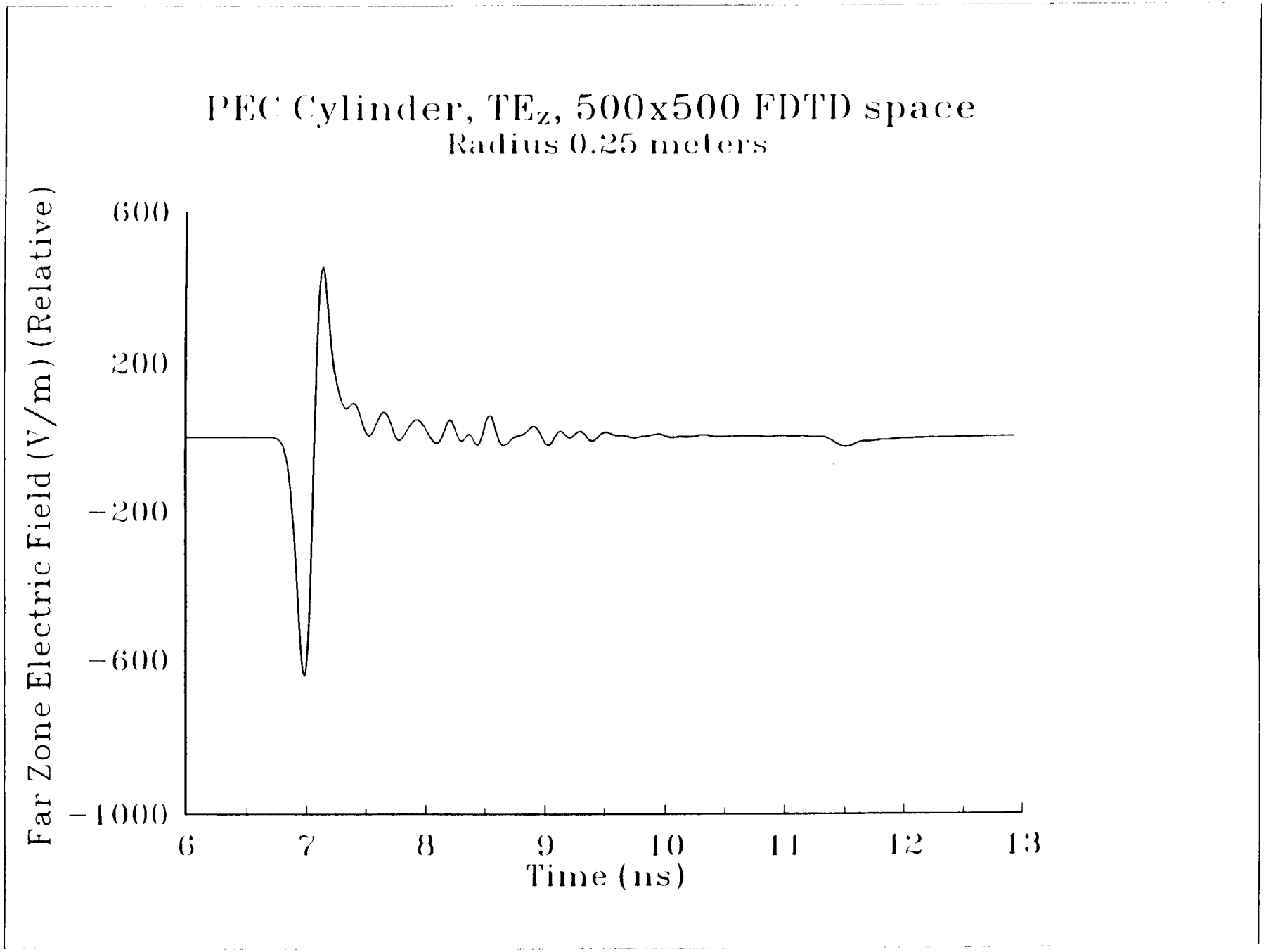
PEC Cylinder, TEz, 500x500 FDTD space
Radius 0.25 meters
Far Zone Electric Field (V/m) (Relative)
600
200
−200
−600
−1000
6
7
8
9
10
11
12
13
Time (ns)

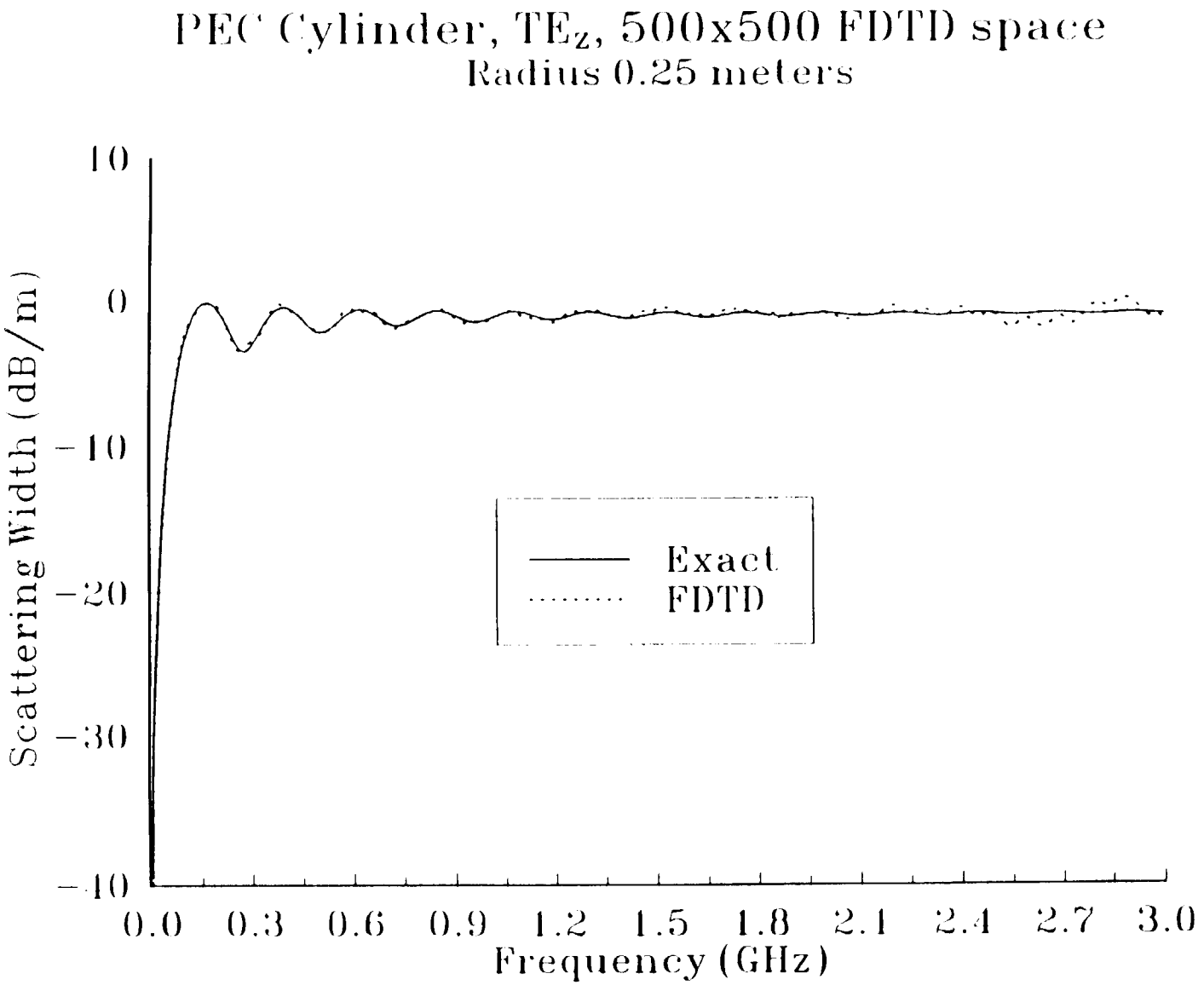
PEC Cylinder, TEz, 500x500 FDTD space
Radius 0.25 meters
Scattering Width (dB/m)
10
0
-10
-20
-30
-40
0.0
0.3
0.6
0.9
1.2
1.5
1.8
2.1
2.4
2.7
3.0
Frequency (GHz)
Exact
FDTD

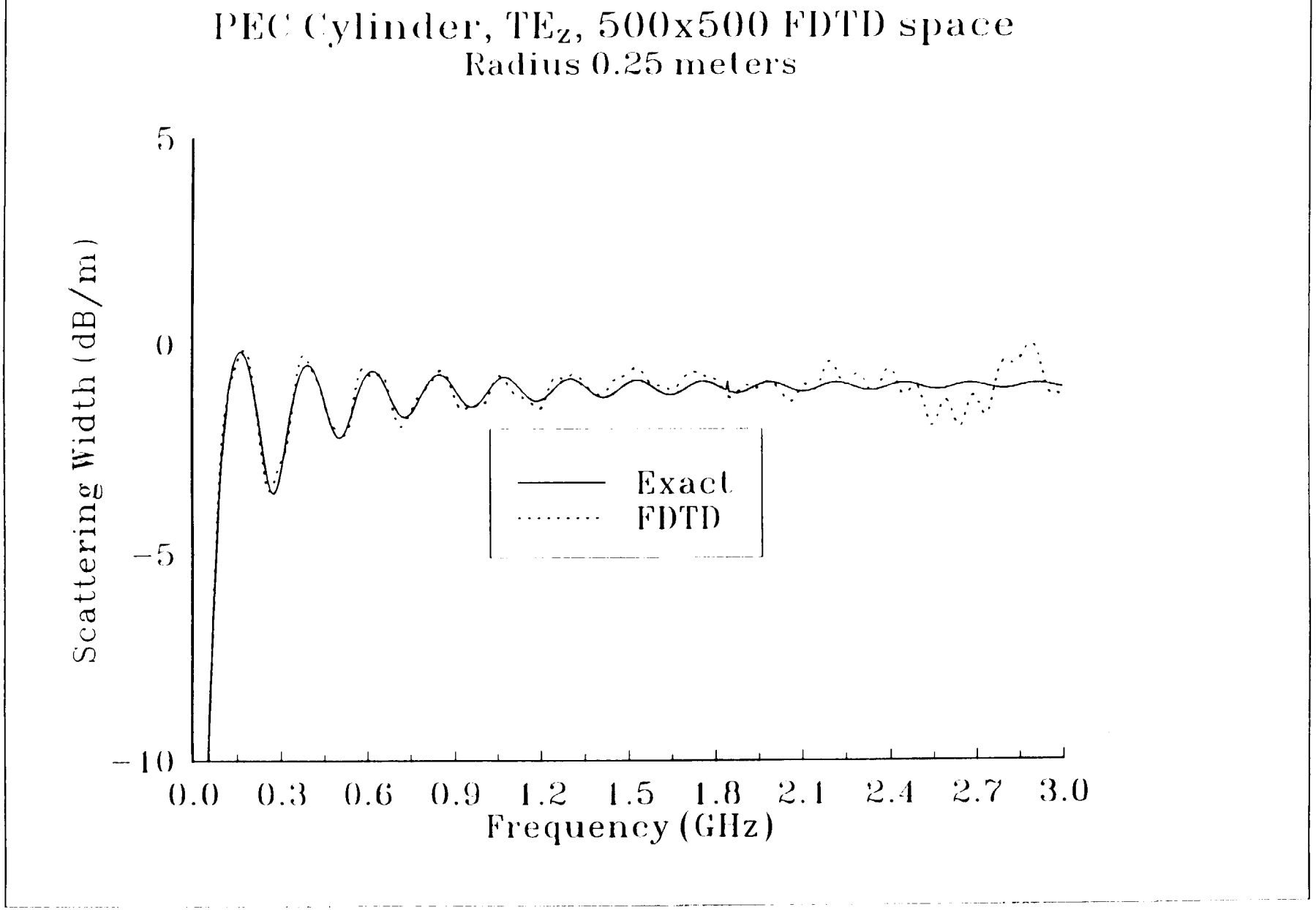
PEC Cylinder, TEz, 500x500 FDTD space
Radius 0.25 meters
Scattering Width (dB/m)
5
0
−5
−10
0.0
0.3
0.6
0.9
1.2
1.5
1.8
2.1
2.4
2.7
3.0
Frequency (GHz)
Exact
FDTD

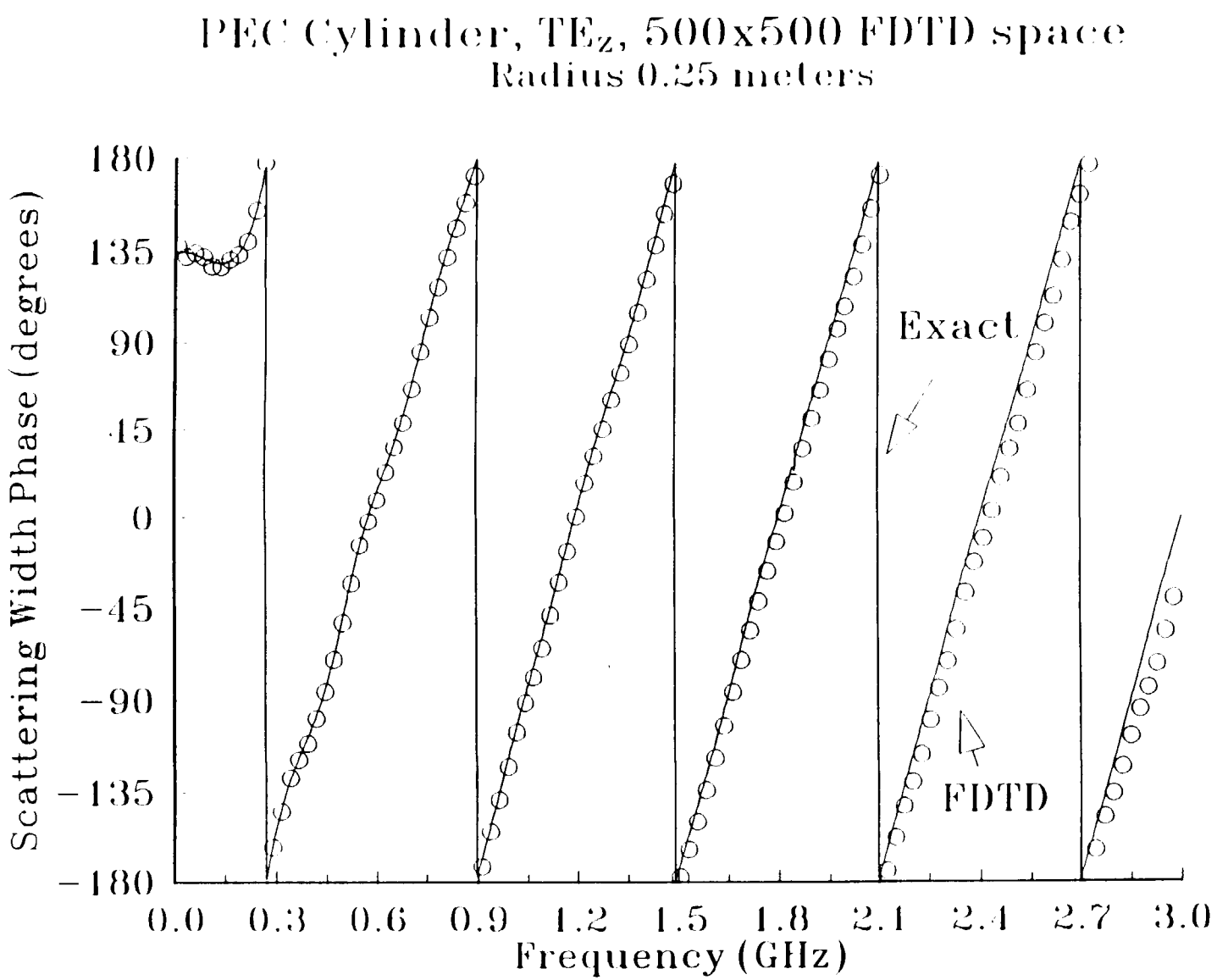
PEC Cylinder, TEz, 500x500 FDTD space
Radius 0.25 meters
Scattering Width Phase (degrees)
180
135
90
45
0
−45
−90
−135
−180
0.0
0.3
0.6
0.9
1.2
1.5
1.8
2.1
2.4
2.7
3.0
Frequency (GHz)
Exact
FDTD

FINITE DIFFERENCE TIME DOMAIN IMPLEMENTATION OF SURFACE IMPEDANCE BOUNDARY CONDITIONS

by

John H. Beggs, Student Member, IEEE
Raymond J. Luebbers, Senior Member, IEEE
Kane S. Yee*, Member, IEEE
Karl S. Kunz, Senior Member, IEEE

Department of Electrical and Computer Engineering
The Pennsylvania State University
University Park, PA 16802

September 1990

Revised

September 1991

Revised

December 1991

* K. S. Yee is with the Lockheed Missiles and Space Company, Sunnyvale, California.

ABSTRACT

Surface impedance boundary conditions are employed to reduce the solution volume during the analysis of scattering from lossy dielectric objects. In a finite difference solution, they also can be utilized to avoid using small cells, made necessary by shorter wavelengths in conducting media throughout the solution volume. The standard approach is to approximate the surface impedance over a very small bandwidth by its value at the center frequency, and then use that result in the boundary condition. In this paper, two implementations of the surface impedance boundary condition are presented. One implementation is a constant surface impedance boundary condition and the other is a dispersive surface impedance boundary condition that is applicable over a very large frequency bandwidth and over a large range of conductivities. Frequency domain results are presented in one dimension for two conductivity values and are compared with exact results. Scattering width results from an infinite square cylinder are presented as a two dimensional demonstration. Extensions to three dimensions should be straightforward.

I. Introduction

The Finite Difference Time Domain (FDTD) technique permits the analysis of interactions of electromagnetic waves with objects of arbitrary shape and material composition. This method was first proposed by Yee [1] for isotropic, non-dispersive materials in 1966; and through various modifications during the past twenty years, it has evolved into a mature computational technique. Reference [2] and the references contained therein provide an account of various extensions and modifications of the original FDTD algorithm. The present FDTD technique is capable of electromagnetic scattering analysis from objects of arbitrary and complicated geometrical shape and material composition over a large band of frequencies. This technique has recently been extended to include dispersive dielectric materials [3], chiral materials [4] and plasmas [5]. Due to these numerous capabilities, the FDTD method has begun to gain widespread acceptance as a viable computational alternative to the classical method of moments (MM) technique for many problems.

To analyze electromagnetic field interaction with lossy dielectric objects, the FDTD method requires that the interior of the object be modeled in order for fields to penetrate the body. Accurate modeling often requires a very fine spatial grid resulting in a relatively large number of cells for moderately sized objects. A highly conducting dielectric object can be replaced by a surface impedance boundary condition (SIBC) that is a function of the material parameters. Thus, this boundary condition eliminates the spatial quantization of the object and reduces the overall size of the solution space not only by eliminating cells within the lossy dielectric, but also by allowing larger cells to be used in the

exterior region. As with any computational electromagnetic tool, a technique that reduces the solution space or number of unknowns is quite welcome.

Of historical interest, surface impedance boundary conditions were first proposed by Leontovich in the 1940's [6] and were rigorously developed by Senior in 1960 [7]. During the past thirty years, researchers have applied surface impedance concepts in the frequency domain to numerous electromagnetic scattering problems. Time domain surface impedance concepts received little attention until recently. Through some impressive work, Maloney and Smith [8] have previously implemented a surface impedance boundary condition in the FDTD method. However, their implementation has a minor disadvantage because the exponential rates and coefficients for recursive updating have to be reevaluated each time the conductivity or loss tangent is changed. With our proposed method, the exponential rates and coefficients only have to be evaluated once. Tesche [9] has also investigated surface impedance concepts in an integral equation time domain solution, but presented limited computational time domain results.

It is the purpose of this paper to introduce a constant surface impedance boundary condition that is applicable for a single frequency and a dispersive surface impedance boundary condition that is applicable over a large frequency bandwidth and range of conductivities. The dispersive surface impedance includes frequency variations which results in a time domain boundary condition involving a convolution. We will then show how to efficiently evaluate this convolved surface impedance using recursion.

II. Motivation

The motivation for implementing a SIBC in the FDTD method is to reduce the computational resource requirements for modeling highly conducting lossy dielectric objects. In the standard FDTD method, modeling highly conducting lossy dielectric objects requires that the cell size be chosen small enough to resolve the field inside the object at the maximum frequency of interest. For example, suppose scattering from a lossy dielectric object with permeability μ, permittivity ϵ and conductivity σ=2.0 S/m is to be studied over the frequency band 0-10 GHz. The cell size must be chosen as some fraction of the wavelength inside the conducting material at the maximum frequency of interest. Thus the cell size is chosen (typically) as

$$\delta x = \delta y = \delta z = \frac{\lambda}{10} = \frac{\lambda_0}{10\sqrt{|\hat{\epsilon}_r|}} \qquad (1)$$

where $\hat{\epsilon}_r$ is the complex relative permittivity constant of the material and λ and λ_0 are the wavelengths inside the material and in free space at 10 GHz, respectively. The complex permittivity for lossy dielectrics in the frequency domain is

$$\hat{\epsilon} = \epsilon + \frac{\sigma}{j\omega} \tag{2}$$

where ω is the radian frequency. The complex relative permittivity is determined using (2) as

$$\hat{\epsilon}_r = \frac{\hat{\epsilon}}{\epsilon_0} = \epsilon_r + \frac{\sigma}{j\omega\epsilon_0} \tag{3}.$$

If the material is a good conductor over all frequencies of interest, then the constitutive parameters satisfy the condition

$$\frac{\sigma}{\omega\epsilon} >> 1 \tag{4}.$$

Therefore, $\hat{\epsilon}_r$ can be approximated as

$$\hat{\epsilon}_r \approx \frac{\sigma}{j\omega\epsilon_0} \tag{5}.$$

Assuming parameters $\mu=\mu_0$ and $\epsilon=\epsilon_0$ and using the values of $\hat{\epsilon}_r$ and λ_0 at 10 GHz, the cell size is $\delta x = \delta y = \delta z = 1.582$ mm. If a SIBC is used, then the cell size need only be chosen to resolve the field in free space and (1) is modified to

$$\delta x_{SIBC} = \delta y_{SIBC} = \delta z_{SIBC} = \lambda_0/10 \tag{6}.$$

Again, using the value for λ_0 at 10 GHz, the cell size is $\delta x_{SIBC} = \delta y_{SIBC} = \delta z_{SIBC} = 3.0$ mm. Thus the cell size has been increased by the factor $\sqrt{|\hat{\epsilon}_r|}$ =1.90, and the computational storage requirements are reduced by the same factor. Therefore, the computational savings, denoted by S, is

$$S = \left[\sqrt{|\hat{\epsilon}_r|}\right]^d \tag{7}$$

where $\hat{\epsilon}_r$ is given by (5), (4) is satisfied for all frequencies of interest and d is the number of dimensions.

III. FDTD Constant Surface Impedance Implementation

To implement the constant SIBC in the FDTD method we consider the planar air-lossy dielectric interface as shown in Figure 1. The conducting material has permittivity ϵ, permeability μ and conductivity σ. We assume that the thickness of the material is large compared to the skin depth. We will also assume that the material is linear and isotropic and a basic familiarity with the Yee algorithm [1]. Figure 1 also shows the one-dimensional FDTD grid.

The first order (or Leontovich) impedance boundary condition relates tangential total field components and is given in the frequency domain as [6]

$$E_x(\omega) = Z_s(\omega) H_y(\omega) \tag{8}$$

where $Z_s(\omega)$ is the surface impedance of the conductor. The frequency domain surface impedance for good conductors is

$$Z_s(\omega) = (1+j)\sqrt{\frac{\omega\mu}{2\sigma}} = \sqrt{\frac{j\omega\mu}{\sigma}} \tag{9}.$$

Using (9), (8) can be rewritten as

$$E_x(\omega) = \left(R_s(\omega) + jX_s(\omega)\right) H_y(\omega) \tag{10}$$

where R_s is the surface resistance and X_s is the surface reactance. Consider rewriting (10) as

$$E_x(\omega) = \left(R_s(\omega) + j\omega L_s(\omega)\right) H_y(\omega) \tag{11}$$

with the resistance and inductance defined by

$$\begin{aligned} R_s(\omega) &= \sqrt{\frac{\omega\mu}{2\sigma}} \\ L_s(\omega) &= \sqrt{\frac{\mu}{2\sigma\omega}} \end{aligned} \tag{12}$$

To remove the frequency dependence of the surface resistance and inductance, these quantities are evaluated at a particular frequency and are subsequently treated as constants. Equation (11) then becomes

$$E_x(\omega) = \left(R_s + j\omega L_s\right) H_y(\omega) \qquad (13).$$

This is the required frequency domain constant surface impedance boundary condition. To incorporate this boundary condition into the FDTD algorithm, the time domain equivalent of (13) must be obtained. Performing an inverse Fourier transform operation on (13) results in

$$E_x(t) = R_s H_y(t) + L_s \frac{\partial}{\partial t} H_y(t) \qquad (14).$$

This equation defines the time domain FDTD constant surface impedance boundary condition.

To implement this constant surface impedance boundary condition, space and time are quantized by defining

$$\begin{aligned} z &\Rightarrow (k\delta z) \Rightarrow (k) \\ t &\Rightarrow (n\delta t) \Rightarrow (n) \end{aligned} \qquad (15).$$

The Faraday-Maxwell law is then used to obtain the H_y component in the free space cell next to the impedance boundary. Since the impedance boundary condition requires that the electric and magnetic fields are co-located in space and time, we assume that the magnetic field 1/2 cell in front of the impedance boundary and 1/2 time step previous is an adequate approximation. The Faraday-Maxwell law yields

$$-\left(\mu_0 \delta x \delta z\right)\left[\frac{\partial}{\partial (n\delta t)} HY^n(k+1/2)\right] = EX^n(k+1)\,\delta x - EX^n(k)\,\delta x \qquad (16).$$

Note the component $EX^n(k+1)$ of (16) is the electric field component at the impedance boundary. Quantizing space and time in (14) and using the result to eliminate $EX^n(k+1)$ in (16) gives

$$-\left(\mu_0 \delta z\right)\left[\frac{\partial}{\partial (n\delta t)} HY^n(k+1/2)\right] = R_s HY^n(k+1/2) + L_s\left[\frac{\partial}{\partial (n\delta t)} HY^n(k+1/2)\right] - EX^n(k) \qquad (17).$$

Notice that the $HY^n(k+1/2)$ term in (17) is time indexed at time step n. This term is approximated as

$$HY^{n}(k+1/2) \approx \frac{1}{2}\left[HY^{n+1/2}(k+1/2) + HY^{n-1/2}(k+1/2)\right] \qquad (18).$$

Using (18), and approximating the time derivatives on the magnetic fields in (17) as finite differences gives

$$-\left(\mu_0\delta z + L_s\right)\left(HY^{n+1/2}(k+1/2) - HY^{n-1/2}(k+1/2)\right) = \frac{R_s\delta t}{2}\left(HY^{n+1/2}(k+1/2) - HY^{n-1/2}(k+1/2)\right) - \delta t\, EX^{n}(k) \qquad (19).$$

Solving for $HY^{n+1/2}(k+1/2)$ in (19) yields

$$HY^{n+1/2}(k+1/2) = \left[\frac{\mu_0\delta z + L_s - R_s\delta t/2}{\mu_0\delta z + L_s + R_s\delta t/2}\right] HY^{n-1/2}(k+1/2) - \frac{\delta t}{\mu_0\delta z + L_s + R_s\delta t/2}\, EX^{n}(k) \qquad (20).$$

This equation implements the constant surface impedance boundary condition in the FDTD method.

IV. FDTD Dispersive Surface Impedance Implementation

To derive a similar relation to (20) valid over a wide frequency band, we begin with the same set of underlying assumptions as for the constant surface impedance. The primary exception is that the surface impedance will vary with frequency and will not be approximated by its value at a particular frequency. All frequency domain information is inversed Fourier transformed to equivalent time domain form. The SIBC is then implemented in the FDTD method with the required convolution using a recursive updating technique.

The standard first order impedance boundary condition remains unchanged and is given by (8). In a similar fashion as Tesche [9], (8) is rewritten as

$$E_x(\omega) = j\omega\left[\frac{Z_s(\omega)}{j\omega}\right] H_y(\omega) \qquad (21).$$

Defining

$$Z_s'(\omega) = \frac{Z_s(\omega)}{j\omega} \tag{22}$$

and substituting (9) into (22) gives

$$Z_s'(\omega) = \sqrt{\frac{\mu}{j\omega\sigma}} \tag{23}.$$

Substituting (23) into (21), a modified surface impedance boundary condition is obtained as

$$E_x(\omega) = Z_s'(\omega)\,[j\omega H_y(\omega)] \tag{24}.$$

The time domain equivalent of (24) is obtained via an inverse Fourier transform operation as

$$E_x(t) = Z_s'(t) * \left[\frac{\partial}{\partial t} H_y(t)\right] \tag{25}$$

where the asterisk denotes convolution,

$$\begin{aligned} E_x(t) &= \mathcal{F}^{-1}[E_x(\omega)] \\ H_y(t) &= \mathcal{F}^{-1}[H_y(\omega)] \\ Z_s'(t) &= \mathcal{F}^{-1}[Z_s'(\omega)] \end{aligned} \tag{26}$$

and the $\mathcal{F}^{-1}$ denotes the inverse Fourier transform operation. Note in (25) that as $\sigma \rightarrow \infty$, the boundary condition becomes $E_x(t)=0.0$, which is required for a perfect conductor. To determine $Z_s'(t)$, the Laplace transform variable $s=j\omega$ is used in (23) to obtain

$$Z_s'(s) = \sqrt{\frac{\mu}{\sigma}}\,\frac{1}{\sqrt{s}} \tag{27}.$$

Using the Laplace transform pair [11]

$$\frac{1}{\sqrt{\pi t}} = \mathcal{L}^{-1}\left[\frac{1}{\sqrt{s}}\right] \tag{28}$$

where the $\mathcal{L}^{-1}$ denotes the inverse Laplace transform operation; and $Z_s'(t)$ is then determined to be

$$Z_s'(t) = \mathcal{F}^{-1}[Z_s'(\omega)] = \begin{cases} \sqrt{\dfrac{\mu}{\pi\sigma t}}, & t > 0 \\ 0, & t < 0 \end{cases} \tag{29}.$$

This is the required time domain surface impedance function. Substituting (29) into (25) and discretizing space and time according to (15) gives

$$EX^n(k+1) = \sqrt{\frac{\mu}{\pi\sigma(n\delta t)}} * \left[\frac{\partial}{\partial(n\delta t)} HY^n(k+1/2)\right] \tag{30}.$$

Substituting (30) into (16) yields

$$-\mu_0\delta z\left[\frac{\partial}{\partial(n\delta t)} HY^n(k+1/2)\right] = \sqrt{\frac{\mu}{\pi\sigma(n\delta t)}} * \left[\frac{\partial}{\partial(n\delta t)} HY^n(k+1/2)\right] - EX^n(k) \tag{31}.$$

The convolution in (31) is expressed as a summation to obtain

$$-\mu_0\delta z\left[\frac{\partial}{\partial(n\delta t)} HY^n(k+1/2)\right] = \sqrt{\frac{\mu\delta t}{\pi\sigma}} \sum_{m=0}^{n-1}\left[\frac{\partial}{\partial((n-m)\delta t)} HY^{n-m}(k+1/2)\right] Z_0(m) - EX^n(k) \tag{32}$$

where $Z_0(m)$ is the discrete impulse response. The discrete impulse response is obtained by assuming the fields are piecewise constant in time as

$$Z_0(m) = \int_{m-1/2}^{m+1/2} \frac{1}{\sqrt{\alpha}} d\alpha \tag{33}$$

If m=0, the lower limit in (33) is 0. Approximating the time derivatives on the magnetic fields in (32) as finite differences results in

$$\left[HY^{n+1/2}(k+1/2) - HY^{n-1/2}(k+1/2)\right] = -Z_1 \sum_{m=0}^{n-1} \left[HY^{n-m+1/2}(k+1/2) - HY^{n-m-1/2}(k+1/2)\right] Z_0(m) + \frac{\delta t}{\mu_0 \delta z} EX^n(k) \tag{34}$$

where

$$Z_1 = \frac{1}{\mu_0 \delta z} \sqrt{\frac{\mu \delta t}{\pi \sigma}} \tag{35}.$$

Equation (34) is suitable for computer implementation and includes the full convolution with all past field components. This full convolution would be impractical for large three dimensional problems; thus it is desirable to obtain a more efficient implementation. The development of a recursive implementation is the subject of the following section.

V. Recursive Implementation

Recently, Luebbers et. al. [3] extended the FDTD technique to dispersive dielectric materials using a time domain susceptibility function for polar dielectrics. In that paper, the time domain susceptibility function was a decaying exponential which permits the convolution summation to be recursively updated, thus avoiding the need for the complete time history of field components. Upon further examination of (34), it is clear that if $Z_0(m)$ can be approximated by a series of exponentials, then the SIBC can be efficiently evaluated using recursion. Figure 2 shows $Z_0(m)$ versus m, and it is clear that it can be approximated by a series of exponentials. $Z_0(m)$ is approximated as

$$Z_0(m) \approx \sum_{i=1}^{N} a_i e^{\alpha_i m} \tag{36}$$

where N is the number of terms in the approximation. One of the most accurate methods for obtaining an exponential approximation to an exact function or to a data set is Prony's method [10]. Figure 2 also shows the Prony approximation to $Z_0(m)$ with N=10 and it is clear that N=10 provides an adequate approximation. Thus, using (36) with N=10 in (34) gives

$$HY^{n+1/2}(k+1/2) = HY^{n-1/2}(k+1/2) - \frac{Z_1}{1+Z_1Z_0(0)} \sum_{i=1}^{10} \sum_{m=1}^{n-1} \left[HY^{n-m+1/2}(k+1/2) - HY^{n-m-1/2}(k+1/2) \right] \cdot a_i e^{\alpha_i m} + \frac{\delta t}{\mu_0 \delta z (1+Z_1Z_0(0))} EX^n(k) \quad (37)$$

where

$$Z_0(0) = \sum_{i=1}^{10} a_i \quad (38).$$

The convolution can now be recursively updated (see Appendix) to give

$$HY^{n+1/2}(k+1/2) = HY^{n-1/2}(k+1/2) - \frac{Z_1}{1+Z_1Z_0(0)} \sum_{i=1}^{10} \psi_i^n(k+1/2) + \frac{\delta t}{\mu_0 \delta z (1+Z_1Z_0(0))} EX^n(k) \quad (39)$$

Note that only one past value of magnetic field is required to update the convolution summation.

VI. One Dimensional Demonstration

To demonstrate the constant and recursive FDTD SIBC, (20) and (39) were implemented in a one dimensional total field FDTD code for the geometry shown in Figure 1. The problem space size is 301 cells, the impedance boundary is located at cell 300, and the electric field is sampled at cell 299. The maximum frequency of interest for each problem was 10 GHz. The incident electric field is a Gaussian pulse with maximum amplitude of 1000 V/m and has a total temporal width of 256 time steps. The frequency response of the incident pulse contains significant information to 12 GHz. Two computations were made with σ=2.0 S/m and σ=20.0 S/m. The loss tangents at 10 GHz are 3.599, 35.99, respectively. The permittivity and permeability for the lossy dielectric were those of free space. The cell size and time step were 750 μm and 2.5 psec, respectively. A tie point of 5.0 GHz was chosen for the FDTD constant SIBC. For each FDTD computation, a reflection coefficient versus frequency was obtained by first dividing the Fourier transform of the scattered field by the transform of the incident field at cell 299. The incident field was obtained by running the FDTD code with free space only and recording the electric field at cell 299. The scattered field is then obtained by subtracting the

time domain incident field from time domain total field. The results are compared with the analytic surface impedance reflection coefficient computed from

$$|R| = \frac{|Z_s(\omega) - \eta_0|}{|Z_s(\omega) + \eta_0|} \tag{40}$$

where $Z_s(\omega)$ is given by (9) and η_0 is the free space wave impedance. The phase of the FDTD reflection coefficient was corrected to account for the round trip phase shift of one cell since the FDTD reflection coefficient is computed from electric fields recorded one cell in front of the impedance boundary.

The high conductivity surface impedance of (9) is an approximation to the general surface impedance for lossy dielectrics given by

$$Z_s(\omega) = \sqrt{\frac{j\omega\mu}{\sigma + j\omega\epsilon}} \tag{41}.$$

The advantage of using (9) over (41) for the FDTD SIBC implementation is that the resulting time domain impulse response is independent of the conductivity. The exponential approximation needs to be performed only once and not each time the conductivity is changed.

Figures 3-4 show the FDTD constant and recursive SIBC reflection coefficient magnitude and phase results versus the analytic SIBC results for σ=2.0 S/m. Notice the agreement between the curves is good, and the maximum error is about 0.02 at 10 GHz in Figure 3.

Figures 5-6 show the FDTD constant and recursive SIBC reflection coefficient magnitude and phase results versus the analytic SIBC results for σ=20.0 S/m. Notice the agreement between the curves is excellent.

Since the FDTD SIBC implementation is an approximation to an analytic SIBC, some amount of divergence between the SIBC curves and the analytic SIBC solution is to be expected with increasing frequency. As frequency increases, the effective number of cells per wavelength decreases and the FDTD SIBC becomes a rougher approximation to the analytic SIBC. To observe this error trend, the same one-dimensional test problems as above (using the dispersive SIBC only) were reevaluated with larger cell sizes equal to twice and four times the original cell size. This is equivalent to having 20 and 10 cells/λ_0 in the free space region, respectively. Figures 7 and 8 show the FDTD dispersive SIBC

reflection coefficient magnitude and phase results versus the analytic SIBC for σ=2.0 S/m using the original cell size and the larger cell sizes. Notice that for each increase in cell size, the agreement between the SIBC curve and the exact solution is reduced by a factor of two. This indicates that the error in the SIBC implementation is $O(\delta z)$ over the range of cell sizes examined here. The constant SIBC exhibited similar agreement reductions at the 5 GHz tie point for larger cell sizes.

VIII. Two Dimensional Demonstration

As a practical application of the FDTD dispersive SIBC, frequency domain scattering width was computed from an infinite square cylinder for two scattering angles, ϕ=0.0 and ϕ=30.0 degrees using a full two dimensional TM scattered field code. The cylinder was 0.99 cm square and had parameters $\epsilon=\epsilon_0$, $\mu=\mu_0$, and σ=20.0 S/m. To illustrate the applicability of the SIBC, the cylinder was modeled in two ways. The first was a normal FDTD computation with a grid size of 10 cells/λ (at 10 GHz) inside the conducting cylinder and the second was a SIBC computation with a grid size of 10 cells/λ in free space (at 10 GHz). Figure 7 shows the two dimensional field components and the cylinder dimensions (in cells) for the FDTD and SIBC computations. For the FDTD computation, the cylinder was modeled using 198 cells in the x and y directions, the cell size was 500 μm, and the time step was 1.18 ps. For the SIBC computation, the cylinder was modeled using 32 cells in the x and y directions, the cell size was 0.003 m and the time step was 7.07 ps. For both computations, a 100 cell border between the cylinder and the absorbing boundary was chosen, the total number of time steps was 1024, and an incident Gaussian pulse with total pulse width of 64 time steps was chosen. The near zone fields were transformed to far zone fields by a two-dimensional near zone to far zone transformation [12].

Figure 10 shows the scattering width magnitude versus frequency for a scattering angle of ϕ=0.0 degrees using the FDTD computation and the SIBC computation. Notice the good agreement over the entire frequency bandwidth for the dispersive SIBC.

Figure 11 shows the scattering width magnitude versus frequency for a scattering angle of ϕ=30.0 degrees using the FDTD computation and the SIBC computation. Notice again the good agreement over the entire frequency bandwidth for the dispersive SIBC.

IX. Summary

One dimensional FDTD implementations of constant and dispersive surface impedance boundary conditions have been presented. The corresponding time domain impedance boundary conditions have been derived and their validity demonstrated by one-dimensional computation of the reflection coefficient at an

air-lossy dielectric interface at a single frequency and over a wide frequency bandwidth. The applicability of the SIBC to two-dimensional scattering problems was demonstrated by scattering width computation from an infinite square cylinder. For both the one and two dimensional cases, the dispersive FDTD results were shown to be in good agreement with exact results over the entire bandwidth. Considerable computational savings were illustrated and a recursive updating scheme was implemented which permits efficient application of a dispersive surface impedance boundary condition to practical scattering problems.

Future extensions of this surface impedance concept currently under investigation are implementation in three dimensions, inclusion of surface curvature, dispersive dielectric and magnetic materials and thin material layers.

X. Acknowledgements

The authors wish to thank the reviewers for helpful comments and suggestions.

Appendix

The purpose of this Appendix is to show how the discrete convolution of the SIBC in (37) can be done recursively. The convolution in (37) is

$$\sum_{i=1}^{10}\sum_{m=1}^{n-1}\left[HY^{n-m+1/2}(k+1/2) - HY^{n-m-1/2}(k+1/2)\right] a_i e^{\alpha_i m} \qquad (42)$$

Consider n=2, and (42) becomes

$$\sum_{i=1}^{10}\left(HY^{3/2}(k+1/2) - HY^{1/2}(k+1/2)\right) a_i e^{\alpha_i} \qquad (43).$$

Now define

$$\psi_i^2(k+1/2) = \left(HY^{3/2}(k+1/2) - HY^{1/2}(k+1/2)\right) a_i e^{\alpha_i} \qquad (44).$$

Next for n=3, (42) becomes

$$\sum_{i=1}^{10}\sum_{m=1}^{2}\left(HY^{7/2-m}(k+1/2) - HY^{5/2-m}(k+1/2)\right) a_i e^{\alpha_i m} \qquad (45).$$

Expanding (45) gives

$$\sum_{i=1}^{10}\left(HY^{5/2}(k+1/2) - HY^{3/2}(k+1/2)\right) a_i e^{\alpha_i} + \left(HY^{3/2}(k+1/2) - HY^{1/2}(k+1/2)\right) a_i e^{2\alpha_i} \qquad (46).$$

Substituting (44) into (46) we obtain

$$\sum_{i=1}^{10}\left[\left(HY^{5/2}(k+1/2) - HY^{3/2}(k+1/2)\right) a_i e^{\alpha_i} + e^{\alpha_i}\psi_i^2(k+1/2)\right] \qquad (47).$$

Equation (47) can be generalized for any time step n as

$$\sum_{i=1}^{10}\left[\left(HY^{n-1/2}(k+1/2) - HY^{n-3/2}(k+1/2)\right) a_i e^{\alpha_i} + e^{\alpha_i}\psi_i^{n-1}(k+1/2)\right] \qquad (48).$$

with

$$\psi_i^n(k+1/2) = \left(HY^{n-1/2}(k+1/2) - HY^{n-3/2}(k+1/2)\right)a_i e^{\alpha_i} + e^{\alpha_i}\psi^{n-1}(k+1/2) \tag{49}$$

and

$$\psi_i^1(k+1/2) = \psi_i^0(k+1/2) = 0.0 \tag{50}$$

REFERENCES

[1] K. S. Yee, "Numerical solution of initial boundary value problems involving Maxwell's equations in isotropic media," IEEE Trans. Antennas Propagat., vol. AP-14, pp. 302-307, May 1966.

[2] A. Taflove and K. Umashankar, "The Finite-Difference Time Domain method for numerical modeling of electromagnetic wave interactions with arbitrary structures," in PIER2: Progress in Electromagnetics Research, M. A. Morgan (editor), New York: Elsevier, pp. 287-373, 1990.

[3] R. J. Luebbers et al, "A frequency dependent Finite Difference Time Domain formulation for dispersive materials,"IEEE Trans. Electromagn. Compat., vol. EMC-32, pp. 222-227, August 1990.

[4] F. P. Hunsberger, R. J. Luebbers and K. S. Kunz, "Application of the Finite-Difference Time-Domain method to electromagnetic scattering from 3-D chiral objects," Proc. IEEE AP-S Int. Symp., Dallas, TX, May 1990, vol. 1, pp. 38-41.

[5] R. J. Luebbers et al, "A frequency dependent Finite Difference Time Domain formulation for transient propagation in plasmas," IEEE Trans. Antennas Propagat., vol. AP-39, pp. 29-34, Jan. 1991.

[6] M. A. Leontovich, "On the approximate boundary conditions for electromagnetic fields on the surface of well conducting bodies," in Investigations of propagation of radio waves, B. A. Vvedensky (editor), Academy of Sciences USSR, Moscow, pp. 5-20, 1948.

[7] T. B. A. Senior, "Impedance boundary conditions for imperfectly conducting surfaces," Appl. Sci. Res. B, vol. 8, pp. 418-436, 1960.

[8] J. G. Maloney and G. S. Smith, "Implementation of surface impedance concepts in the Finite Difference Time Domain (FD-TD) technique," Proc. 1990 IEEE AP-S Int. Symp., Dallas, TX, May 1990, vol. 4, pp. 1628-1631.

[9] Frederick M. Tesche, "On the inclusion of loss in time-domain solutions of electromagnetic interaction problems," IEEE Trans. Electromagn. Compat., vol. EMC-32, pp. 1-4, Feb. 1990.

[10] F. B. Hildebrand, Introduction to Numerical Analysis, New York: McGraw-Hill, 1956, pp. 378-382.

[11] Ruel V. Churchill, Operational Mathematics, New York: McGraw-Hill, 1972, p. 459.

[12] R. J. Luebbers, D. A. Ryan, J. H. Beggs and K. S. Kunz, "A Two-Dimensional Time Domain Near Zone to Far Zone Transformation," submitted to IEEE Trans. Antennas Propagat. for publication, May 1991.

FIGURE TITLES

1. Problem geometry showing one-dimensional FDTD grid and planar free space-conductor interface.

2. FDTD dispersive SIBC discrete impulse response $Z_0(m)$ versus m and Prony approximation using 10 terms.

3. Reflection coefficient magnitude versus frequency for normal incidence plane wave calculated for σ=2.0 S/m using FDTD constant and dispersive SIBC and analytic solution.

4. Reflection coefficient phase versus frequency for normal incidence plane wave calculated for σ=2.0 S/m using FDTD constant and dispersive SIBC and analytic solution.

5. Reflection coefficient magnitude versus frequency for normal incidence plane wave calculated for σ=20.0 S/m using FDTD constant and dispersive SIBC and analytic solution.

6. Reflection coefficient phase versus frequency for normal incidence plane wave calculated for σ=20.0 S/m using FDTD constant and dispersive SIBC and analytic solution.

7. Reflection coefficient magnitude versus frequency for normal incidence plane wave calculated for σ=2.0 S/m using FDTD dispersive SIBC with original and larger cell size and analytic solution.

8. Reflection coefficient phase versus frequency for normal incidence plane wave calculated for σ=2.0 S/m using FDTD dispersive SIBC with original and larger cell size and analytic solution.

9. Two dimensional geometry for scattering width computations from an infinite square cylinder with σ=20.0 S/m using normal FDTD and FDTD dispersive SIBC.

10. Scattering width magnitude versus frequency at scattering angle ϕ=0.0 degrees from an infinite square cylinder with σ=20.0 S/m using normal FDTD and FDTD dispersive SIBC.

11. Scattering width magnitude versus frequency at scattering angle ϕ=30.0 degrees from an infinite square cylinder with σ=20.0 S/m using normal FDTD and FDTD dispersive SIBC.

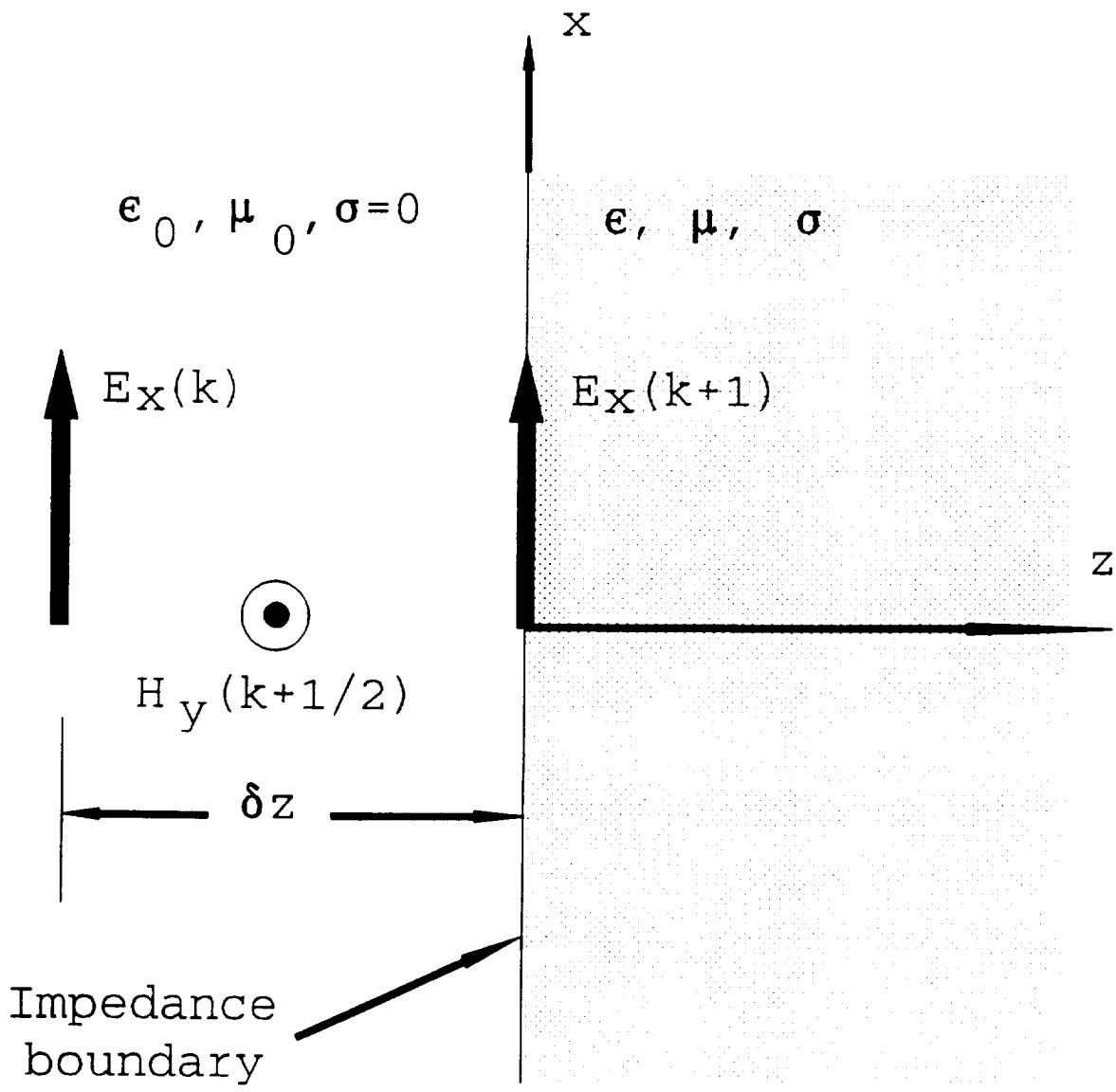
x
$\epsilon_0, \mu_0, \sigma=0$
ϵ, μ, σ
$E_x(k)$
$E_x(k+1)$
z
$H_y(k+1/2)$
δz
Impedance
boundary

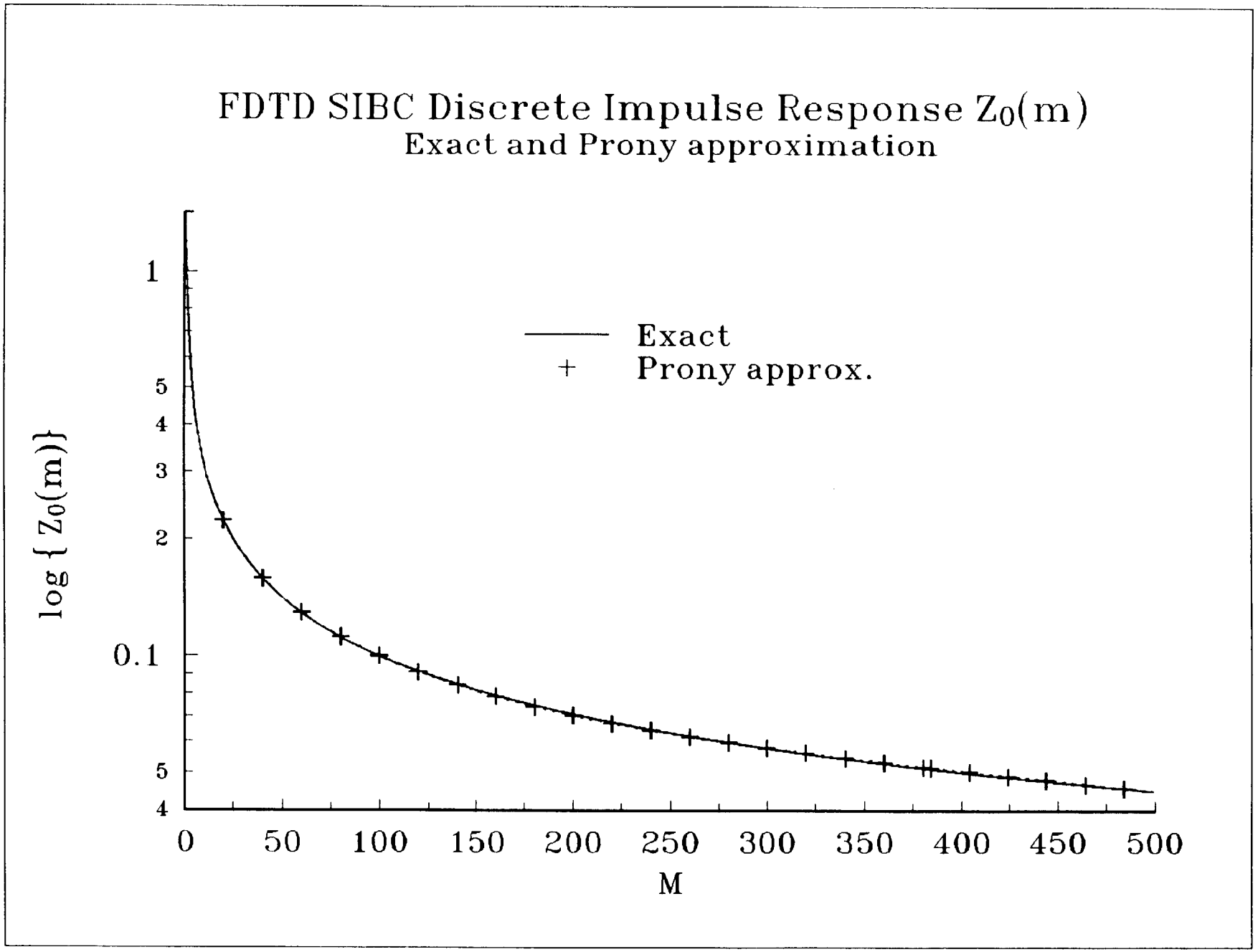
FDTD SIBC Discrete Impulse Response $Z_0(m)$
Exact and Prony approximation
Exact
Prony approx.
log { $Z_0(m)$ }
1
5
4
3
2
0.1
5
4
0
50
100
150
200
250
300
350
400
450
500
M

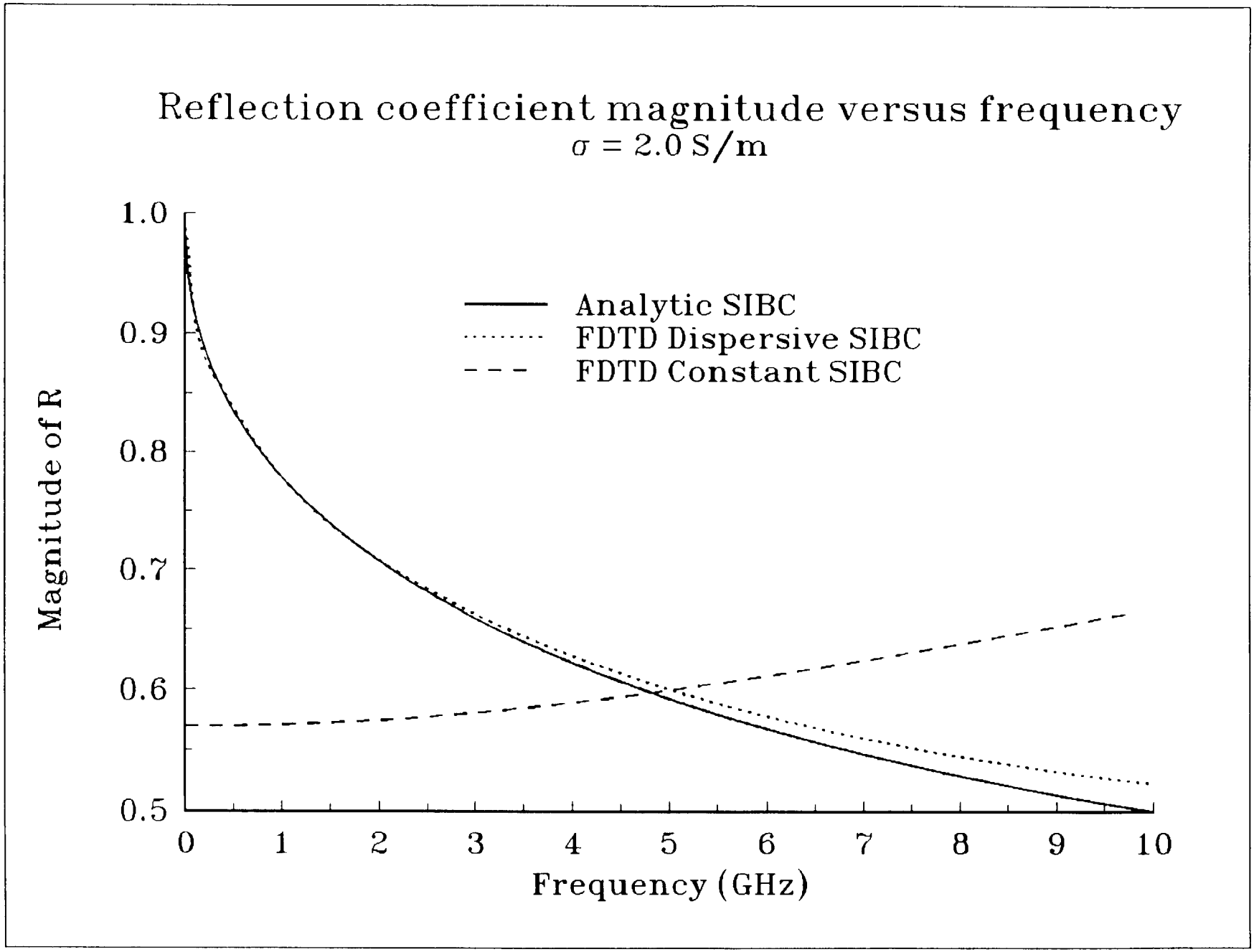
Reflection coefficient magnitude versus frequency
σ = 2.0 S/m
Analytic SIBC
FDTD Dispersive SIBC
FDTD Constant SIBC
Magnitude of R
1.0
0.9
0.8
0.7
0.6
0.5
0
1
2
3
4
5
6
7
8
9
10
Frequency (GHz)

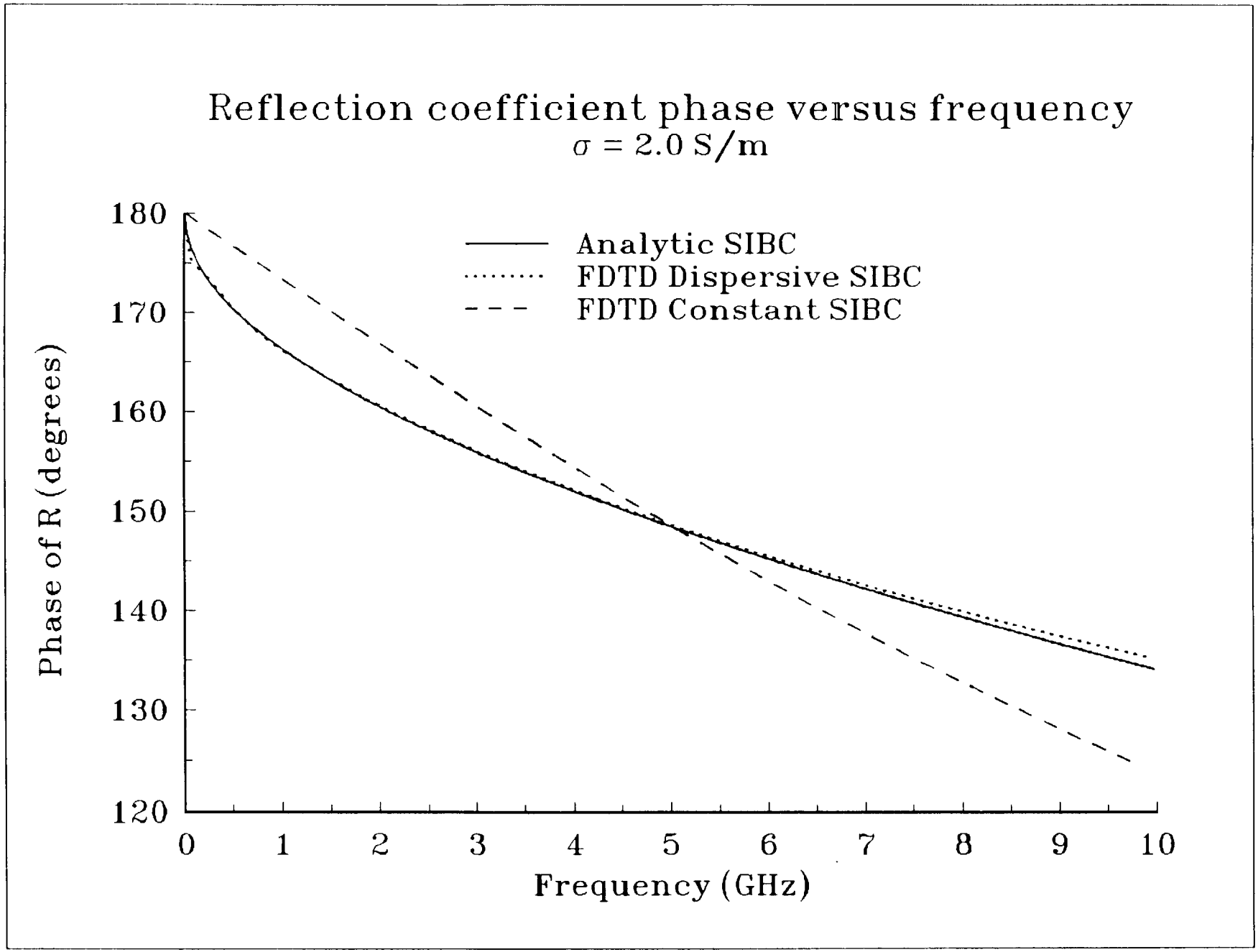
Reflection coefficient phase versus frequency
σ = 2.0 S/m
Analytic SIBC
FDTD Dispersive SIBC
FDTD Constant SIBC
Phase of R (degrees)
180
170
160
150
140
130
120
0
1
2
3
4
5
6
7
8
9
10
Frequency (GHz)

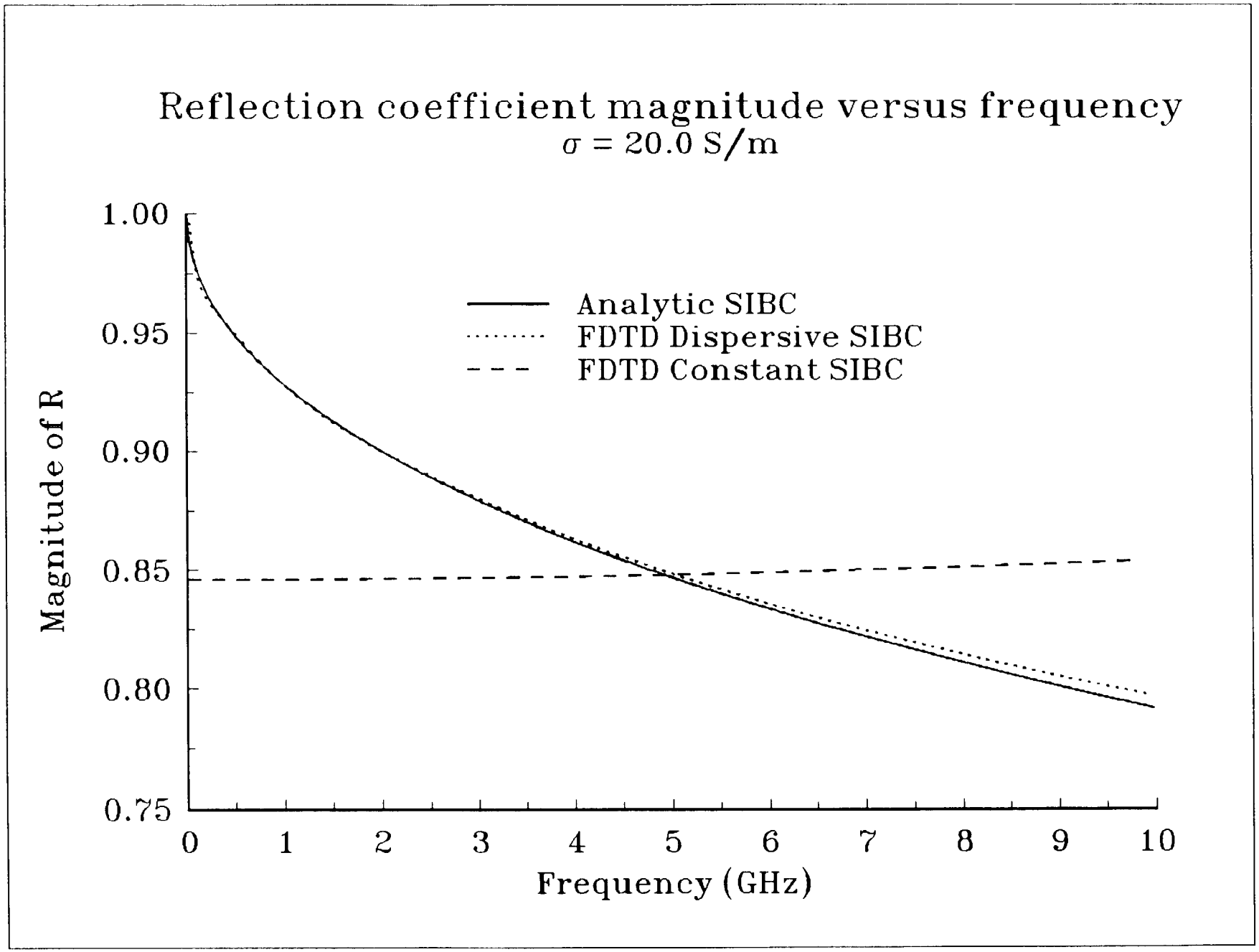
Reflection coefficient magnitude versus frequency
σ = 20.0 S/m
Analytic SIBC
FDTD Dispersive SIBC
FDTD Constant SIBC
Magnitude of R
1.00
0.95
0.90
0.85
0.80
0.75
0
1
2
3
4
5
6
7
8
9
10
Frequency (GHz)

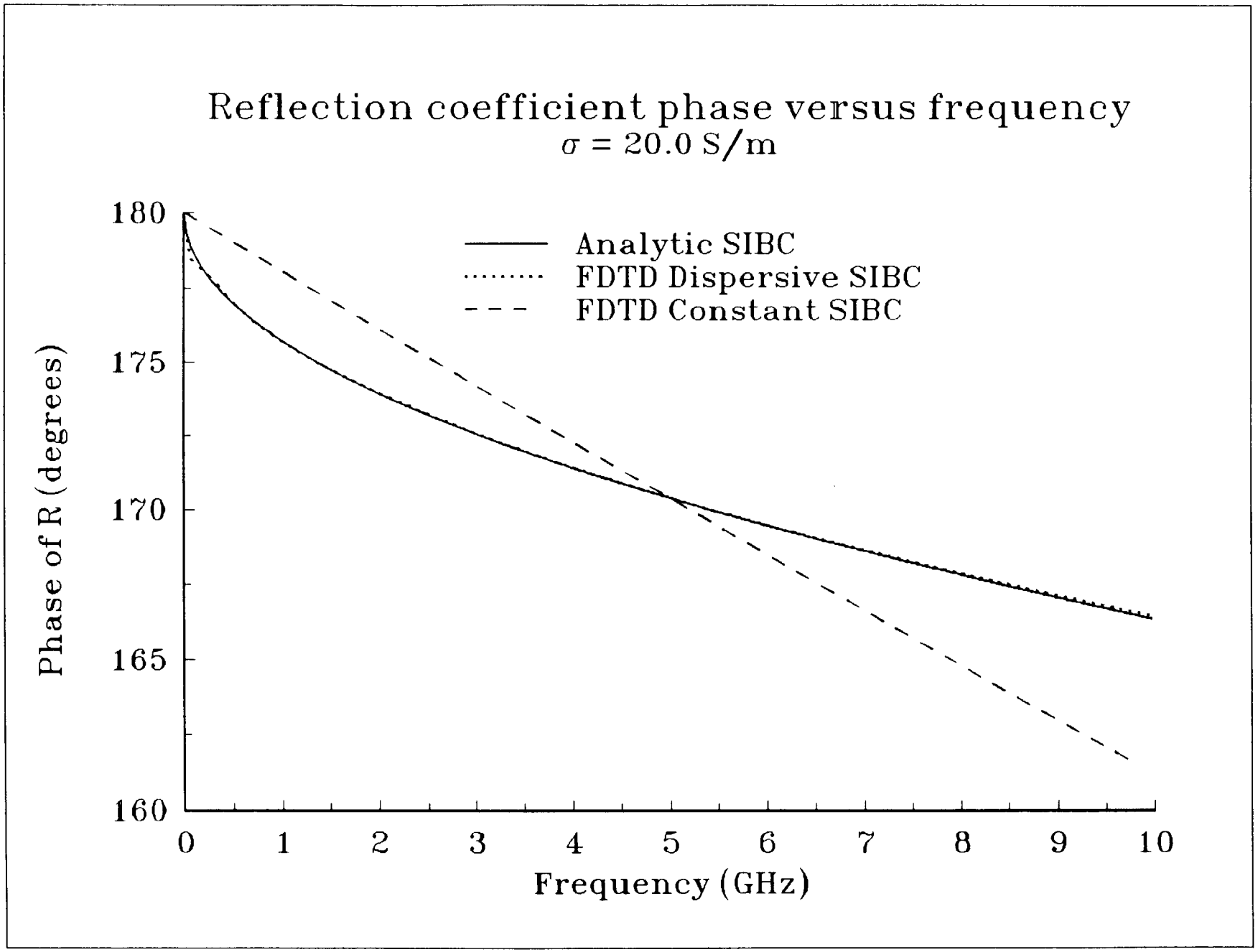
Reflection coefficient phase versus frequency
σ = 20.0 S/m
Analytic SIBC
FDTD Dispersive SIBC
FDTD Constant SIBC
Phase of R (degrees)
180
175
170
165
160
0
1
2
3
4
5
6
7
8
9
10
Frequency (GHz)

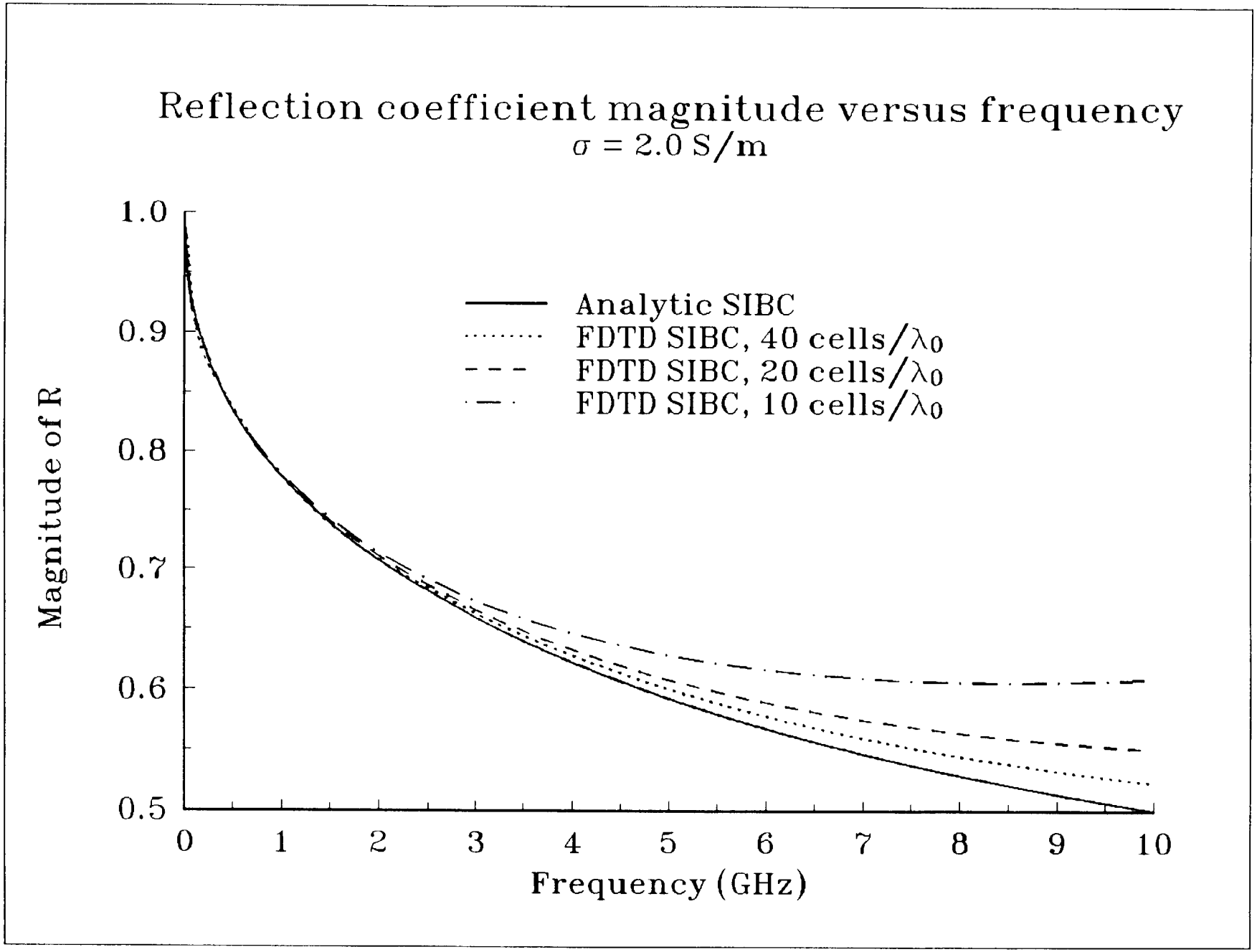
Reflection coefficient magnitude versus frequency
σ = 2.0 S/m
Magnitude of R
1.0
0.9
0.8
0.7
0.6
0.5
0
1
2
3
4
5
6
7
8
9
10
Frequency (GHz)
Analytic SIBC
FDTD SIBC, 40 cells/λ0
FDTD SIBC, 20 cells/λ0
FDTD SIBC, 10 cells/λ0

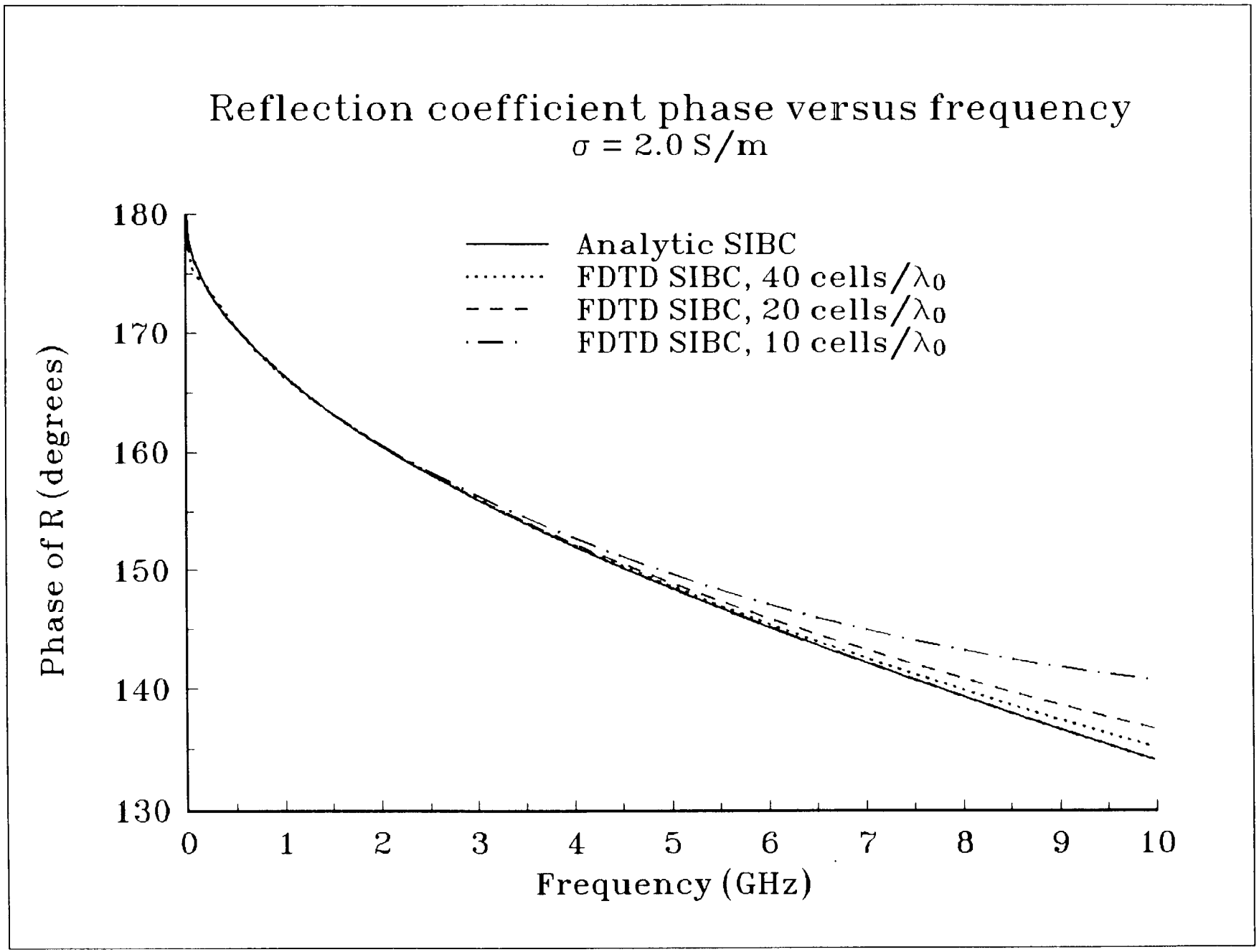
Reflection coefficient phase versus frequency
σ = 2.0 S/m
Analytic SIBC
FDTD SIBC, 40 cells/λ0
FDTD SIBC, 20 cells/λ0
FDTD SIBC, 10 cells/λ0
Phase of R (degrees)
180
170
160
150
140
130
0
1
2
3
4
5
6
7
8
9
10
Frequency (GHz)

2D TM FDTD grid

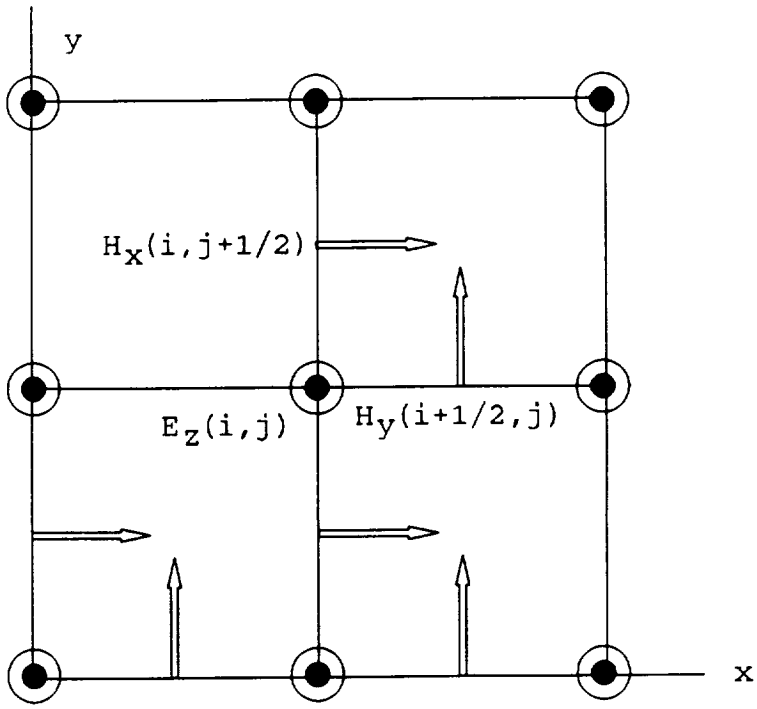

Normal FDTD computation

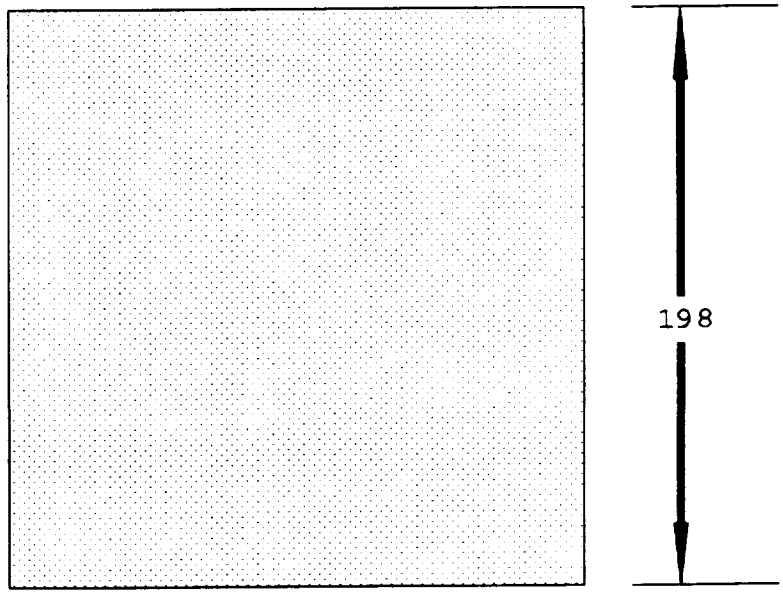

FDTD SIBC computation

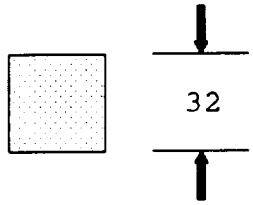

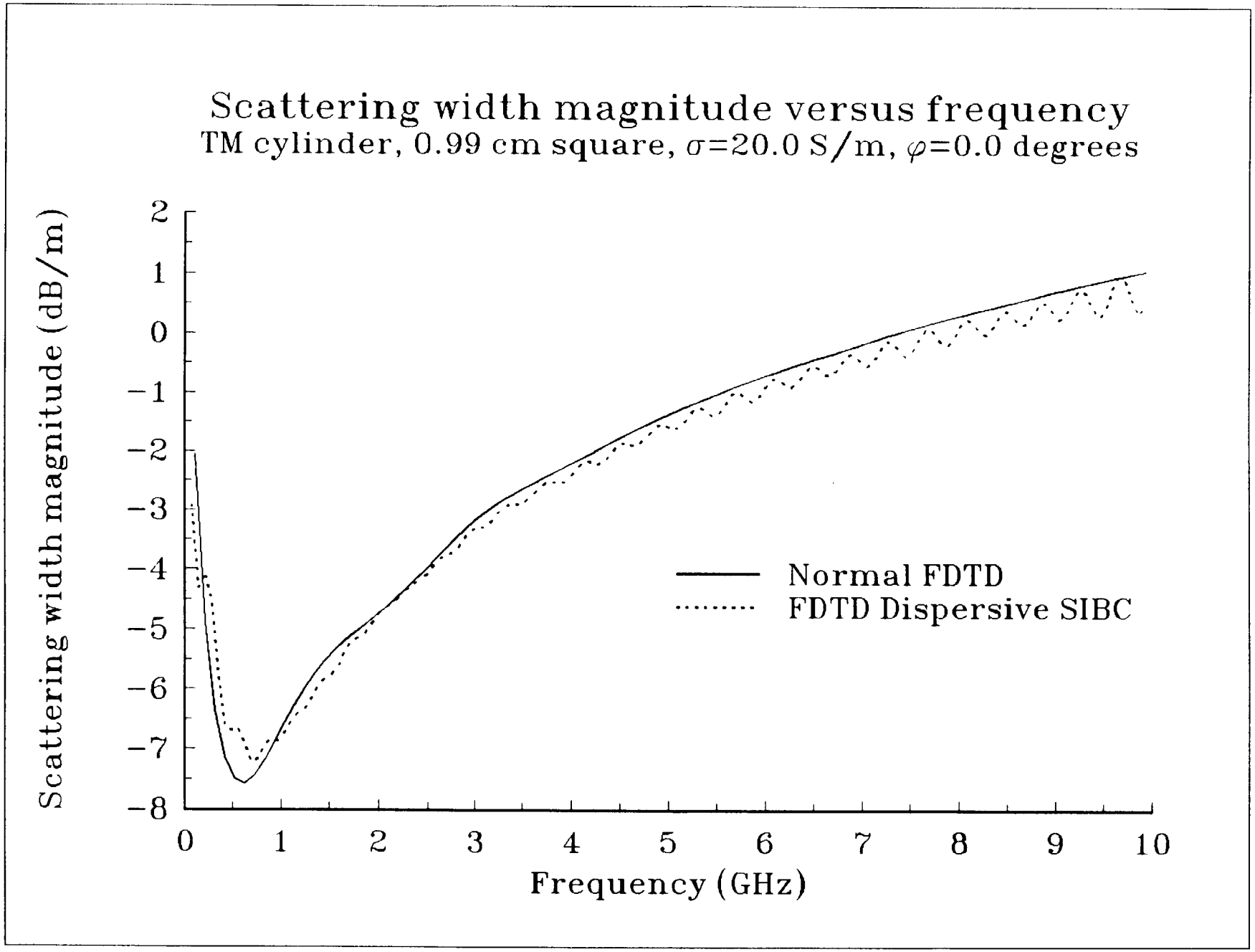
Scattering width magnitude versus frequency
TM cylinder, 0.99 cm square, σ=20.0 S/m, φ=0.0 degrees
Scattering width magnitude (dB/m)
2
1
0
−1
−2
−3
−4
−5
−6
−7
−8
0
1
2
3
4
5
6
7
8
9
10
Frequency (GHz)
Normal FDTD
FDTD Dispersive SIBC

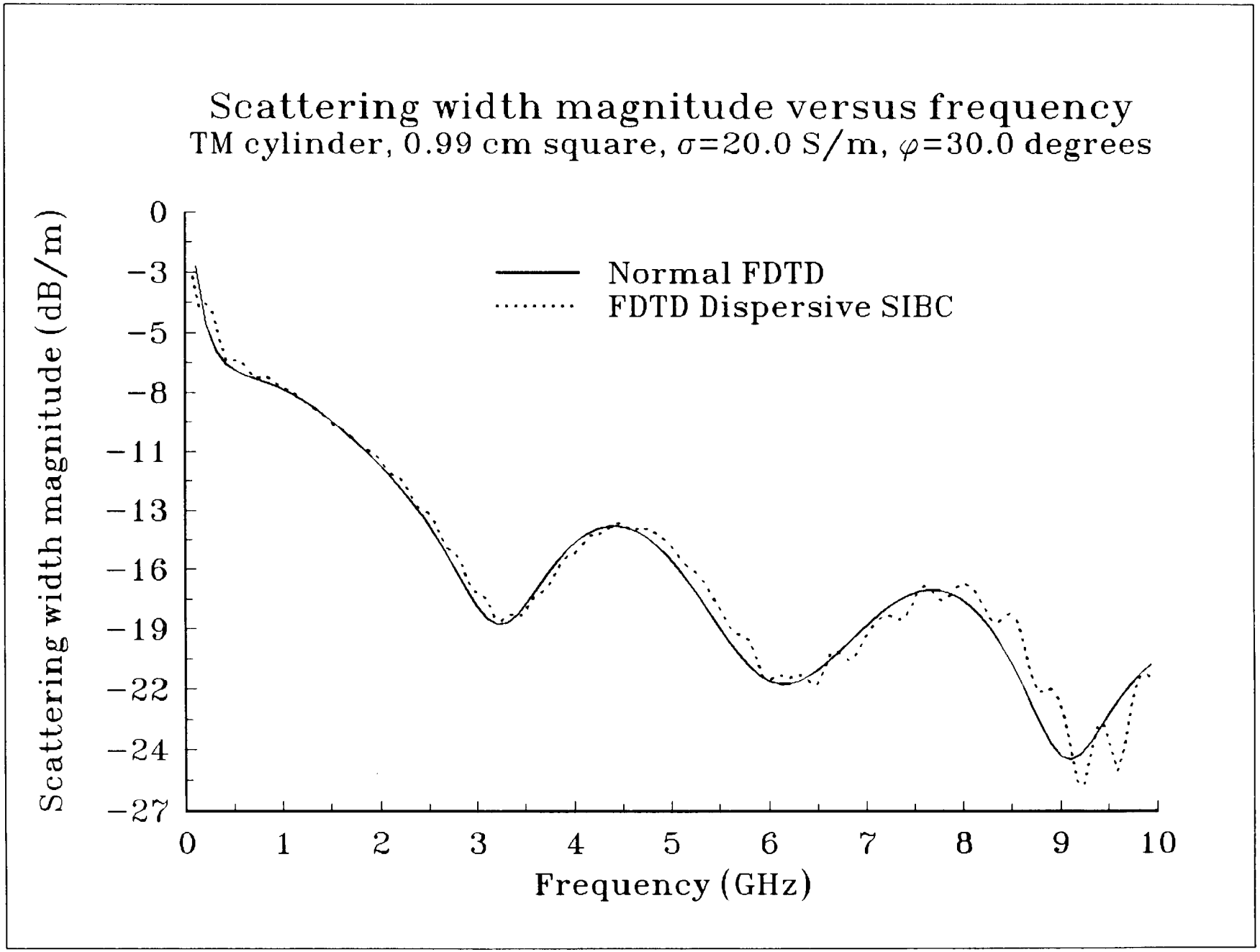
Scattering width magnitude versus frequency
TM cylinder, 0.99 cm square, σ=20.0 S/m, φ=30.0 degrees
Normal FDTD
FDTD Dispersive SIBC
Scattering width magnitude (dB/m)
0
-3
-5
-8
-11
-13
-16
-19
-22
-24
-27
0
1
2
3
4
5
6
7
8
9
10
Frequency (GHz)

WIDEBAND FINITE DIFFERENCE TIME DOMAIN IMPLEMENTATION OF SURFACE IMPEDANCE BOUNDARY CONDITIONS FOR GOOD CONDUCTORS

John H. Beggs, Raymond J. Luebbers *, and Karl S. Kunz

Department of Electrical and Computer Engineering
The Pennsylvania State University
University Park, PA 16802

Kane S. Yee
Lockheed Missiles and Space Company
Sunnyvale, California

SUMMARY

Surface impedance boundary conditions are employed to reduce the solution volume during the analysis of scattering from lossy dielectric objects. In a finite difference solution, they also can be utilized to avoid using small cells, made necessary by shorter wavelengths in conducting media, throughout the solution volume. This paper presents a one dimensional implementation for a surface impedance boundary condition for good conductors in the Finite Difference Time Domain (FDTD) technique.

In order to illustrate the FDTD surface impedance boundary condition, we considered a planar air-lossy dielectric interface as shown in Figure 1. The incident field has polarization TE_z, and is propagating in the +z direction. The one-dimensional FDTD grid is also shown in Figure 1. To begin our implementation for a FDTD surface impedance boundary condition, we assume that the lossy dielectric has permittivity ϵ, permeability μ, and conductivity σ; and that it is a good conductor. Thus, these constitutive parameters are real and satisfy the relation

$$\frac{\sigma}{\omega\epsilon} > 1 \qquad (1)$$

where ω is the radian frequency. We also assume that the radius of curvature is large compared to the maximum wavelength in the material and that the thickness of the material is large compared to the skin depth.

The first order (or Leontovich) impedance boundary condition in the frequency domain is [1]

$$E_x^t(\omega) = \eta_s(\omega) H_y^t(\omega) \qquad (2).$$

where $\eta_s(\omega)$ is the surface impedance of the conductor. A superscript "t" is used in equation (2) to indicate the boundary condition is applied to the total field in free space. The frequency domain surface impedance for good conductors is

$$\eta_s(\omega) = \sqrt{\frac{\omega\mu}{2\sigma}}(1+j) = \sqrt{\frac{j\omega\mu}{\sigma}} \qquad (3).$$

Separating incident and scattered E_x terms in (2) yields

$$E_x^s(\omega) = \eta_s(\omega) H_y^t(\omega) - E_x^i(\omega) \qquad (4).$$

where the superscripts "s" and "i" are used to denote scattered and incident field components respectively. This equation is the required surface impedance boundary condition for scattered field components. The corresponding time domain expression involves a convolution integral and is given as

$$E_x^s(t) = \eta_s'(t) * H_y^t(t) - E_x^i(t) \qquad (5)$$

where the '*' denotes convolution and the time domain surface impedance impulse response is given by

$$\eta_s'(t) = F^{-1}\{\eta_s'(\omega)\} = F^{-1}\{\frac{\eta_s(\omega)}{j\omega}\} \qquad (6).$$

We have approximated this time domain impulse response by a series of exponentials to obtain an efficient recursive updating scheme requiring only four running sum variables similar to [2]. Figures 2 and 3 show reflection coefficient comparison versus frequency for conductivities of 10.0 S/m and 50.0 S/m. The FDTD reflection coefficients are compared against the standard analytical solution. Note that the agreement is quite good for the entire frequency band.

Overall, the surface impedance boundary condition implementation works well in eliminating the conductor volume from the solution space. This method has a distinct advantage over other possible implementations because the coefficients of the exponential approximation of the impulse response are independent of the conductivity of the scattering object and do not need to be reevaluated for different conductivities. Extensions of this surface impedance concept to two and three dimensions are currently under investigation.

REFERENCES

[1] T. B. A. Senior, "Impedance boundary conditions for imperfectly conducting surfaces," Appl. Sci. Res. B, vol. 8, pp. 418-436, 1960.

[2] R. J. Luebbers et al, "A Frequency-Dependent Finite-Difference Time-Domain Formulation for Dispersive Materials," IEEE Trans. Electromagn. Compat., vol. EMC-32, pp. 222-227, August 1990.

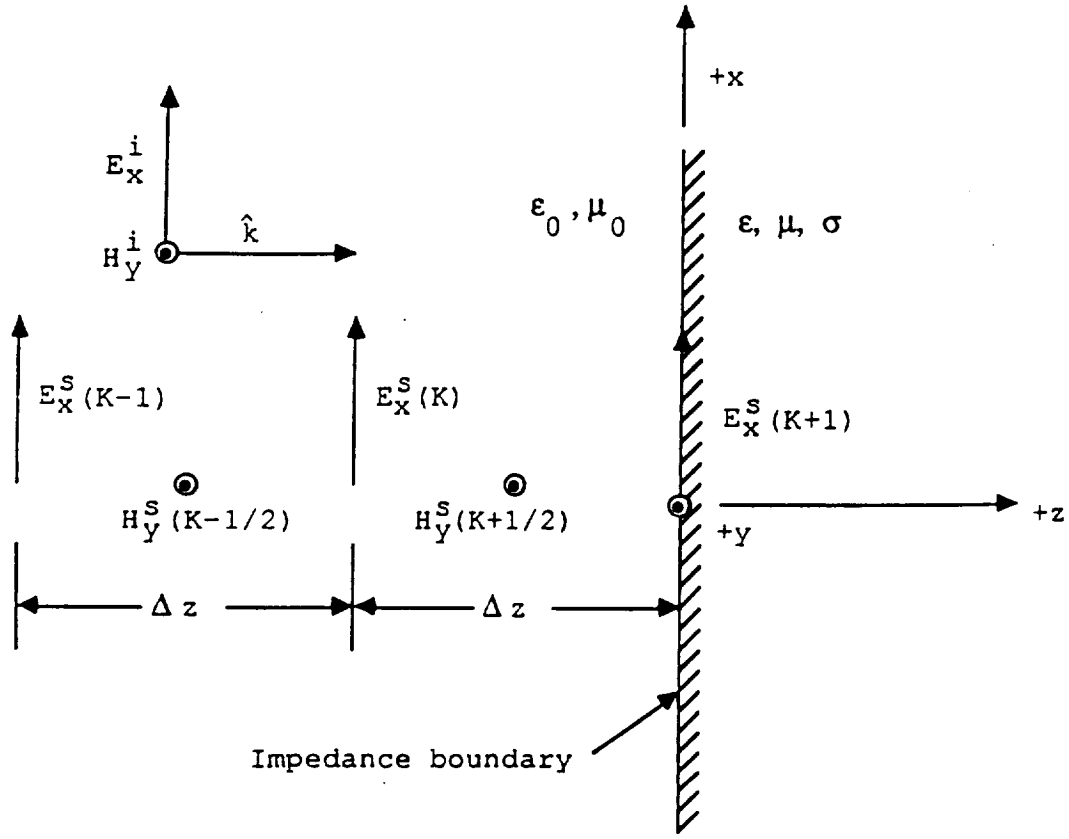

Figure 1. Problem geometry showing incident plane wave, planar air-lossy dielectric interface and one dimensional FDTD grid.

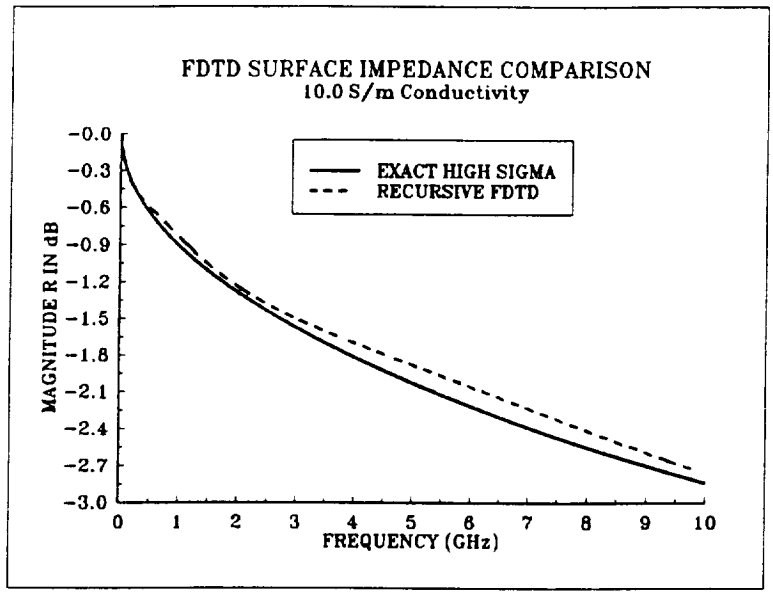

Figure 2. Reflection coefficient magnitude versus frequency for normal incidence plane wave calculated for 10.0 S/m conductivity using FDTD surface impedance and analytical evaluation of high conductivity approximation.

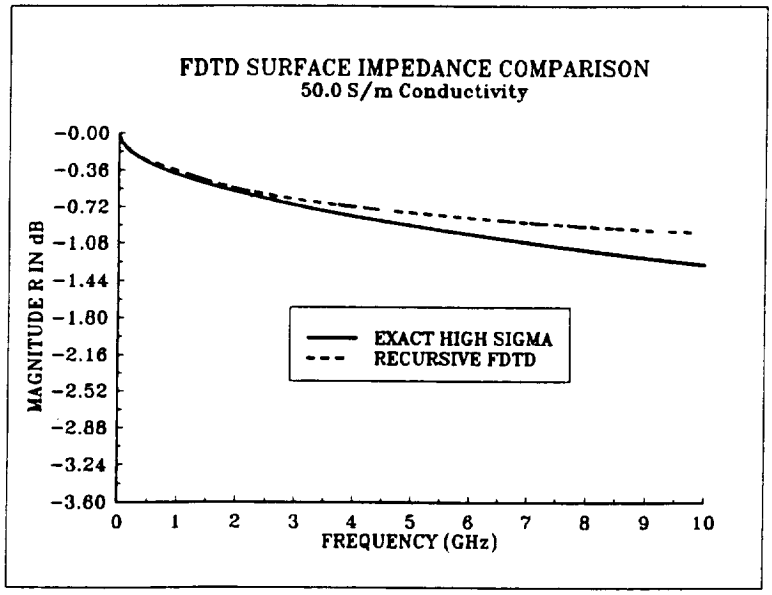

Figure 3. Reflection coefficient magnitude versus frequency for normal incidence plane wave calculated for 50.0 S/m conductivity using FDTD surface impedance and analytical evaluation of high conductivity approximation.

TIME DOMAIN SCATTERING AND RADAR CROSS SECTION CALCULATIONS FOR A THIN, COATED PERFECTLY CONDUCTING PLATE

furnished to

Captain Doug Havens
AFEWC/ESAS
San Antonio, TX 78243-5000

and to

Dr. Randy Jost
AFWAL/CDJ
Wright-Patterson AFB, OH 45433-6523

submitted by

Raymond J. Luebbers and John H. Beggs
Electrical and Computer Engineering Department
The Pennsylvania State University
University Park, PA 16802

(814) 865-2362

February 1991

Abstract

Radar Cross Section (RCS) calculations for flat, perfectly conducting plates are readily available through the use of conventional frequency domain techniques such as the Method of Moments (MOM). However, if the plate is covered with a dielectric material that is relatively thick in comparison with the wavelength in the material, these frequency domain techniques become increasingly difficult to apply. In this paper, we present the application of the Finite Difference Time Domain (FDTD) technique to the problem of electromagnetic scattering and RCS calculations from a thin, perfectly conducting plate that is coated with a thick layer of lossless dielectric material. Both time domain and RCS calculations will be presented and discussed.

I. Introduction

The Finite Difference Time Domain (FDTD) technique has become increasingly popular in recent years for modeling electromagnetic scattering problems. It is based upon the time domain form of Maxwell's equations, in which temporal and spatial derivatives are approximated by finite differences, and the electric and magnetic fields are interleaved spatially and temporally. Transient scattering behavior is easily examined and through the use of non-sinusoidal plane wave excitation, wideband frequency results can be obtained. The technique was first proposed by Yee [1] in 1966 and is inherently volumetric, which makes it ideal for modeling volumetric scatterers. Thin scatterers can easily be accommodated, and recently the technique has been expanded to include dispersive materials [2], plasmas [3], and chiral materials [4]. Through the use of a near to far zone transformation [5], far zone scattered fields (and thus RCS data) are readily available. This paper presents time domain scattering and RCS calculations over 0-3 GHz for several incidence angles from a thin, perfectly conducting (PEC) plate that is coated with a uniform lossless dielectric layer.

II. Problem Description

The scattering problem was a 3λ by 6λ (at 3 GHz) perfectly conducting plate that was coated with a 5 cm thick lossless dielectric layer with relative dielectric constant of $\epsilon_r = 4.0$. Figure 1 shows the problem geometry with the dielectric layer on top of the plate. The wavelength (at 3 GHz) inside the dielectric layer is $\lambda_0/\sqrt{\epsilon_r} = 5.0$ cm, where λ_0 is the free space wavelength at 3 GHz. Thus, the dielectric coating is relatively thick at 1λ. The spatial increment (cell size) was chosen to be 1 cm, which provides a spatial resolution of 5 cells/λ inside the dielectric coating and 10 cells/λ_0 in free space.

The problem space size was chosen to be 61 by 121 by 49 cells in the x, y and z directions respectively. The plate was centered within the problem space in the x and y directions. The plate was positioned low in the problem space in the z direction

to allow any specular reflections multiple encounters with the outer radiation boundary condition (ORBC).

The plate was constructed with 30 by 60 by 5 cells in the x, y and z directions for the dielectric coating, and with 30 by 60 by 0 cells for the PEC plate. The dielectric coating was constructed first, and the PEC plate was constructed on the bottom of the dielectric layer to avoid any air gaps within the scatterer. A 15 cell and 30 cell border on each side of the scatterer in the x and y directions provided adequate margin for the near to far zone transformation integration surface and for the ORBC.

A θ-polarized, Gaussian pulse incident plane wave with a maximum amplitude of 1000 V/m and a total temporal width of 128 time steps was chosen. The time step was 0.0192 ns and the total number of time steps was 2048.

III. Computations and Discussion

Calculations were made at incidence angles $\theta = 0.0$, $\theta = 60.0$, $\theta = 85.0$ and $\theta = 90.0$ degrees for both an uncoated and coated plate. The incidence angle was taken from the $+z$ axis, the ϕ incidence angle was $\phi = 0.0$ degrees for all computations, and the far field computations were for backscatter only. The θ-polarized scattered and incident fields were then transformed to the frequency domain via an FFT and RCS was determined. Each computational problem required slightly more than one hour of CPU time on a Cray Y-MP supercomputer.

Figure 2 shows the θ-polarized time domain far zone scattered electric field for incidence angle $\theta = 0.0$ degrees. Note for the coated plate the early reflection from the top edge of the dielectric layer. Also note the time domain response for the coated plate is not markedly different from the uncoated plate except for some additional "ringing" due to energy being confined within the dielectric coating. Figure 3 shows the RCS computations versus frequency again for both the uncoated and coated plate, and the RCS for both cases does not differ substantially.

Figure 4 shows the θ-polarized time domain far zone scattered field for incidence angle $\theta = 60.0$ degrees. Note the time responses differ more substantially for this case as more energy is being confined within surface wave modes of the dielectric layer. Figure 5 shows the corresponding RCS. Note the small peaks that have appeared in the RCS for the coated plate. We postulate these peaks correspond to surface wave modes that have been excited and radiate energy to the far field. As an approximation, we computed cutoff frequencies for waveguide modes for an infinite, dielectric covered ground plane according to Balanis [6]. These waveguide modes and corresponding cutoff frequencies are tabulated in Table 1. Examining the RCS of the coated plate, it is easily seen that a peak in the RCS is in close proximity to each cutoff frequency from Table 1. The peaks in the RCS are not located exactly at the cutoff frequencies of Table 1, probably due to the finite size of the plate.

Mode	Cutoff Frequency (GHz)
TM_0	0.00000
TE_1	0.86589
TM_2	1.73718
TE_3	2.59767

Table 1. Modes and cutoff frequencies for an infinite ground plane covered with a 5 cm thick dielectric layer of $\epsilon_r = 4.0$.

Figure 6 shows the θ-polarized time domain far zone scattered field for incidence angle $\theta = 85.0$ degrees. Also shown in Figure 6 is the far zone scattered field for a 5 cm thick 3λ by 6λ dielectric layer. Since this incidence angle is near grazing, we expect to see little scattered field for the uncoated plate. Examining the time responses in Figure 6, the uncoated plate response is indeed quite small in comparison to the dominant coated plate response. The dielectric layer response has the same general form as the coated plate response but is smaller in magnitude. Figure 7 shows the corresponding RCS. Note the large peaks and lobing structure for the coated plate and dielectric layer RCS. These can be attributed to radiation from surface wave modes of the dielectric cavity.

Figure 8 shows the θ-polarized time domain far zone scattered field for incidence angle $\theta = 90.0$ degrees. The response for the zero-thickness uncoated plate is zero, while the coated plate time response does not differ substantially from that for incidence angle $\theta = 85.0$ degrees. Figure 9 shows the RCS for the coated plate only, and it is also similar to the coated plate RCS for incidence angle $\theta = 85.0$ degrees.

IV. Conclusions

In this paper, the FDTD technique has been applied to model electromagnetic scattering from a perfectly conducting plate coated with a uniform, lossless dielectric layer. Time domain scattering results and frequency domain Radar Cross Section computations were presented and discussed. Large peaks in the RCS were found for the coated plate at large incidence angles (near grazing) due to energy being radiated from surface wave modes of the dielectric layer.

The next step would be to provide a rigorous analytical treatment of the problem of a dielectric layer on a finite sized plate (ground plane) and to derive the surface wave structure of the layer and the far field scattering pattern. To the best of the authors' knowledge, no such treatment has yet been presented. Results obtained from a rigorous theoretical treatment would then be used for comparison with the FDTD scattering computations and measured data.

V. Acknowledgement

The authors would like to thank the NASA Ames Research Center for providing the necessary supercomputer resources, and Dr. Randy Jost for suggesting the problem.

References

[1] K. S. Yee, "Numerical solution of initial boundary value problems involving Maxwell's equations in isotropic media," IEEE Trans. Antennas Propagat., vol. AP-14, pp. 302-307, May 1966.

[2] R. J. Luebbers et al, "A frequency dependent Finite Difference Time Domain formulation for dispersive materials," IEEE Trans. Electromagn. Compat., vol. EMC-32, pp. 222-227, August 1990.

[3] R. J. Luebbers et al, "A frequency dependent Finite Difference Time Domain formulation for transient propagation in plasmas,"IEEE Trans. Antennas Propagat., accepted for publication.

[4] F. P. Hunsberger, R. J. Luebbers and K. S. Kunz, "Application of the Finite-Difference Time-Domain method to electromagnetic scattering from 3-D chiral objects," Proc. IEEE AP-S Int. Symp., Dallas, TX, vol. 1, pp. 38-41, May 1990.

[5] R. J. Luebbers et al, "A Finite Difference Time Domain near to far zone transformation," IEEE Trans. Antennas Propagat., accepted for publication.

[6] C. A. Balanis, Advanced Engineering Electromagnetics, New York: Wiley, pp. 441-444, 1989.

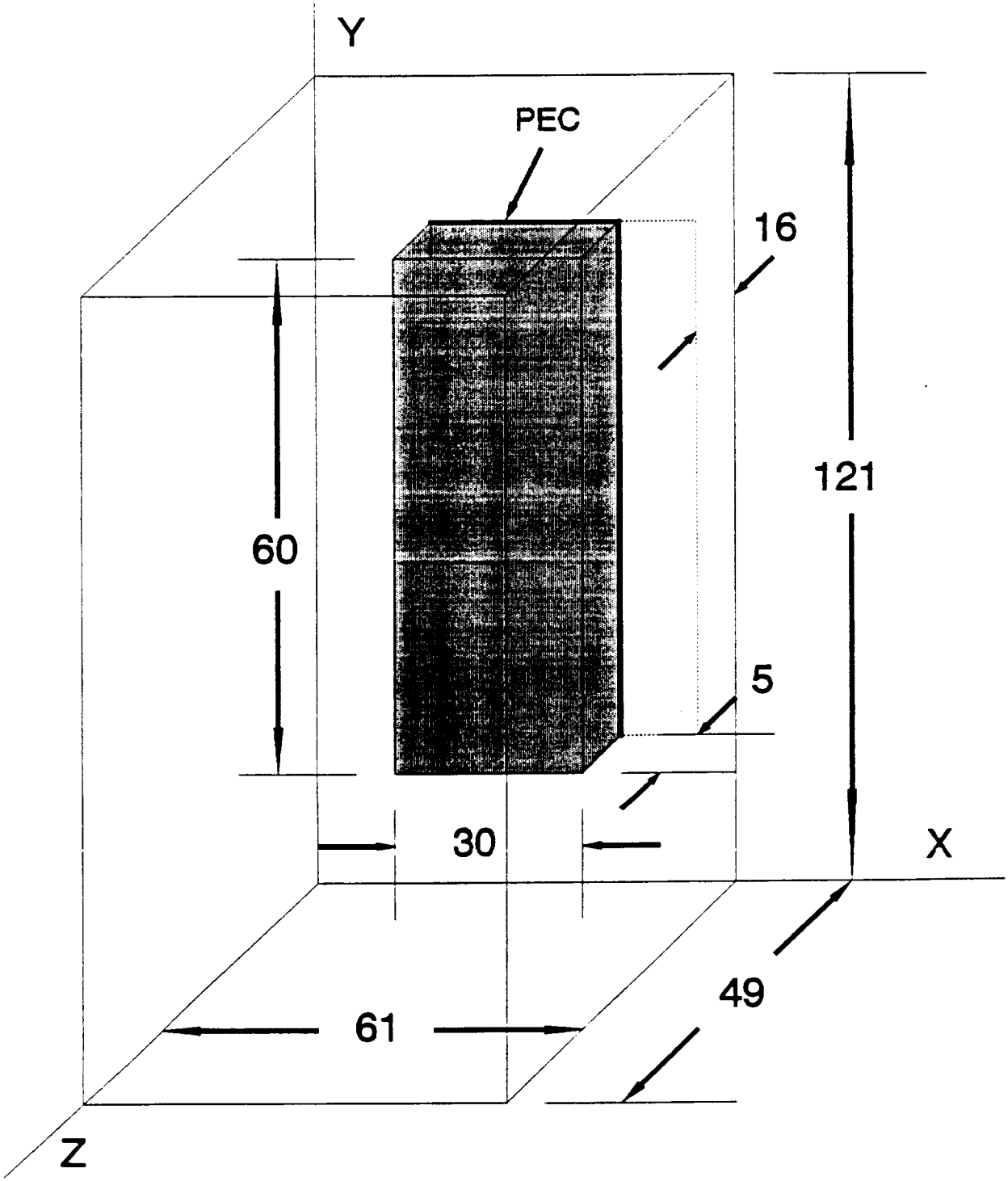

Figure 1. Problem geometry showing problem space size, plate size and plate position.

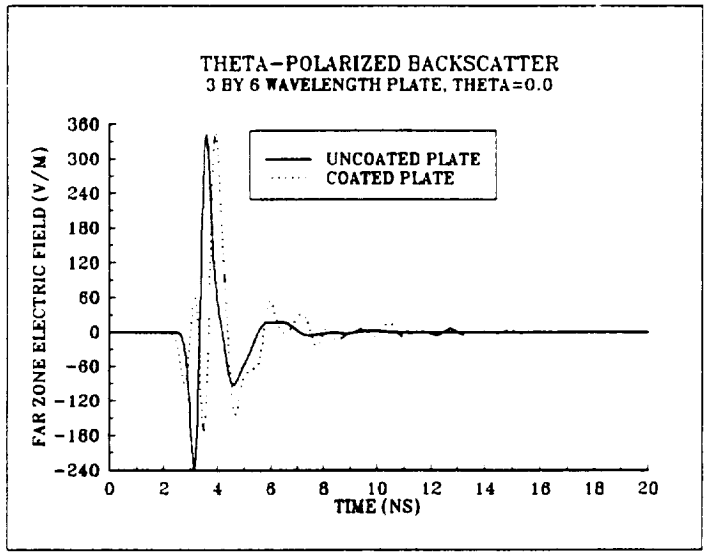

Figure 2. Monostatic, far zone, θ-polarized scattered field for uncoated and coated 3λ by 6λ plate at scattering angle θ =0.0 degrees.

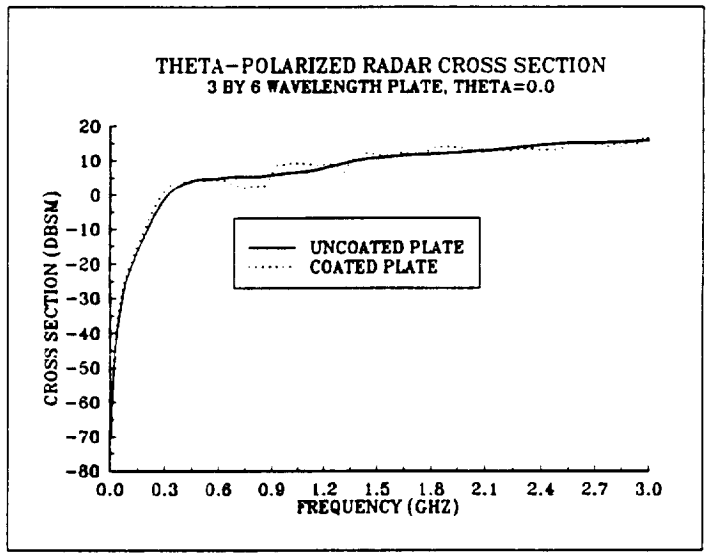

Figure 3. Monstatic Radar Cross Section versus frequency for an uncoated and coated 3λ by 6λ plate at scattering angle θ =0.0 degrees.

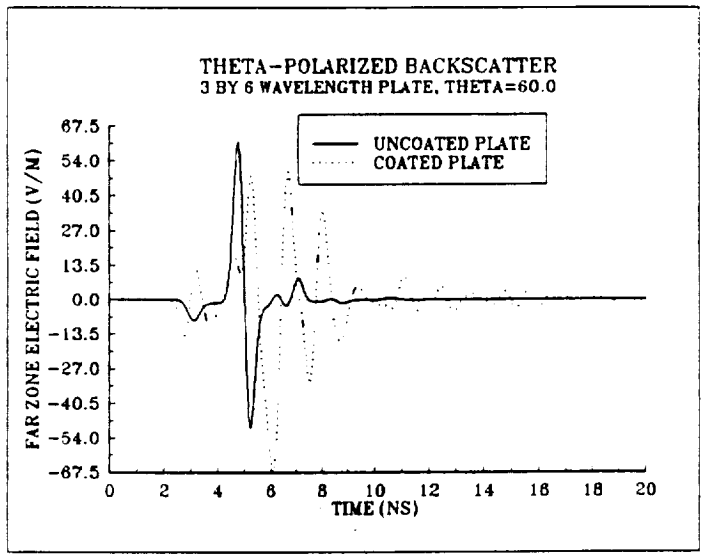

Figure 4. Monostatic, far zone, θ-polarized scattered field for uncoated and coated 3λ by 6λ plate at scattering angle θ =60.0 degrees.

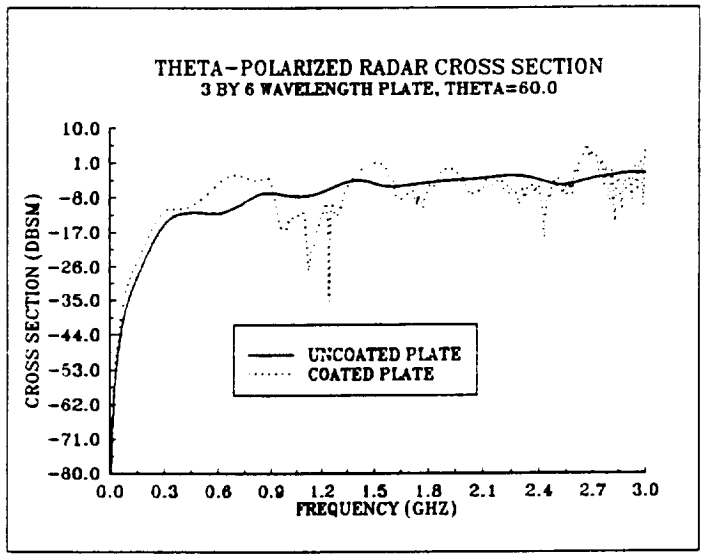

Figure 5. Monostatic Radar Cross Section versus frequency for an uncoated and coated 3λ by 6λ plate at scattering angle θ =60.0 degrees.

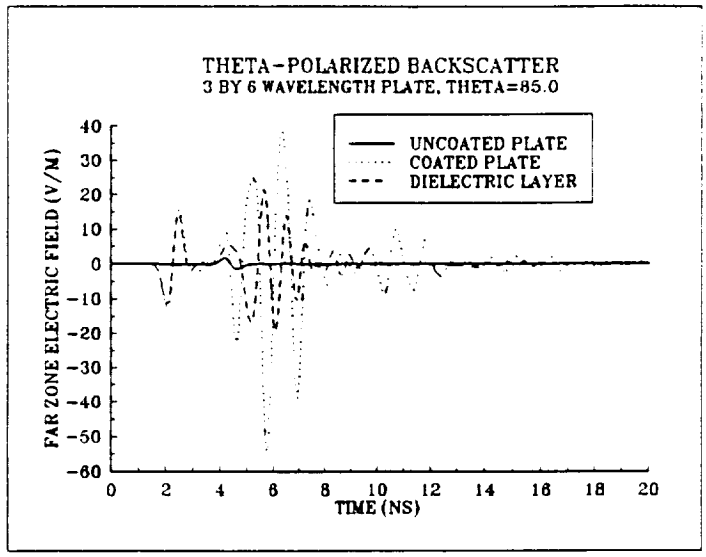

Figure 6. Monostatic, far zone, θ-polarized scattered field for uncoated and coated 3λ by 6λ plate and for 5 cm thick 3λ by 6λ dielectric layer at scattering angle θ = 85.0 degrees.

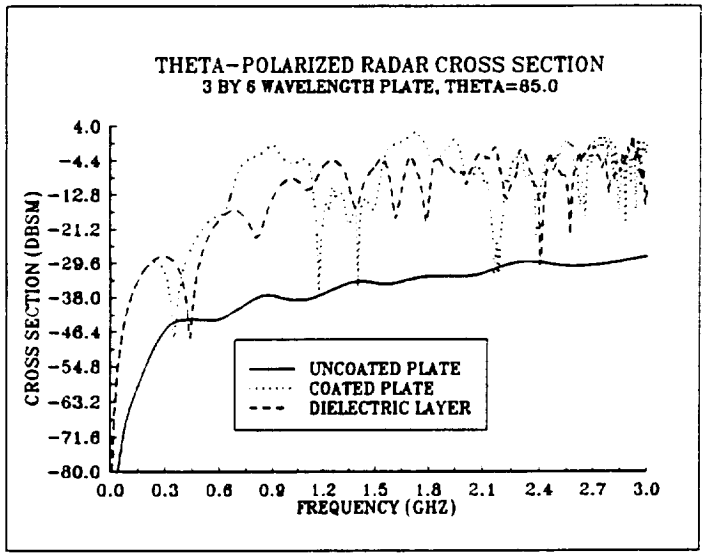

Figure 7. Monostatic Radar Cross Section versus frequency for an uncoated and coated 3λ by 6λ plate and for a 5 cm thick 3λ by 6λ dielectric layer at scattering angle θ = 85.0 degrees.

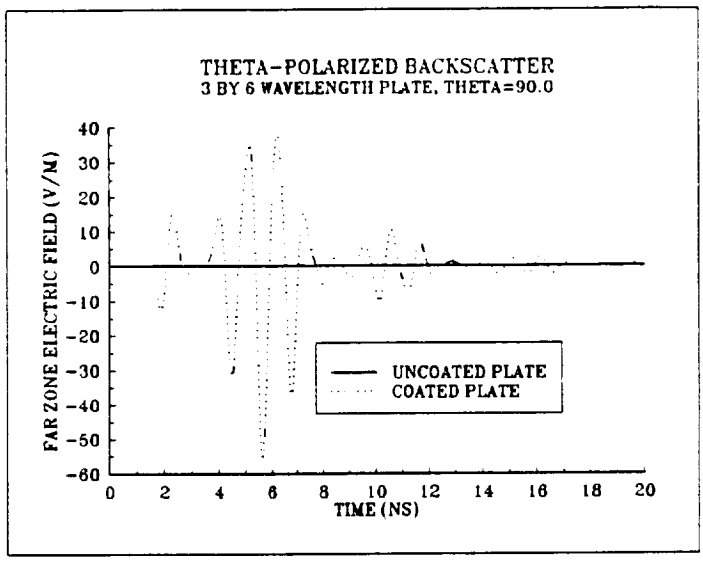

Figure 8. Monostatic, far zone, θ-polarized scattered field for uncoated and coated 3λ by 6λ plate at scattering angle θ =90.0 degrees.

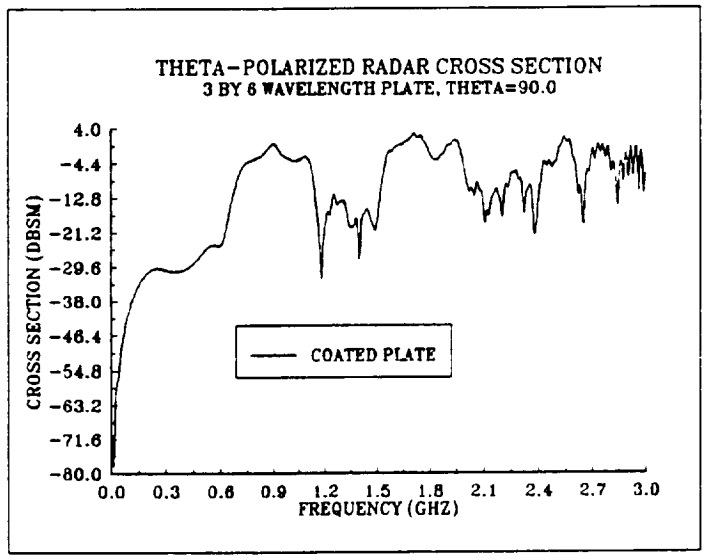

Figure 9. Monostatic Radar Cross Section versus frequency for a coated 3λ by 6λ plate at scattering angle θ =90.0 degrees.

CONICAL CUT RADAR CROSS SECTION CALCULATIONS FOR A THIN, PERFECTLY CONDUCTING PLATE

furnished to

Dr. Alex Woo
Mail Stop 227-6
NASA Ames Research Center
Moffet Field, CA 94035

submitted by

Raymond J. Luebbers and John H. Beggs
Electrical and Computer Engineering Department
The Pennsylvania State University
University Park, PA 16802

(814) 865-2362

March 1991

Abstract

Radar Cross Section (RCS) calculations for flat, perfectly conducting plates are readily available through the use of conventional frequency domain techniques such as the Method of Moments. However, if time domain scattering or wideband frequency domain results are desired, then the Finite Difference Time Domain (FDTD) technique is a suitable choice. In this paper, we present the application of the Finite Difference Time Domain (FDTD) technique to the problem of electromagnetic scattering and RCS calculations from a thin, perfectly conducting plate for a conical cut in the scattering angle ϕ. RCS calculations versus angle ϕ will be presented and discussed.

I. Introduction

The Finite Difference Time Domain (FDTD) technique has become increasingly popular in recent years for modeling electromagnetic scattering problems. It is based upon the time domain form of Maxwell's equations, in which temporal and spatial derivatives are approximated by finite differences, and the electric and magnetic fields are interleaved spatially and temporally. Transient scattering behavior is easily examined and through the use of non-sinusoidal plane wave excitation, wideband frequency results can be obtained. The technique was first proposed by Yee [1] in 1966 and is inherently volumetric, which makes it ideal for modeling volumetric scatterers. Thin scatterers can easily be accommodated, and recently the technique has been expanded to include dispersive materials [2], plasmas [3], and chiral materials [4]. Through the use of a near to far zone transformation [5], far zone scattered fields (and thus RCS data) are readily available. This paper presents RCS calculations at several frequencies of a conical cut in scattering angle ϕ for a 3.5λ by 2λ perfectly conducting plate. Results obtained with FDTD computations are compared with results obtained with the ESP4 electromagnetic code.

II. Problem Description

This particular scattering problem first came to the authors' attention when Dr. Woo indicated he was obtaining significant discrepancies between measurements and numerical analyses using several Method of Moments electromagnetic codes. He then suggested that a scattering analysis by the Penn State FDTD code may provide some insight as to where problems may exist.

The scattering problem was a 3.5λ by 2λ (at 3 GHz) perfectly conducting plate that was oriented within the FDTD solution space as shown in Figure 1. The free space wavelength (at 3 GHz) is λ_0=10.0 cm. The spatial increment (cell size) was chosen to be 1 cm, which provides a spatial resolution of 10 cells/λ_0 in free space.

The problem space size was chosen to be 66 by 41 by 49 cells in the x, y and z directions respectively. The plate was centered within the problem space in the x and y directions. The plate was positioned low in the problem space in the z direction to allow any specular reflections multiple encounters with the outer radiation boundary condition (ORBC).

The plate was constructed with 35 by 20 by 0 cells in the x, y and z directions for the PEC plate. Thus the physical plate size was 35 cm by 20 cm. A 15 cell and 10 cell border on each side of the scatterer in the x and y directions provided adequate margin for the near to far zone transformation integration surface and for the ORBC.

A ϕ-polarized, Gaussian pulse incident plane wave with a maximum amplitude of 1000 V/m and a total temporal width of 128 time steps was chosen. The time step was 0.0192 ns and the total number of time steps was 1024.

III. Computations and Discussion

At the recommendation of Dr. Woo, calculations were made for $\theta = 80.0$ degrees; and the angle ϕ was varied from 0.0 to 10.0 degrees in steps of 0.5 degrees. The incidence angles θ and ϕ were taken from the +z and +x axes respectively and the incident field was ϕ-polarized for all computations. The far field computations were for backscatter only. For each incidence angle, the ϕ-polarized (co-pol) and θ-polarized (cross-pol) scattered and incident fields were then transformed to the frequency domain via an FFT and RCS was determined. From each RCS data file, the θ-polarized and ϕ-polarized RCS at 3 GHz for each angle ϕ were chosen and then entered into separate data files of RCS versus angle ϕ. Each incidence angle computation required 1.5 hours on a 486/25 personal computer.

Figure 2 shows a sample time domain co-pol backscatter for $\theta = 80.0$ degrees and $\phi = 5.0$ degrees. Figure 3 shows a sample time domain cross-pol backscatter for $\theta = 80.0$ degrees and $\phi = 5.0$ degrees.

Figure 4 shows the co-pol radar cross section versus scattering angle ϕ. Note the extreme disagreement between the FDTD result and the ESP4 result.

Figure 5 shows the cross-pol radar cross section versus scattering angle ϕ. Note the change in scale of the cross section and the relatively good agreement between the FDTD result and the ESP4 result. Since the co-pol RCS results for FDTD and ESP4 were very much different and the cross-pol RCS results were similar, this indicates a possible problem with either the FDTD code or the ESP4 code.

IV. Investigation

The original calculations for ESP4 were made at 3 GHz with a plate size of 35 cm by 20 cm. These results were compared with FDTD RCS frequency domain data at 3 GHz. In order to gain some insight as to possible problems with the FDTD or ESP4 electromagnetic codes, three additional RCS computations were made with ESP4 at frequencies of 2.25 GHz, 2.47 GHz and 2.70 GHz with $\theta = 80.0$ degrees and a ϕ-polarized incident field. These frequencies were chosen as approximate frequencies for two peaks (2.25 and 2.70 GHz) and one null (2.47 GHz) in the co-pol frequency domain RCS from Figure 6. The data points from the resulting FDTD RCS files were chosen for each frequency and entered into a separate data file for comparison with ESP4 results.

Figure 6 shows the co-pol radar cross section versus frequency and incidence angle ϕ. Figure 7 shows the cross-pol radar cross section versus frequency and incidence angle ϕ.

Figures 8 and 9 show the co-pol and cross-pol radar cross section versus scattering angle ϕ for both FDTD and ESP4 at 2.25 GHz. Note also the extreme disagreement between the co-polarized RCS results and the good agreement between the cross-polarized RCS results.

Figures 10 and 11 show the co-pol and cross-pol radar cross section versus scattering angle ϕ for both FDTD and ESP4 at 2.47 GHz. Again, note the disagreement between the FDTD and ESP4 co-polarized RCS and the good agreement between the cross-polarized RCS results.

Figures 12 and 13 show the co-pol and cross-pol radar cross section versus scattering angle ϕ for both FDTD and ESP4 at 2.7 GHz. Note the co-polarized RCS results are in slightly better agreement and the cross-polarized results again are in good agreement.

V. Conclusions

In this paper, the FDTD technique has been applied to model electromagnetic scattering in a conical cut from a perfectly conducting plate. Radar Cross Section versus scattering angle ϕ was presented and discussed. The ϕ-polarized FDTD and ESP4 RCS results were very dissimilar, while the θ-polarized RCS results were in good agreement. Thus a problem may exist with one or both of the FDTD or ESP4 electromagnetic codes.

References

[1] K. S. Yee, "Numerical solution of initial boundary value problems involving Maxwell's equations in isotropic media," IEEE Trans. Antennas Propagat., vol. AP-14, pp. 302-307, May 1966.

[2] R. J. Luebbers et al, "A frequency dependent Finite Difference Time Domain formulation for dispersive materials," IEEE Trans. Electromagn. Compat., vol. EMC-32, pp. 222-227, August 1990.

[3] R. J. Luebbers et al, "A frequency dependent Finite Difference Time Domain formulation for transient propagation in plasmas," IEEE Trans. Antennas Propagat., accepted for publication.

[4] F. P. Hunsberger, R. J. Luebbers and K. S. Kunz, "Application of the Finite-Difference Time-Domain method to electromagnetic scattering from 3-D chiral objects," Proc.IEEE AP-S Int. Symp., Dallas, TX, vol. 1, pp. 38-41, May 1990.

[5] R. J. Luebbers et al, "A Finite Difference Time Domain near to far zone transformation," IEEE Trans. Antennas Propagat., accepted for publication.

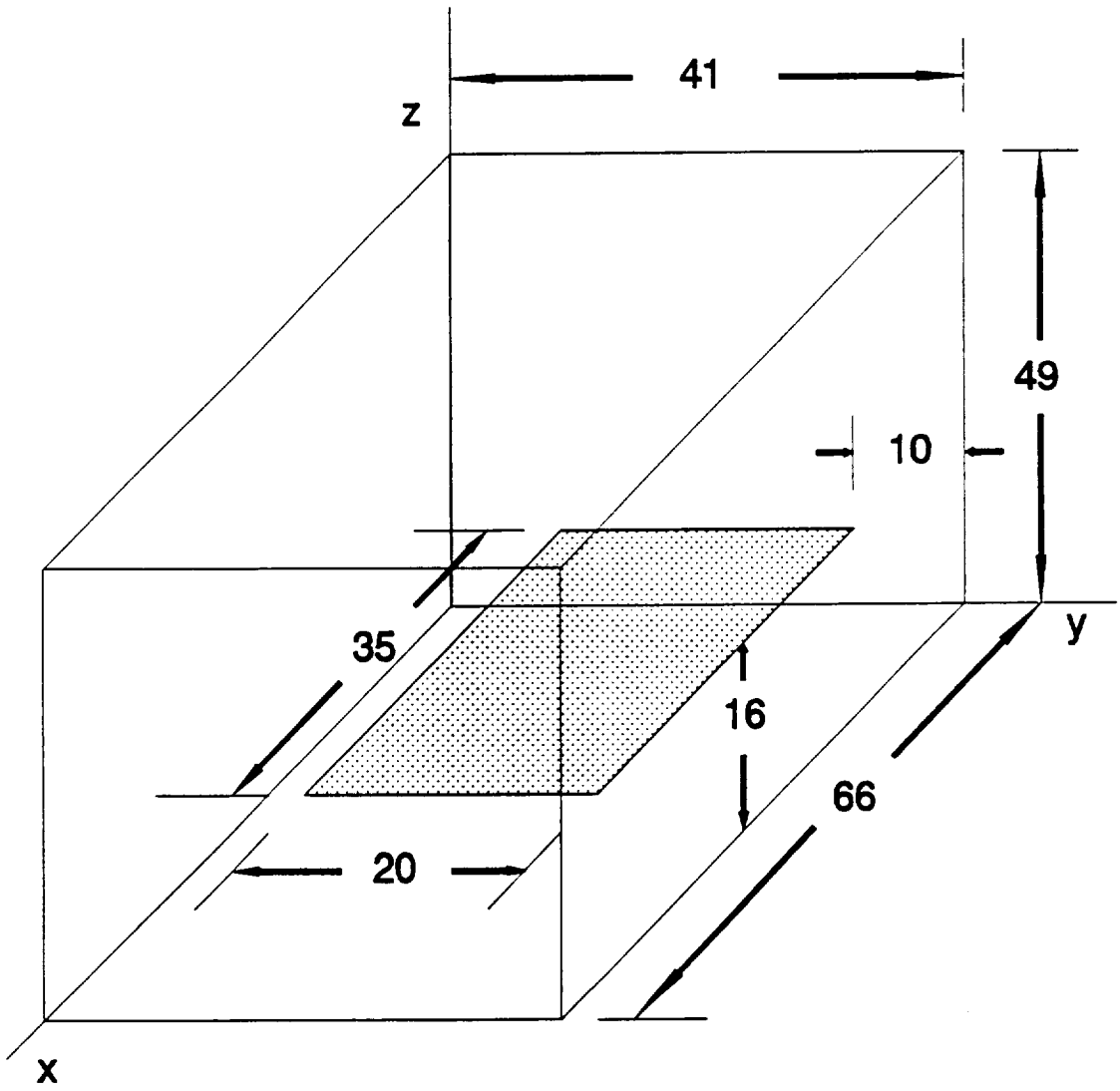

Figure 1. Problem geometry showing FDTD solution space size, and the size and spatial placement of the perfectly conducting plate. Dimensions are in cells, with each cell being a 1 cm cube.

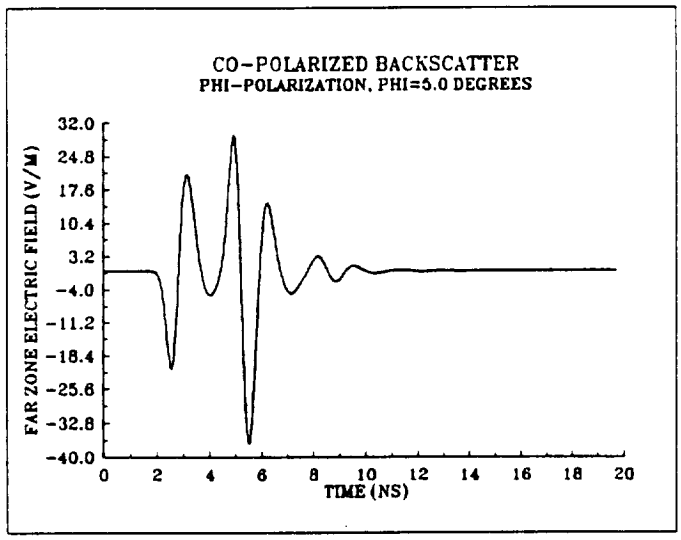

Figure 2. Sample time domain far zone, backscattered, co-polarized electric field from a 35 cm by 20 cm perfectly conducting plate. The scattering angles are $\theta = 80.0$, $\phi = 5.0$ degrees.

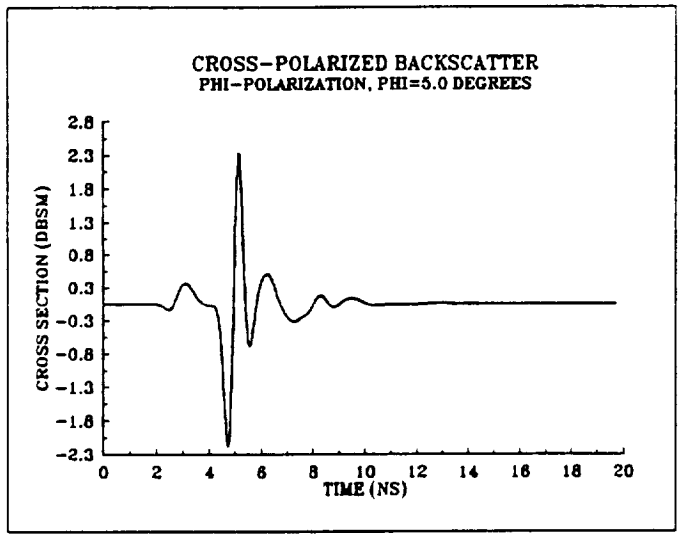

Figure 3. Sample time domain far zone, backscattered, cross-polarized electric field for a 35 cm by 20 cm perfectly conducting plate. The scattering angle is $\theta = 80.0$, $\phi = 5.0$ degrees.

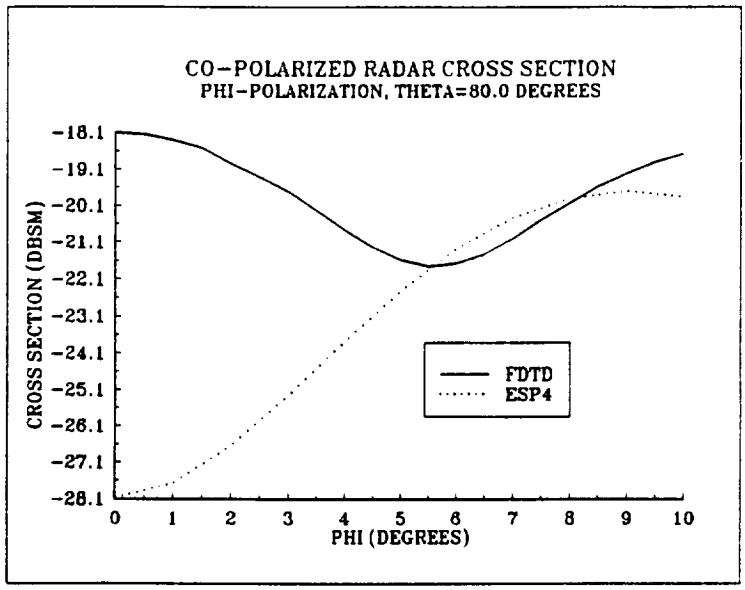

Figure 4. Co-polarized radar cross section versus angle ϕ for a 35 cm by 20 cm perfectly conducting plate at 3.00 GHz using FDTD and ESP4.

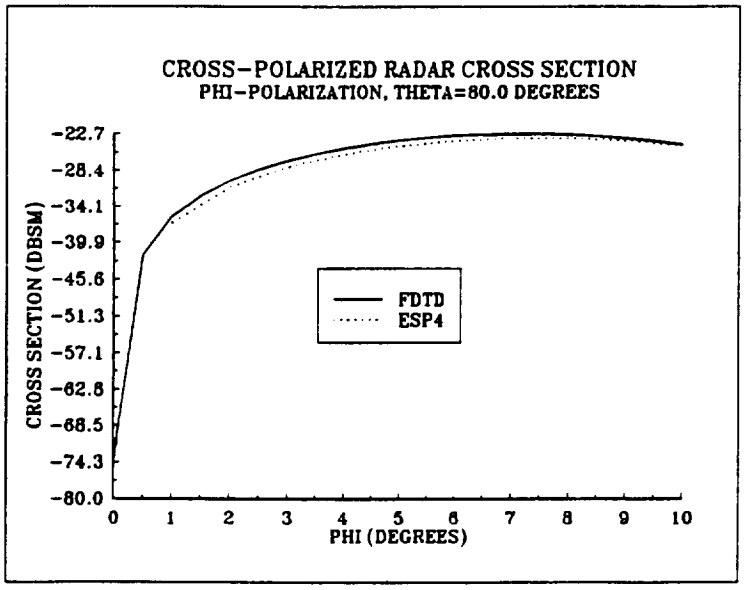

Figure 5. Cross-polarized radar cross section versus angle ϕ for a 35 cm by 20 cm perfectly conducting plate at 3.00 GHz using FDTD and ESP4.

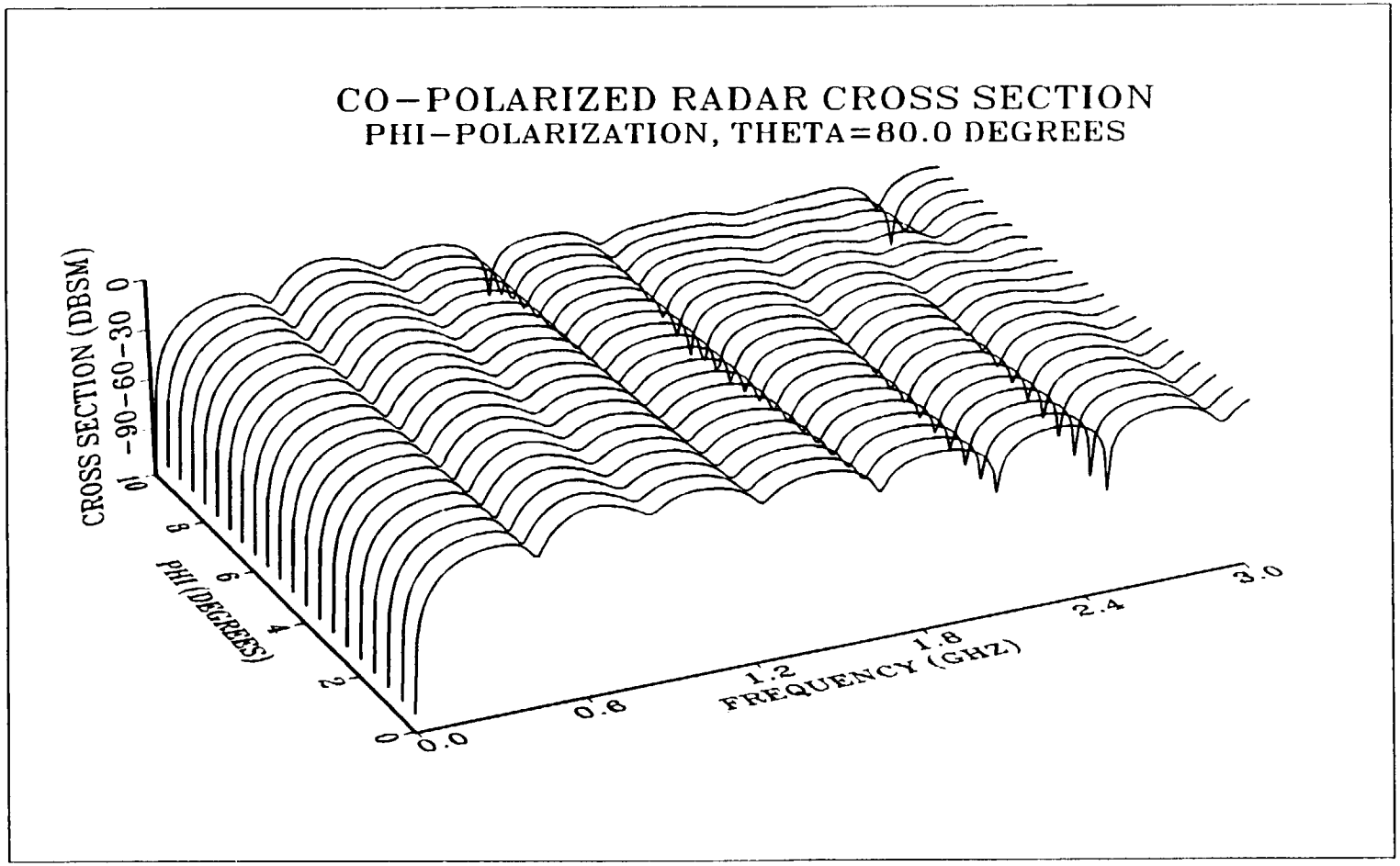

Figure 6. Co-polarized radar cross section versus frequency and incidence angle ϕ from a 35 cm by 20 cm perfectly conducting plate using FDTD.

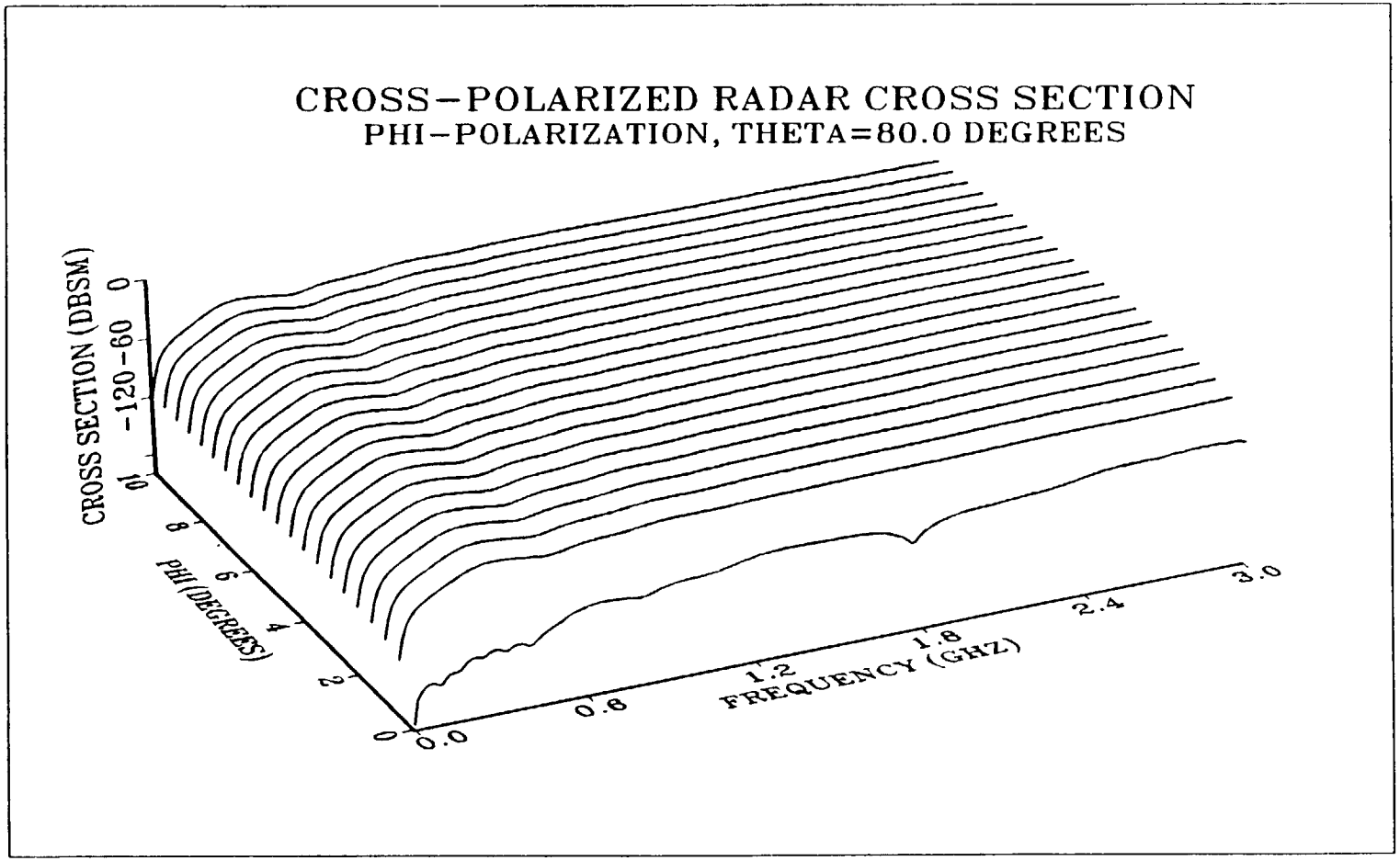

Figure 7. Cross-polarized radar cross section versus frequency and incidence angle ϕ from a 35 cm by 20 cm perfectly conducting plate using FDTD.

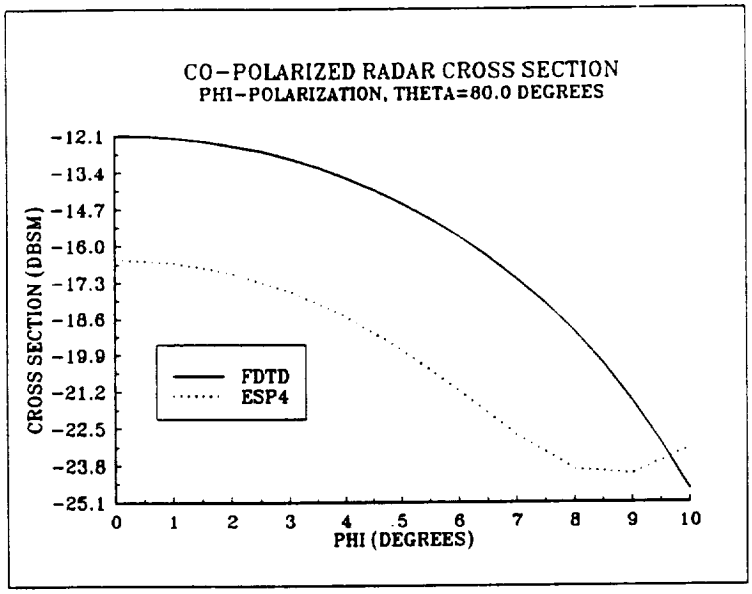

Figure 8. Co-polarized radar cross section versus angle ϕ from a 35 cm by 20 cm perfectly conducting plate at 2.25 GHz using FDTD and ESP4.

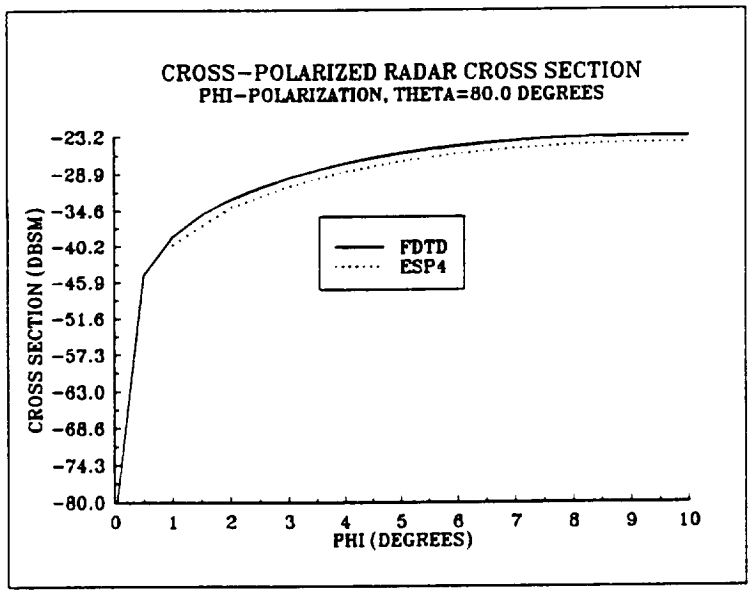

Figure 9. Cross-polarized radar cross section versus angle ϕ from a 35 cm by 20 cm perfectly conducting plate at 2.25 GHz using FDTD and ESP4.

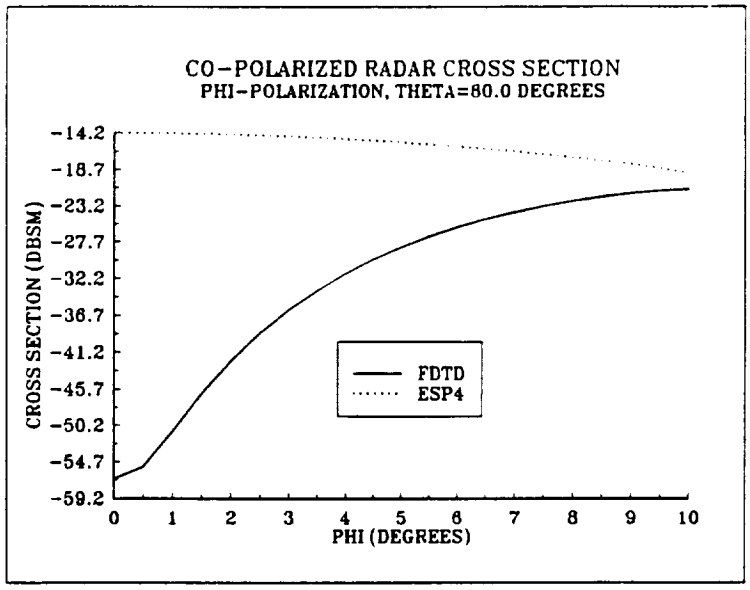

Figure 10. Co-polarized radar cross section versus angle ϕ from a 35 cm by 20 cm perfectly conducting plate at 2.47 GHz using FDTD and ESP4.

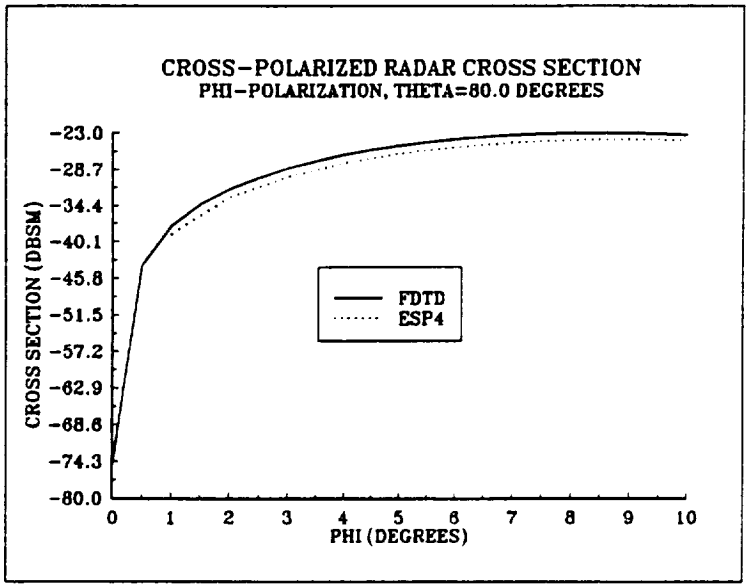

Figure 11. Cross-polarized radar cross section versus angle ϕ from a 35 cm by 20 cm perfectly conducting plate at 2.47 GHz using FDTD and ESP4.

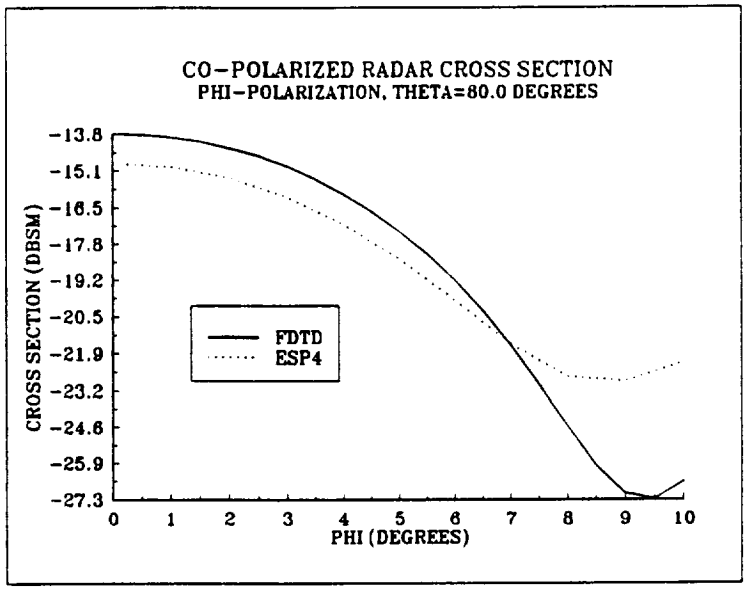

Figure 12. Co-polarized radar cross section versus angle ϕ from a 35 cm by 20 cm at 2.70 GHz using FDTD and ESP4.

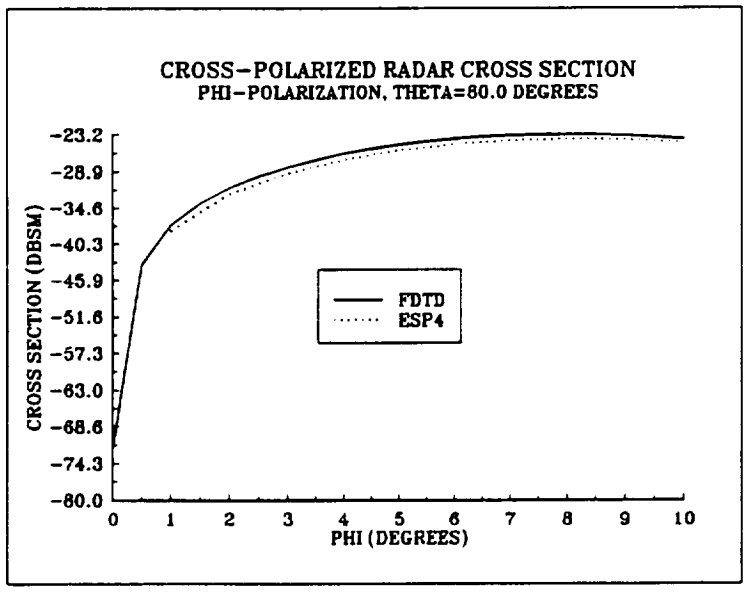

Figure 13. Cross-polarized radar cross section versus angle ϕ from a 35 cm by 20 cm perfectly conducting plate at 2.70 GHz using FDTD and ESP4.

FDTD Modeling of Thin Impedance Sheets

by

Raymond Luebbers and Karl Kunz

Department of Electrical Engineering
The Pennsylvania State University
University Park, PA 16802

(814) 865-2362

Abstract

Thin sheets of resistive or dielectric material are commonly encountered in radar cross section calculations. Analysis of such sheets is simplified by using sheet impedances. In this paper it is shown that sheet impedances can be modeled easily and accurately using Finite Difference Time Domain (FDTD) methods.

Introduction

In [1] a review of various approximate boundary conditions is given, including several for thin sheets and layers. These are applicable to sheets which are thin relative to the free space wavelength, so that they can be approximated by an electric current sheet. If the thin sheet is primarily conductive the sheet impedance will be resistive, as is the case for resistance cards. A thin lossless dielectric sheet will have a purely reactive sheet impedance, while in general the sheet impedance will be complex. These sheets are characterized by a discontinuity in the tangential magnetic field on either side of the sheet but no discontinuity in tangential electric field. This continuity, or single valued behavior of the electric field, allows the sheet current to be expressed in terms of an impedance multiplying this electric field.

Approach

The sheet impedance can be defined in several ways. A convenient definition can be obtained by combining eqs. (3.3) and (3.5) of [2]

$$Y_s = \sigma T + j\omega\epsilon_0(\epsilon_r - 1)T \tag{1}$$

with

$$Z_s = 1/Y_s \tag{2}$$

where Y_s is the sheet admittance, Z_s the sheet impedance, σ and ϵ_r the conductivity and relative permittivity of the sheet material, T the sheet thickness, and ϵ_0 the free space permittivity.

Let us now consider how to incorporate this approximation into the FDTD method. The surface impedance approximation

requires the impedance sheet to be small compared with the free space wavelength. In most FDTD calculations the FDTD cell size (Yee [3] cells are used here) must be on the order of 1/10 wavelength or less for reasonably accurate results. Scattering from an infinitesimally thin perfectly conducting plate was has been calculated by approximating the plate as being one FDTD cell thick with good results [4]. If it is assumed that the same approach can be applied to infinitesimally thin impedance sheets, then the plate thickness T in (1) merely becomes the thickness of the FDTD cell, and the conductivity and/or relative permittivity to be used in the FDTD calculations are merely adjusted in accordance with (1) to give the desired sheet impedance. Note that the FDTD cell dimension need not correspond to the thickness of the actual physical plate. The FDTD cell thickness is used only to determine the conductivity and relative permittivity of the FDTD electric field location so that the desired sheet impedance is approximated. Note also that, even if the wavelength in the material forming the impedance sheet is much smaller than a free space wavelength, the FDTD cell size need not be correspondingly reduced.

Demonstration

The first demonstration will consist of calculating the far zone backscatter from a 29 x 29 cm flat plate of sheet impedance Z_s = 500 Ω. The FDTD calculations will use cubical Yee cells with 1 cm edges. Using T = 1 cm, the corresponding FDTD conductivity is σ = 0.2 S/m. The FDTD calculations shown in Figures 1-8 are all made with the plate modeled by setting the conductivity to 0.2 S/m for x and y polarized electric field locations corresponding to single z dimension index over a range of x and y dimension indices to model the plate. The FDTD approach used and the transformation to the far zone is described in [4]. The problem space size, orientation and position of the

plate, incident Gaussian pulse plane wave, and time step size are also consistent with those in [4].

Figure 1 shows the far zone backscattered electric field for a Gaussian pulsed plane wave normally incident on the plate. In Figure 2 this result is Fourier transformed, converted to cross section, and compared with results using the Method of Moments [2]. The agreement is quite good, with the approximately 20 dB reduction in radar cross section relative to a perfectly conducting plate of the same size [4] consistently predicted by both methods.

In Figures 3-8 the same plate geometry and composition is considered but for non-normal incidence. The plate is perpendicular to the z axis, with edges parallel to the x and y axes, and the plane wave is incident from θ=45, ϕ=30 degrees. Figures 3-5 show the co-polarized backscatter far zone electric field for ϕ and θ polarizations and the cross-polarized backscatter as well. In Figures 6-8 these time domain results are Fourier transformed and converted to radar cross section for comparison with Moment Method [2] results. Again the agreement is quite good, except at the highest frequencies considered. These results indicate that perhaps 12 cells/wavelength are required for good accuracy for off-normal incidence. Comparing the results in Figure 6 with those in Figure 5 of [4], it is clear that changing from a perfectly to a finitely conducting plate changes the scattering level and frequency behavior, and that the FDTD and Moment Method results agree quite well on these effects.

In Figure 9 both FDTD and Moment Method [4] results for scattering by a plate with a complex sheet impedance are shown. The sheet impedance is determined by applying eqs. (1,2) with conductivity 0.25 S/m, relative permittivity 3.0, and thickness 1 cm., corresponding to the FDTD parameters used. Again the plane

wave is a Gaussian pulse incident from θ=45, ϕ=30 degrees. The FDTD results agree with the Moment Results for frequencies up to about 12 cells/wavelength.

The final result is for a plate with edge treatment. For this demonstration a 21 x 21 cm thin perfectly conducting plate is given a 4 cm border of sheet impedance Z_s = 500 Ω, resulting in a square plate 29 x 29 cm. This edged plate is modeled in FDTD by setting x and y polarized electric field locations for a single z dimension index as being either perfect conductor for the central portion of the plate or with a conductivity of 0.2 S/m for the edges. The ESP4 calculations were made with a central perfectly conducting plate surrounded by 4 plates of sheet impedance Z_s = 500 Ω attached to the central plate using overlap modes. The results are compared in Figure 10 with excellent agreement between the two methods, both showing a significant difference due to the edge treatment when compared with the results of Figure 6.

Conclusions

The ability of the FDTD method to easily and accurately model scattering by sheet impedances was demonstrated by comparing FDTD results for scattering from flat plates modeled using sheet impedances with Method of Moment results. The approach described here is directly applicable to the Yee cell, and demonstrated good accuracy for frequencies up to approximately 12 cells per wavelength.

References

1. T. B. A. Senior, "Approximate Boundary Conditions," IEEE Transactions on Antennas and Propagation, vol. AP-29, pp 826-829, September 1981.

2. E. Newman, "A user's manual for the electromagnetic surface patch code: ESP Version IV," The Ohio State University Research Foundation, ElectroScience Laboratory, Department of Electrical Engineering, Columbus, Ohio 43212.

3. K. S. Yee, "Numerical solution of initial boundary value problems involving Maxwell's equations in isotropic media," IEEE Transactions on Antennas and Propagation, vol. AP-14, pp 302-307, May 1966.

4. R. Luebbers, K. Kunz, M. Schneider, F. Hunsberger, "A Finite Difference Time Domain Near-Zone to Far-Zone Transformation", IEEE Transactions on Antennas and Propagation, vol. AP-39, pp 429-433, April 1991.

Figure Titles

1. Co-Polarized far zone electric field vs time scattered by a 29 x 29 cm flat plate of sheet impedance 500 ohms for a θ-polarized normally incident Gaussian pulse plane wave computed using FDTD.

2. Radar cross section for a 29 x 29 cm flat plate of sheet impedance 500 ohms, normal incidence, obtained from FDTD results of Figure 1 compared with Moment Method [2] results.

3. Co-Polarized far zone electric field vs time scattered by a 29 x 29 cm flat plate of sheet impedance 500 ohms for a ϕ-polarized incident Gaussian pulse plane wave from θ=45, ϕ=30 degrees computed using FDTD.

4. Co-Polarized far zone electric field vs time scattered by a 29 x 29 cm flat plate of sheet impedance 500 ohms for a θ-polarized incident Gaussian pulse plane wave from θ=45, ϕ=30 degrees computed using FDTD.

5. Cross-Polarized far zone electric field vs time scattered by a 29 x 29 cm flat plate of sheet impedance 500 ohms for a ϕ-polarized incident Gaussian pulse plane wave from θ=45, ϕ=30 degrees computed using FDTD.

6. Co-Polarized radar cross section for a 29 x 29 cm flat plate of sheet impedance 500 ohms, θ=45, ϕ=30 degree incidence, ϕ-polarized, obtained from FDTD results of Figure 3 compared with Moment Method [2] results.

7. Co-Polarized radar cross section for a 29 x 29 cm flat plate of sheet impedance 500 ohms, θ=45, ϕ=30 degree incidence, θ-polarized, obtained from FDTD results of Figure 4 compared with Moment Method [2] results.

8. Cross-Polarized radar cross section for a 29 x 29 cm flat plate of sheet impedance 500 ohms, θ=45, ϕ=30 degree incidence, obtained from FDTD results of Figure 5 compared with Moment Method [2] results.

9. Co-Polarized radar cross section for a 29 x 29 cm flat plate of sheet impedance corresponding to conductivity of 0.25, relative permittivity of 3.0, and thickness 1 cm, for θ=45, ϕ=30 degree ϕ-polarized incident plane wave calculated using FDTD and compared with Method of Moments [2].

10. Co-Polarized radar cross section for a 21 x 21 cm perfectly conducting flat plate with a 4 cm 500 ohm edge treatment on all sides (total plate size 29 x 29 cm) for θ=45, ϕ=30 degree ϕ-polarized incident plane wave calculated using FDTD and compared with Method of Moments [2].

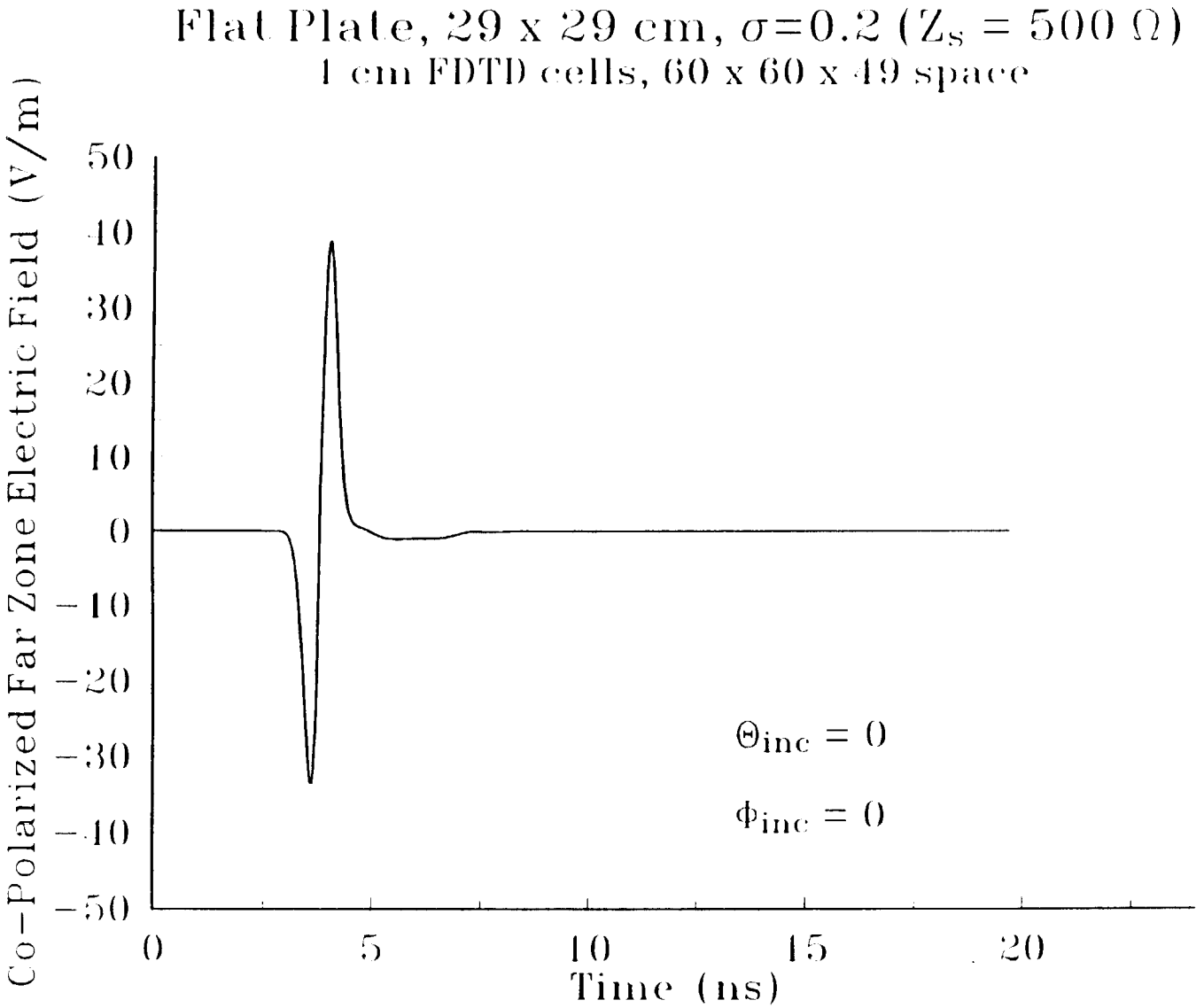
Flat Plate, 29 x 29 cm, σ=0.2 (Zs = 500 Ω)
1 cm FDTD cells, 60 x 60 x 49 space
Co-Polarized Far Zone Electric Field (V/m)
50
40
30
20
10
0
-10
-20
-30
-40
-50
0
5
10
15
20
Time (ns)
Θinc = 0
Φinc = 0

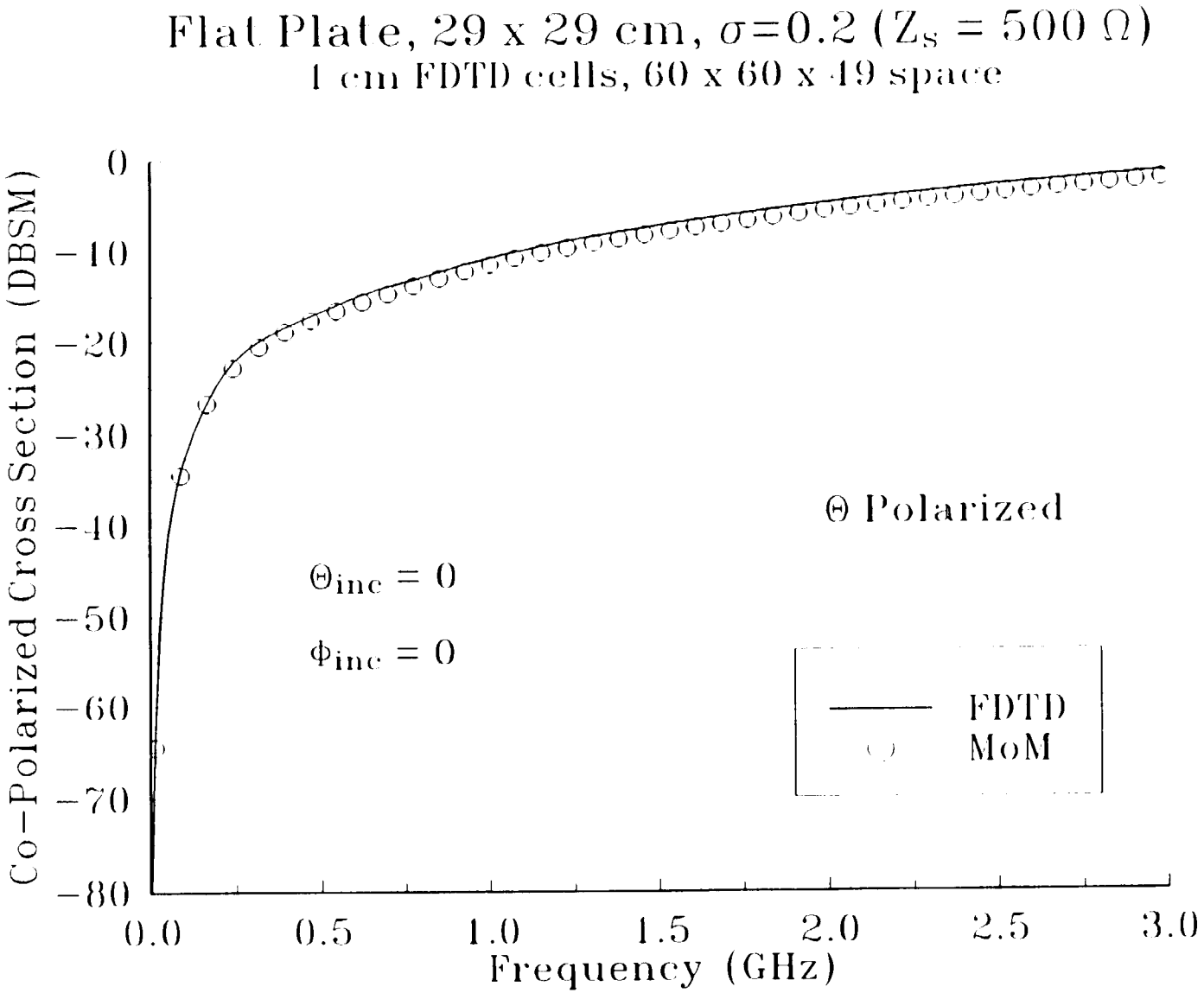
Flat Plate, 29 x 29 cm, σ=0.2 (Zs = 500 Ω)
1 cm FDTD cells, 60 x 60 x 49 space
Co-Polarized Cross Section (DBSM)
0
-10
-20
-30
-40
-50
-60
-70
-80
0.0
0.5
1.0
1.5
2.0
2.5
3.0
Frequency (GHz)
Θ Polarized
Θinc = 0
Φinc = 0
FDTD
MoM

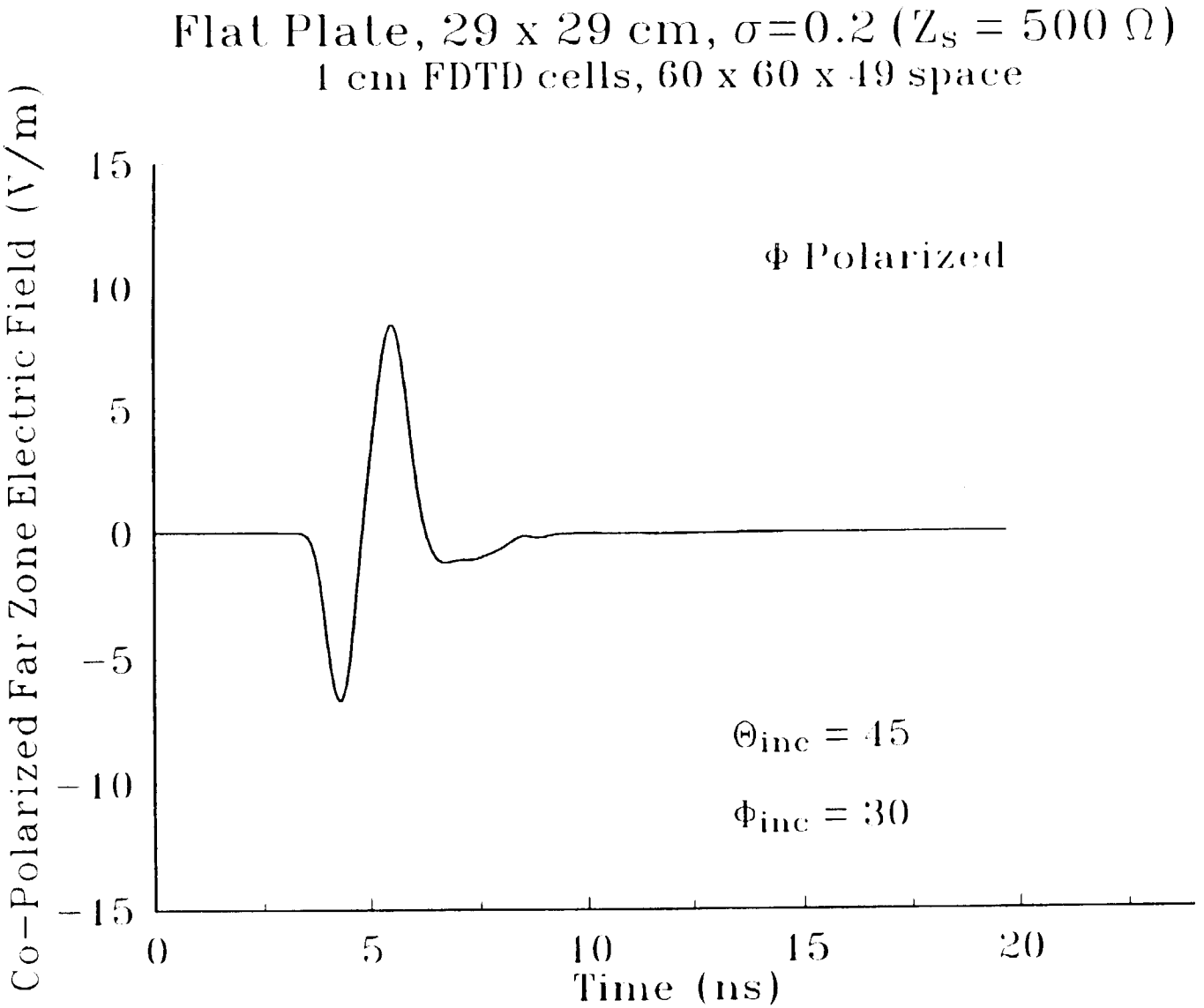
Flat Plate, 29 x 29 cm, σ=0.2 (Zs = 500 Ω)
1 cm FDTD cells, 60 x 60 x 49 space
Co-Polarized Far Zone Electric Field (V/m)
15
10
5
0
-5
-10
-15
0
5
10
15
20
Time (ns)
Φ Polarized
Θinc = 45
Φinc = 30

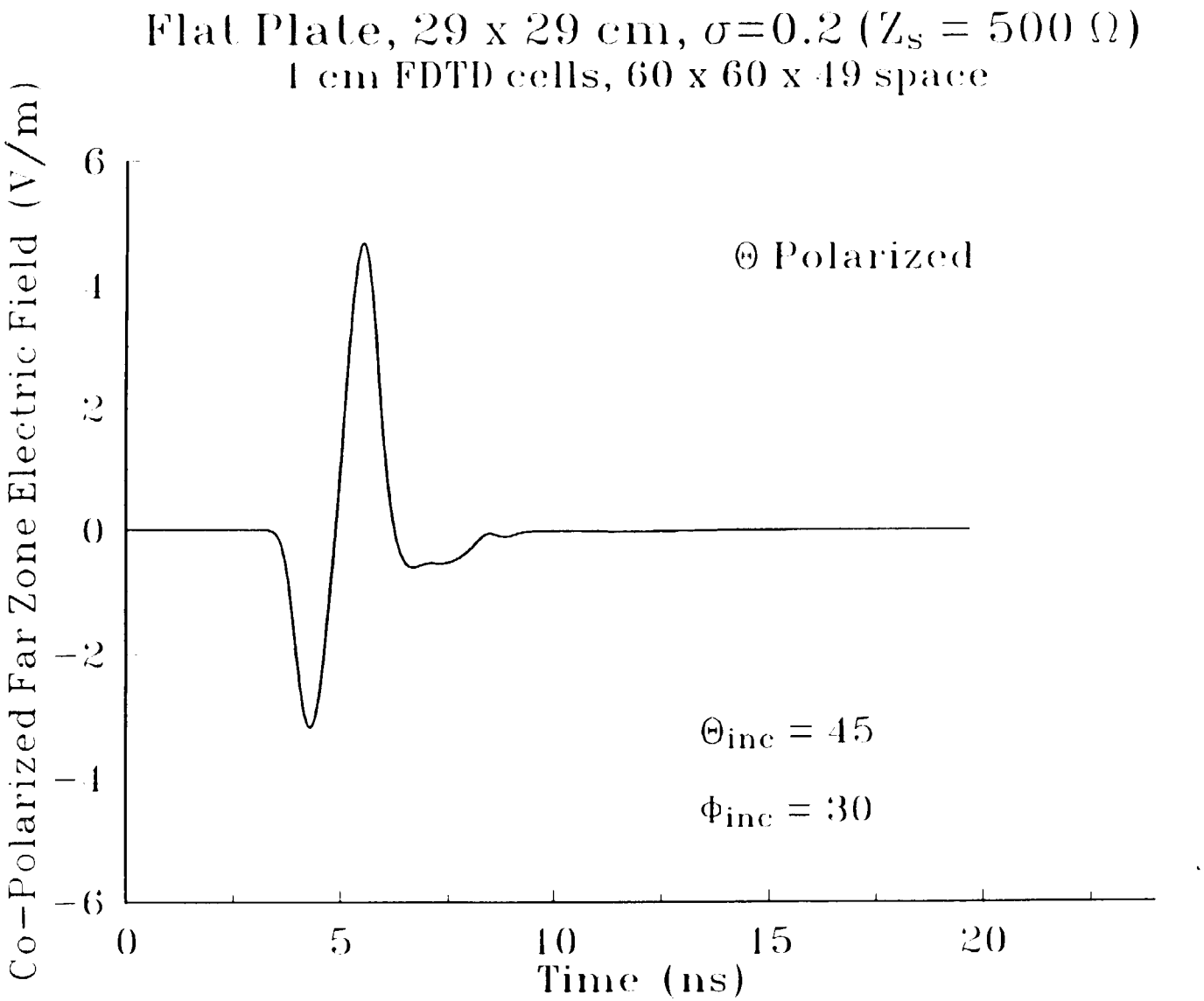
Flat Plate, 29 x 29 cm, σ=0.2 (Zs = 500 Ω)
1 cm FDTD cells, 60 x 60 x 49 space
Co-Polarized Far Zone Electric Field (V/m)
6
4
2
0
-2
-4
-6
0
5
10
15
20
Time (ns)
Θ Polarized
Θinc = 45
Φinc = 30

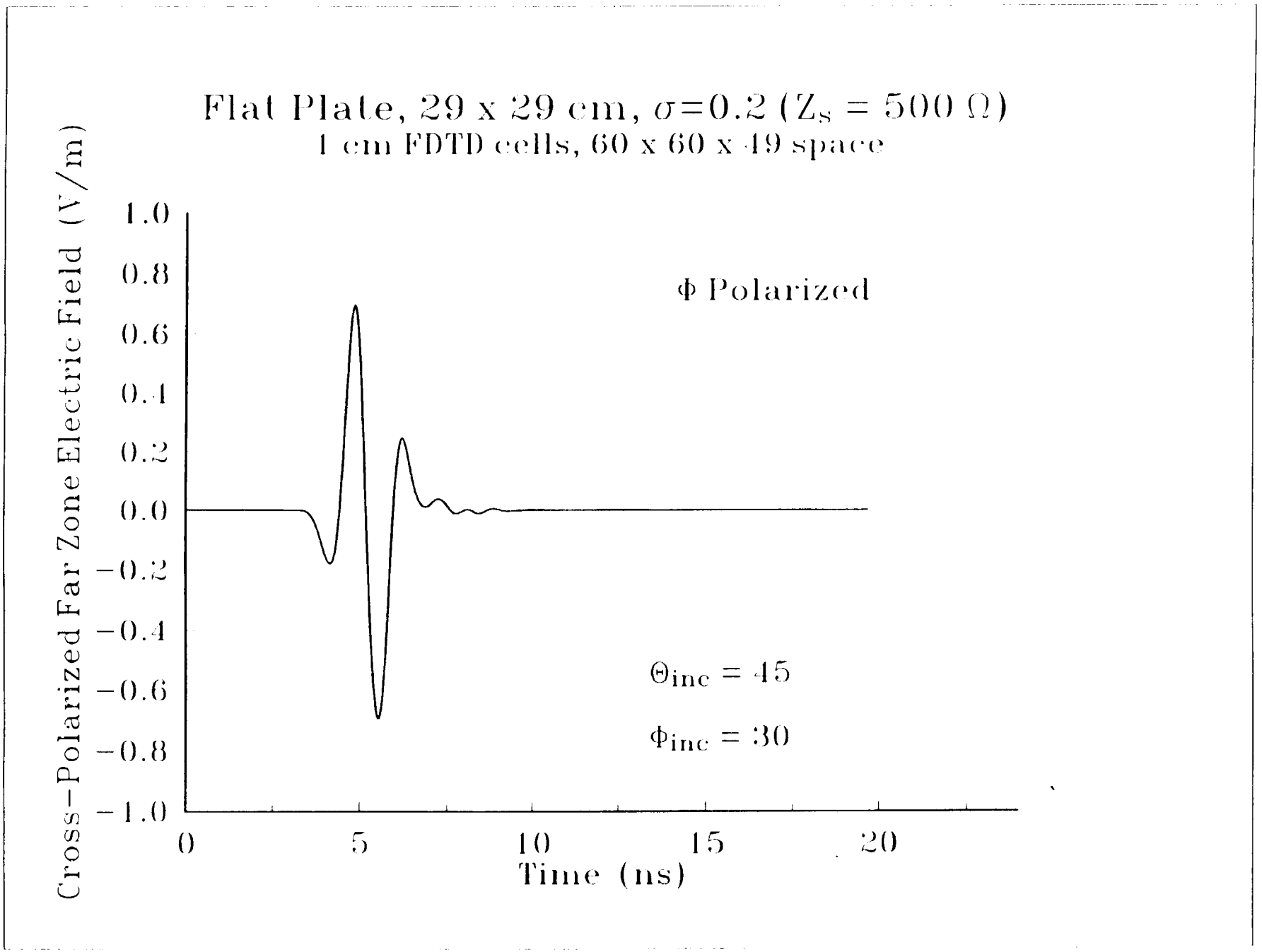
Flat Plate, 29 x 29 cm, σ=0.2 (Zs = 500 Ω)
1 cm FDTD cells, 60 x 60 x 49 space
Cross-Polarized Far Zone Electric Field (V/m)
1.0
0.8
0.6
0.4
0.2
0.0
−0.2
−0.4
−0.6
−0.8
−1.0
Φ Polarized
Θinc = 45
Φinc = 30
0
5
10
15
20
Time (ns)

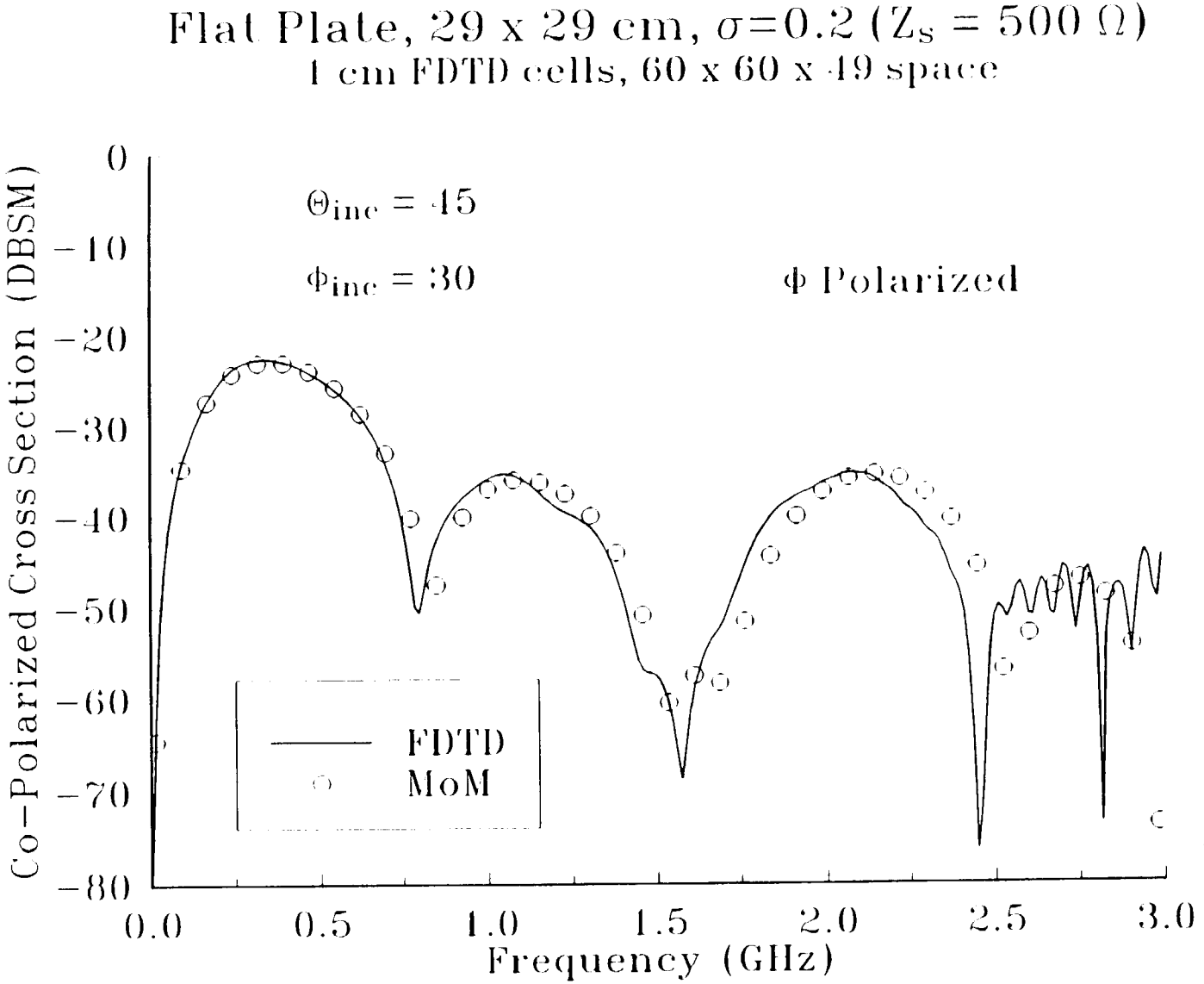
Flat Plate, 29 x 29 cm, σ=0.2 (Zs = 500 Ω)
1 cm FDTD cells, 60 x 60 x 49 space
Θinc = 45
Φinc = 30
Φ Polarized
Co-Polarized Cross Section (DBSM)
0
−10
−20
−30
−40
−50
−60
−70
−80
FDTD
MoM
0.0
0.5
1.0
1.5
2.0
2.5
3.0
Frequency (GHz)

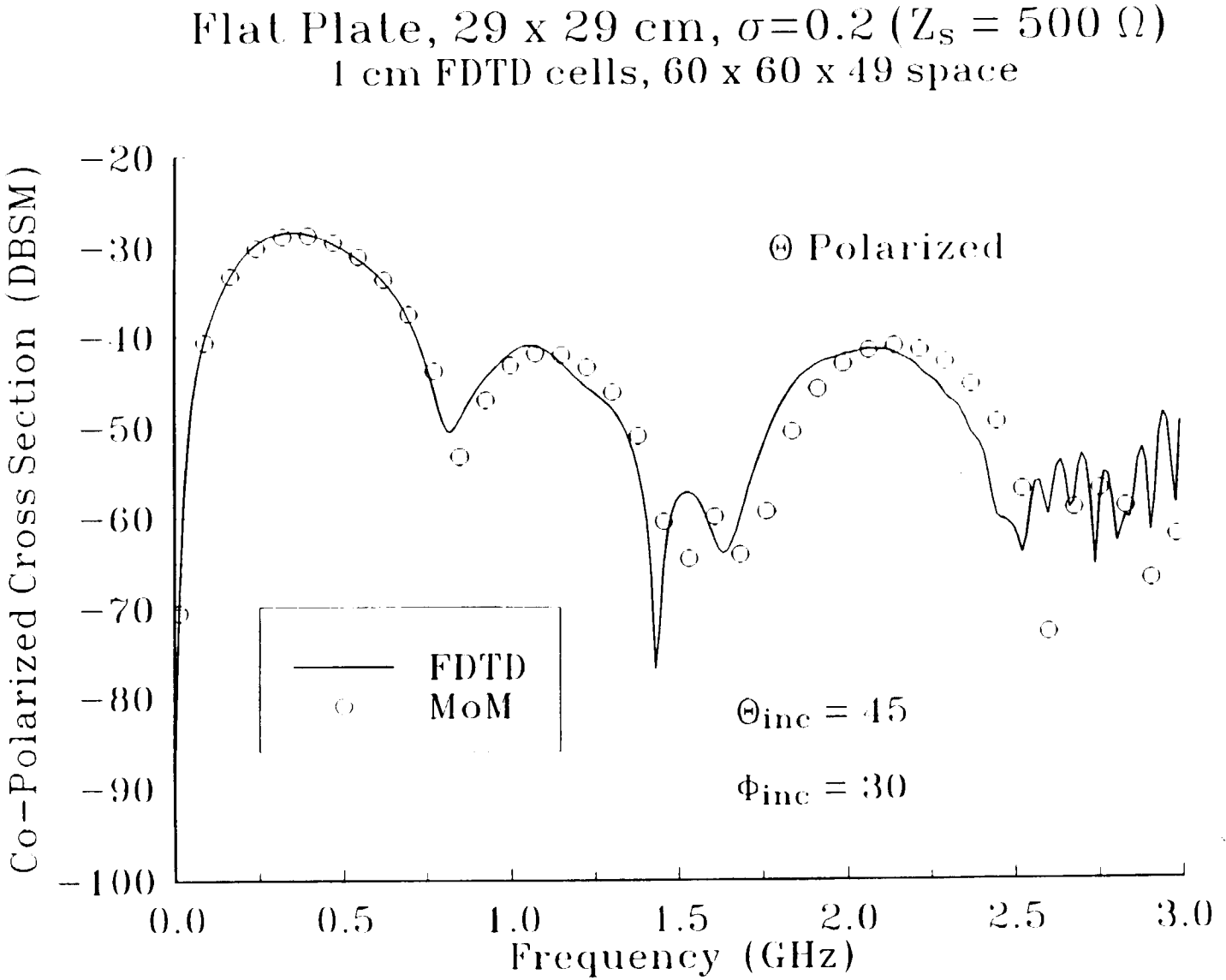
Flat Plate, 29 x 29 cm, σ=0.2 (Zs = 500 Ω)
1 cm FDTD cells, 60 x 60 x 49 space
Co-Polarized Cross Section (DBSM)
−20
−30
−40
−50
−60
−70
−80
−90
−100
Θ Polarized
FDTD
MoM
Θinc = 45
Φinc = 30
0.0
0.5
1.0
1.5
2.0
2.5
3.0
Frequency (GHz)

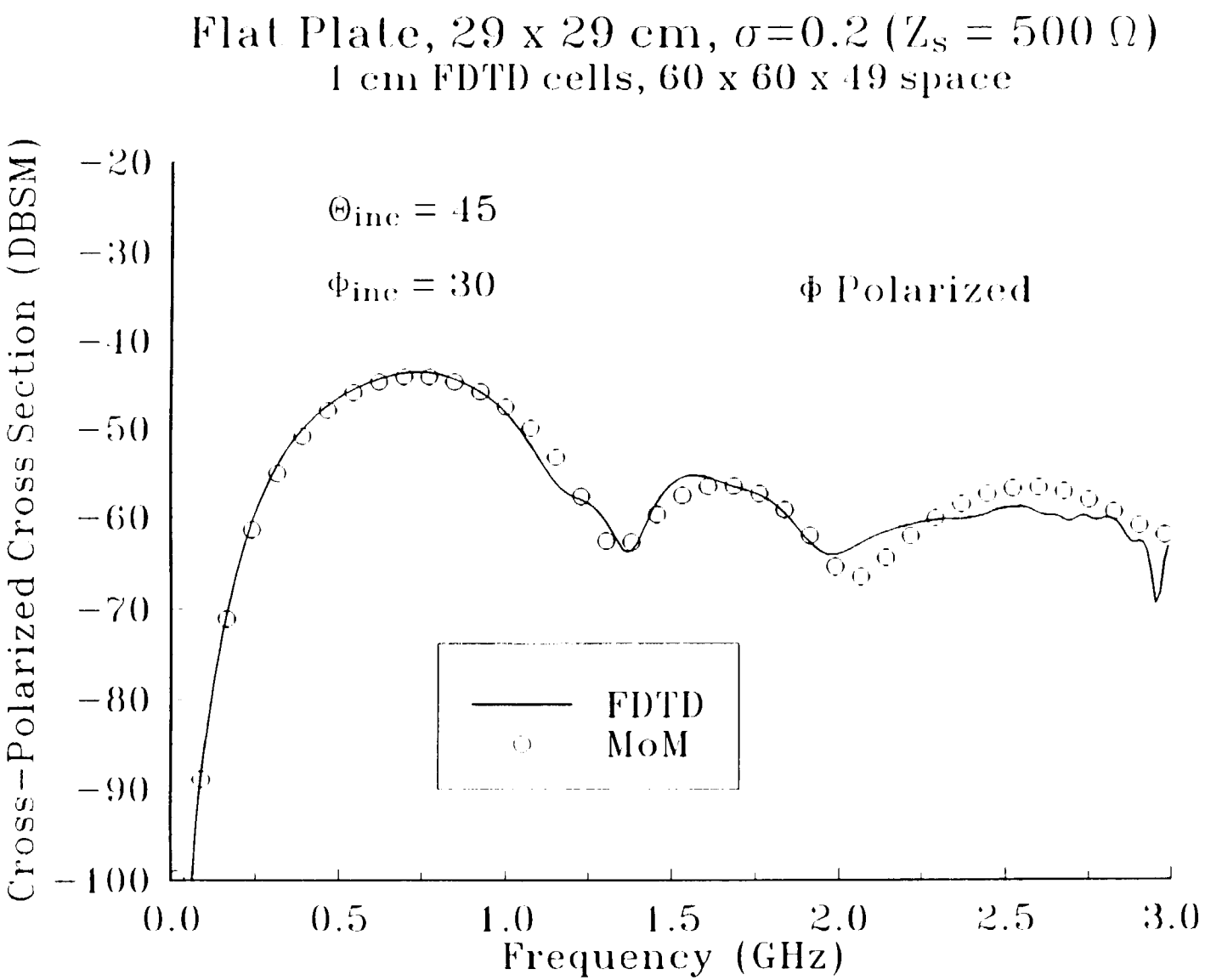
Flat Plate, 29 x 29 cm, σ=0.2 (Zs = 500 Ω)
1 cm FDTD cells, 60 x 60 x 49 space
Θinc = 45
Φinc = 30
Φ Polarized
FDTD
MoM
Cross-Polarized Cross Section (DBSM)
-20
-30
-40
-50
-60
-70
-80
-90
-100
0.0
0.5
1.0
1.5
2.0
2.5
3.0
Frequency (GHz)

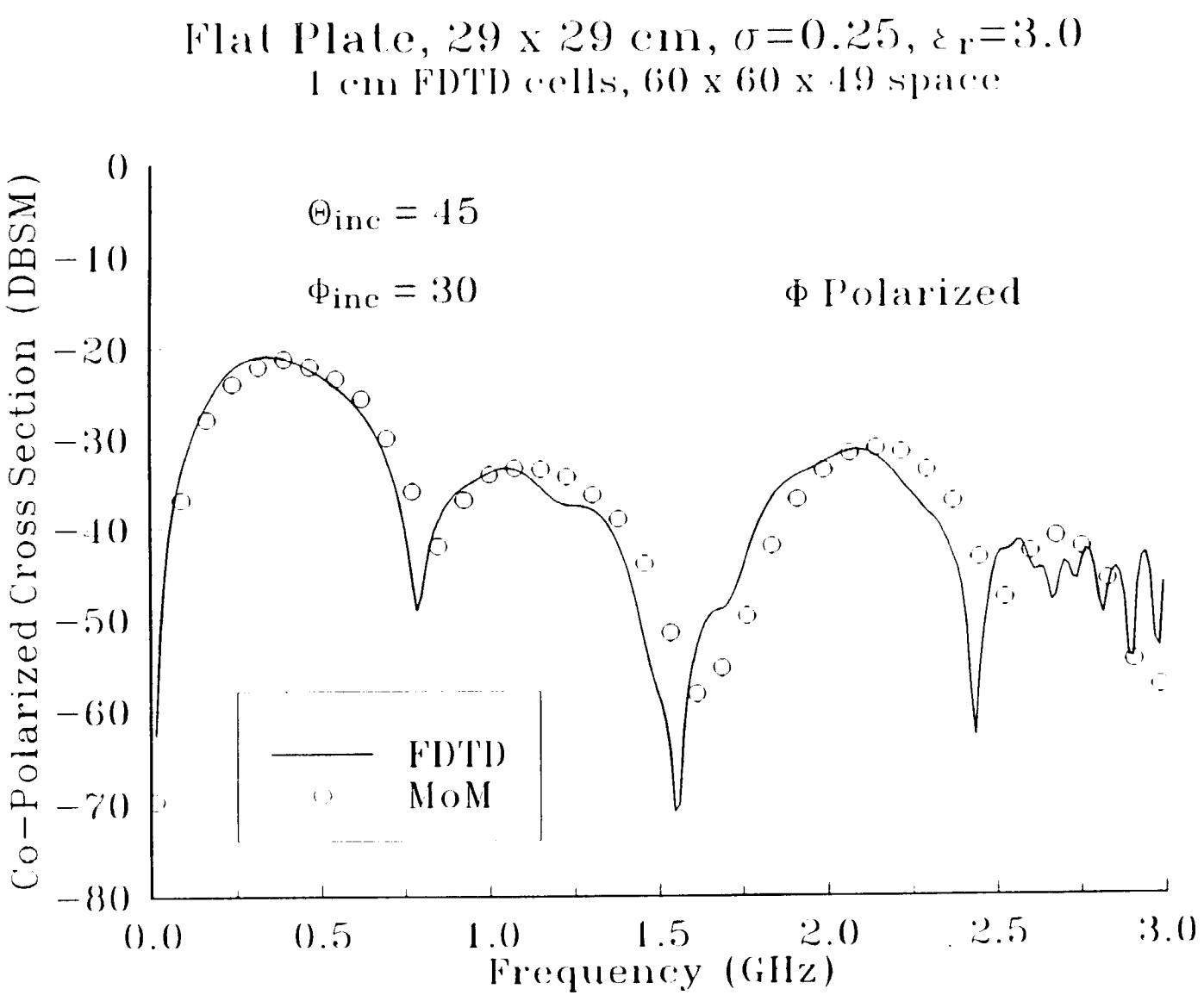
Flat Plate, 29 x 29 cm, σ=0.25, ε r=3.0
1 cm FDTD cells, 60 x 60 x 49 space
Θinc = 45
Φinc = 30
Φ Polarized
Co-Polarized Cross Section (DBSM)
0
-10
-20
-30
-40
-50
-60
-70
-80
0.0
0.5
1.0
1.5
2.0
2.5
3.0
Frequency (GHz)
FDTD
MoM

PEC Plate, 21 x 21 cm, with 4 cm 500 Ω Edge Treatment

1 cm FDTD cells, 60 x 60 x 49 space

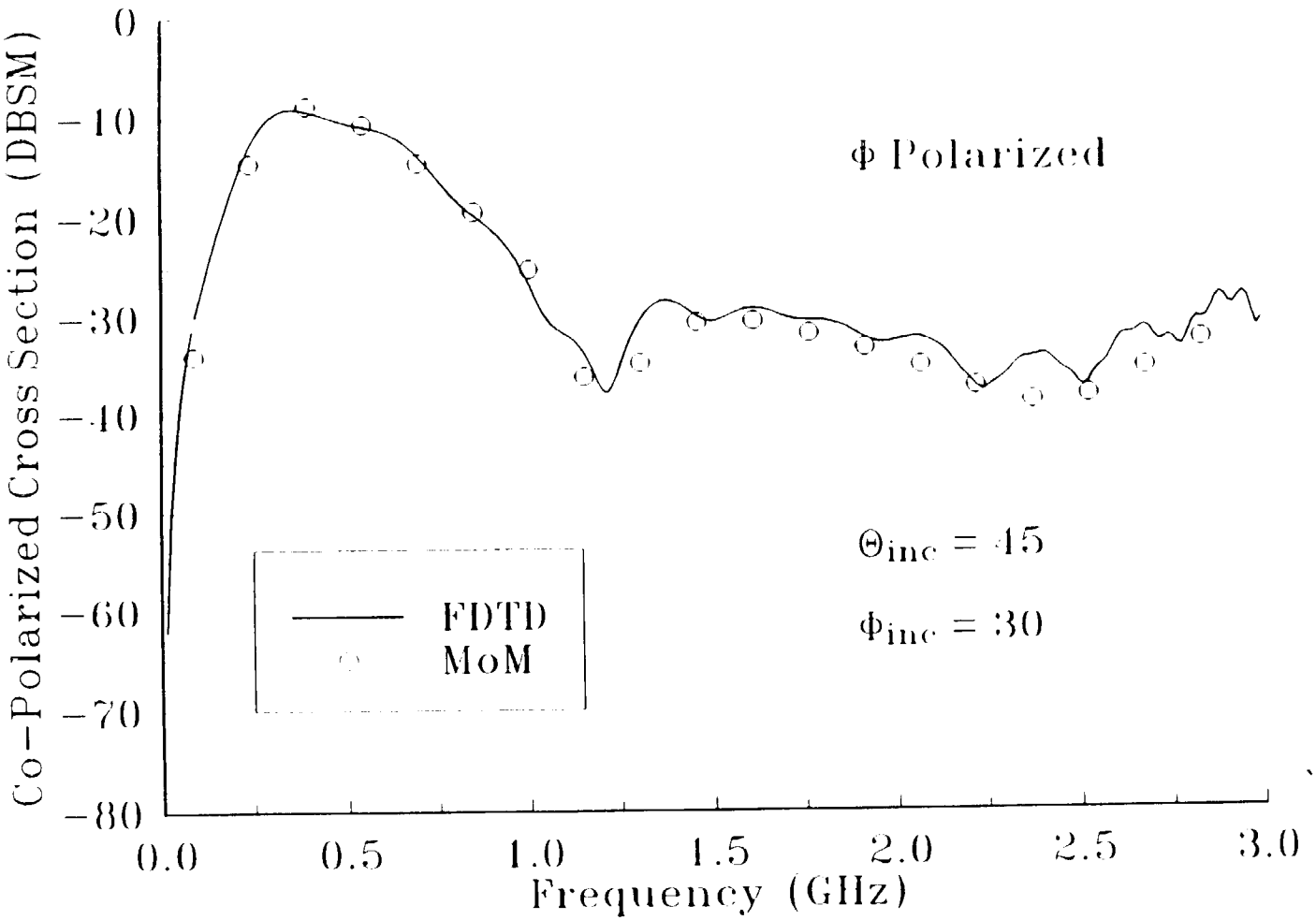

Finite Difference Time Domain Calculation of Transients in Antennas with Nonlinear Loads

by

Raymond Luebbers, John Beggs, and Karl Kunz
Department of Electrical and Computer Engineering
The Pennsylvania State University
University Park, PA 16802

and by

Kent Chamberlin
Department of Electrical and Computer Engineering
University of New Hampshire
Durham, New Hampshire

July 1991

Abstract

Determining transient electromagnetic fields in antennas with nonlinear loads is a challenging problem. Typical methods used involve calculating frequency domain parameters at a large number of different frequencies, then applying Fourier transform methods plus nonlinear equation solution techniques. If the antenna is simple enough so that the open circuit time domain voltage can be determined independently of the effects of the nonlinear load on the antenna current (an infinitesimal dipole, for example), time stepping methods can be applied in a straightforward way. In this paper transient fields for antennas with more general geometries are calculated directly using Finite Difference Time Domain methods. In each FDTD cell which contains a nonlinear load, a nonlinear equation is solved at each time step. As a test case the transient current in a long dipole antenna with a nonlinear load excited by a pulsed plane wave is computed using this approach. The results agree well with both calculated and measured results previously published. The approach given here extends the applicability of the FDTD method to problems involving scattering from targets including nonlinear loads and materials, and to coupling between antennas containing nonlinear loads. It may also be extended to propagation through nonlinear materials.

INTRODUCTION

Calculating the transient electromagnetic fields in antennas and scatterers containing nonlinear loads or material is a difficult problem. The traditional approach has been to apply frequency domain methods at a large number of harmonic frequencies. Sarkar and Weiner [1] used this approach in combination with a Volterra series analysis to determine scattering from antennas with nonlinear loads. Liu and Tesche [2,3] separated the problem into linear and nonlinear portions, calculated wideband frequency domain characteristics for the linear portion of the problem, transformed this to the time domain, and then solved the nonlinear portion by time marching. They achieved good agreement with measurements using this approach, and their results presented in [3] will be used to validate the results obtained in this paper. However, obtaining the frequency domain results for a complicated antenna at the large number of frequencies involved may be quite tedious and involve significant computer resources. And this approach cannot be extended to situations involving scattering from bulk regions of nonlinear materials, or to propagation through nonlinear materials as can the FDTD approach presented here.

For the simpler situation where the time domain open circuit voltage on the antenna terminals can be determined independently from the effects of the nonlinear load the frequency domain portion of the approach of Liu and Tesche can be dispensed with, and the open circuit voltage can be used as the input to a nonlinear circuit model of the load, with the resulting problem solved directly using time marching or other methods applied to nonlinear circuits. This approach was used by Kanda [4], who also gives an excellent review of previous work in this area.

Finally, Schuman [5] applied a time domain method of moments approach to a thin straight wire. However, his method appears difficult to apply to more general geometries.

In this paper the Finite Difference Time Domain (FDTD) approach will be extended to include nonlinear lumped loads. The

reader is assumed to have some familiarity with this method. The literature is extensive, with some representative papers included in the following references [6-8]. The authors are using the scattered field formulation of [8], but with linear time differencing.

APPROACH

To illustrate the method, let us consider the specific example of interest, taken from [3]. A wire dipole with half length 0.6 meters and a diameter of 0.81 mm is loaded at its midpoint, as shown in Figure 1. The dipole is located parallel to the z axis. The FDTD cell at the center of the wire is used to model the lumped load. As described in [3], this load is two diodes in series with a 100 ohm resistor (the actual measurements were made using a single diode at the base of a monopole). The total diode junction capacitance of 0.5 pF must also be included in the model for accurate results at the frequencies contained in the pulse.

In order to describe the approach used to model the diode circuit in FDTD, let us first consider an approach to approximating a linear lumped load consisting of a capacitor in parallel with a resistor (conductance) in an FDTD cell. Starting with

$$\nabla \times \bar{H} = \epsilon \frac{\partial \bar{E}}{\partial t} + \sigma \bar{E} \qquad (1)$$

where H, E, ϵ and σ are the magnetic and electric fields, the permittivity, and the conductivity, and following the Yee [6] approach for discretizing space and time, with $t=n\Delta t$, $x=I\Delta x$, $y=J\Delta y$, $z=K\Delta z$, eq. (1) becomes, for the z component of electric field in a particular FDTD cell,

$$(\nabla \times H^{n+1/2})_z = \epsilon \frac{E_z^{n+1} - E_z^n}{\Delta t} + \sigma E_z^{n+1} \qquad (2)$$

where ϵ and σ pertain to the particular cell location of E_z and the superscripts denote the time reference of the particular component. Usually in applying FDTD this equation is solved for E^{n+1} in terms of the previous time values of E^n and $H^{n+\frac{1}{2}}$, with the curl H term computed using spatial finite differences. Instead, consider the physical meanings of the terms. The curl H term gives the total current density flowing in the cell surrounding the electric field component. The next term involving ϵ and the time derivative of E is the displacement current density flowing through the cell in the z direction. The σE^{n+1} term is the conduction current density flowing through the cell in the z direction. Using the cell dimensions Δx, Δy and Δz, and assuming fields are constant across the cell, we can rewrite the above equation in terms of lumped elements, voltages, and currents as

$$\Delta x \Delta y (\nabla \times H^{n+1/2})_z = C \Delta z \frac{E_z^{n+1} - E_z^n}{\delta t} + G \Delta z E_z^{n+1} \qquad (3)$$

where now the first term is the total current flowing through the cell, C is the lumped "parallel plate" capacitance of the cell, and G is the lumped conductance in parallel with the capacitance. Note that one can identify $\Delta z E^{n+1}$ as the voltage across the cell. Clearly a lumped capacitance C can be equivalent to setting an appropriate value of the ϵ of the cell based on the cell dimensions, and similarly for a lumped resistance and the σ of the cell. Thus a lumped load that is a parallel combination of a capacitor and a conductance (resistance) can be modeled simply by setting the cell values of ϵ and σ appropriately. Equations (2) and (3) are interchangeable in terms of solving for E^{n+1}.

However, one warning is that the cell permittivity cannot be set too low. FDTD in the form presented in this paper cannot in general model materials with an epsilon that is too small (much less than free space) without becoming unstable. Such materials can be modeled using FDTD modified for frequency dependent materials [9], but with additional computational effort. If the conductance G (conductivity σ) is great enough so that the displacement current term in eq. (2) (or (3)) can be neglected then this term may be dropped. Indeed, if (2) or (3) is solved for E^{n+1} and G (or equivalently σ) is allowed to go to infinity, the correct result of $E^{n+1}=0$ is obtained. However, making G (or σ) small enough so that the conduction current is smaller than the displacement current through the cell filled with free space, but nevertheless neglecting this displacement current term, will result in instabilities. A physical argument for this is that the capacitance of an FDTD cell cannot be made lower than the capacitance of the cell filled with free space by adding lumped elements in parallel with the cell capacitance.

Now let us proceed to extend this approach to the circuit of interest, shown in Figure 2. In this figure the resistance R models the input resistance of the oscilloscope used to measure the current [3]. The capacitance C represents the capacitance of the free space FDTD cell plus the junction capacitance of the diode. The diode junction capacitance of the diode is not actually in parallel with the resistor, but this approximation simplifies the following derivation and does not appreciably affect the results for the circuit element sizes under consideration. Letting i_d represent the current through the diode, which is also the total conduction current through the cell, we can solve (3) for i_d obtaining

$$i_d = \Delta x \Delta y \left(\nabla x H^{n+1/2}\right)_z - \frac{C\Delta z}{\Delta t}\left(E_z^{n+1} - E_z^n\right) \qquad (4)$$

Once i_d is determined from (4), the diode voltage v_d can be obtained from the equation

$$2\ v_d + i_d\ R = v_c = \Delta z\ E_z^{n+1} \tag{5}$$

Since the diodes are in the circuit, i_d must also satisfy the nonlinear equations

$$i_d = 1.0\text{x}10^{-8}\ v_d, \quad v_d \leq 0 \tag{6a}$$

$$i_d = 2.9\text{x}10^{-7}\ [\exp(15v_d) - 1], \quad v_d \geq 0 \tag{6b}$$

where (6) are the nonlinear diode equations given in [3]. Since i_d as given in both eqs. (4) and (6a,b) must be equal, a Newton-Raphson iteration method can be applied to solve for the E^{n+1} value which produces required equality. This was the approach taken in this paper. The convergence was very fast since an initial guess for E^{n+1} of the previous value of E, E^n, provided the Newton-Raphson iteration with a good starting value.

DEMONSTRATION

The dipole considered in [3] is excited by a pulsed plane wave. As shown in [3], this plane wave has a peak electric field strength of approximately 390 volts. For simplicity, this pulse has been approximated for our calculations by a Gaussian pulse. The FDTD excitation pulse used for the calculations in this paper is shown in Figure 3. The actual pulse shown in [3] rings at a low amplitude out to about 3 ns, but this was neglected in the FDTD calculations.

In order to provide the necessary temporal resolution FDTD cells were chosen as 0.006 m cubes, providing a time step of 11.55 ps. For the FDTD Gaussian pulse used in this demonstration this allowed 64 time steps between the 1% of peak amplitude values. The transient currents given in [3] have a duration of

approximately 14 ns. The corresponding FDTD calculation was 1300 time steps (allowing for the incident pulse to reach the dipole), requiring 200 minutes on a 25 MHz 486 PC clone running Lahey fortran.

To approximate the wire dipole 200 FDTD cells were used. Since the wire diameter is smaller than the FDTD cell width, subcell modeling was used to adjust for this [10]. The FDTD problem space was 39 x 39 x 240 cells, and was terminated in second order Mur [11] absorbing boundaries.

Three calculations of the current through the dipole load were made and compared with results calculated by Liu and Tesche [3]. For all FDTD results the total current flowing through the FDTD cell, determined by evaluating the curl of H around the cell containing the lumped load, is plotted. In the first calculation only the 100 ohm resistor (in parallel with the free space capacitance of the FDTD cell) was included, with the results shown in Fig. 4. The agreement with the results of Liu is quite reasonable.

Next the diodes were added in series with the 100 ohm resistor, and the FDTD cell capacitance C, shown in Fig 2, was set to 0.5 pF to model the combined diode junction capacitance. FDTD results for the two cases considered in [3] were then calculated. These are shown in Figs. 5 and 6, and differ only in that the pulse initially forward biases the diode for the results in Fig. 5, but reverse biases the diode in Fig. 6. Some points taken from calculated results in [3] are included in Figs. 5 and 6 for comparison, but the interested reader on referring to [3] directly will see that the agreement between the FDTD results and both the calculated and measured results in [3] is excellent considering the different assumptions and approximations made in the analysis.

CONCLUSIONS

In this paper an approach to model nonlinear lumped elements in the context of FDTD was presented. It was used to compute the transient current in a diode loaded long dipole antenna, and excellent agreement with previously published results was obtained. This capability extends the applicability of the FDTD method to a wide range of problems, including scattering from nonlinear loaded antennas and harmonic product generation by nonlinear elements. The method can be further extended to considering regions of nonlinear material, since the (nonlinear) material content of each FDTD cell can be specified independently. Thus extensions to scattering from targets containing nonlinear material, or to propagation through nonlinear media should be straightforward. In combination with FDTD methods for frequency dependent materials, it may also be possible to extend the method to model electromagnetic propagation through dispersive nonlinear materials, including soliton propagation through such media.

REFERENCES

1. T. K. Sarkar and D. D. Weiner, "Scattering Analysis of Nonlinearly Loaded Antennas," IEEE Trans. Antennas and Propagat., vol. AP-24, pp 125-131, March 1976.

2. T. K. Liu and F. M. Tesche, "Analysis of Antennas and Scatterers with Nonlinear Loads," IEEE Trans. Antennas and Propagat., vol. AP-24, pp 131-139, March 1976.

3. T. K. Liu, F. M. Tesche and F. J. "Transient Excitation of an Antenna with a Nonlinear Load: Numerical and Experimental Results," IEEE Trans. Antennas and Propagat., vol. AP-25, pp 539-542, July 1977.

4. M. Kanda, "Analytical and Numerical Techniques for Analyzing an Electrically Short Dipole with a Nonlinear Load," IEEE Trans. Antennas and Propagat., vol. AP-28, pp 71-78, January 1980.

5. H. Schuman, "Time Domain scattering from a Nonlinearly loaded Wire," IEEE Trans. Antennas and Propagat., vol. AP-22, pp 611-613, July 1974.

6. K. S. Yee, "Numerical solution of initial boundary value problems involving Maxwell's equations in isotropic media," IEEE Trans. Antennas and Propagat., vol. AP-14, pp 302-307, May 1966.

7. A. Taflove and M. E. Brodwin, "Numerical solution of steady-state electromagnetic scattering problems using the time-dependent Maxwell's equations,' IEEE Trans. Microwave Theory Tech., vol. MTT-23, pp 623-630, Aug. 1975.

8. R. Holland, L. Simpson, and K. Kunz, "Finite difference analysis of EMP coupling to lossy dielectric structures," IEEE Trans. Electromagnetic Compat., vol. EMC-22, pp 203-209, Aug. 1980.

9. R. Luebbers, F. Hunsberger, K. Kunz, "A Frequency-Dependent Time Domain Formulation for Transient Propagation in Plasma", IEEE Transactions on Antennas and Propagat., vol. 39, pp 29-34, January 1991.

10. K. Umashankar, A. Taflove, and B. Beker, "Calculation and experimental validation of induced currents on coupled wires in an arbitrary shaped cavity," IEEE Trans. Antennas and Propagat., vol. AP-35, pp 1248-1257, November 1987.

11. G. Mur, "Absorbing boundary conditions for the Finite Difference Approximation of the Time-Domain Electromagnetic Field Equations," IEEE Trans. on Electromagnetic Compatibility, vol. EMC-23, pp 377-382, November 1981.

FIGURE TITLES

Fig 1. Pulsed plane wave incident on vertical wire dipole with nonlinear load.

Fig 2. Approximate equivalent circuit of lumped nonlinear load. Capacitance C includes both the FDTD cell capacitance and the diode junction capacitances. Resistance R simulates the input resistance of the oscilloscope used to measure the current [3].

Fig. 3 Gaussian pulse used in the FDTD calculations to simulate the pulse used by Liu et al in [3].

Fig. 4 Transient current flowing through 100 ohm load and parallel FDTD cell capacitance at the terminals of the wire dipole calculated using FDTD and compared with calculated results of Liu et al [3].

Fig. 5 Total transient current flowing through equivalent circuit of Fig. 2 located at the terminals of the wire dipole calculated using FDTD and compared with calculated results of Liu et al [3]. Diode is initially forward conducting.

Fig. 6 Total transient current flowing through equivalent circuit of Fig. 2 located at the terminals of the wire dipole calculated using FDTD and compared with calculated results of Liu et al [3]. Diode is initially reverse conducting.

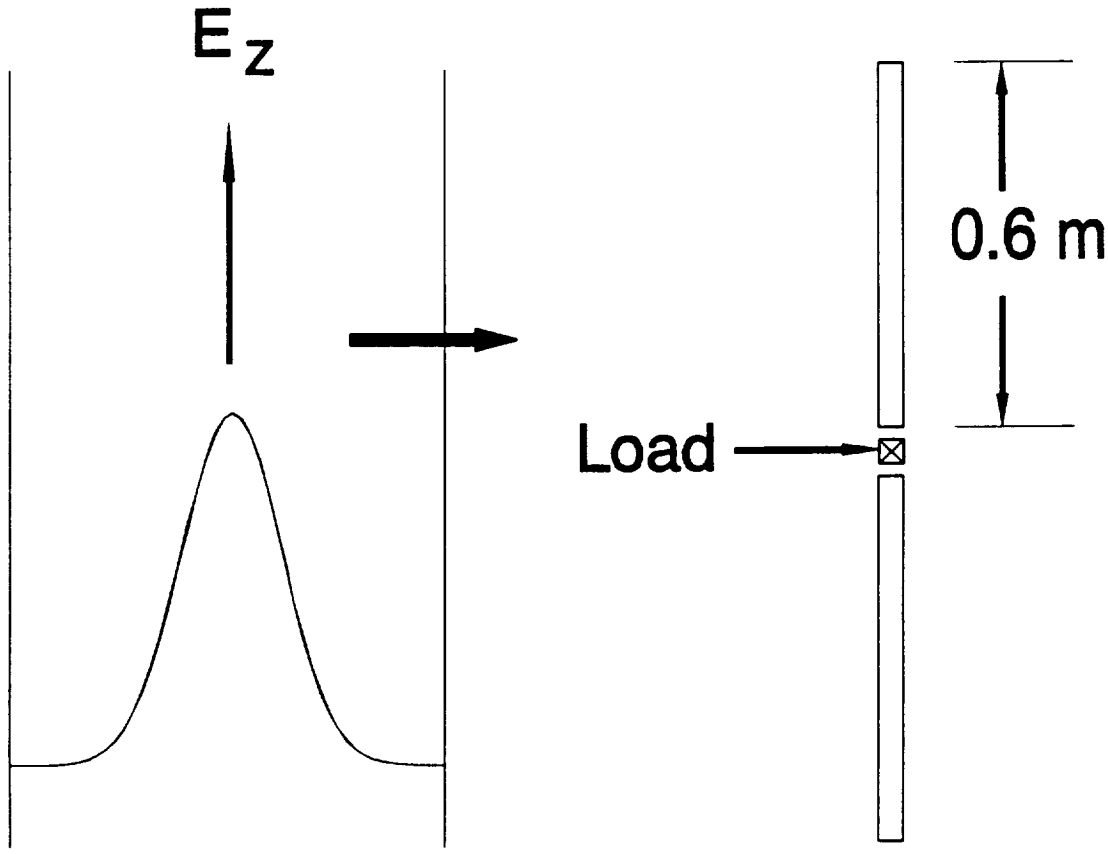
E_z
0.6 m
Load

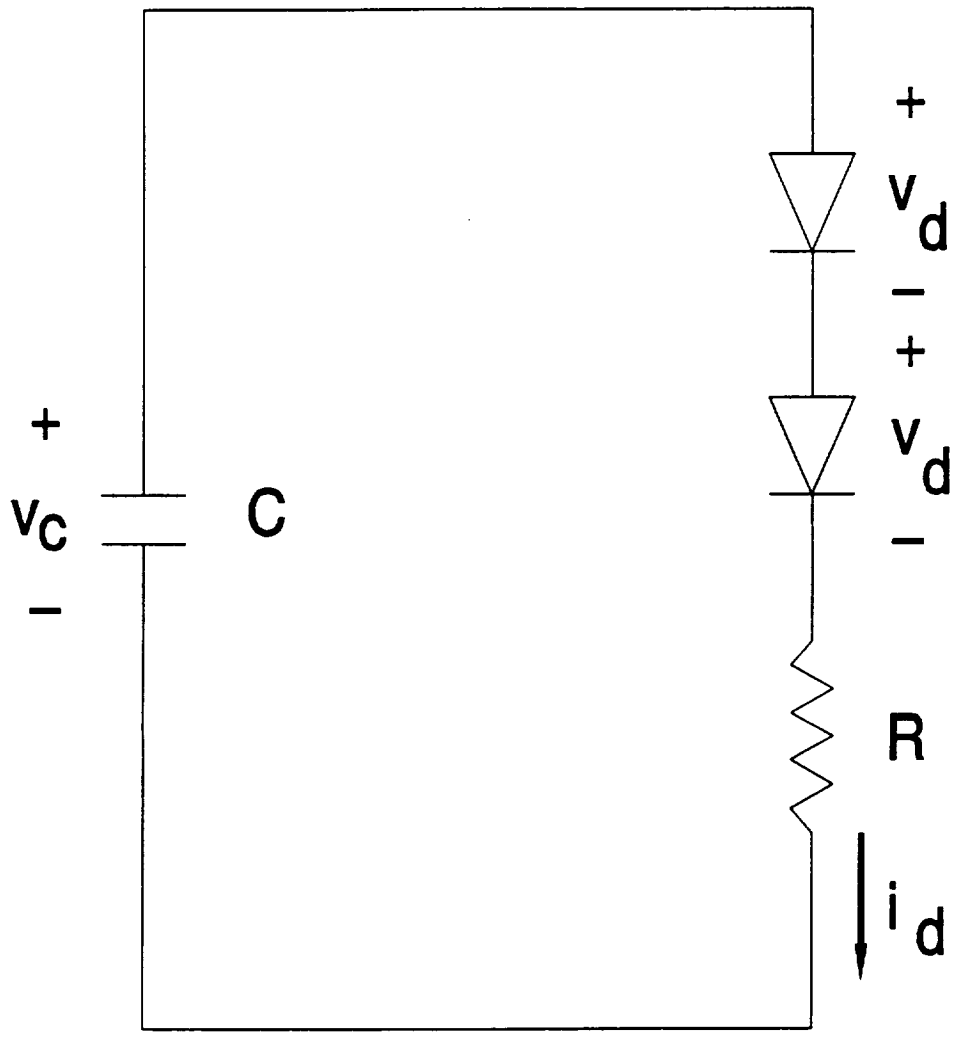
+
v_d
−
+
v_d
−
+
v_C
−
C
R
i_d

Incident Pulse used for FDTD Calculations

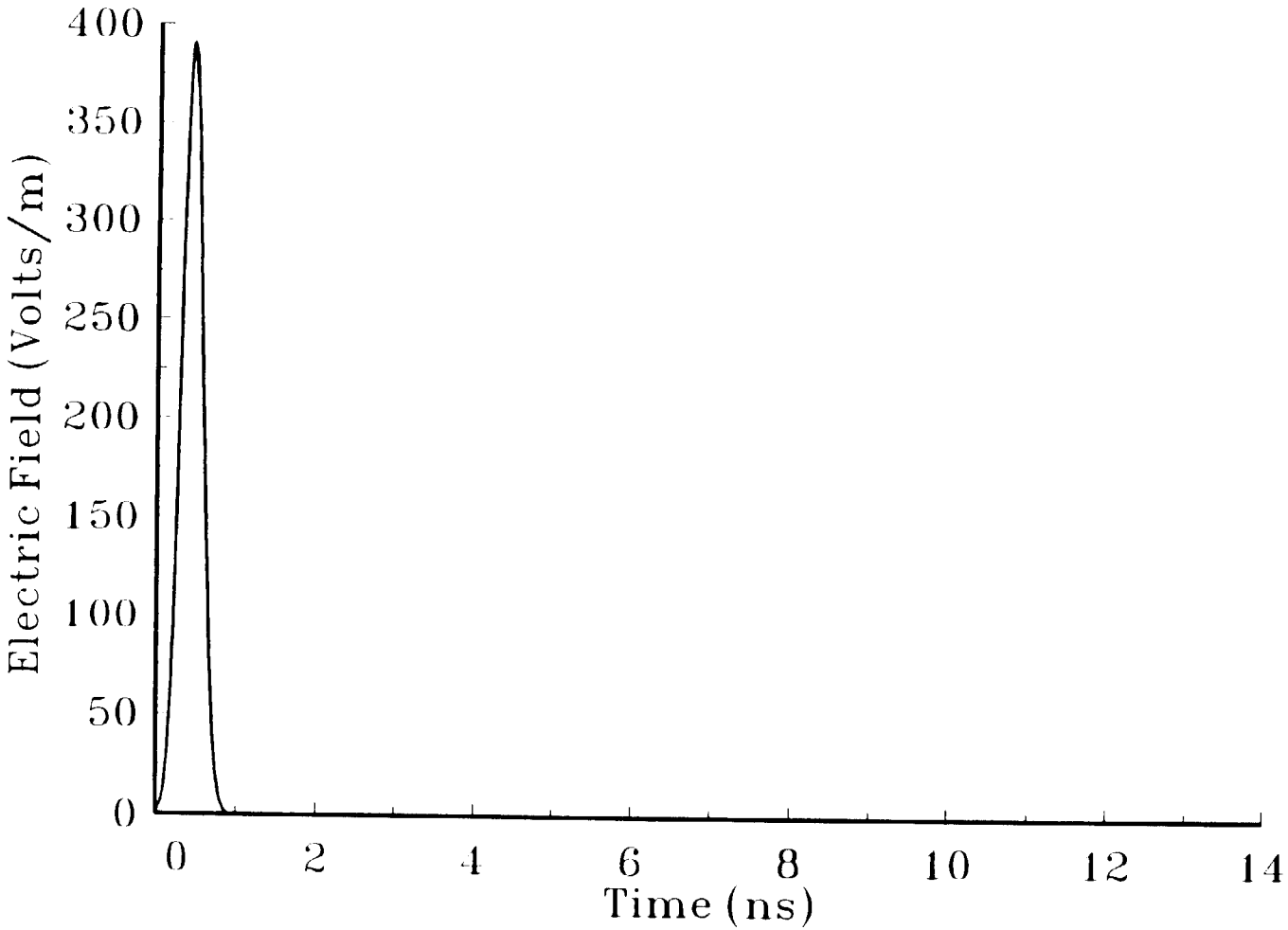

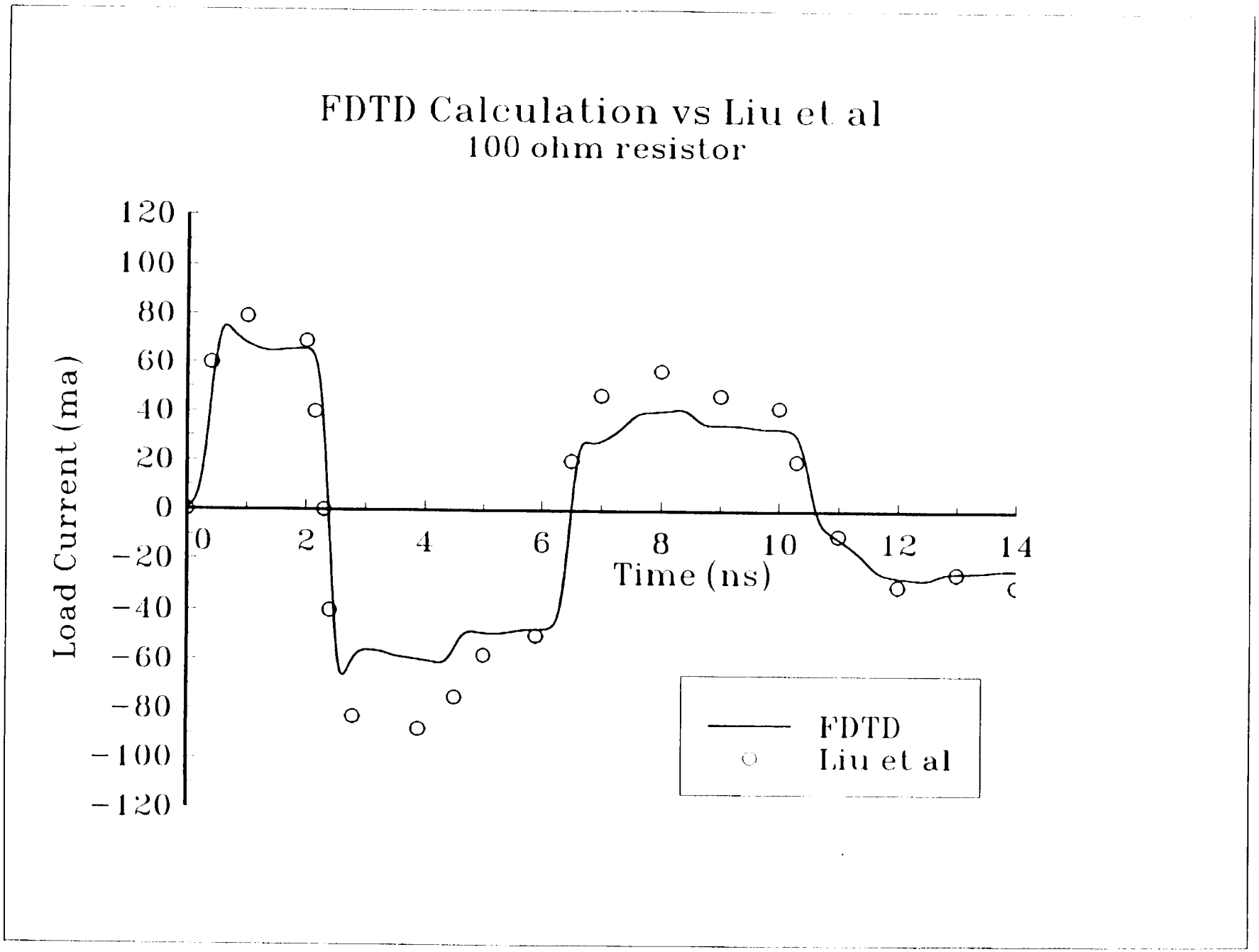
FDTD Calculation vs Liu et al
100 ohm resistor
Load Current (ma)
120
100
80
60
40
20
0
-20
-40
-60
-80
-100
-120
0
2
4
6
8
10
12
14
Time (ns)
FDTD
Liu et al

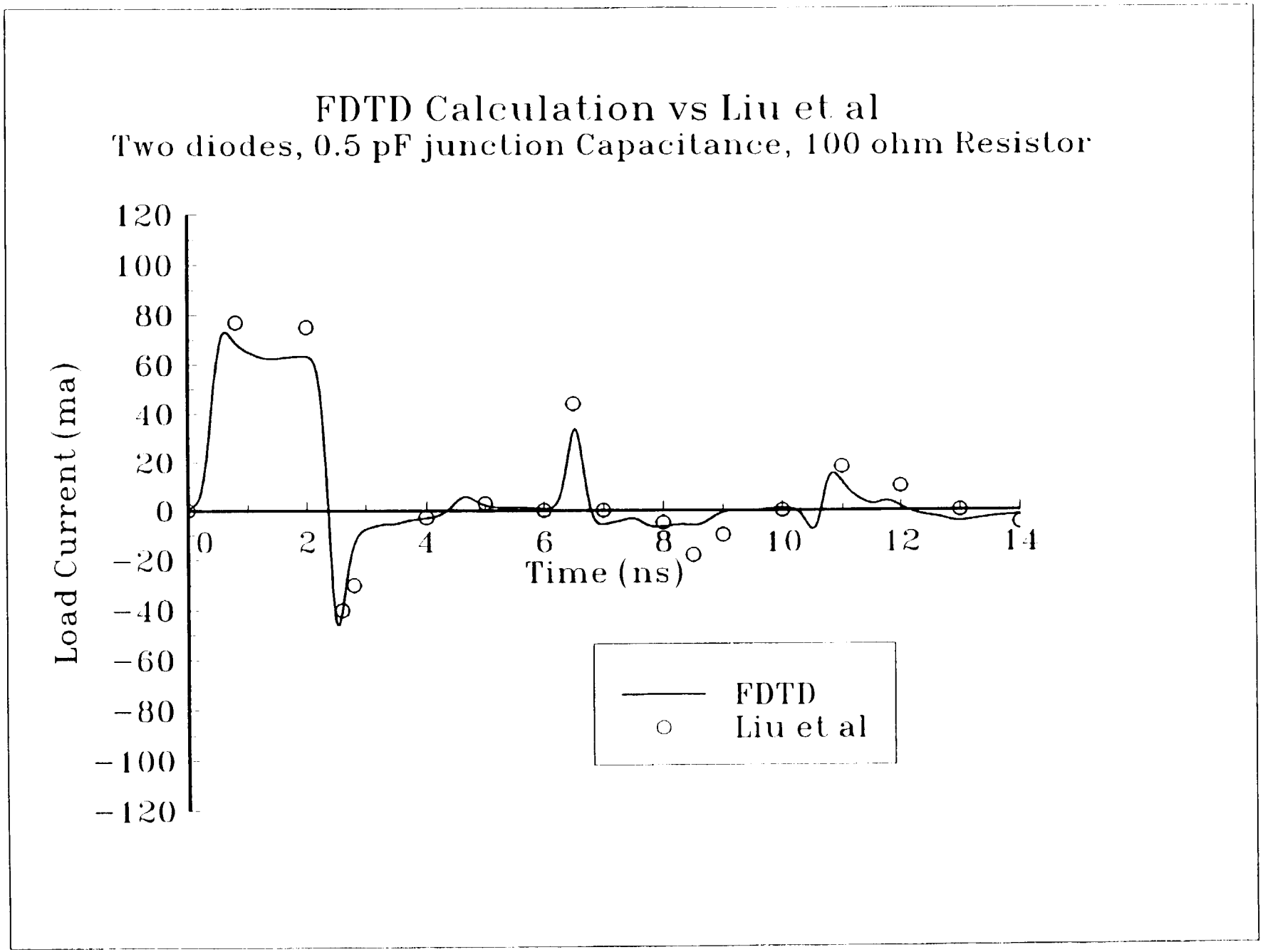
FDTD Calculation vs Liu et al
Two diodes, 0.5 pF junction Capacitance, 100 ohm Resistor
Load Current (ma)
120
100
80
60
40
20
0
-20
-40
-60
-80
-100
-120
0
2
4
6
8
10
12
14
Time (ns)
FDTD
Liu et al

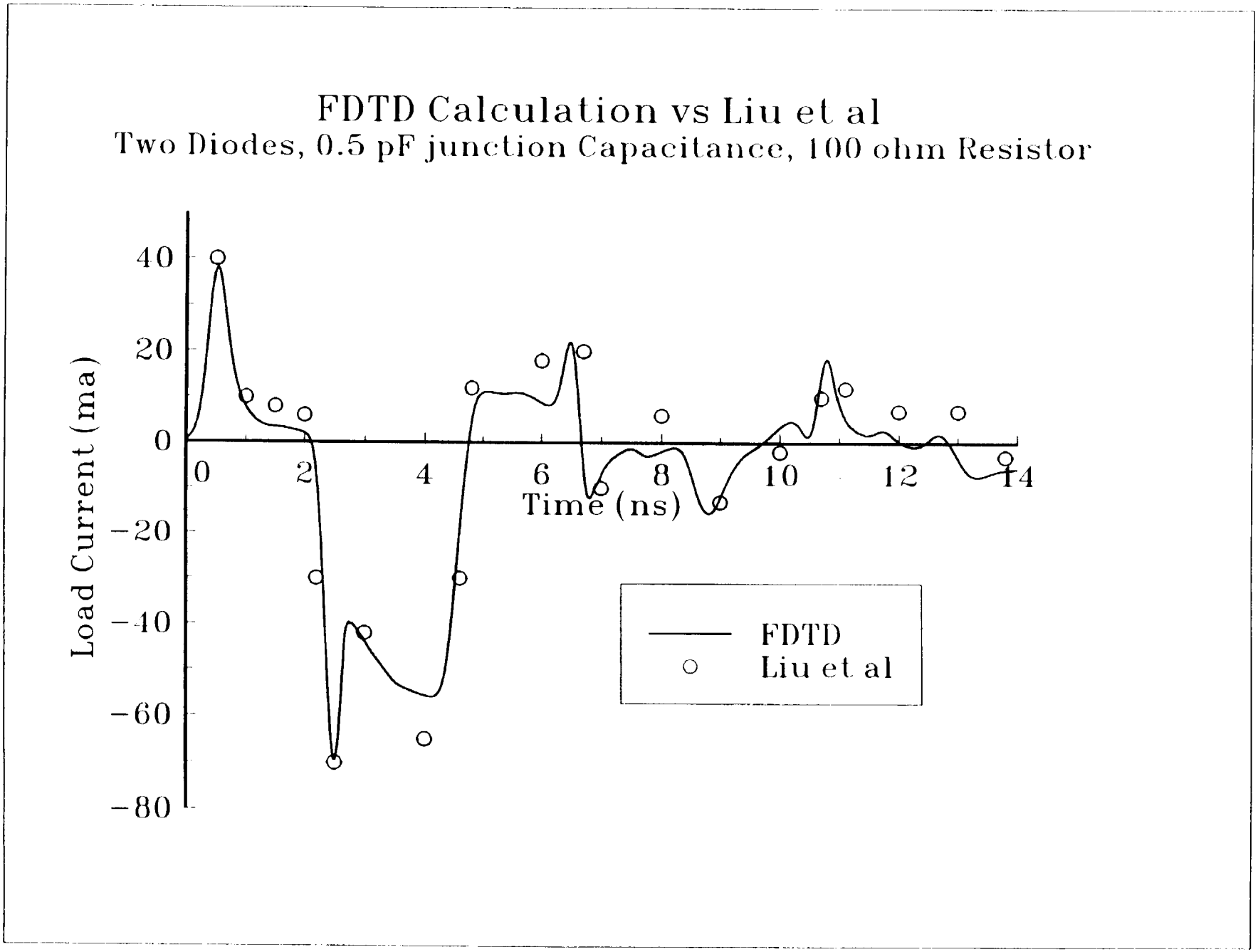
FDTD Calculation vs Liu et al
Two Diodes, 0.5 pF junction Capacitance, 100 ohm Resistor
Load Current (ma)
40
20
0
-20
-40
-60
-80
0
2
4
6
8
10
12
14
Time (ns)
FDTD
Liu et al

Finite Difference Time Domain Calculations of Antenna Mutual Coupling

by

Raymond Luebbers and Karl Kunz

Electrical Engineering Department
The Pennsylvania State University
University Park, PA 16802

April 1991

Abstract

The Finite Difference Time Domain (FDTD) technique has been applied to a wide variety of electromagnetic analysis problems, including shielding and scattering. However, the method has not been extensively applied to antennas. In this short paper calculations of self and mutual admittances between wire antennas are made using FDTD and compared with results obtained using the Method of Moments. The agreement is quite good, indicating the possibilities for FDTD application to antenna impedance and coupling.

I Introduction

The Finite Difference Time Domain (FDTD) technique has had only limited application to antennas. This is somewhat surprising, since the geometrical and material generality of the method suggests that it might have significant application to antenna analysis, especially in situations where other structures, especially electromagnetically penetrable ones, are nearby. This is due to the relative ease with which the FDTD method accommodates modeling of volumetric electromagnetic interactions with materials as compared to the Method of Moments.

Earlier work [1] has shown that the FDTD method could compute the self impedance of a wire antenna in three dimensions, however, the approach used in [1], plane wave incidence, did not lend itself to mutual coupling calculations. Accurate self-admittance FDTD results for two-dimensional antenna geometries were presented in [2]. In this paper we demonstrate both self and mutual admittance FDTD calculations for three dimensional wire antennas.

II Approach

The test problem geometry is shown in Figure 1. Two wire dipoles of length 57 and 43 cm are parallel and separated by 10.5 cm. Both are center fed, and are symmetrically positioned. The goal is to determine the self admittance of the driven dipole and the mutual admittance between the two dipoles.

The FDTD computations were made using a three dimensional computer code based on the Yee [3] cell, with second order Mur [4] absorbing boundaries. The problem space was chosen as 61x51x80 cells, with the cell dimensions $\Delta x=\Delta y=0.5$ cm, $\Delta z=1.0$ cm. Making the two transverse dimensions smaller results in a greater length to diameter ratio, so that a thin wire Moment Method code may be used to provide comparison results over a wider band of frequencies. Thinner wires may be modeled in FDTD using sub-cell methods [5,6].

For the FDTD calculations the longer dipole is fed at the center with a Gaussian pulse of 100 volts maximum amplitude that reached its 1/e amplitude in 16 time steps. The time steps were 11.11 picoseconds, the Courant stability limit for the cell size chosen.

During the progress of the FDTD calculations the currents at the center of each dipole were saved for each time step. They were computed by evaluating the line integral of the magnetic field around the dipoles at the center. Along with the applied Gaussian voltage pulse the currents were Fourier transformed to the frequency domain. Then, based on the admittance parameter equations

$$I_1 = V_1 Y_{11} + V_2 Y_{12}$$

$$I_2 = V_1 Y_{21} + V_2 Y_{22}$$

and taking V_1 to be the driven dipole voltage and V_2 zero, we easily obtain the self admittance of dipole 1 and the mutual admittance (since $Y_{12} = Y_{21}$) between the dipoles by dividing the appropriate complex Fourier transforms of V_1, I_1, and I_2.

The Moment Method results were obtained using the Electromagnetic Surface Patch Version 4 [7] computer code. The wire radius for the Moment Method calculations was taken as 0.281 cm, providing the same cross section area as the 0.5 cm square FDTD cells. While the FDTD calculations should be valid up to approximately 3 GHz based on having 10 FDTD cells per wavelength, the thin wire approximation for the Moment Method code becomes questionable at

approximately 1 GHz and this was taken as the upper frequency limit for comparison of results.

III Results

Figure 2 shows the Gaussian pulse voltage applied to the 1 cell gap at the center of the longer, driven dipole. Figures 3 and 4 show the current flowing in the center cell of the driven and passive dipole respectively. All are plotted on the same time scale, corresponding to 8,192 time steps. This calculation required approximately 7 hours on a 25 MHz 486-based personal computer.

Figures 5-7 show the magnitude of the Fourier transforms of the voltage and current results of Figures 2-4. The current results indicate the complicated frequency domain behavior of the coupled dipole system.

The self admittance was obtained by dividing the complex Fourier transform of the driven dipole current by that of the Gaussian voltage pulse at each frequency. The results are shown in magnitude and phase in Figures 8 and 9 and compared with ESP4 Moment Method results. Considering the differences in how the feed region is modeled (a 1 cm gap in the FDTD calculations vs an infinitesimal gap in ESP4) the agreement is quite good.

The mutual admittance was obtained in a similar manner, dividing the complex passive dipole current by that of the Gaussian pulse. The results are shown in Figures 9 and 10. Again the agreement is quite good considering the different approximations and assumptions made in the FDTD approach relative to the ESP4 computer code.

IV Conclusions

The capability of the FDTD method to predict mutual coupling between antennas was demonstrated. The test case was two parallel wire dipoles of different lengths, with one driven by a Gaussian pulse. The complex self and mutual admittance results obtained using FDTD showed good agreement with results obtained using the Method of Moments.

V References

1. K. Kunz, R. Luebbers, F. Hunsberger, "A Thin Dipole Antenna Demonstration of the Antenna Modeling Capabilities of the Finite Difference Time Domain Technique", Applied Computational Electromagnetics Society Journal, Summer 1990.

2. J. G. Maloney, G. S. Smith, and W. R. Scott, Jr., "Accurate computation of the Radiation from Simple Antennas using the Finite-Difference Time Domain Method," IEEE Trans. Antennas and Propagat., vol. AP-38, pp 1059-1068, July 1990.

3. K. S. Yee, "Numerical solution of initial boundary value problems involving Maxwell's equations in isotropic media," IEEE Trans. Antennas and Propagat., vol. AP-14, pp 302-307, May 1966.

4. G. Mur, "Absorbing boundary conditions for the Finite Difference Approximation of the Time-Domain Electromagnetic Field Equations," IEEE Trans. on Electromagnetic Compatibility, vol. EMC-23, pp 377-382, November 1981.

5. R. Holland and L. Simpson, "Finite-difference analysis of EMP coupling to thin struts and wires," IEEE Trans. on Electromagnetic Compatibility, vol. EMC-23, May 1981.

6. K. Umashankar, A. Taflove, and B. Beker, "Calculation and experimental validation of induced currents on coupled wires in an arbitrary shaped cavity," IEEE Trans. Antennas and Propagat., vol. AP-35, pp 1248-1257, November 1987.

7. E. Newman, "A user's manual for the electromagnetic surface patch code: ESP Version IV," The Ohio State University Research Foundation, ElectroScience Laboratory, Department of Electrical Engineering, Columbus, Ohio 43212.

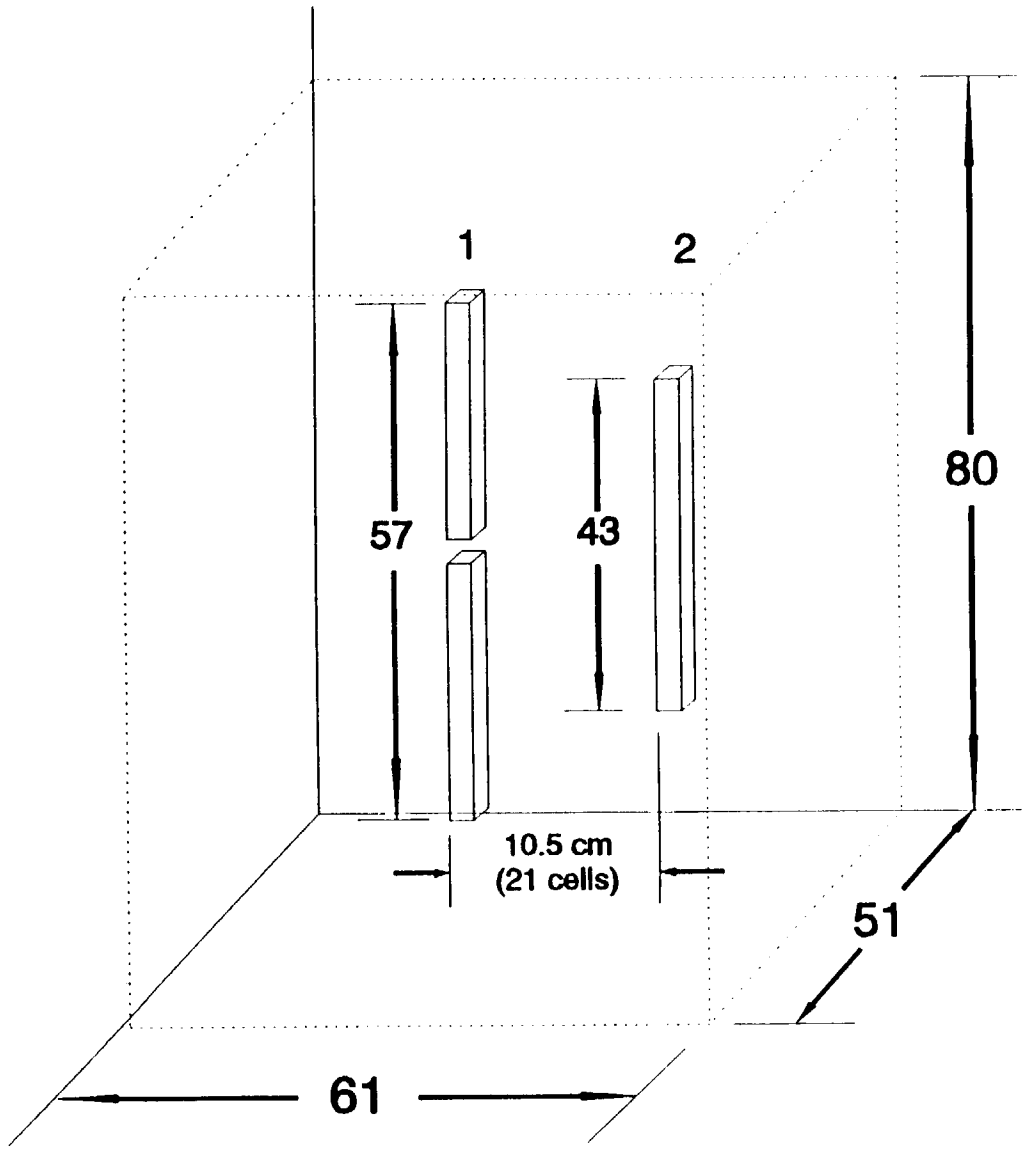
1
2
57
43
80
10.5 cm
(21 cells)
51
61

RJL Apr. 5, 1991 9:29:50 AM

57 CM Dipole Feed Voltage

10.5 cm spacing, 43 cm passive dipole, 61x51x80 Space

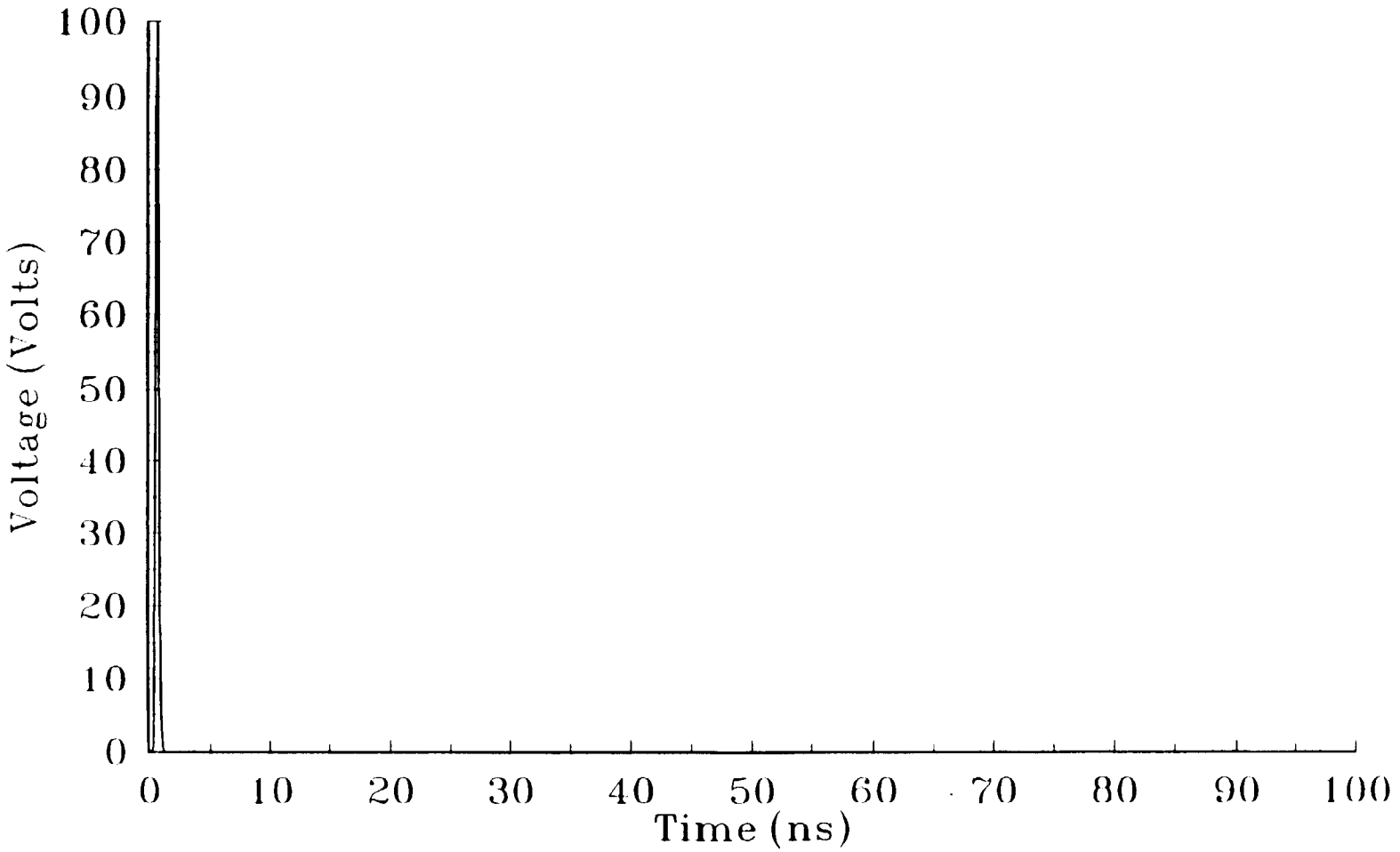

RJL Apr. 5, 1991 9:26:14 AM

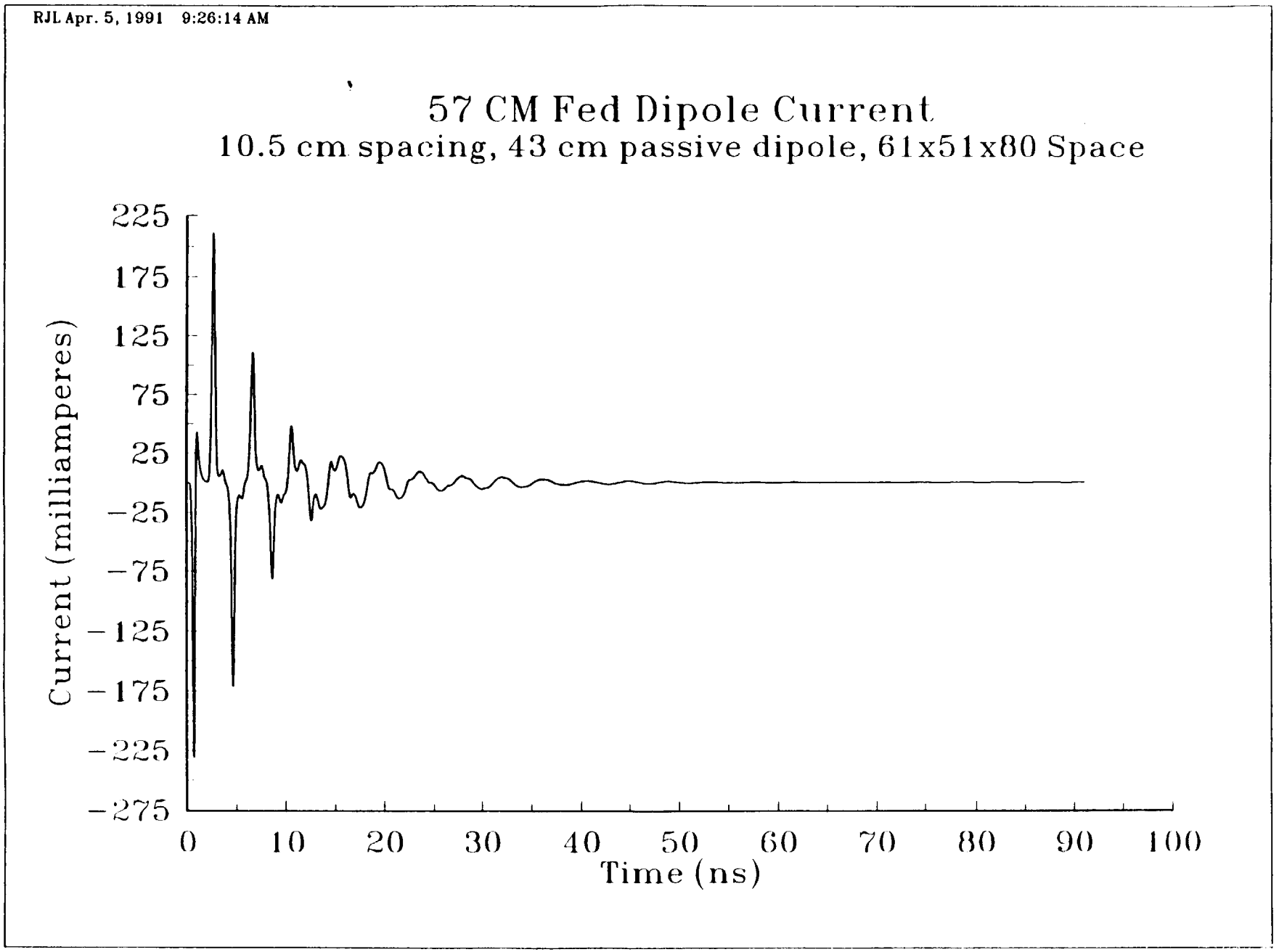

RJL Apr. 5, 1991 9:28:09 AM

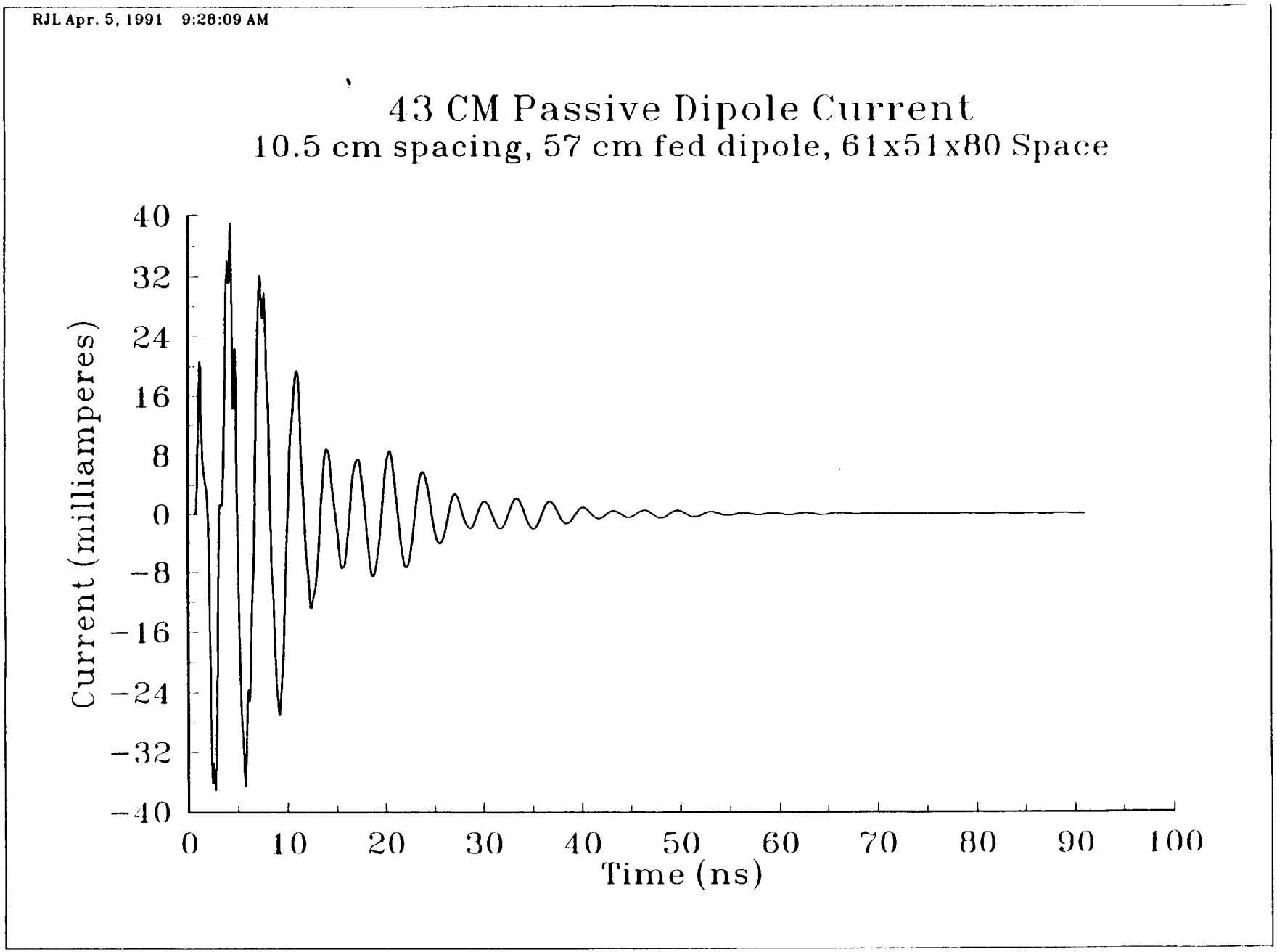

RJL Apr. 5, 1991 5:50:23 PM

57 CM Dipole Feed Voltage

10.5 cm spacing, 43 cm passive dipole, 61x51x80 Space

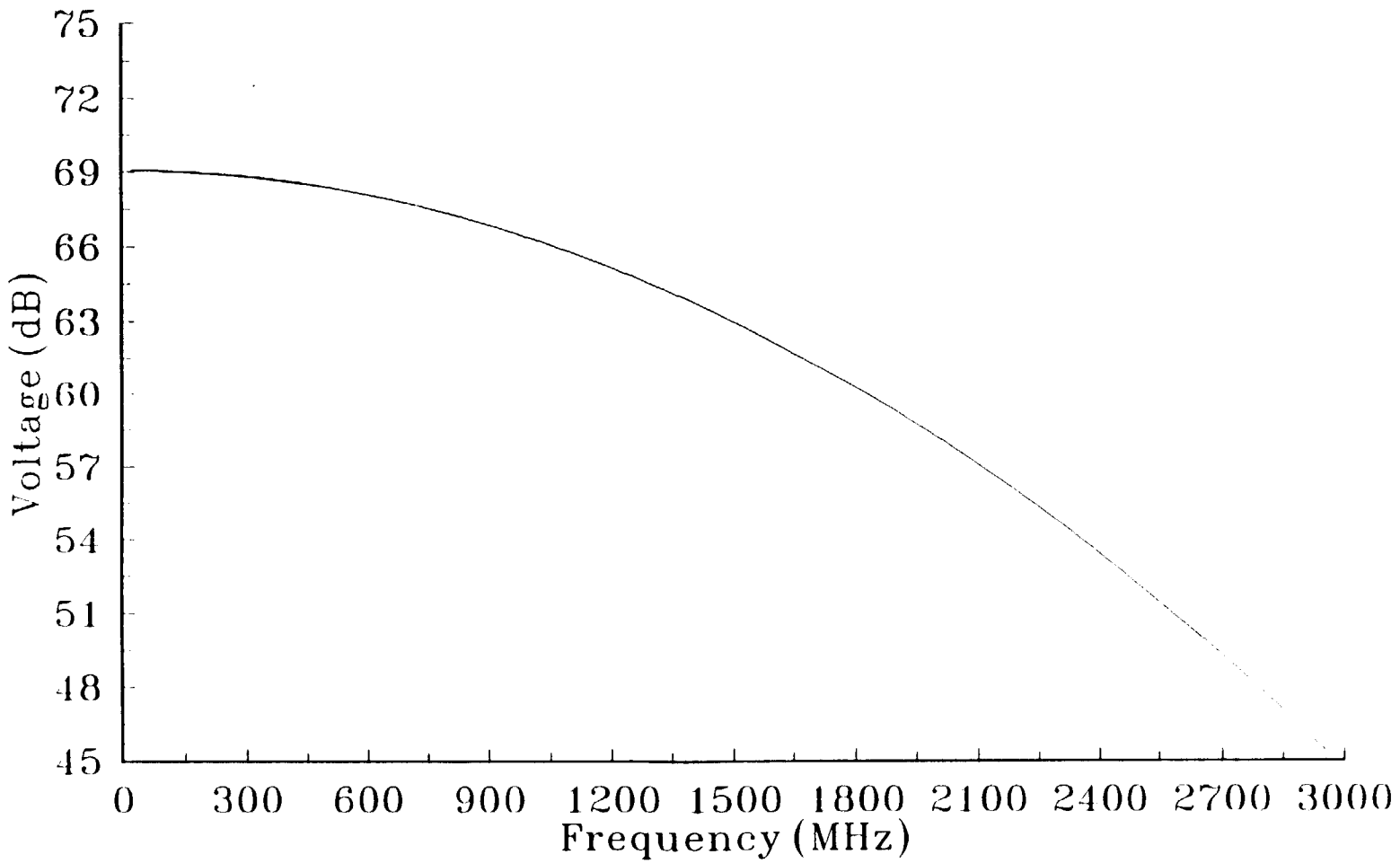

RJL Apr. 5, 1991 5:52:23 PM

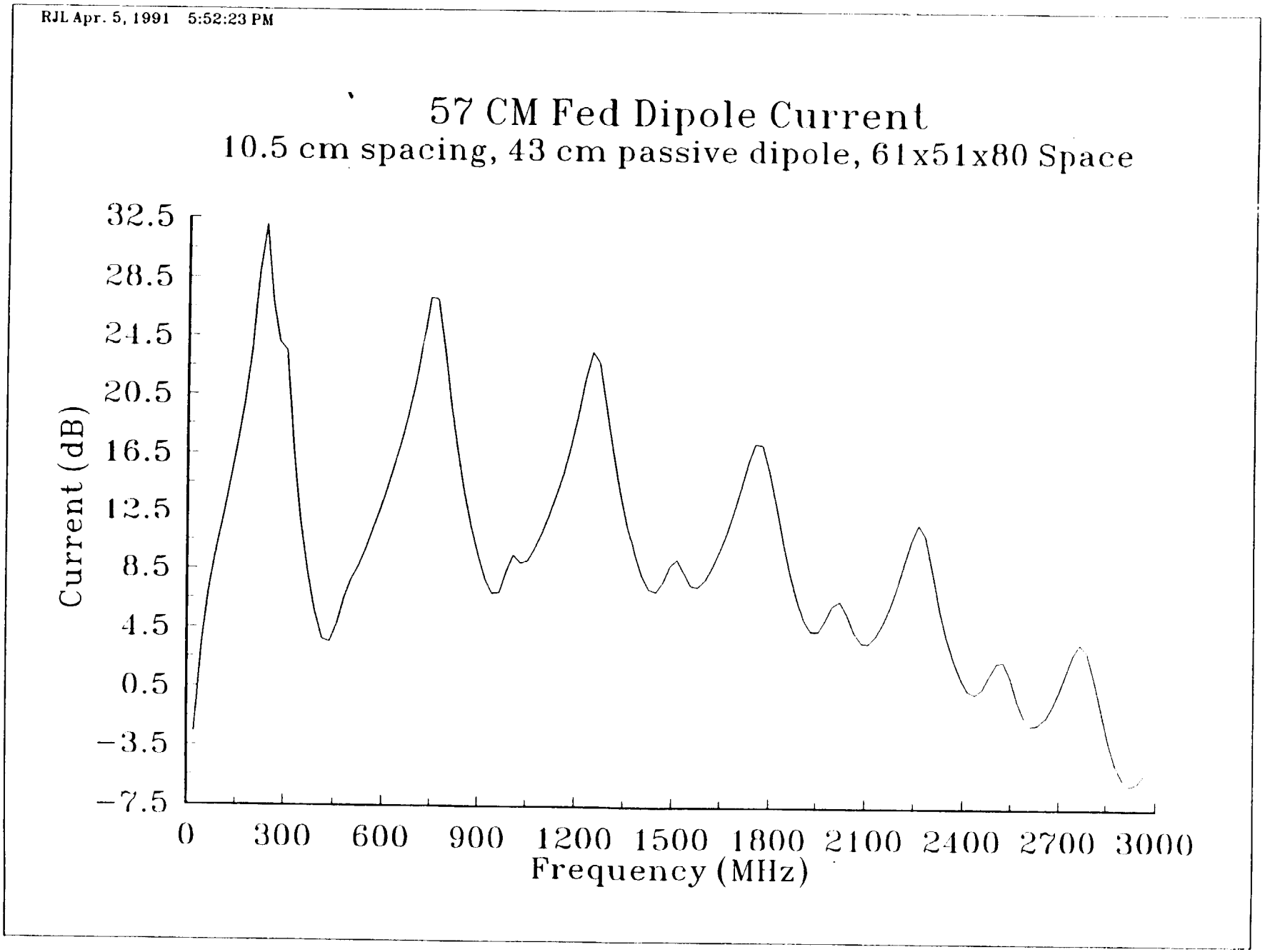

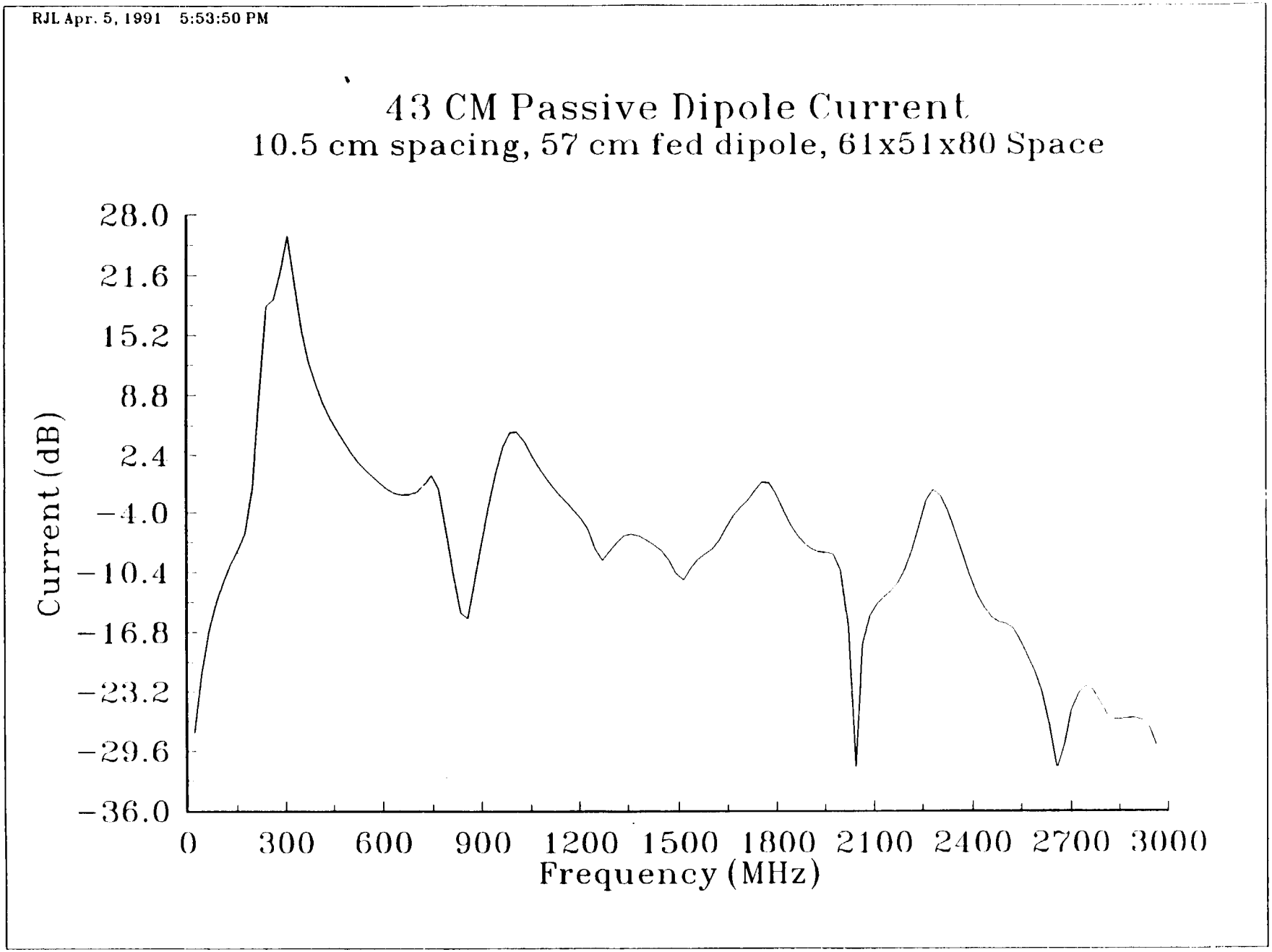
RJL Apr. 5, 1991 5:53:50 PM
43 CM Passive Dipole Current
10.5 cm spacing, 57 cm fed dipole, 61x51x80 Space
28.0
21.6
15.2
8.8
2.4
-4.0
-10.4
-16.8
-23.2
-29.6
-36.0
Current (dB)
0
300
600
900
1200
1500
1800
2100
2400
2700
3000
Frequency (MHz)

RJL Apr. 15, 1991 8:52:39 AM

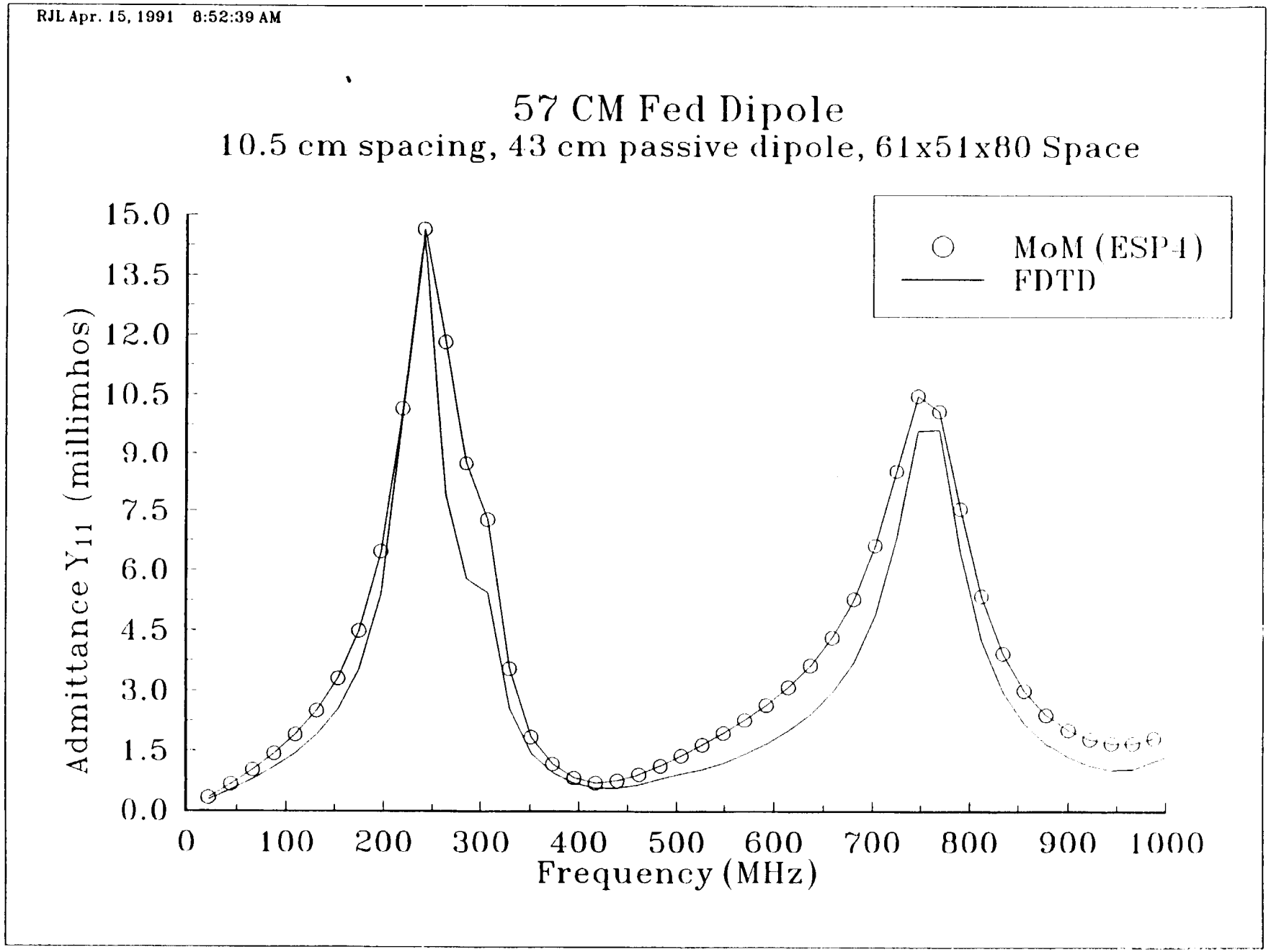

RJL Apr. 15, 1991 8:47:58 AM

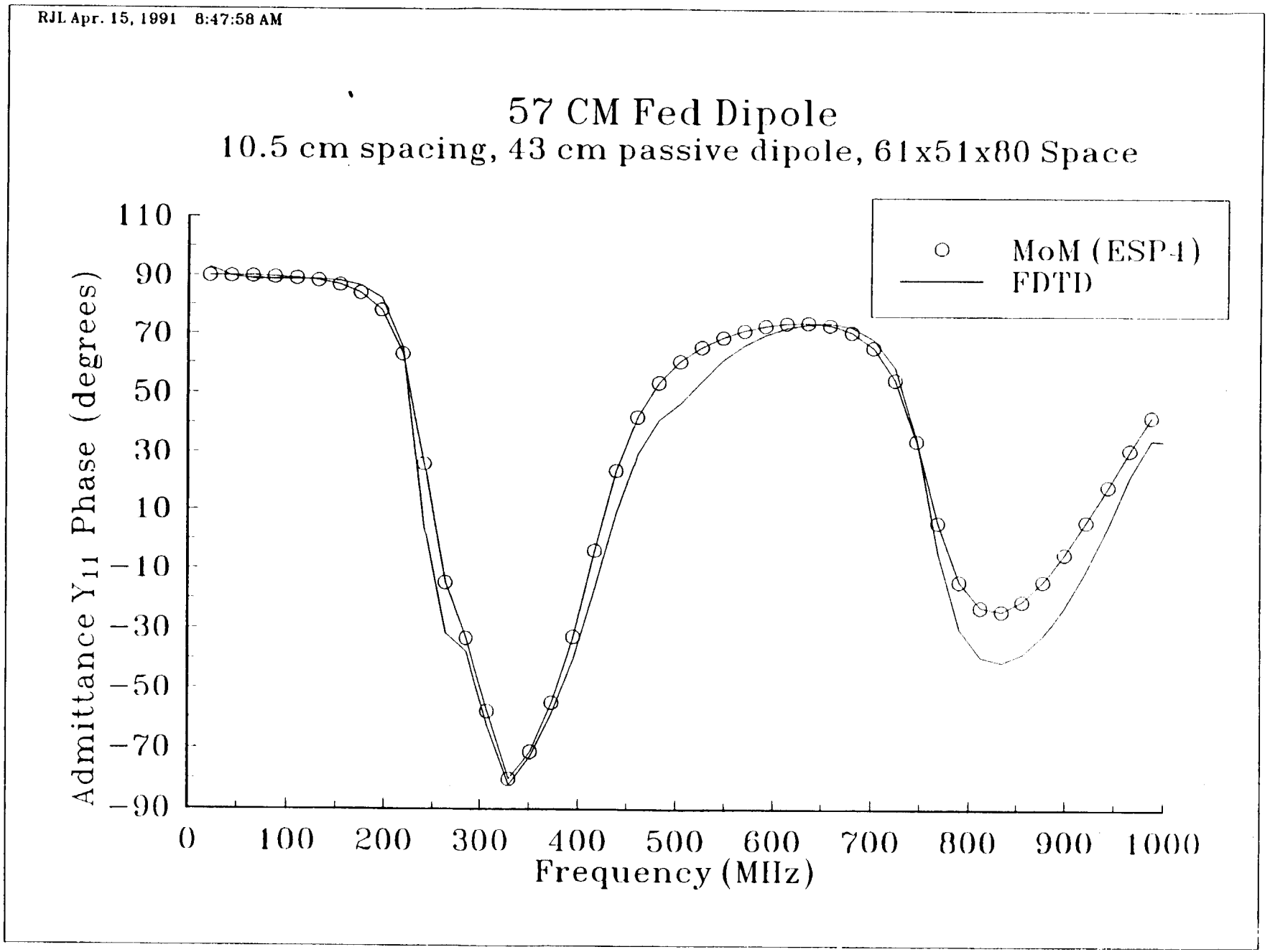

RJL Apr. 15, 1991 12:42:33 AM

43 CM Passive Dipole

10.5 cm spacing, 57 cm fed dipole, 61x51x80 Space

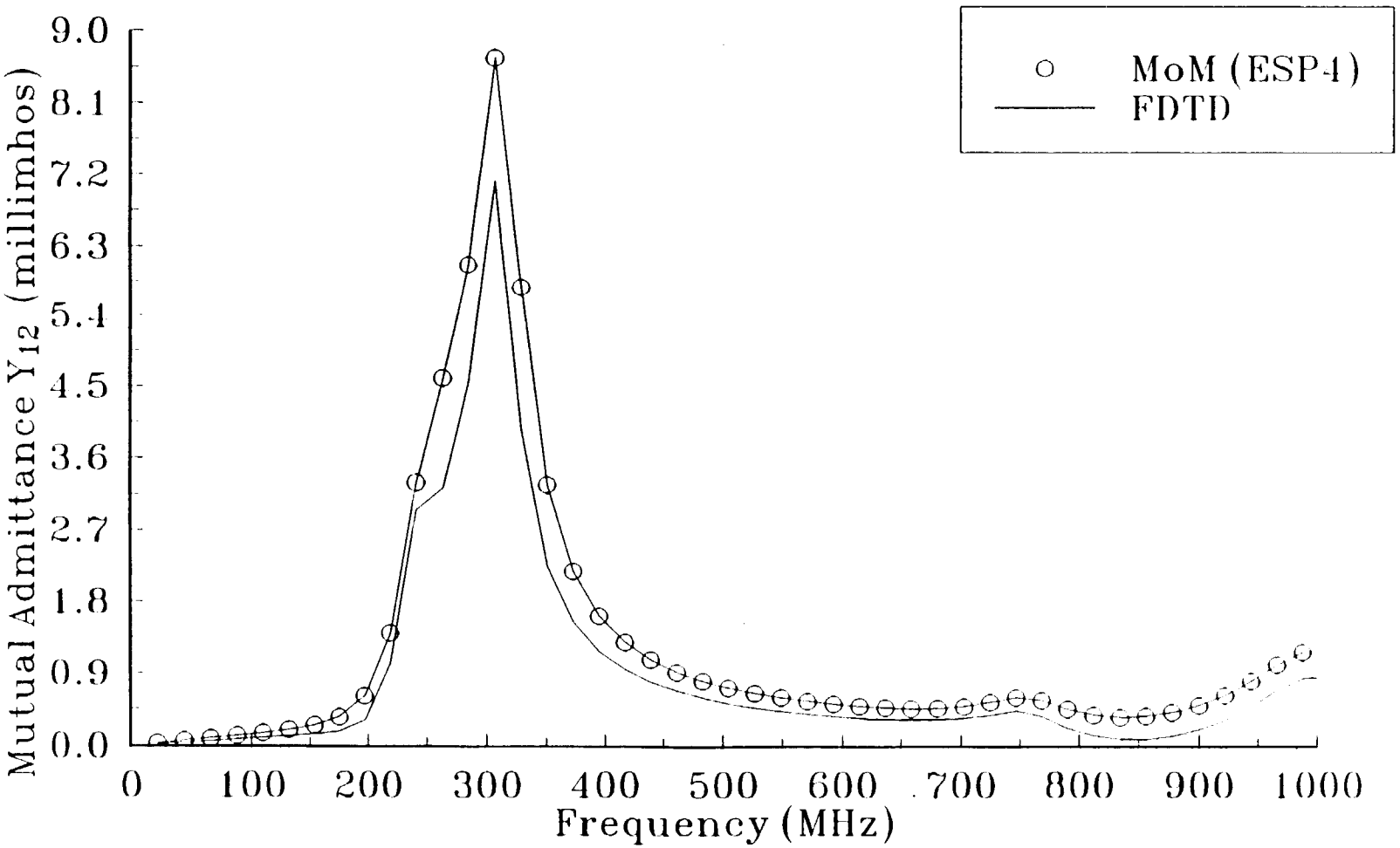

4-D

RJL Apr. 15, 1991 12:43:26 AM

43 CM Passive Dipole

10.5 cm spacing, 57 cm fed dipole, 61x51x80 Space